Antibacterial Activity and Potential Therapeutic Applications of Pyridine-based Synthetic Amphiphiles

A Thesis

Submitted in Partial Fulfillment of the Requirements for the Degree of

DOCTOR OF PHILOSOPHY

by

SUDEEP GOSWAMI

Department of Biosciences and Bioengineering
Indian Institute of Technology Guwahati
Guwahati-781039, Assam, India

May 2015

TH-1410_10610607

Antibacterial Activity and Potential Therapeutic Applications of Pyridine-based Synthetic Amphiphiles

A Thesis

Submitted in Partial Fulfillment of the Requirements for the Degree of

DOCTOR OF PHILOSOPHY

by

SUDEEP GOSWAMI

Department of Biosciences and Bioengineering
Indian Institute of Technology Guwahati
Guwahati-781039, Assam, India

May 2015

TH-1410_10610607

TH-1410_10610607

Dedicated to My Parents
Teachers
And
Almighty God

TH-1410_10610607

TH-1410_10610607

INDIAN INSTITUTE OF TECHNOLOGY GUWAHATI

DEPARTMENT OF BIOSCIENCES AND BIOENGINEERING

STATEMENT

I do hereby declare that the research findings of this thesis is the result of research work carried out by me in the Department of Biosciences and Bioengineering, Indian Institute of Technology Guwahati, Guwahati, India, under the supervision of Professor Aiyagari Ramesh.

As per the general norms of reporting research findings, due acknowledgements have been made, wherever the research findings of other researchers have been cited in this thesis.

Date: 25 May, 2015 **Sudeep Goswami**

TH-1410_10610607

TH-1410_10610607

TH-1410_10610607

TH-1410_10610607

INDIAN INSTITUTE OF TECHNOLOGY GUWAHATI

DEPARTMENT OF BIOSCIENCES AND BIOENGINEERING

CERTIFICATE

It is certified that the work described in this thesis entitled "***Antibacterial Activity and Potential Therapeutic Applications of Pyridine-based Synthetic Amphiphiles***" by Mr. Sudeep Goswami for the award of degree of Doctor of Philosophy is an authentic record of the results obtained from the research work carried out under my supervision in the Department of Biosciences and Bioengineering, Indian Institute of Technology Guwahati, India, and this work has not been submitted elsewhere for the award of any other degree.

CERTIFIED

Sudeep Goswami

(Candidate)

Roll No: 10610607

Aiyagari Ramesh, Ph.D.

(Thesis Supervisor)

Date: 25 May, 2015

TH-1410_10610607

TH-1410_10610607

TH-1410_10610607

TH-1410_10610607

ACKNOWLEDGEMENT

I would like to take this opportunity to offer my heartfelt thanks to a number of people without whose help and support this thesis would never have been possible.

It gives me immense pleasure and satisfaction to express my sincere reverence and heartfelt gratitude towards my Ph.D. supervisor Professor Aiyagari Ramesh, for allowing me to work under his esteemed guidance which made this achievement possible. His commendable dedication towards research and teaching has been my constant source of inspiration. His invaluable guidance, moral support and never ending kindness throughout my Ph.D. tenure has helped me to grow as a researcher and as an individual. I am very fortunate to have worked with him.

I am thankful to my doctoral committee members, Dr. Debasish Das, Dr. G. K. Saini and Dr. Biplab Mondal. Their constructive suggestions, support and motivation has improved the quality and richness of my research experience.

I am extremely grateful to Professor Gopal Das, Department of Chemistry for helping me in data analysis and providing valuable suggestions that often gave new perspectives to my research work. I owe him my most sincere gratitude for giving me the opportunity to work with him.

I would like to extend my sincere gratitude towards Professor V. V. Dasu, Head of the Department of Biosciences and Bioengineering, IIT Guwahati. I am also grateful to Professor Arun Goyal and Professor Pranab Goswami, Former Heads of the Department Biosciences and Bioengineering, IIT Guwahati for providing me the necessary facilities that helped me to pursue my research at IIT Guwahati.

I am also grateful to all faculty members and staff of the department for supporting me as a student and as a person. I would like to thank Department of Biosciences and Bioengineering for providing infrastructural facility. I would also like to thank Central Instrumentation Facility (CIF) of IIT Guwahati for providing ambient atmosphere of research and freedom to execute experiments.

I acknowledge the state-of-art facility at the Center for Excellence under the aegis of Program Support Grant provided by Department of Biotechnology (DBT), Government of India. I am grateful to Department of Biotechnology (DBT) and Science and Engineering Board, Department of Science & Technology (DST) for supporting my research through grants. I am also grateful to University Grants Commission (UGC) for providing research fellowship.

TH-1410_10610607

I am grateful to our collaborators Dr. Chirantan Kar, Abhijit Gogoi, Barun Dutta and Soham Samanta from the Department of Chemistry, IIT Guwahati for synthesizing and characterizing molecules. I would also like to thank Center for the Environment, IIT Guwahati for their help and assistance in AAS analysis.

I sincerely acknowledge my project supervisor in master degree -Dr. Manabendra Mandal. I am indebted for his constant support and encouragement. It is my pleasure to thank my seniors Dr. Manab Deb Adhikari, Dr. Asim Bikas Das, for their helpful guidance at the initial stages of my research work. It is my pleasure to thank my current lab members Thiyagarajan, Sandipan and Poulomi and former lab members Umakanth, Pallavi, Vidushi and Rajanikant for their support and unconditional gesture of assistance in the time of need. I have also spent many memorable moments with them.

I wish to thank my all seniors and friends Mahitosh, Seraj, Shubamoy, Chockalingam, Pojul, Ashok, Debi prasad, Santosh, Asif, Archita, Neha, Sharmila, Koushik, Mahesh, and all other COE labmates for their co-operation during my work and sharing light moments with them.

I would like to extend my appreciation for my friends at IIT Guwahati Mousumi, Soumyadeep, Sukhomoy, Tulsi, Nand Kishor, Arghya, Ankita, Balaji, Nilanjan and all other well-wishers because of whom my stay at IIT Guwahati has become more memorable and wonderful. I would also like to thank my other friends in the department and IIT Guwahati campus for the wonderful time and fun I had with them.

Lastly, and also most importantly, I would like to thank my parents for their blessings, my brother, sister and their respective family members for their endless and unconditional love and affection.

Sudeep Goswami

TH-1410_10610607

CONTENTS

Contents

TH-1410_10610607

ABBREVIATIONS

µM	Micromolar
A_{600}	Absorbance at 600 nm
AFM	Atomic force microscope
AMPs	Antimicrobial peptides
ANOVA	Analysis of variance
AU	Arbitrary unit
BHI	Brain-heart infusion broth
BSA	Bovine serum albumin
C6-HNC	**Compound 6**-loaded HSA nanocarrier
CCCP	Carbonyl cyanide m-chlorophenylhydrazone
cFDA-SE	5(and 6)-carboxyfluorescein diacetate succinimidyl ester
CFS	Cerebrospinal fluid
cF-SE	5(and 6)- carboxyfluorescein succinimidyl ester
CFU	Colony forming unit
cps	Counts per second
CR	Congo red
CTAB	Cetyltrimethylammonium bromide
CTAC	Cetyltrimethylammonium chloride
CV	Crystal violet
$DiSC_35$	3,3′-dipropylthiadicarbocyanine iodide
DMEM	Dulbecco's modified eagles medium
DMSO	Dimethyl sulfoxide
EDTA	Ethylene Diamine tetra Acetic Acid
EPS	Extracellular polymeric substances
FBS	Fetal bovine serum
FCS	Fetal calf serum
FDA	Food and Drug Administration
FESEM	Field emission scanning electron microscope
FIC	Fractional inhibitory concentration
FSC	Forward scattering
FTIR	Fourier Transform Infrared Spectroscopy
HEPES	N-2-Hydroxyethyl Piperazine N-2 Ethane Sulphonic acid

Abbreviations

HNPs	Human serum albumin (HSA)-based nanoparticles
HSA	Human serum albumin
IC	Inhibitory concentration
K_a	Association constant
LC	Loading capacity
LPS	Lipopolysaccharide
MBC	Minimum bactericidal concentration
MIC	Minimum inhibitory concentration
MRGs	Metal reactive groups
MRSA	Methicillin resistant *Staphylococcus aureus*
MSCRAMMs	Microbial surface components recognizing adhesive matrix molecules proteins
MTCC	Microbial Type Culture Collection
MTT	3-(4,5-Dimethylthylthiazol-2-yl)-2,5-diphenyltetrazolium bromide
NB	Nutrient broth
NPN	1-N-phenylnaphthylamine
NPs	Nanoparticles
PBS	Phosphate buffered saline
PI	Propidium iodide
SBF	Simulated body fluid
SD	Standard deviation
SDS	Sodium dodecyl sulphate
SEM	Scanning electron microscope
SGF	Simulated gastric fluid
SRL	Sisco research laboratories
SSC	Side scattering
TEM	Transmission electron microscope
TFA	Trifluoacetic acid
VNC	Viable but non-culturable cells
WTA	Wall teichoic acid
λ_{Em}	Emission wavelength
λ_{Ex}	Exitation wavelength

LIST OF TABLES

List of Tables

CHAPTER 6

LIST OF FIGURES

Chapter 1

Introduction and Literature Review

TH-1410_10610607

TH-1410_10610607

Chapter 1

Introduction and Literature Review

Introduction

Conventional antibiotics and chemotherapeutic drugs have undoubtedly rescued us from several life threatening infectious microbial ailments from the day of their discovery. However, in recent times, the rapid evolution of drug-resistant pathogenic bacterial strains has reached alarming proportions and is a cause of great healthcare concern. The genesis of drug-resistance in pathogenic bacteria can be attributed to an array of inherent molecular mechanisms, which include enzyme-catalyzed target modification, drug impermeability, drug inactivation and others. Further, a diminishing armory of antibiotics to counter the challenge of drug-resistant pathogenic bacteria has triggered a serious therapeutic crisis worldwide. This crisis has undoubtedly fuelled a perpetual need for a vigorous drug discovery program that aims to produce novel and potent antimicrobial agents. Such an endeavor demands judicious drug design and rational medicinal chemistry in order to develop bactericidal agents that can act on irrefutable cellular targets and are counterproductive to resistance development.

In this regard, membrane-targeting antimicrobial agents hold considerable therapeutic promise since the probability of developing resistance against them would require restoration of membrane components, which is physiologically challenging for the bacteria. Amongst the known membrane-acting antimicrobial agents, cationic antimicrobial peptides (AMPs) are considered to be viable candidates. Structure-function studies have established the key role of positive charge and amphiphilic scaffold in AMPs that enables electrostatic interaction with the negatively charged bacterial cell surface and subsequent insertion into the hydrophobic core region of the membrane, which results in membrane disruption and eventually cell death. Such a mode of action is likely to thwart resistance development in the bacterial strain. In spite of the profound mode of action of AMPs, their therapeutic potential is hampered owing to the high manufacturing cost formulation difficulties, poor pharmacokinetics, protease sensitivity and lower efficacy in

animal models. Under these circumstances and given the pressing need to develop potent antibacterials against drug-resistant pathogens, a major emphasis has been in the discovery of novel and structurally diverse synthetic amphiphiles as antimicrobial agents, which mimic AMPs in their mode of action. Conceivably, synthetic amphiphiles constitute a radical paradigm as antibacterial therapeutics against drug-resistant pathogens because of their facile synthesis, structural diversity, resistance to proteolytic inactivation and membrane targeting ability. Importantly, modulation of their activity is also possible by subtle alterations in their structure so as to leverage bactericidal activity and minimize host cell toxicity.

To realize the therapeutic promise of synthetic amphiphiles as antibacterial agents, a complete understanding of the mechanism of action of these molecules is imperative. In this regard it would be paramount to undertake specific studies pertaining to structure-function relationship of synthetic amphiphiles. Such an endeavor is expected to unravel the descriptors that govern antibacterial selectivity and cytotoxicity and thus provide a holistic picture of the therapeutic potential of synthetic amphiphiles. Since the bactericidal action of synthetic amphiphiles is primarily mediated through cell surface interactions followed by membrane disruption, this mode of action is radically different from conventional antibiotics, which act mostly on internal targets. It is also conceivable that the membrane-targeting activity of synthetic amphiphiles can thus be explored in adjuvant applications to breach the membrane barrier in pathogenic bacteria and thereby sensitize them against low concentrations of antibiotics. It is also foreseen that membrane-targeted amphiphiles could also be exploited to prevent the formation of biofilm, which is significantly implicated in nosocomial infections.

The present investigation is essentially based on the aforementioned rational. Recognizing the enormous scope of developing synthetic amphiphiles as novel and potent bactericidal agent, the present investigation is an endeavor to demonstrate the structure-function activity and potential therapeutic application of pyridine-based synthetic amphiphiles. In the age of unbridled antibiotic-resistance and at a time when several therapeutic antibiotics are rendered ineffective against life-threatening infections, this study, which strives to generate potent therapeutic antibacterials, addresses a very important and contemporary global healthcare problem.

The following section provides a detailed literature review pertinent to the research area of the present investigation.

Literature Review

1.1. Overview of Antibiotic-resistance in Pathogenic Bacteria

Prevalence of antibiotic-resistant pathogenic bacterial strains is a burgeoning healthcare issue. The rising menace of drug-resistant pathogenic bacteria coupled with the sluggish progress in the discovery of new antibiotics to counter their challenge is posing serious concerns worldwide. Antibiotic-resistant pathogenic bacteria display myriad strategies to acquire resistance against therapeutic drugs. Further, the ever mounting risk of this new threat to public health has heightened the use of antibiotics and disinfectants. This irrational and excessive use of antibiotics has been counterproductive as it has, in turn, contributed to the evolution of drug-resistant strains. A number of seminal review articles discuss the emergence and healthcare implications of antibiotic-resistant pathogenic bacteria (Fair and Tor 2014, Fischbach and Walsh 2009, Gootz 2010, Nikaido 2009). As discussed in the review article of Fischbach and Walsh 2009, the prevalent antibiotic-resistant pathogenic bacteria can be categorized as:

(a) Methicillin-resistant *Staphylococcus aureus* (MRSA), which is responsible for several nosocomial and life-threatening infections.

(b) Multidrug-resistant (MDR) Gram-negative pathogenic bacterial strains such as *Acinetobacter baumannii*, *Escherichia coli*, *Klebsiella pneumoniae* and *Pseudomonas aeruginosa*, which are empowered with an outer membrane as a drug permeability barrier and efflux pumps to purge out antimicrobial agents.

(c) Multidrug-resistant (MDR) and extensively-drug-resistant (XDR) strains of *Mycobacterium tuberculosis* (MDR-TB and XDR-TB), which is a serious threat in the developing countries.

From the available literature reports, the major clinically relevant drug-resistant pathogens encompass β-lactam resistant *Pneumococci*, penicillin and chloramphenicol resistant *Neisseria meningitides*, vancomycin-resistant enterococci (VRE), vancomycin-resistant

Staphylococcus aureus (VRSA) (Kaye and Kaye, 2000, Yang et al. 2007) and methicillin-resistant *Staphylococcus aureus* (MRSA), penicillin-resistant *Streptococcus pneumoniae* (Lowy, 2003), multidrug-resistant *Salmonella Typhimurium* (MRST) (Mather et al. 2013), multidrug-resistant *Acinetobacter*, carbapenem-resistant Enterobacteriaceae (CRE) and several others (Fair and Tor 2014).

In recent times, metallo-β-lactamase-resistance gene ($bla_{NDM.1}$)-mediated resistance against penicillin, cephalosporins and other antimicrobial agents exhibited by *Klebsiella pneumonia* NDM-1 is a grave cause of concern (Hawkey and Jones 2009). Another case in point is the rampant spread of MDR strains of *Salmonella enterica*, and fatal infections caused by *Escherichia coli* contaminated vegetables in Germany (Bush et al. 2011). Methicillin-resistant *S. aureus* (MRSA) is the most prevalent and a formidable nosocomial pathogen which is implicated significantly in hospital-acquired infections (20-40%), in particular bacteremia and sepsis (Lowy, 2003). According to the Center for Disease Control and Prevention's 2013 report, of nearly 2.0 million people getting affected, the number of deaths per year is 23,000 in United States alone due to an outbreak of resistant bacterial strain infections. A schematic highlighting the major implications of antibiotic-resistant pathogenic bacteria is indicated in Figure 1.1.

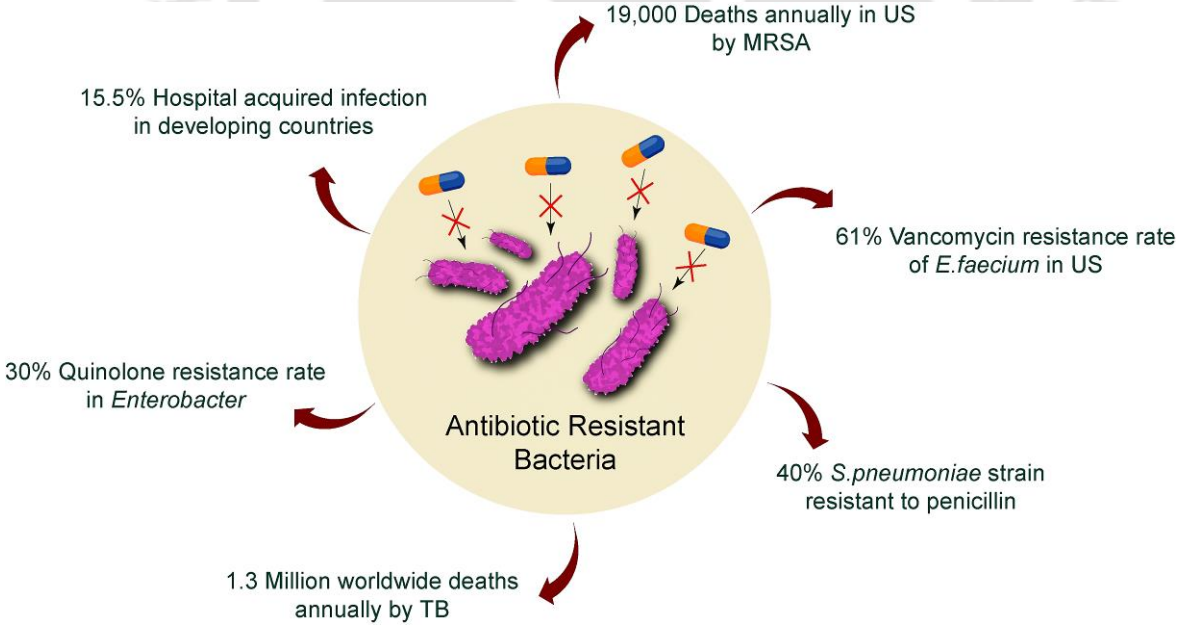

Figure 1.1. Major implications of antibiotic-resistant pathogenic bacteria. The represented statistics in the figure is obtained from Fair and Tor, 2014.

From the facts presented in Figure 1.1, it is quite clear that there is an urgent need to discover novel classes of antibacterial drugs in order to combat the global problem of drug resistance. However, there is a severe dearth in the turnover of new antibacterials. All major groups of antibiotics were discovered between 1930s-1960s and since then only a few new classes of antibiotics have been introduced, which indicates the innovation gap and stagnancy in drug discovery research (Fischbach and Walsh 2009, Silver 2011).

1.2. Mechanism of Antibiotic-resistance

Antibiotic-resistant pathogenic bacterial strains are evolving at an overwhelming rate. Acquisition of the resistance trait not only empowers the pathogen to defy host defense, it also renders most of the clinically relevant antibiotics ineffective. The drug-resistant pathogenic bacterial strains are equipped with highly evolved, complex and effective countermeasures that could evade the action of most therapeutic antibiotics (Blair et al. 2015, Fernandes 2006, Wright 2011). In order to mitigate the persistent problem of drug-resistance, it is important to acquire a nuanced understanding of various mechanisms involved in triggering drug-resistance and dissemination of the resistance trait. Therapeutic antibiotics essentially target various physiological processes in cells such as DNA synthesis (Collin et al. 2011, Kohanski et al. 2010), cell wall synthesis (Hurdle et al. 2011, Lewis, 2013), protein synthesis (McCoy et al. 2011, Wilson, 2014) and folate synthesis (Lange et al. 2007, Palmer and Kishony 2014). However, to evade the host defense mechanism and foil the action of many antibiotics, drug-resistant bacteria are equipped with a armory of versatile mechanisms which may include (a) the presence of a permeability barrier that prevents drug diffusion, (b) an active efflux pump that expels specific drugs and reduces its availability at target sites, (c) alterations in molecular targets, (d) presence of metabolic bypass that renders the cell insensitive to the drug, (e) presence of antibiotic-altering and antibiotic-degrading enzymes (Nikaido 2009, Wright 2011). Further, it is also considered that excessive use of antibiotics may in turn contribute to the spread of the resistance trait. Conceivably, use of antibiotics preferably select and favor the

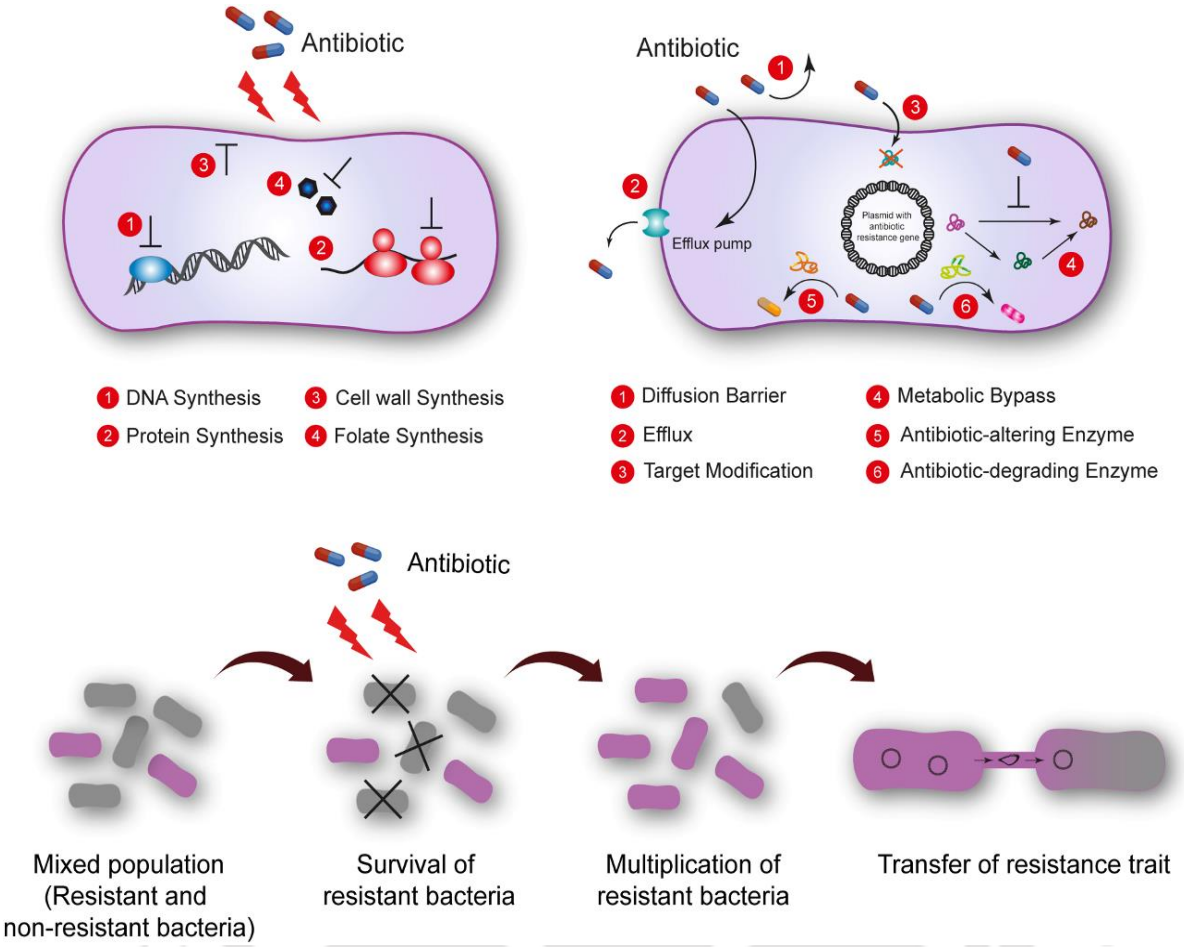

Figure 1.2. (A) Cellular targets of common antibiotics. (B) Mechanisms of antibiotic-resistance in pathogenic bacteria. (C) Spread of antibiotic-resistance trait by excess use of antibiotic followed by genetic transfer of trait.

growth of resistant cells and subsequent dissemination of the resistance trait can then be mediated through horizontal gene transfer (Davies and Davies 2010, Fair and Tor 2014, Toprak et al. 2012). A schematic representation of the conventional targets for antibiotics in bacterial cells, mechanism of antibiotic-resistance in bacteria and the spread of resistance through excessive antibiotic usage and gene transfer is illustrated in Figure 1.2. A comprehensive overview of various antibiotic-resistance mechanisms prevalent in pathogenic bacteria is represented in Table 1.1.

Table 1.1. General mechanisms of antibiotic-resistance in bacteria

Mechanism	Mediator	Effect	Reference
Permeability barrier	Lipopolysaccharide (LPS) in outer membrane	Drug resistance in Gram-negative bacteria	Delcour 2009 Lavigne et al. 2012
	Peptidoglycan and wall teichoic acid (WTA) in cell wall	Drug resistance in Gram-positive bacteria	Kohler et al. 2009, Weidenmaier and Peschel 2008
	Altered porin proteins (Opr and Omp)	Reduces drug eynt	Fernandez and Hancock 2012
Genetic basis of drug resistance [Drug resistance genes carrying plasmids and mutations]	Mutations in *kat*G, *inh*A, *ahp*C, *kas*A and *ndh*	Develops MDR-TB	Almeida Da Silva and Palomino 2011
	bla_{CTX-M} *mec*A operon,	Beta-lactamase, Methicillin-resistant *S. aureus*	Chambers and Deleo 2009, Hawkey and Jones 2009
	*acr*B, *efr*, *qep*, *msrA (*for macrolide), *cml* (for chloramphenicol), *rob*A, *mar*A and *emr gene locus* (in *E. coli*)	Drug efflux pump genes and altered porins	Fernández Fuentes et al. 2014
	qac genes,	Quaternary ammonium compounds resistance in *Staphylococcus* species	Wassenaar et al. 2015
	*tet*A gene *nor* genes, *aph*,and *aadA1* genes	Tetracycline, norfloxacin, Quinolone and aminoglycoside resistance gene	Blair et al. 2015, Nikaido, 2009
	*msr*A/B, *mph*A, and *mef*A	Macrolide resistance gene	Fernández Fuentes et al. 2014
Multidrug efflux pumps	Major families of bacterial drug efflux pumps	1. ATP-binding cassette (ABC) 2. Major facilitator superfamily (MFS) 3. Multidrug and toxic compound extrusion (MATE) 4. Small multidrug resistance (SMR)	Fernández Fuentes et al. 2014, Li and Nikaido 2009, Sun et al. 2014

Mechanism	Mediator	Effect	Reference
Enzymatic degradation and modification of Drug	Enzymatic processes (such as hydrolysis phosphorylation, acetylation, redox process etc.)	Inactivates β-lactams (β-lactamases), inactivates macrolides (esterases), (Acetyl & methyl) transferase (inactivates aminoglycosides and choramphenicol)	Gootz 2010, Kumar and Varela 2013, Wright 2005
Target modification	LPS remodeling by (L-Arap4N)	Reduces net electro-negativity of LPS, favours resistance development against cationic antibiotics such as Polymyxin B	Gutsmann and Seydel 2010, Kaye and Kaye 2000
	Altering Gyrase	Quinolones resistance	
	Altering DNA polymerase binding	Rifamycin resistance	
	rRNA methylation	Macrolides resistance	
	Mutation in penicillin binding protein (PBP)]	β-lactams resistance	
Overexpression of target	Overexpression of dihydropteroate synthase	Resistance against Sulfonamide and Trimethoprim Antibiotics	Alekshun and Levy 2007, Palmer and Kishony 2014
Bypass drug targets	Resistance against glycopeptide antibiotics (e.g. vancomycin)		Wright 2011

1.3. Considerations to Counter Resistance and Develop Candidate Drugs

In the process of drug discovery against emerging antibiotic-resistant pathogenic strains, the following can be regarded as critical elements: (a) identification of new and compelling targets for inhibition, which play a pivotal role in the survival as well as virulence of the target strain, (b) prevent host cell toxicity by judicious selection of targets that lack structural homologs in the mammalian host, (c) develop candidate drugs which fulfill optimum pharmacodynamic and pharmacokinetic criteria (Craig 1998, Craig 2003, Mueller et al. 2004, Silver, 2011), (d) candidate drugs should be essentially non-toxic to host cells, since they are likely to be administered at concentrations higher than their MIC depending to achieve effective *in vivo* killing concentrations (Wispelwey 2005),

(e) it is vital that the candidate drug should exhibit potent bactericidal activity and a minimal propensity to trigger resistance development.

1.4. Bacterial Membrane as a Potential Drug Target

The bacterial cell membrane has a unique structural organization, which enables it to perform a plethora of vital cellular functions. It is the focal point for several biochemical processes and a conduit for bacterial cells to interact with the external environment. Considering these points, antimicrobial agents that can target the bacterial membrane hold considerable therapeutic potential against antibiotic-resistant bacteria. Unlike most conventional antibiotics whose targets constitute specific physiological processes and are liable to resistance development, the probability of developing resistance against membrane-acting agents would require extensive restoration of damaged membrane components, which is physiologically taxing for the bacteria (Chen et al. 2010, Van Bambeke et al. 2008). Further, membrane acting agents are also effective against infections caused by dormant bacterial cells such as biofilm or slow-growing bacteria like *Mycobacterium tuberculosis*, unlike β-lactam antibiotics, which are known to act on only growing cells (Hurdle et al. 2011). Interestingly, there are marked differences in the composition and topological arrangement of lipids in the bacterial membrane vis-a-vis membrane in mammalian cells. Bacterial membranes have a higher content of anionic phospholipids like phosphatidylglycerol (PG), cardiolipin, phosphatidylserine (PS) as opposed to mammalian cytoplasmic membranes, which are predominantly composed of neutral, zwitterionic lipids such as phosphatidylcholine, phosphatidylethanolamine, sphingomyelin and sterols like cholesterol and ergesterol (van Meer and de Kroon, 2011, Zasloff 2002) Moreover, the presence of lipopolysaccharides (LPS) in Gram-negative bacteria and acidic polysaccharides (teichoic acids) in Gram-positive bacteria imparts a negative charge to the bacterial cell surface (Glukhov et al. 2005, Van Bambeke et al. 2008). This fundamental difference in the membrane characteristic renders cationic membrane acting antimicrobial agents as potential therapeutics that is likely to exhibit high antibacterial selectivity and thus eliminate the target pathogenic bacteria without imparting unwarranted host cell toxic effects.

1.5. Antimicrobial Peptides (AMPs): Prototype Membrane-acting Agents

Antimicrobial peptides (AMPs) are naturally occurring membrane acting agents which are unequivocally present amongst all classes of organisms and exhibit broad-spectrum antibacterial activity (Hancock and Sahl 2006, Shai 2002, Zasloff 2002). A large number of studies have deciphered the mechanism of action of AMPs on target membrane. The general understanding is that the cationic residues of AMPs facilitate initial electrostatic interaction with the negatively charged bacterial cell surface, whereas the hydrophobic residues allow AMPs to form an overall amphiphilic membrane-spanning structure that disrupts membrane architecture and functional integrity (Wimley 2010, Brogden 2005, Yeaman and Yount 2003, Chen et al. 2010). It is also opined that cationic AMPs render a "self-promoted uptake" wherein they can competitively displace divalent cations (Ca^{2+} or Mg^{2+}) present in the lipopolysaccharide (LPS) layer. This destabilizes the outer membrane, which facilitates further uptake of AMPs and other classical antibiotics for e.g. polymyxin B (Hancock 1997, Piers et al. 1994, Yeaman and Yount 2003, Zhang et al. 2000). The typical models that provide plausible explanations for AMP-mediated membrane permeabilization are the barrel-stave, toroidal pore and carpet model (Hurdle et al. 2011, Wimley 2010). Studies on AMPs have also indicated that membrane depolarization and formation of lesion or holes that leads to leakage of cellular contents eventually trigger cell death (Zasloff 2002, Klocek et al. 2009). In the endeavor of discovering potent antibacterial agents, AMP-inspired functional mimetics have come to the forefront. The fundamental goal of generating AMP-mimics is to enhance the antimicrobial activity, impart protease resistance and improve other pharmacological properties. Studies based on this rational include altering the primary amino acid sequence to acquire the desired charge and hydrophobicity (Pag et al. 2008, Wiradharma et al. 2011, Unger et al. 2001, Chen et al. 2010), integration of D-amino acids, non-peptide scaffolds or bulky side chains to impart protease resistance (Hancock and Sahl 2006, Findlay et al. 2010, Verdurmen et al. 2011) and conjugation with lipophilic acids for enhanced antibacterial activity (Avrahami and Shai 2002).

AMPs hold superior therapeutic potential over conventional antibiotics owing to their rapid membrane directed bactericidal activity and lower propensity to induce

resistance development. However, realization of their true therapeutic potential is hindered by several factors such as:

(a) The prohibitive manufacturing cost involved in the generation of AMPs is by far a major obstacle in their use as antibacterial chemotherapeutic agents (Marr et al. 2006).

(b) Challenges in drug formulations due to the size and large number of amide groups are considered to be a bottleneck for the routine clinical use of AMPs (Findlay et al., 2010).

(c) Many peptides have been shown to be ineffective in the physiological milieu as they are liable to lose their *in vivo* activity in presence of mono and divalent cations (Bowdish et al. 2005).

(d) The pharmacological attributes of AMPs need to be further deciphered. For instance, a nuanced understanding with regard to peptide aggregation, *in vivo* half-life of peptides and their proteolytic inactivation and their dosing frequency is paramount prior to the widespread therapeutic applications of AMPs (Marr et al., 2006, Yeaman and Yount 2003).

1.6. Synthetic Amphiphiles as Alternate and Potent Bactericidal Agents

In the pursuit of developing novel and potent membrane-acting antibacterial agents medicinal chemistry-based research has grown in recent times and has demonstrated the feasibility of generating structurally tunable and highly potent bactericidal amphiphilic scaffolds, which mimic the quintessential membrane-targeting activity of antimicrobial peptides. In contrast to AMPs, synthetic amphiphiles offer distinct advantages, which enhance their merit as potential therapeutic antibacterials. Some of the significant features include:

(1) Facile and inexpensive synthesis, which permits large scale production.

(2) Membrane-directed activity, which augers well to tackle antibiotic-resistant pathogens.

(3) Structural tunability, which allows a library of scaffolds to be generated readily.

(4) Resistance to proteolytic degradation, which imparts stability and robustness to these molecules.

(5) Possibility of functionalization with fluorophore moiety, which renders tracking of interactions with target cell.

(6) High antibacterial selectivity and reduced host cell toxicity achieved through judicious tethering of functional groups in the amphiphile.

A schematic representation of the noteworthy attributes of synthetic amphiphiles is shown in Figure 1.3.

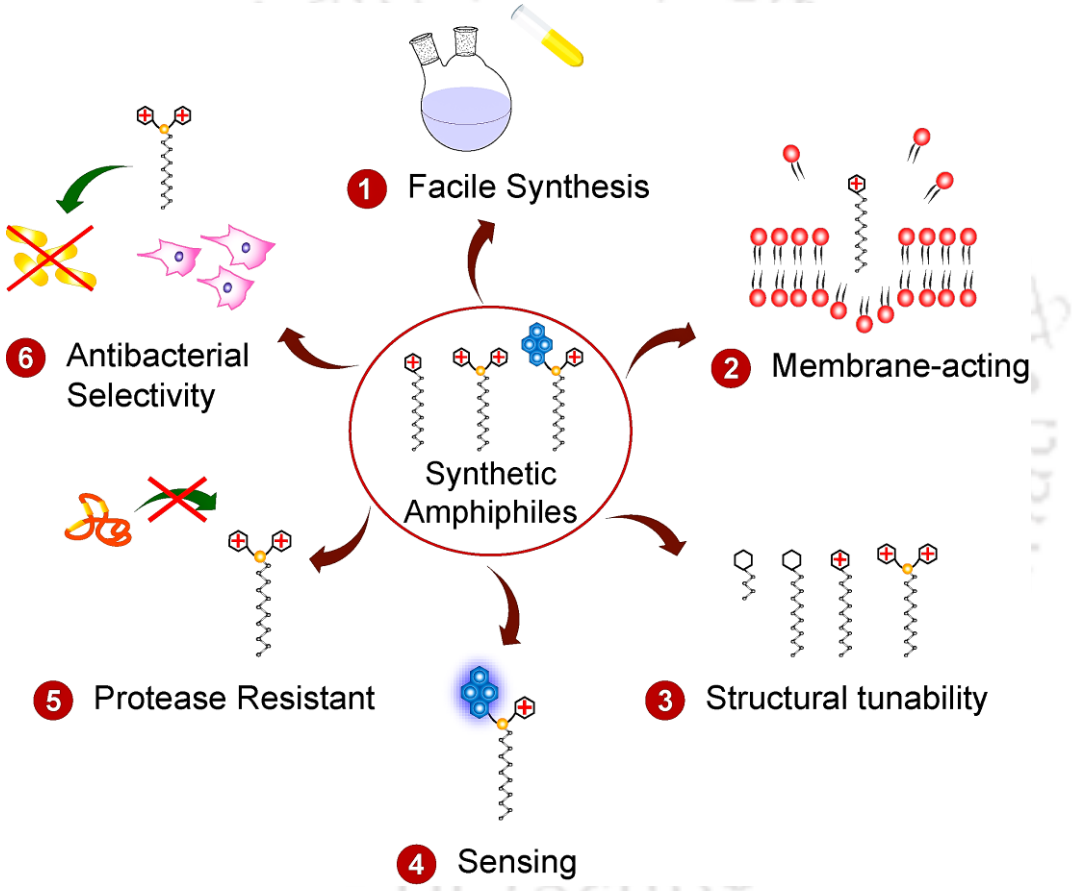

Figure 1.3. Schematic representation of the beneficial attributes of synthetic amphiphiles.

1.7. An Overview on Bactericidal Synthetic Amphiphiles

Recognizing the promise of synthetic amphiphiles as potent antibacterial agents, the present investigation was undertaken to demonstrate the structure-activity relationship and the potential therapeutic applications of pyridine-based synthetic amphiphiles. In the following sections a brief overview on the fundamentals of amphiphiles, structure-function

relationship in the context of antibacterial activity, factors contributing to cytotoxicity and the adjuvant potential of amphiphiles in combination therapy with antibiotics is presented.

1.7.1. Synthetic Amphiphiles-Essential Concepts

Synthetic amphiphiles are essentially generated through tethering of hydrophilic and hydrophobic domains. Their hydrophilic/polar head group may consist of phosphates, heterocyclic aromatic/non-aromatic rings, amines, hydroxyl or acidic groups whereas, the hydrophobic group is usually a long hydrocarbon moiety. Cationic amphiphiles consists of a positively charged head group such as quaternary ammonium and halide ion as a counter ion. Such amphipathic nature allows them to solubilize to an extent in both polar (e.g. water) and a non-polar (e.g. organic solvents). Anionic amphiphiles are characterized by the presence of negatively charged polar headgroups and positively charged counterions such as sodium, potassium or ammonium ions. Anionic surfactants are powerful detergents and are widely used as soap. A third category of amphiphile is the amphoteric amphiphile, which consist of headgroups that have both positive and negative charge and are thus zwitterions. Nonionic amphiphile are used in cleaning applications with anionic surfactants and consist of a chain of oxyethylene groups, also called ethoxylates.

Synthetic amphiphiles are also considered as surface-active molecules and hence exhibit the quintessential features of surfactants. Another archetypical attribute of synthetic amphiphiles is their propensity to self-assemble. This phenomenon is driven by non-covalent interactions among themselves and the medium that can lead to the formation of different levels of complex molecular aggregates. Scanning electron microscope and other powerful techniques have revealed a plethora of morphology for these aggregates such as micelles, micellar rods, bilayers, vesicles and inverted aggregates. Formation of distinct self-aggregated supramolecular assemblies depends on the ratio between the size of the hydrophilic and the hydrophobic moiety as well as the nature of the solvent.

1.7.2. Structure-Activity Relationship in Bactericidal Synthetic Amphiphiles

Membrane-targeting synthetic amphiphile having low molecular mass is an emerging and promising candidate for developing potent therapeutic agents against antibiotic-resistant pathogenic bacteria (Findlay et al. 2010). A large number of reports highlight the

correlation between amphiphile structure and their bactericidal activity. In an early study, the pH-dependent hydrolysis of a set of betaine and fatty alcohols esters of quaternary ammonium amphiphiles having hydrocarbon chain of varying length and its subsequent effect on bactericidal activity was reported (Lindstedt et al. 1990). In another study, the structure-dependent antimicrobial activity of methyl substituted cationic phosphonium salts with single or multiple long alkyl chains were investigated. It was observed that synthetic di- and trimethyl-substituted phosphonium salts containing alkyl chains of various lengths were found to display higher antibacterial activity as compared to polymeric quaternary ammonium salts having the same hydrophobic structure (Kanazawa et al. 1994). In an interesting study, aminoglycoside antibiotics-derived amphiphiles were synthesized based on scaffold of Neomycin B, Kanamycin A, Amikacin, and Neamine with polycarbamates and polyethers. The most potent neomycin B-derived heptaphenyl carbamate exhibited manifold higher activity against MRSA as compared to unmodified neomycin B (Bera et al. 2010).

A group of synthetic macrocyclic pore-forming amphiphiles called hydraphiles were reported whose head groups were made up of crown ethers or other polar residues. They are membrane-acting ionophore that forms ion channels, disrupts cellular ion gradients causing osmotic stress and subsequent cell death (Gokel and Negin 2012). Cholic acid-derived facial amphiphiles bear anionic, cationic, or nonionic functional groups. They can act as potent membrane-acting antibacterial agent (Zhong, Yan, and Zhao 2005). Cationic ceragenin is a cholic acid derived steroid and a semi-synthetic antimicrobial agent that has an ability to depolarize and permeabilize bacterial cell membrane (Epand et al. 2010, Van Bambeke et al. 2008). Cationic quinine-derived amphiphiles have been synthesized and characterized for its antimicrobial activity against methicillin resistant *S. aureus*. It was proposed that the cationic nitrogen group probably interacts with the negatively charged membrane phospholipids and their aromatic ring promotes insertion into the hydrophobic interior of the phospholipid layer (Lv et al. 2007). A similar kind study of was also performed with biocompatible quinoline-based synthetic amphiphiles where, the antimicrobial activity had been shown to augment with cationic charge and increasing hydrophobicity i.e., alkyl chain length (Vudumula et al. 2012). In another study the cationic and amphiphilic nature of phenylene ethynylene antimicrobial

oligomers (AMOs) was implicated in interactions with the membrane (Yang et al. 2007). It has also been demonstrated that amongst a group of low molecular weight random methacrylamide copolymers, the antimicrobial activity was significantly increased with an increase in the length of the alkyl side chain (Palermo et al. 2009). In case of macrocycle trimer of cholate-derived facial amphiphile, it was found that cyclic trimer exhibited greater penetration into the hydrophobic region of the membrane as compared to linear trimer (Widanapathirana and Zhao 2012). Based on a structure-activity study, it has been demonstrated that the antimicrobial activity of cationic amphiphilic polymethacrylate derivatives can be enhanced by altering the charge, hydrophobicity and molecular weight (Kuroda and DeGrado 2005).

The role of cationic charge and hydrophobicity in the bactericidal activity of synthetic amphiphiles has also been highlighted in additional studies (LaDow et al. 2011, Lowery et al. 2009). Multiplicity of cationic head groups can elevate bactericidal activity of an amphiphile through multi-dentate interactions with the bacterial cell surface. Compared to single-headed amphiphiles, there is a systematic increase in the antimicrobial activity of amphiphilic molecules such as alpha-helical AMPs with an increase in the cationic head groups (Jiang et al. 2008). It is envisaged multiple headgroups and higher cationic charge density will render superior interaction of amphiphiles with the bacterial cell surface which is likely to translate into higher bactericidal activity (Haldar et al. 2005). Head group structure was also shown to have an influence on antimicrobial activity of the cationic dipeptide-based amphiphiles (Mitra et al. 2009). A series of bicephalic (double-headed) cationic amphiphiles with aromatic core bearing multiple trimethylammonium head groups and a single linear alkoxy tail were prepared. It was reported that the antimicrobial activity was governed by chain length and relative positioning of the head groups on the aromatic core (LaDow et al. 2011).

A homologous series of dendritic amphiphiles having varying sizes of saturated linear alkyl chains were synthesized. It was noticed that there was a decrease in critical micelle concentration (CMC) with an increase in the chain length, which in turn influenced water-solubility and antimicrobial activity of the amphiphile (Sugandhi et al. 2007). In another study it was observed that amongst a series of synthetic methacrylate monomers containing quaternary ammonium with alkyl chains of varying length, 2-

dimethyl-2-hexadecyl-1-methacryloxyethyl ammonium iodide having 16 carbon chain length demonstrated highest antibacterial activity against *S. mutans* (He et al. 2011). In case of gemini amphiphiles having two hydrophilic cationic quaternary ammonium head groups connected with a hydrocarbon tail as well as interlinked with different methylene spacers and cleavable amide linkages, greater antimicrobial activity was observed as against monomeric amphiphiles. Further, the activity was observed to increase with increase in the spacer chain length upto a critical extent and thereafter there was a reduction in the activity with further increase in spacer chain length (Hoque et al. 2012). Random and sequence-specific copolymers with lipophilic and hydrophilic side chains have been shown to mimic host-defense peptides in their antibacterial activity (Mowery et al. 2007). Based on available literature reports, an overview of bactericidal synthetic amphiphiles is presented in Table 1.2.

1.7.3. Factors Affecting Cytotoxicity of Synthetic Amphiphiles

Literature reports have unequivocally established that the antimicrobial activity of amphiphilic molecules are enhanced with increase in cationic charge and hydrophobicity (Findlay et al. 2010, LaDow et al. 2011, Vudumula et al. 2012, Lowery et al. 2009). However, an increase in hydrophobicity of the amphiphile may also contribute to its pronounced cytotoxic effect (Dymond and Attard 2008). Hence to achieve optimum antimicrobial activity and biocompatibility, a judicious balance between hydrophilic and hydrophobic moieties is imperative as illustrated in pyridinium head group-based amphiphilic hydrogelators (Brahmachari et al. 2010) and quaternary ammonium head group based gemini amphiphile (Hoque et al. 2012). High bactericidal activity with minimal cytotoxic effect against mammalian cell lines was observed in a set of anionic amphiphilic dendrimers, which were shown to form supramolecular assemblies (Meyers et al. 2008). In another report, a series of amino acid-based hydrogelating amphiphiles were prepared with a counterion. Interestingly, anionic counterions with greater hydrophobicity and nanocomposite formed by AgNP-amphiphile interaction could enhance the antimicrobial activity and biocompatibility (Dutta et al. 2011). Studies on a series of synthetic dipeptide-based cationic amphiphiles with different head groups have demonstrated the importance of charge and the number of hydrophobic amino acids

Table 1.2. An overview of bactericidal synthetic amphiphiles.

Sl. No.	Amphiphilic Molecule	Target Organism	MIC Range	Cytotoxic Effect	Reference
1.	Triple-headed, double-tailed amphiphiles	*S. aureus, E. coli P. aeruginosa*	1.0–16 µM	Not determined	Marafino et al. 2015
2.	Polyamine derived amphiphiles	*S.aureus, E. faecalis , E. coli , P. aeruginosa*	0.5-125 µM	Not determined	Paniak et al. 2014
3.	Quinoline-based amphiphiles	*S. aureus, E. coli*	5.0-20 µM	Non cytotoxic	Vudumula et al. 2012
4.	Cationic dimeric amphiphiles (gemini amphiphile)	*E. coli, S. aureus*	10−13 µM	Non-toxic (HC_{50} = 128 µM)	Hoque et al. 2012
5.	Bicephalic amphiphile	*S. aureus, E. coli*	4.0-31 µM	Not determined	LaDow et al. 2011
6.	Hydrogelating amphiphiles	*B. subtilis, S. aureus, E. coli*	1.0-12.5 µg/mL	Cytotoxic above 20 µg/mL	Dutta et al. 2011
7.	Methacrylate amphiphile	*Streptococcus mutans*	1.0-25 µg/ml	Not determined	He et al. 2011
8.	Random and uniform side chain polymers	*P. aeruginosa, E. coli, B. cereus, S. aureus*	8.0- 256 µg/ml	Hemolytic	Song et al. 2011
9.	Amphiphilic block and random copolymers	*E. coli*	1-63 µg/ml	Non-hemolytic	Oda et al. 2011
10.	Poly-methacrylate amphiphile	*E. coli, M. luteus, L.. monocytogenes, P. aeruginosa*	0.1-1.0 mg/mL	IC_{50} = 0.2-2 mg/mL	Rawlinson et al. 2010

Sl. No.	Amphiphilic Molecule	Target Organism	MIC Range	Cytotoxic Effect	Reference
11.	Amphiphilic Neamine Derivatives	*S. aureus, P. aeruginosa, and E. coli*	4.0-32 µg/ml	Not determined	Baussanne et al. 2010
12.	Aminoglycoside antibiotics-derived amphiphiles	*S. aureus,, E. faecalis, E. coli*	0.25 µg/ml – 1.0 µg/ml	Not determined	Bera et al. 2010
13.	Pyridinium based amphiphilic hydrogelators	*B. subtilis, M. luteus, E. coli*	0.4-20 µg/ml	(IC_{50} = 100 µg/mL)	Brahmachari et al. 2010
14.	Fmoc functionalized cationic amphiphiles	*B. subtilis, S. aureus, E. coli, P. aerugenosa*	20-200 µg/mL	Not determined	Debnath et al. 2010
15.	Tetramic acid based amphiphile	*B. subtilis, E. coli, S. aureus*	EC_{50} = 49.0 µM.	Non-toxic (upto 100 µM)	Lowery et al. 2009
16.	Dipeptide-based cationic amphiphiles	*B. subtilis, S. aureus, E. coli, P. aeruginosa*	0.1-150 µg/mL	Cytotoxic at higher conc.	Mitra et al. 2009
17.	Random methacrylamide copolymers	*E. coli, S. aureus*	14 µM -340 µM	HC_{50} = 5.0-100	Palermo et al. 2009
18.	Anionic amphiphilic dendrimers	*Bacillus subtilis*	EC_{50} = 40-60 µM	EC_{50} =130-1500 µM	Meyers et al. 2008
19.	Random and sequence-specific copolymers	*E. coli, B.subtilis, S. aureus*	3-25 µg/mL	Hemolytic (MHC=100 µg/mL)	Mowery et al. 2007
20.	Antimicrobial oligomers (AMO)	*E. coli, B. subtilis,* MRSA	0.8-100 µg/mL	Hemolytic (3.2-100 µg/ml)	Yang et al. 2007
21.	Quinine-derived amphiphiles	MRSA, *B.* subtilis, *E. coli, P. aeruginosa*	0.4-1.6 ug/mL	Non Haemolytic	Lv et al. 2007

Sl. No.	Amphiphilic Molecule	Target Organism	MIC Range	Cytotoxic Effect	Reference
22.	Homologous dendritic amphiphile	*Mycobacterium Smegmatis*	0.35 µM	Not determined	Sugandhi et al. 2007
23.	Amphiphilic Polymethacrylate	*E. coli*	16 µM	HC_{50} < 1 µg/mL	Kuroda and DeGrado 2005
24.	Multiple pyridinium headgroup amphiphile	*E. coli, S. aureus, E. faecalis*	4.9-11.3 µM	Not determined	Haldar et al. 2005
25.	Synthetic hydraphile	*E. coli, B. subtilis,* *S. cerevisiae*	0.6-175 µM	Cytotoxic	Leevy et al. 2005
26.	Phosphonium and quaternary ammonium	*S. aureus, B. subtilis, E. coli, E. aerogenes, P. aeruginosa*	3.13-200 µg/ml	Not determined	Kanazawa et al. 1994
27.	Betaine and quaternary ammonium amphiphiles	*E. coli, P. aeruginosa,*	2-50 µM	Not determined	Lindstedt et al. 1990

present in the peptide chain for attaining biocompatibility and selectively high antimicrobial activity (Mitra et al. 2009). An interesting approach reported in a study is the use of an amino acid-based (L-tryptophan based) cationic amphiphilic peptide that exhibited broad spectrum antimicrobial activity and biocompatibility was demonstrated against mammalian cell lines (Roy and Das 2008). In case of low molecular weight random methacrylamide copolymers, the hemolytic trait and membrane-disrupting ability was influenced by alkyl chain length and mole fraction of alkyl chain (Palermo, Sovadinova, and Kuroda 2009). In case of hydrocarbon polymers (alternating copolymers, random copolymers, and homopolymers) with cationic and hydrophobic groups distributed along its backbone the significance of proper balance of spacer distance, hydrophobicity, and charge was highlighted to attain higher biocompatibility and antimicrobial activity (Song et al. 2011). In another study on polymeric amphiphiles it has been emphasized that

biocompatibility is largely influenced by molecular weight, charge density, cationic functionalities, structure and sequence and conformational flexibility of the molecule (Fischer et al. 2003). In a fundamental study, it was deciphered that the structure of the macromolecular amphiphilic copolymer, in particular the presence of block copolymers is a key determinant of their selectivity against bacteria over human cells (Oda et al. 2011).

1.7.4. Synthetic Amphiphiles in Combination Therapy

Antibacterial therapy using a combination of drugs is considered to render several benefits. Combinatorial therapy is a viable strategy to overcome bacterial resistance mechanism and refurbish drug effectiveness (Chan et al. 2011, Li et al. 2011). Most multicellular organisms secrete a plethora of antimicrobial peptides (AMPs). Apart from their fundamental role in host innate immunity, many of the AMPs are known to synergistically enhance the activity of conventional antibiotics (Yeaman and Yount 2003, Marret al. 2006). Several antimicrobial polymers were well known to enhance the efficacy of some existing conventional antimicrobial agents. For instance, it has been demonstrated that the muco-adhesive amphiphilic polymer pDMAEMA disrupts outer membrane of the Gram-negative bacteria and enhances activity of erythromycin (Rawlinson et al. 2010). Administration of these synthetic crown ether-based pore forming hydraphiles could sensitize microbes towards conventional antibiotics such as erythromycin, kanamycin, rifampicin, and tetracycline by creating ion channels on the bacterial membrane (Atkins et al. 2010). Several cationic-membrane permeabilizing agents including amphiphilic molecules are known to synergistically enhance the bactericidal activity of conventional antibiotics like erythromycin (Naghmouchi et al. 2010, Matsuzaki et al. 1998, Westerhoff et al. 1995, Yeaman and Yount 2003, Saha et al. 2008). In a recent study, the potential of the cationic quinolinium-based amphiphile to act as an adjuvant and thereby enhance the efficacy of erythromycin against Gram-negative bacteria has been reported (Uday et al. 2014).

1.8. Bacterial Biofilms

In the present study, the prospect of synthetic amphiphiles as antibiofilm agents is investigated. In order to realize the therapeutic challenges posed by bacterial biofilms and devise strategies to generate antibiofilm agents, it is paramount to understand the essential physiology of biofilms, the key stages in their development and the fundamental basis of their resistance to antibiotic-mediated therapy. In the following section a detailed overview of the key features of biofilms, essential stages of their development, prevalence of biofilm-based infections and potential therapeutic agents for antibiofilm therapy are highlighted.

1.8.1. Salient Features of Biofilm

Bacterial biofilms are characterized as an organized cluster of surface-adherent bacterial cells encased in a self-secreted extracellular polymeric substance (EPS), also called "matrix", that are important mediating agents for bacterial attachment (Archer et al. 2011, Flemming and Wingender 2010, Kostakioti et al. 2013). Bacterial biofilms are essentially typified as communities in which polymeric molecules enforce intercellular bonds, while signaling molecules mediate intercellular communications. Formation of biofilm is a survival strategy in microorganisms to prevail over stress conditions such as nutritional deprivation, challenge of antibiotics, host immune response, oxidation and desiccation (Bordi and de Bentzmann, 2011, Hall-Stoodley et al. 2004). Owing to a specialized niche, biofilm-associated cells exhibit an altered physiology, variations in nutrient utilization, and express an array of genes, proteins, surface molecules and virulence factors (Archer et al. 2011, Donlan and Costerton 2002, Kostakioti et al. 2013).

Drug resistance in bacterial biofilms is a major healthcare concern and its clinical implication can be realized as biofilms are responsible for approximately 80% of all microbial infections, and cause 100,000 deaths annually in the USA alone (Chambers and Deleo 2009, Stone 2009). Biofilms are known to cause chronic infections such as periodontitis and chronic lung infection in cystic fibrosis patients (Parsek and Singh 2003, Stewart and Costerton 2001). In addition, there has been an alarming rise in biofilm-based nosocomial infections, which are often device-associated (Arciola et al. 2012, Davies 2003, Singh et al. 2000). The clinically relevant and most commonly encountered biofilm

forming bacteria are *Staphylococcus aureus*, *Staphylococcus epidermidis* and *Pseudomonas aeruginosa*. In particular, *S. aureus* mediated biofilm infection has been prevalent and is a cause of great concern with the recent emergence of methicillin-resistant *S. aureus* (MRSA) (Archer et al. 2011, Chambers and Deleo 2009, Periasamy et al. 2012). Owing to the relevance of biofilms in healthcare and the inherent defiance exhibited by biofilms towards antibiotic-mediated therapy, development of bactericidal agents with antibiofilm potential has acquired considerable significance (Bordi and de Bentzmann 2011, Mintzer et al. 2012, Piletska et al. 2011, Thompson et al. 2012).

1.8.2. Stages in the Formation of Biofilm

On the basis of *in vitro* experimental models, the typical stages of biofilm formation constitute the following:

(I) At the outset, reversible interaction of planktonic cells with the surface of a substratum is mediated by relatively weak forces such as hydrophobic, van der Waals and electrostatic interactions (Arciola et al. 2012). Subsequently, stronger adhesion of cells to the substratum is promoted by proteinaceous adhesion ligands such as autolysins, lecithin and adhesins and polysaccharides such as glucomannan (Danhorn and Fuqua 2007).

(II) The second step of biofilm formation is is largely governed by Microbial Surface Components Recognizing Adhesive Matrix Molecules (MSCRAMMs) and intercellular adhesion, which leads to accretion of multiple layers of cells (Patti et al. 1994, Speziale et al. 2009). The cells are protected by an exopolysaccharide matrix and a heterogeneous multicellular community called micro-colony begins to emerge (Parsek and Tolker-Nielsen 2008).

(III) In the subsequent stage, maturation of the micro-colony is accomplished wherein the characteristic structural and physiological features of the biofilm such as high cell density, elaboration of EPS, nutritional starvation, reduced growth rate and establishment of cell-cell communication gradually unfold (Bordi and de Bentzmann 2011).

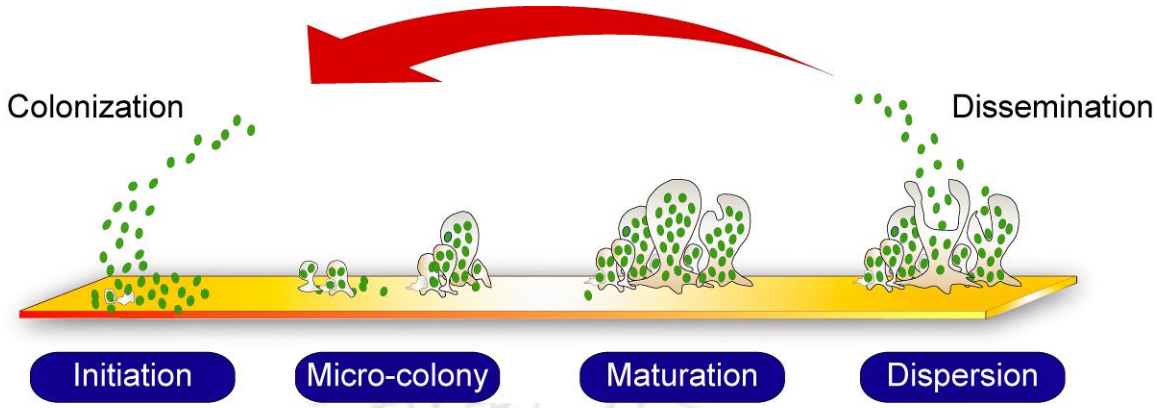

Figure 1.4. Schematic representation of various stages in the formation of bacterial biofilm.

(IV) In the final step, bacterial cell dispersion is observed as the planktonic cells entrenched in the matrix detach and initiate a subsequent round of invasion and colonization of a new substratum (Molin and Tolker-Nielsen 2003). Detachment of planktonic cells can be mediated through enzymes (Kaplan et al. 2004) or quorum-sensing molecules (Otto 2008). A cartoon indicating the various stages during a typical biofilm formation is indicated in Figure 1.4.

1.8.3. Biofilm Matrix

The matrix is a significant component of the biofilm and is often referred to as extracellular polymeric substance (EPS). The slimy EPS is characterized by the presence of a dynamic microenvironment, which supports cellular adhesion and aggregation, which in turn elicits the formation of a robust and refractory biofilm (Flemming and Wingender 2010). Biofilm matrix is amphiphilic in nature as it consists of both hydrophilic e.g. hydroxyl, carboxyl, charged groups and hydrophobic moieties e.g., aromatic, phenolic groups, hydrophobic regions in proteins and carbohydrates (Flemming and Wingender 2010). Apart from water which constitutes nearly 97% of the matrix, self-secreted exopolysaccharide glycocalyx polymers such as D-alanylated lipoteichoic acid (LTA) and poly-β-1,6-N-acetyl-D-glucosamine (PGA) play the role of intercellular polysaccharide adhesins and are major components in bacterial biofilm matrix (Diemond-Hernandez et al. 2010, Izano et al. 2008). The structural components of the biofilm matrix include cells (dormant, persistent and metabolically active), water, enzymes, lipids (LPS, phospholipids,

surfactin, viscosin and emulsan), and other cellular metabolic products such as slimy exopolysaccharide and proteinaceous adhesins. In addition, extracellular DNA (eDNA) is known to be a key component of the biofilm matrix (Flemming and Wingender, 2010). The presence of eDNA renders structural stability to biofilm matrix and increases cell-to-cell and cell-surface interactions (Allesen-Holm et al. 2006, Whitchurch et al. 2002).

1.8.4. Biofilm-associated Ailments

Biofilms are often observed as highly resilient cellular communities that can colonize either host tissues or medical devices. The most common biofilm-forming bacteria are *Staphylococcus aureus, Staphylococcus epidermidis, Pseudomonas aeruginosa, Enterococcus faecalis, Streptococcus viridans, Escherichia coli, Klebsiella pneumoniae* and *Proteus mirabilis* (Donlan 2001). Chronic and sometimes life-threatening ailments are manifested through biofilms formed either on medical devices such as implants or in host-tissues. Majority of implant-mediated infections are caused by staphylococci, enterococci and *Candida* species (Arciola et al. 2012, Hetrick and Schoenfisch, 2006, Noimark et al. 2009, Otto 2008). Biofilm-forming *S. aureus* and *S. epidermidis* are frequently detected on cardiovascular devices (Otto 2008, 2009). *S. aureus* and *P. aeruginosa* have been implicated in development of biofilms on the surface of Foley's urinary catheter and thereby causing urinary tract infections (Muder et al. 2006, Singh et al. 2012). Biofilm-forming pathogenic bacteria are also known as causative agents for chronic and recalcitrant host-tissue infections. Common examples of such infections include respiratory infections caused by *P. aeruginosa* (Govan and Deretic 1996; Koch and Hoiby 1993). There are known instances of urinary tract infections caused by uropathogenic *E. coli* [UPEC] (Foxman 2010), periodontitis caused by mixed biofilms of *Streptococcus mutans* and other bacteria (Kuramitsu and Wang 2011). A schematic representation of the major infections in humans caused by bacterial biofilms is depicted in Figure 1.5.

1.8.5. Antibiotic-resistance in Biofilms

Biofilms are known to exhibit high resistance towards conventional therapeutic antibiotics (Burton et al. 2006, Hogan and Kolter 2002, Jones et al. 2001, Kostakioti et al. 2013, Mah and O'Toole, 2001). The presence of an extracellular polymeric matrix is widely regarded

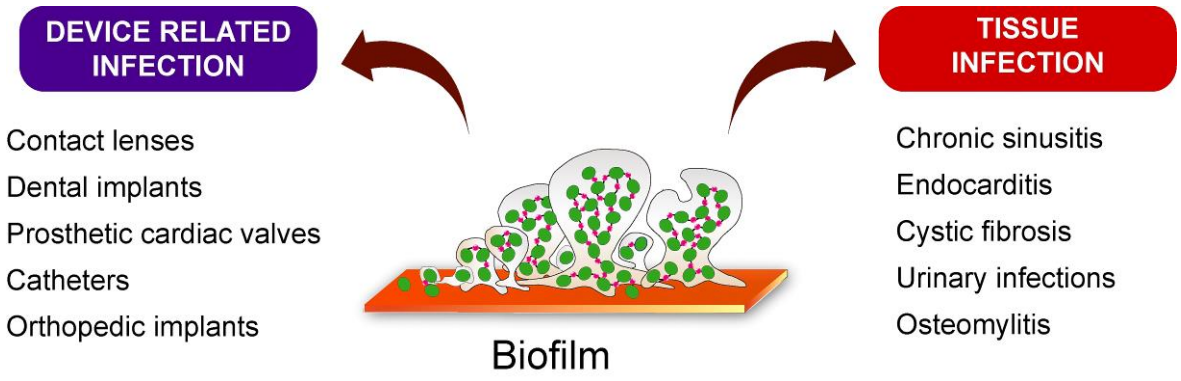

Figure 1.5. Schematic representation of various biofilm-related infections in humans.

as a prominent barrier for diffusion of antibiotics (Bordi and de Bentzmann, 2011, Flemming and Wingender, 2010, Kostakioti et al. 2013). Various reports suggest the role of biofilm matrix in developing resistance towards antibiotics such as tobramycin (Tseng et al. 2013), gentamycin or beta-lactams like ampicillin (Stewart 2002) and other antibiotics such as oxacillin, cefotaxime and vancomycin (Singh et al. 2010). Literature reports indicate that persister cells can emerge in a biofilm. Owing to depletion of nutrients and elaboration of waste products, cells in the core of the biofilm matrix exhibit slow growth. These persister cells have been shown to display an innate resistance towards antibiotics, which target metabolically active cells (Lewis 2008, Stewart and Costerton 2001). eDNA is known to be an integral component of biofilms and can sequester cationic aminoglycosides such as tobramycin and reduce their efficacy against cystic fibrosis causing *P. aeruginosa* (Purdy Drew et al. 2009). Studies have shown that elaboration of enzymes such as β-lactamase, aminoglycoside-modifying enzymes, or chloramphenicol acetyltransferases by biofilm-associated cells could inactivate several antibiotics (Fux et al. 2005). In addition, high levels of metal ions and a considerably low pH associated with the biofilm matrix also contributes to antibiotic inactivation (Jones et al. 2001, Kostakioti et al. 2013). It has been also been suggested that antibiotic resistance trait can also develop through horizontal gene transfer of resistance factors in bacterial biofilm (Madsen et al. 2012).

1.8.6. Potential Antibiofilm Agents

Treatment of bacterial biofilms is accomplished by therapeutic agents, which essentially target various stages involved in the formation of biofilm. The viable approaches include: (1) application of anti-adhesion agents and small molecules that interfere with signal transduction and hamper the onset of cell adhesion to substratum, (2) use of lytic phages, nanocomposites, EPS-degrading enzymes, DNAse I, Dispersin B and chelating agents that impede the formation of micro-colony formation and biofilm maturation and (3) modulation of c-di-GMP to induce motility and deployment of D-amino acids or norspermidine and their analogs that are known to trigger dispersion of biofilm (Bordi and de Bentzmann 2011, Kostakioti et al. 2013). Some of the representative examples of antibiofilm agents are illustrated in Table 1.3.

Table 1.3. Examples of Antibiofilm Agents.

Sl. No.	Antibiofilm Agent	Molecule	Target Organism	Mode of Action	References
1	Anti-adhesion agent	Mannoside Fim H inhibitor	*E. coli*	Inhibit adhesion to the surface	Cusumano et al. 2011
2	Chelating agent	Sodium citrate	*S. aureus*	Chelate cations	Shanks et al. 2006
3	Motility promoting agent	Norspermidine	*E. coli* *S. aureus*	Trigger biofilm disassembly by targeting EPS	Kolodkin-Gal et al. 2012
4	Signal transduction interference	3-Acyltetramic aci	*S. aureus*	Target quorum sensing	Murray et al. 2014
5	Antimicrobial peptide	Cathelicidin peptides	*S. aureus* *P. aeruginosa*	Membrane acting	Pompilio et al. 2011
6	Synthetic antimicrobial peptide	A3K, A6K, and A9K	*S. aureus* *E. coli*	Membrane acting	Chen et al. 2010
7	Quinolinium-based cationic amphiphile	Quinolinium-based amphiphiles	*P. aeruginosa*	Membrane acting	Uday et al. 2014
8	Lytic phages	Enzyme	*E. agglomerans*	EPS degradation	Sutherland et al. 2004
9.	Antimicrobial compound	Pentasilver hexaoxoiodate (Ag_5IO_6)	*P. aeruginosa, S. aureus*	Antimicrobial activity of silver	Incani et al. 2015
10.	Antibiotics	Reutericyclin, ranbezolid	*S. aureus*	Membrane acting	Hurdle et al. 2011

Sl. No.	Antibiofilm Agent	Molecule	Target Organism	Mode of Action	References
11.	Proton pump inhibitors	Esomeprazole	*S. aureus, P. aeruginosa*	Inhibits biofilm associated cells.	Singh et al. 2012
12.	Combination therapy	Tobramycin and 2-aminoimidazole	MRSA, VRE	Synergistic activity of 2-aminoimidazole potentiates the activity of tobramycin	Rogers et al. 2010
13.	Mucolytic agent	N-acetylcysteine	*P. aeruginosa*	Reduces the production of EPS	Zhao and Liu 2010
14.	Anti-biofilm polysaccharides	Pel and Psl	*S. aureus, S. aureus*	Destabilizes biofilm	Jiang et al. 2011
15.	Antimicrobial Peptides mimics	Quaternary ammonium amphiphiles	*S. aureus and E. faecalis*	Cationic character and alkyl side chains are vital for biofilm eradication	Jennings et al. 2014
16.	Porphyrin antibacterial agents	XF-70 and XF-73	*S. aureus*	Membrane damage	Ooi et al. 2010
17.	Synthetic anti-adhesion agents	5, 6-dimethyl-2-aminobenzimidazole (DMABI)	*Pseudomonas aeruginosa*	Non-bactericidal, prevent biofilm attachment	Broderick et al. 2013
18.	Flustramine analogues	pyrroloindoline triazole amides	*A. baumannii, E. coli, and* MRSA	Membrane damage	Bunders et al. 2011

1.8.7. Nanoscale Materials as Antibiofilm Agents

Nanomaterials are increasingly coming to the forefront as antibiofilm agents. The desirable attributes of nanomaterials such as high surface area to volume ratio, facile surface functionalization and possibility of generating nanocomposites with known antibiofilm agents are likely to facilitate biofilm eradication. Nanoscale materials that exhibit bactericidal activity are considered to be efficient in combating the menace of antibiotic-resistance and mitigating the toxicity commonly associated with therapeutic antibiotics (Huh and Kwon 2011). Further, literature reports seem to suggest that nanomaterials are tailored to achieve superior delivery of antibacterial agents and render a number of beneficial attributes such as improved solubility, high half-life of payload drug, sustained and stimuli-responsive drug release, targeted delivery of therapeutic agent and delivery of

multiple drugs in combination for attaining synergistic activity (Moghimi et al. 2005, Pinto-Alphandary et al. 2000, Risbud et al. 2000, Zhang et al. 2010). **S**uper paramagnetic iron oxide nanoparticles (SPIONs) in combination with a metabolic stimuli (fructose) has been shown to demonstrate high antibiofilm activity against MRSA and Gram-negative *E.coli* and *Pseudomonas* (Durmus et al. 2013). In another study, the potential of gold nanoparticle-polythiophene composite as an antibiofilm agent was demonstrated (Adhikari et al. 2013). The use of nitric oxide releasing polymer-bearing nanocomposites that are effective in dispersion of biofilm matrix has been reported (Duong et al. 2014, Slomberg et al. 2013). Representative example of nanomaterials as antibiofilm agents are illustrated in Table 1.4.

Table 1.4. Examples of Nanomaterials as Antibiofilm Agents.

Sl. No.	Nanomaterials	Target Organism	Mode of Action	References
1.	Super-paramagnetic Iron oxide nanoparticle in presence of fructose	*S. aureus* *E. coli*	Oxidative stress leads to DNA damage and cell death	Durmus et al. 2013
2.	Nitric oxide releasing silica nanoparticle	*MRSA* *P. aeruginosa*	Disruption of membrane due to nitrosative or oxidative stress	Slomberg et al. 2013
3.	Amphiphile- loaded BSA nanoparticle	*S. aureus*	Membrane-acting	Uday et al. 2014
4.	(Gold nanoparticle)-polythiophene composite	*P. aeruginosa*	Membrane-acting	Adhikari et al. 2013
5.	Graphene oxide-poly N-vinyl carbazole (GO-PVK) nanocomposite	*E. coli* *B. subtilis*	Perturbation of cell membrane leads to leakage of electrolytes	Mejias Carpio et al. 2012
6.	Silver nanoparticle	*E. coli* *B. subtilis*	Inhibit respiratory chain and damage membrane protein	Taglietti et al. 2014
7.	ZnO-PVC nanocomposite	*P. aeruginosa*	Reactive species generation	Geilich and Webster 2013
8.	Antibiotic encapsulated in gamma aminobutyric acid-silica nanaoparticle	*S. aureus*	Inhibition of protein synthesis and cell wall synthesis	Grumezescu et al. 2014
9.	Nitric oxide-releasing porous silicon nanoparticles	*S. epidermidis*	Membrane destruction via lipid peroxidation	Kafshgari et al. 2014

MOTIVATION AND OBJECTIVES OF THE PRESENT INVESTIGATION

TH-1410_10610607

TH-1410_10610607

MOTIVATION AND OBJECTIVES OF THE PRESENT INVESTIGATION

Bacterial pathogens have evolved mechanisms to elude the action of most clinically relevant antibiotics. To address this crisis, there is an urgent need to develop novel and potent antibacterial agents that can act on compelling targets and display a mode of action, which is different from conventional antibiotics. It is envisaged that antibacterial agents that exhibit a membrane-targeting activity hold considerable therapeutic implications as the probability of developing resistance against such molecules would necessitate large scale renovation of the membrane components, which is considered to be a physiologically daunting task for the bacterium. Antimicrobial peptides (AMPs) have long been recognized as potent membrane-acting antibacterial agents. Despite their potency, the high manufacturing cost, challenges in formulation, inferior pharmacokinetic traits and susceptibility to proteolytic inactivation are some of the major hindrances limiting their therapeutic promise. In this backdrop, there is an enormous scope to synthesize novel and structurally diverse cationic amphiphiles, which mimic the bactericidal activity of AMPs. In an age of unbridled antibiotic-resistance fraught with a dwindling drug armory to combat several life-threatening infections caused by antibiotic-resistant bacteria, studies on synthetic amphiphiles as antibacterials and elucidation of their therapeutic potential would auger well in the context of a contemporary global healthcare problem. The present study is essentially based on this premise and the salient motivating factors for undertaking the study can be stated as follows:

1. Synthetic amphiphiles are conceivably attractive as antibacterial agents against antibiotic-resistant pathogens owing to their facile synthesis, structural tunability, propensity to disrupt bacterial membranes and their resistance to proteolysis.

2. Although literature reports have described several classes of synthetic cationic peptide- and polymer-based amphiphiles as potent antimicrobial agents, it is imperative to critically ascertain the therapeutic potential of synthetic amphiphiles based on structure-guided bactericidal activity and a nuanced evaluation of their cytotoxic potential. In order to render beneficial therapeutic attributes such as

higher solubility in biological fluids, efficient passage through membranes and superior tissue distribution, the choice of low molecular weight and biocompatible functional groups as building blocks for synthetic amphiphiles is critical.

3. Based on the potent membrane-directed activity of synthetic amphiphiles, it would be worthwhile to explore the use of membrane-acting amphiphiles as adjuvants in combination with conventional therapeutic antibiotics. Deployment of such a combination therapy regime could perhaps breach the membrane barrier of pathogenic bacteria and thereby enhance the antibiotic uptake and subsequent killing of target bacteria.

4. The high prevalence of life-threatening bacterial biofilm-associated infections is a contemporary healthcare concern, which is assuming alarming proportions. It is conceived that synthetic amphiphiles are likely to pervade through the biofilm matrix, access the encased cells and render membrane disruption. Hence, it would be interesting to investigate whether membrane-acting synthetic amphiphiles could be employed either alone, or as adjuvant in combination with antibiotics for eradication of bacterial biofilm.

5. In order to harness the therapeutic prospect of synthetic amphiphile as an antibiofilm agent, it would be pertinent to develop a biocompatible non-toxic nanocarrier that renders sustained release of the bactericidal payload and retains the antibiofilm activity of the amphiphile in the complex niche of the biofilm matrix.

6. The knowledge generated from previous research investigations point out that cationic charge, functional groups that impart cationic charge, charge density, hydrophobicity and conformational flexibility have a paramount effect on the bactericidal activity and therapeutic index of synthetic amphiphiles. Hence, in the endeavor of developing new bactericidal amphiphiles, there is considerable scope to adopt a prudent approach and tweak the structure of the amphiphiles rationally so as to maximize bactericidal activity without a concomitant risk of host cell toxicity. Given the prevalence of metal reactive groups (MRGs) in bacterial cell

envelope, deployment of a biocompatible and physiologically relevant metal ion to impart charge and hydrophilicity to an amphiphile may be an interesting approach in this direction. It is conceived that synthetic amphiphiles based on such design principles may leverage interactions with metal-reactive groups in bacterial cell surface envelope and emerge as potent therapeutic antibacterials.

A schematic representation of the aforementioned features, which essentially constitute the rational of the present investigation, is depicted in Scheme 1.

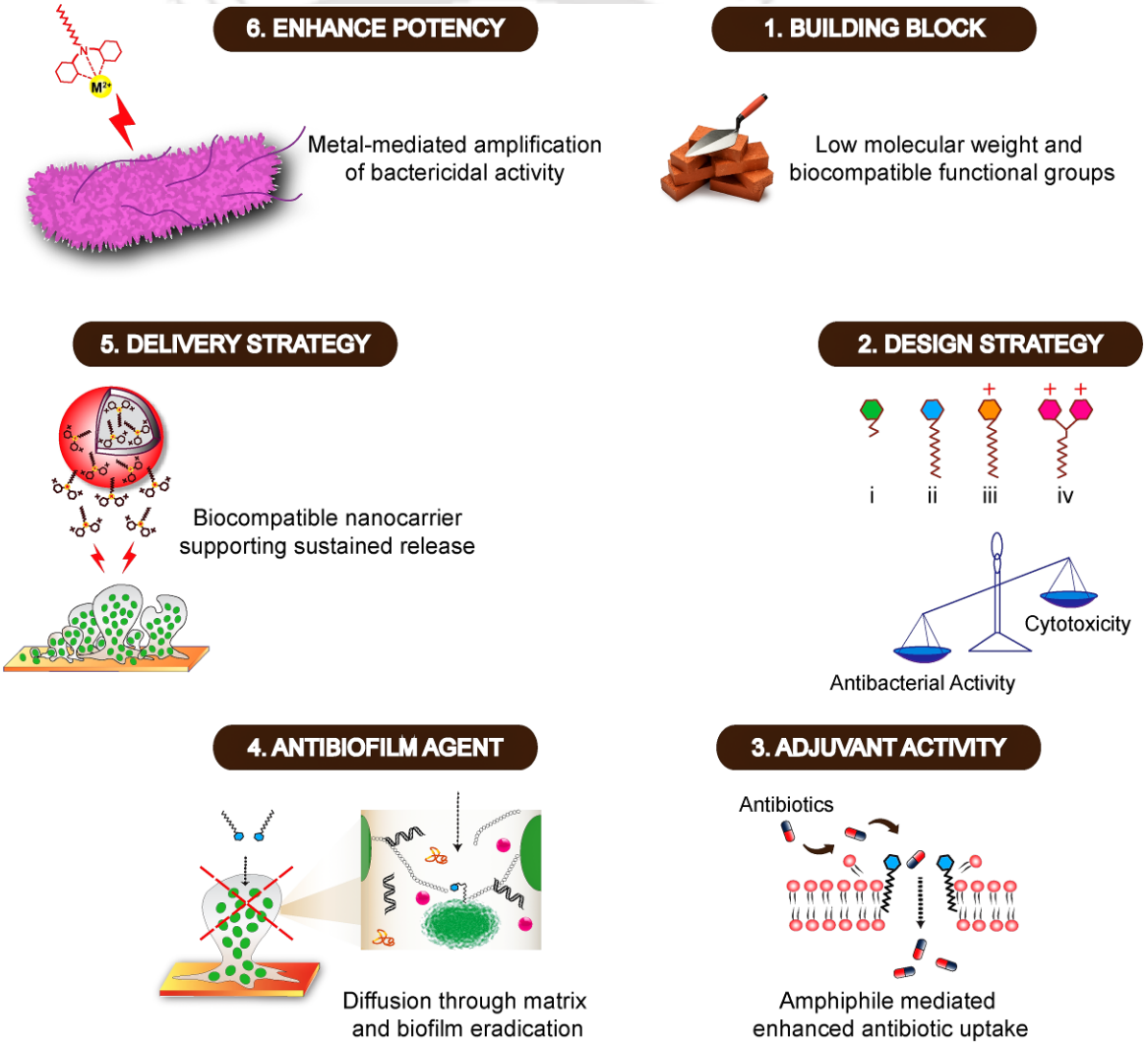

Scheme 1. Schematic representation of the rational of the present investigation.

In the backdrop of the enormous scope for developing synthetic amphiphiles as potent antibacterial agents, the essential objectives of the investigation encompassed the following:

1. Determination of the bactericidal activity and *in vitro* cytotoxic effect of structurally diverse pyridine-based synthetic amphiphiles (**compound 1-6**).

2. Prospect of the synthetic amphiphile - N,N-bis((methylpyridinium-2-yl)methyl) dodecan-1-amine (**Compound 6**) as an adjuvant to potentiate the bactericidal activity of model therapeutic antibiotics in combination.

3. Evaluation of the antibiofilm activity of **Compound 6** against *S. aureus* and *P. aeruginosa* biofilm.

4. Generation of **Compound 6**-loaded biocompatible human serum albumin (HSA)-based nanocarrier system for eradication of biofilm.

5. Generation of a zinc complex of the synthetic amphiphile - N,N-bis((methylpyridin-2-yl)methyl) dodecan-1-amine (**compound 5**) with enhanced bactericidal activity and therapeutic index.

Chapter 2

Structure-Guided Bactericidal Activity and Mode of Action of Pyridine-based Synthetic Amphiphiles

This chapter reports the structure-function studies with pyridine-based synthetic amphiphiles. A nuanced discussion on the hierarchical antibacterial activity and cytotoxic effect of the amphiphiles is presented.

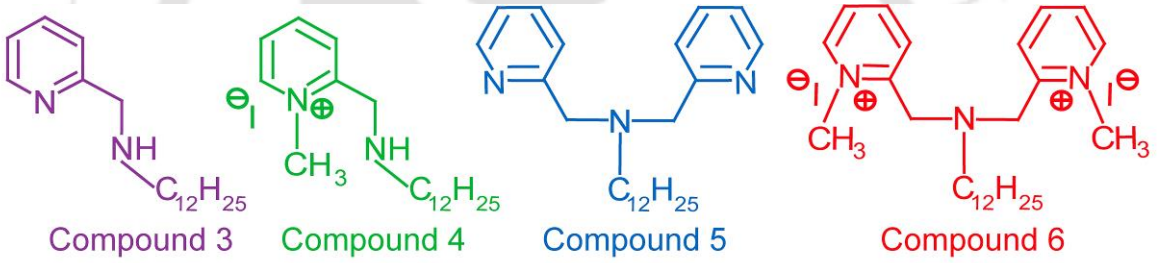

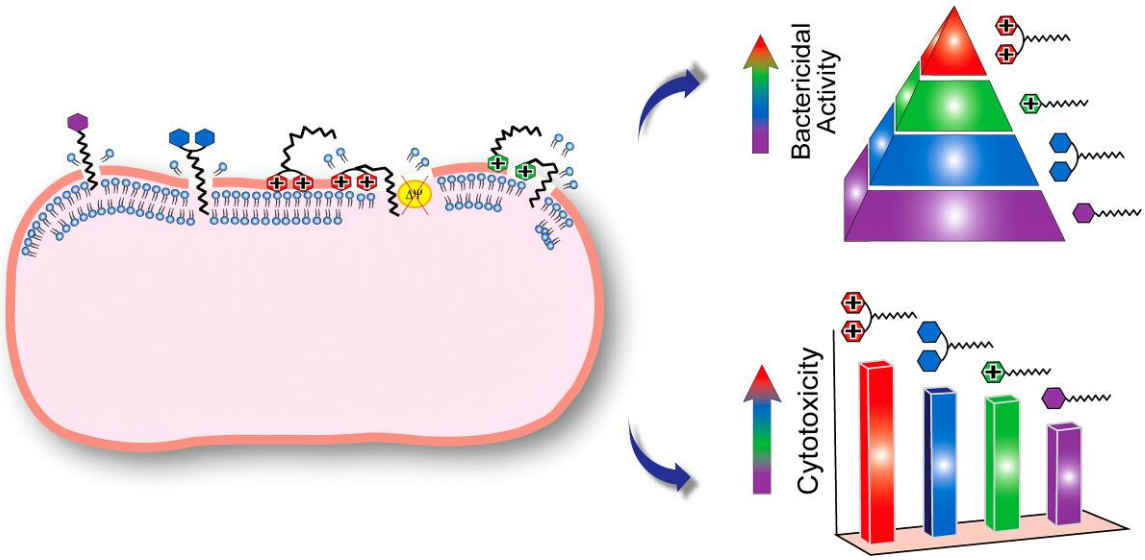

TH-1410_10610607

ABSTRACT

The investigation outlined in this chapter describes the structure-guided bactericidal activity of low molecular weight pyridine-based synthetic amphiphiles and presents a critical assessment of their cytotoxic potential. The synthetic amphiphiles selected for the present study (**compound 1**- **Compound 6**) displayed varying charge densities and differed in their alkyl chain length. Fluorescence-based structure-function studies revealed that the amphiphiles were membrane-acting and exhibited a hierarchical pattern of bactericidal activity, which could be correlated to their charge density and hydrophobicity. The membrane-directed activity of the most potent cationic amphiphile (**Compound 6**) was substantiated through fluorescence-based assays, flow cytometric analysis, time-kill curve, scanning electron microscope (SEM) analysis and fluorescence microscopic analysis. At concentrations equivalent to the minimum inhibitory concentration (MIC) against the Gram-positive target bacteria *Staphylococcus aureus* MTCC 96, none of the amphiphiles rendered any cytotoxic effect on model human cell lines (HeLa, MCF-7 and HT-29). However, at higher concentrations, a distinct gradation in the cytotoxic effect was manifested, which is perhaps accounted by charge density and conformational flexibility of the amphiphiles.

2.1. Introduction

The emergence of antibiotic-resistant pathogenic bacteria coupled with a critical dearth of new therapeutic agents to counter their challenge is a contemporary healthcare problem of great concern (Fischbach and Walsh 2009, Nikaido 2009, Gootz 2010, Gwynn et al. 2010, Bush et al. 2011). Conventional therapeutic antibiotics are mostly known to act on definite physiological targets in pathogenic bacteria However, antibiotic-resistant bacteria are armed with a plethora of highly evolved molecular mechanisms, which include enzyme-catalyzed target modification, drug inactivation, presence of an impermeability barrier for drugs and presence of efflux pumps, which enable them to thwart the action of clinically relevant antibiotics (Yeaman and Yount 2003, Morar and Wright 2010, Wright 2011). This therapeutic crisis has fuelled a perpetual need for developing potent antibacterial agents that can act on compelling cellular targets and counter development of resistance in target bacteria. In this regard, membrane-targeting bactericidal agents hold special significance, since the probability of developing resistance against them demands extensive reconstruction of membrane components, which is a physiologically challenging task for the target bacteria (Van Bambeke et al. 2008, Hurdle et al. 2011).

Amongst the known membrane-acting antibacterial agents, cationic antimicrobial peptides (AMPs) have been extensively studied. Structure-activity studies have revealed that the positive charge of AMPs is key to initiating electrostatic interactions with the negatively charged bacterial cell surface, while the hydrophobic domain promotes insertion into the target membrane, which results in large scale membrane disruption and cell death (Zasloff 2002, Brogden 2005, Mangoni et al. 2003, Hancock and Chapple 1999). However, the therapeutic application of AMPs is hindered owing to a prohibitive production cost, poor pharmacokinetics and susceptibility to proteolytic degradation (Marr et al. 2006, Yeaman and Yount 2003). To circumvent this bottleneck, the current thrust is in the discovery and characterization of novel and structurally diverse AMP-mimetic synthetic amphiphiles as bactericidal agents (Tang et al. 2006, Tew et al. 2002, Patch and Barron 2003, Mowery et al. 2007) Synthetic amphiphiles are conceivably attractive as bactericidal agents because of their facile synthesis, possibility of generating a library of bactericidal scaffolds through judicious choice of functional descriptors, resistance to proteolytic cleavage and their ability to disrupt bacterial cell membrane. Several research investigations report the

synthesis and bactericidal activity of structurally diverse AMP-mimicking polymeric amphiphiles (Rawlinson et al. 2010, Paslay et al. 2012, Oda et al. 2011, Kuroda and DeGrado 2005). Previous studies have also demonstrated that synthetic cationic amphiphiles provide a repertoire of bactericidal scaffolds, which hold considerable therapeutic promise against pathogenic bacteria (Findlay, Zhanel, and Schweizer 2010, Gokel and Negin 2012, LaDow et al. 2011, Vudumula et al. 2012).

Structure-function studies have indicated that determinants of polymeric and low molecular weight synthetic amphiphiles that constitute the cornerstone of their bactericidal activity are cationic charge (Paslay et al. 2012, Vudumula et al. 2012), functional groups that impart cationic charge (Paslay et al. 2012, Palermo and Kuroda 2009), charge density (Haldar et al. 2005, LaDow et al. 2011) and hydrophobicity (Kuroda and DeGrado 2005, Palermo et al. 2009) Recent investigations have clearly demonstrated the membrane-targeting activity of bactericidal amphiphilic polymers (Rawlinson et al. 2010, Song et al. 2011), facially amphiphilic oligomers (Tang et al. 2006) and cationic quinoline-based amphiphiles (Vudumula et al. 2012). With regard to membrane-targeting activity of synthetic amphiphiles, it has also been shown that a cationic amphiphile can displace the metal ion from the outer membrane of Gram-negative pathogenic bacteria, and the subsequent insertion of the amphiphile into the hydrophobic core of the membrane leads to loss of membrane integrity (Miller et al. 2005).

In order to comprehend the true therapeutic potential of bactericidal amphiphiles, it is paramount to critically assess their biocompatibility and potential cytotoxic effect on human cells. The overall number of cationic charges and the degree of hydrophobicity has an overwhelming influence on the cytotoxic effect and antibacterial selectivity of synthetic amphiphiles. Hence, in the endeavor of developing new bactericidal amphiphiles, it is important to adopt a rational approach and tweak the structure of the amphiphiles so as to maximize bactericidal activity without a concomitant risk of unwarranted cytotoxicity. In case of amphiphilic molecules it has been shown that a balance between cationic charge, spacing of cationic charge and hydrophobicity is critical to ensure high bactericidal activity and minimize cytotoxicity (Song et al. 2011, Brahmachari et al. 2010). Additional studies have revealed that the high cationic charge density and conformational flexibility of amphiphilic polymers are likely to result in cytotoxic effects on human

cells (Palermo et al2009, Fischer et al. 2003). It has been shown that the target cell selectivity of amphiphilic polymers can be enhanced by moderating the hydrophobicity and chemical nature of the cationic group (Palermo and Kuroda 2009) and also by designing amphiphilic block copolymers in lieu of random copolymers (Oda et al. 2011).

The knowledge generated from previous research investigations provide a broad structural guideline that render high bactericidal activity and selectivity to synthetic amphiphiles. However, a nuanced understanding of how a new amphiphilic bactericidal agent makes a distinction between target pathogen and human cells is imperative in order to foster the development of potent antibacterials with therapeutic utility. Further, in order to afford beneficial therapeutic attributes such as higher solubility in biological fluids, efficient transit through membranes and superior tissue distribution, the choice of low molecular weight and biocompatible functional groups as building blocks for synthetic amphiphiles is also critical. The aforementioned tenet formed the rationale of the investigation in this chapter, wherein the bactericidal activity and cytotoxic effect of pyridine-based low molecular weight synthetic amphiphiles of varying charge and alkyl chain length (**compound 1**- **Compound 6**) were critically analyzed. Structure-function studies and mode of action of the amphiphiles on target bacteria were pursued through fluorescence-based assays, which provided a comparative assessment of the membrane-directed activity of the amphiphiles. Based on the cytotoxic effect exerted by the amphiphiles on model human cell lines (HeLa, MCF-7, HT-29 cells), a critical appraisal of the therapeutic potential of the bactericidal amphiphiles is reported in the present study.

2.2. Materials and Methods

2.2.1. Growth Media and Chemicals

Nutrient Broth (NB) and Brain-Heart Infusion (BHI) broth were procured from HiMedia, Mumbai, India. Dimethyl sulfoxide (DMSO) and glutaraldehyde were obtained from Merck, India. N-2-Hydroxyethyl piperazine-N-2-ethane sulphonic acid (HEPES buffer) was procured from Sisco Research Laboratories SRL, Mumbai, India. 5 (and 6)-carboxyfluorescein diacetate succinimidyl ester (cFDA-SE), propidium iodide (PI), carbonylcyanide m-chlorophenyl hydrazone (CCCP), 1-N-phenyl-naphthylamine (NPN), valinomycin, polymyxin B, Dulbecco's Modified Eagle Medium (DMEM), trypsin–EDTA and 3-(4,5-dimethyl-2-thiazolyl)-2,5- diphenyl-2H-tetrazolium bromide (MTT) were procured from Sigma-Aldrich (USA). Fetal bovine serum (FBS) was procured from PAA Laboratories, USA.

2.2.2. Synthetic Amphiphiles

The general structure of the synthetic amphiphiles **(compounds 1-6)** used in the present study is shown in Figure. 2.1. In the present investigation, **compounds 1-6** are referred to as **C1-C6**. Representative steps involved in the synthesis of these amphiphiles are illustrated in Figure. 2.2. Detailed information regarding synthesis and characterization of the amphiphiles is indicated in the Appendix of Chapter 2. Stock solutions of the amphiphiles were prepared in DMSO and stored at room temperature in dark condition.

2.2.3. Bacterial Strains and Growth Conditions

The bacterial strains used in the present investigation consisted of Gram-positive strains of *Staphylococcus aureus* MTCC 96 (*S. aureus*), *Listeria monocytogenes* Scott A (*L. monocytogenes*), *Bacillus subtilis* MTCC 441 (*B. subtilis*) and *Enterococcus faecalis* MTCC 439 (*E. faecalis*). Gram-negative bacterial strains used in the present investigation included *Escherichia coli* MTCC 433 (*E. coli*), *Enterobacter aerogenes* MTCC 2822 (*E. aerogenes*), *Pseudomonas aeruginosa* MTCC 2488 (*P. aeruginosa*) and. *Yersinia enterocolitica* MTCC 859 (*Y. enterocolitica*). *B. subtilis*, *E. coli* MTCC 433, *P. aeruginosa* and *E. aerogenes* were grown in NB medium at 37^{o}C and 180 rpm for 12 h whereas

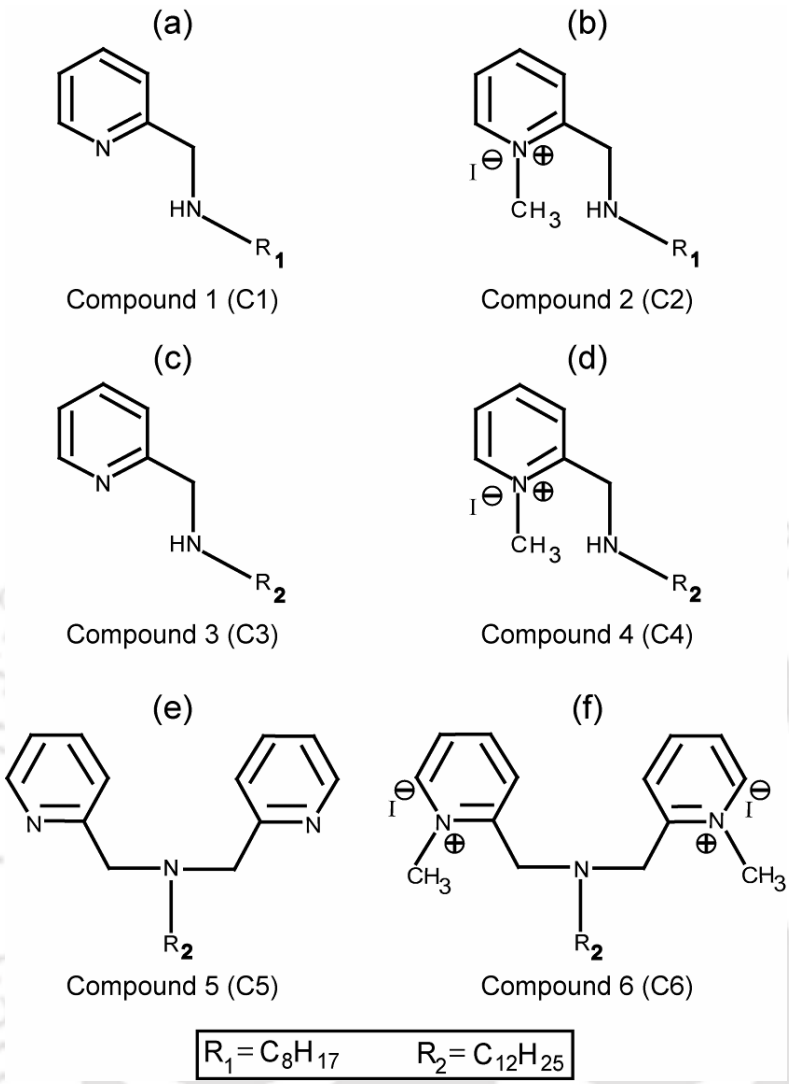

Figure 2.1. General structure of pyridine-based synthetic amphiphiles used in the present investigation.

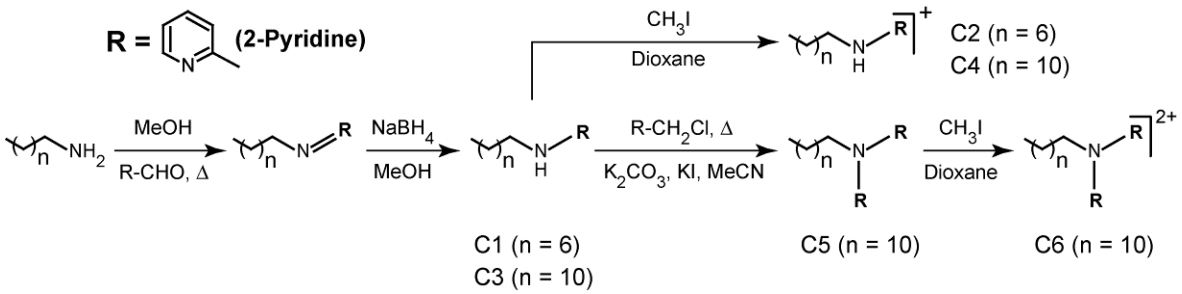

Figure 2.2. Schematic representation of general steps involved in the synthesis of the synthetic amphiphiles.

S. aureus, *L. monocytogenes* Scott A, *E. faecalis* and *Y. enterocolitica* were propagated in BHI broth at 37°C and 180 rpm for 12 h.

2.2.4. Antibacterial Activity of Synthetic Amphiphiles

Stock solutions of the synthetic amphiphiles were prepared in DMSO and stored at -20°C. Prior to experiments, amphiphile solutions were freshly reconstituted to achieve the desirable concentrations for the specific experiments. The bactericidal activity of the amphiphiles (**C1-C6**) was determined against a group of Gram-positive and Gram-negative bacteria. Target bacterial strains were grown in requisite growth medium in the presence of varying concentrations of the amphiphile (50 µg/mL and 100 µg/mL) for 24 h. The growth of amphiphile-treated bacterial cells was recorded periodically by measuring absorbance at 600 nm from replica samples in a spectrophotometer (Beckman Coulter DU 800 HP, USA) and was expressed as percentage growth compared to the control (untreated cells).

2.2.5. Minimum Inhibitory Concentration (MIC) and Minimum Killing Concentration (MKC) of Amphiphiles

The minimum inhibitory concentration (MIC) and minimum killing concentration (MKC) of the synthetic amphiphiles **(C3**, **C4**, **C5** and **C6)** were determined against *S. aureus* MTCC 96, *L. monocytogenes* Scott A, *E. coli* MTCC 433 and *E. aerogenes* MTCC 2822 by using a microtiter broth dilution method (Vudumula et al., 2012). Target bacterial cultures were inoculated at 1% level in microtitre wells (approximately 5×10^5 CFU/well) having 100 µL of the requisite growth medium and propagated overnight at 37°C and 180 rpm in presence of varying concentrations of the amphiphiles. The growth of the bacterial strains was verified by measuring absorbance at 600 nm in a microtitre plate reader (Infinite M200, TECAN, Switzerland). UV-visible absorbance (A_{600}) for negative growth control was also measured and the value was subsequently subtracted from the absorbance readings of the test samples. MIC of the amphiphile was defined as the minimum concentration that resulted in growth inhibition of the target bacteria (A_{600}<0.1). An aliquot (1% v/v) from all the wells that indicated a lack of cell growth (A_{600}<0.1) was re-inoculated into separate microtitre wells with fresh growth medium in the absence of amphiphile and incubated overnight at 37°C and 180 rpm. MKC of the amphiphile was

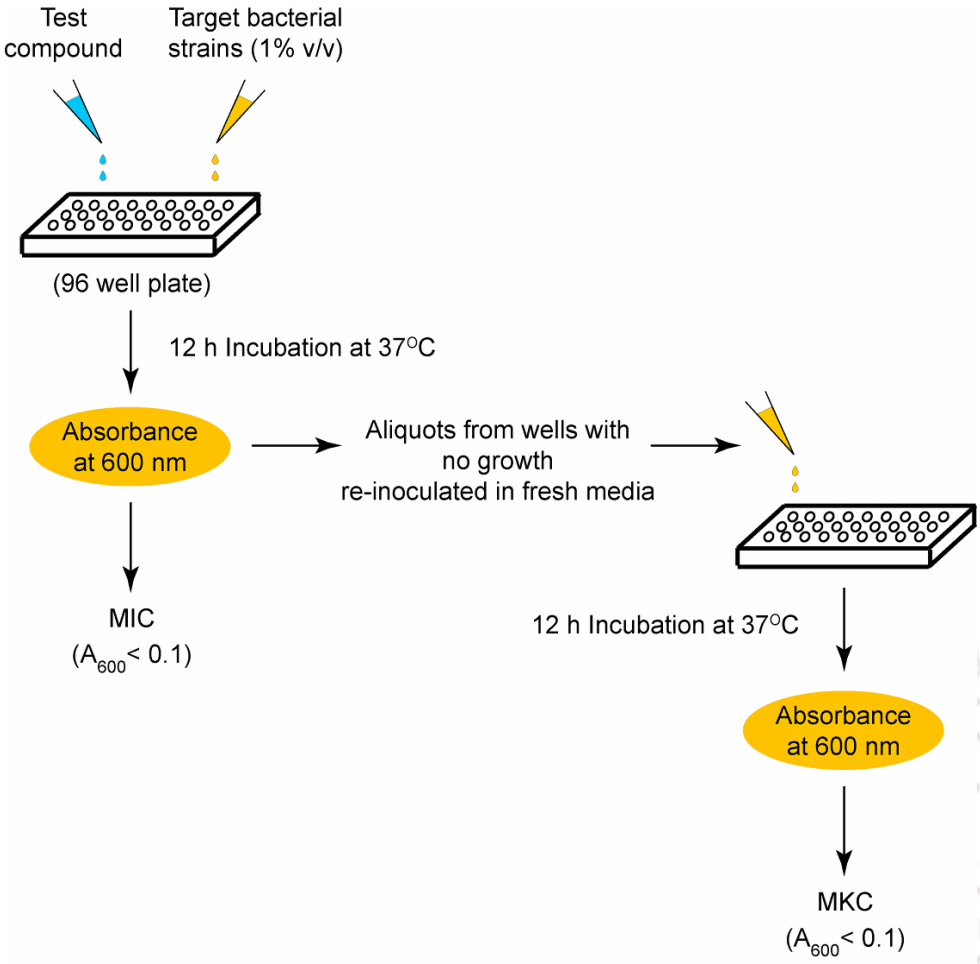

Figure 2.3. Schematic representation of the experimental protocol for determining MIC and MKC of amphiphiles.

defined as the lowest concentration that inhibited the growth of the target bacterial cells following re-inoculation (A_{600}<0.1). MIC and MKC values were expressed as average values of six independent experiments. A schematic of the protocol used to determine MIC and MKC of the amphiphiles is indicated in Figure 2.3.

2.2.6. Structure-Function Studies

A comparative structure-function study was conducted with equimolar concentration of the amphiphiles (**C3-C6**). The experimental details are described in the following section.

2.2.6.1. cFDA-SE Leakage Assay

A stock solution of cFDA-SE (500 μM) was prepared in ethanol and stored at -20°C.

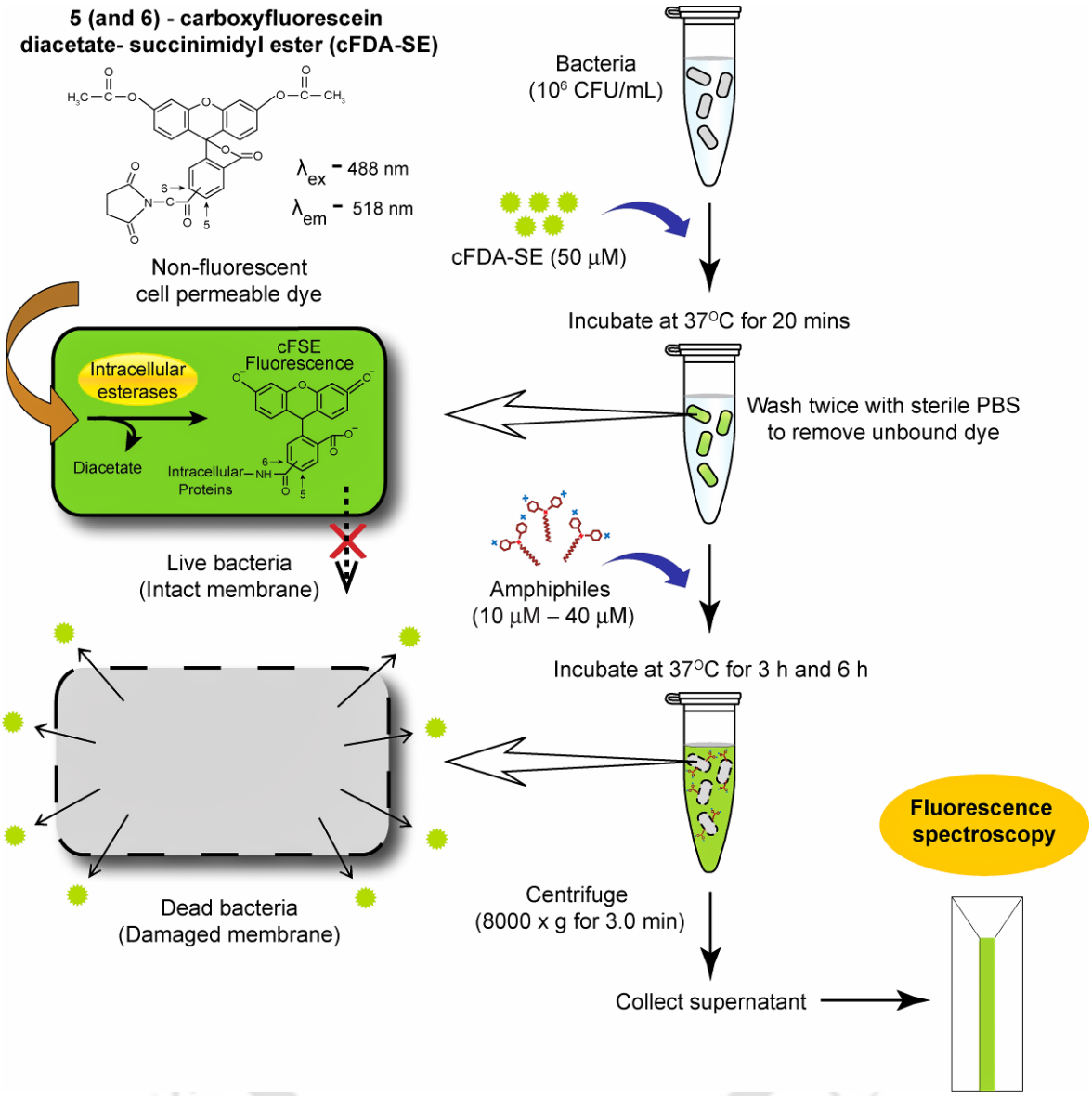

Figure 2.4. Schematic representation of experimental protocol for cFDA-SE leakage assay.

Overnight grown cells of *S. aureus* MTCC 96 and *E. coli* MTCC 433 were harvested by centrifugation at 3,000 x g for 10 min. The cell pellet was washed twice with sterile phosphate buffer, resuspended in the same and labelled with cFDA-SE (final concentration of 50 µM) at 37°C for 20 min. The labelling reaction was terminated by pelleting the cells followed by washing twice with sterile phosphate buffer to remove excess dye molecules. Equimolar concentration of **C3**, **C4**, **C5** and **C6** (10 µM, 20 µM and 40 µM) were added to 10^6 CFU/mL cFDA-SE labelled target bacteria and incubated at 37°C and 180 rpm for 3 h. In case of control experiments, only DMSO solution devoid of amphiphile was added to

labelled cells and incubated under the same conditions. Following incubation, cells were pelleted by centrifugation and leakage of carboxyfluorescein from amphiphile-treated cells was determined by measuring fluorescence of the cell free supernatant at an excitation wavelength of 488 nm and emission wavelength of 518 nm in a spectrofluorimeter (FluoroMax-3, HORIBA). The fluorescence measurements were recorded after subtracting the fluorescence of effluxed dye from control samples. For every amphiphile concentration and control sample, fluorescence measurements were acquired from three independent experimental samples. A schematic illustrating the basic steps of the cfDA-SE leakage assay is represented in Figure 2.4.

2.2.6.2. PI Uptake Assay

A stock solution of PI (1.5 mM) was prepared in sterile MilliQ water and stored at 4ºC. Target bacterial cultures of *S. aureus* MTCC 96 and *E. coli* MTCC 433 (10^6 CFU/mL) were treated with equimolar concentration of **C3**, **C4**, **C5** and **C6** (10 μM, 20 μM and 40 μM) at 37ºC and 180 rpm for 3 h. In case of control sample, only DMSO was added to cells and incubated under the same conditions. Following incubation, cells were washed with sterile phosphate buffered saline (PBS), resuspended in the same and incubated with PI (final concentration of 30 μM) for 30 min at 37°C in a circulating water bath incubator (Amersham, USA). Subsequently, the cells were centrifuged and washed in distilled water to remove excess dye, resuspended in sterile PBS and fluorescence was measured in a spectrofluorimeter (FluoroMax-3, HORIBA) at an excitation wavelength of 535 nm and emission wavelength of 617 nm. The values obtained for untreated cells were subtracted from all experimental values. For every amphiphile concentration and control sample, fluorescence measurements were acquired from three in independent experimental samples. A schematic representation of PI uptake assay is shown in Figure 2.5.

2.2.6.3. Fluorescence Microscope Analysis

Cell suspensions of *S. aureus* MTCC 96 and *E. coli* MTCC 433 in sterile PBS (10^6 CFU/mL) were treated with 40 μM of amphiphile (**C3**, **C4**, **C5** and **C6**) at 37ºC and 180 rpm for 3 h. Control sample consisted of DMSO treated cells incubated under the same conditions. Following incubation, both the treated and control cells were washed

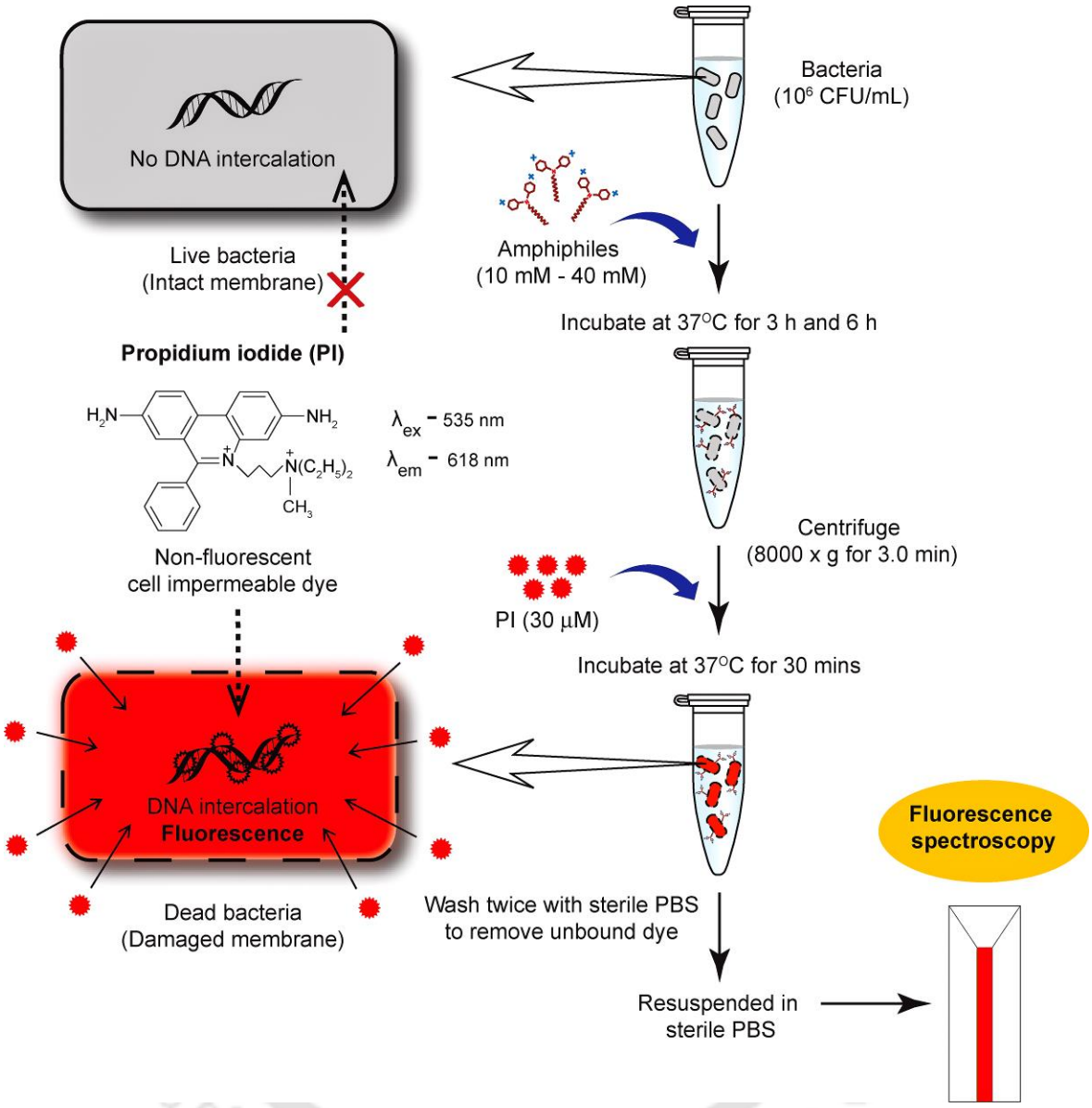

Figure 2.5. Schematic representation of experimental protocol for PI uptake assay.

twice with sterile PBS, resuspended in the same and labelled with cFDA-SE and PI as mentioned before in section 2.2.6.1. and 2.2.6.2., respectively. The stained samples were fixed in 2.5% glutaraldehyde and subsequently washed twice with sterile PBS. A 10 µl aliquot of the stained sample was gently spotted on a clean glass slide, air dried and observed under a fluorescence microscope (Eclipse Ti-U, Nikon, USA) with a filter that allowed blue light excitation for cFDA-SE and green light excitation in case of PI stained cells. Images of the control and treated cell were recorded.

2.2.7. Bactericidal Potency and Membrane-directed Activity of ***Compound 6***

The following experiments were performed to ascertain the antibacterial activity and membrane-targeting activity of **C6**:

2.2.7.1. Time- kill Curve

Target cells of Gram-positive *S. aureus* MTCC 96 and Gram-negative *E. coli* MTCC 433 (approximately 10^6 CFU/mL each suspended in sterile PBS) were treated with varying concentration (3.0 μM - 15 μM) of **C6** at 37ºC and 180 rpm. Samples were withdrawn at regular intervals of 3 h, 6 h, 12 h and 24 h and subjected to serial dilution and plating to the ascertain the viable cell number (Log_{10} CFU/mL). The viability of cells suspended in sterile PBS as well as cells treated with DMSO alone was also determined.

2.2.7.2. Scanning Electron Microscope (SEM) Analysis

Overnight grown cells of *S. aureus* MTCC 96 and *E. coli* MTCC 433 were washed twice in sterile PBS and resuspended in the same buffer. Approximately 10^6 CFU/mL cells were treated with 50 μM of **C6** for 6 h at 37ºC. Control samples consisted of untreated cells incubated in sterile PBS under the same conditions. Treated as well as untreated cells were washed twice with sterile PBS and fixed in 2.5% glutaraldehyde for 90 mins at 4ºC. Following fixation, cells were washed and resuspended in sterile MilliQ water. A 2.0 μl aliquot of each sample was spotted on SEM stubs and air dried in a laminar hood. Subsequently, the cells were coated with gold plasmon and observed under scanning electron microscope (Leo, 1430 vp) at 15 kV and the images were recorded.

2.2.7.3. Flow Cytometry Analysis

The effect of **C6** on the viability of *S. aureus* MTCC 96 and *E. coli* MTCC 433 was studied by flow cytometry (FCM), which was performed on a FACS Calibur flow cytometer (Becton-Dickinson Immunocytometry Systems, San Jose, CA, USA). Target bacterial cells were pre-labelled with cFDA-SE following the protocol as mentioned earlier. Labelled bacterial cells were treated with 50 μM of **C6** for 6 h at 37°C in a circulating water bath incubator (Amersham, USA). Following treatment, cells were analyzed along with unlabelled-untreated cells as well as labelled-untreated cells (control).

For FCM analysis, approximately 10^8 cells per ml were analyzed at a low flow rate setting and the FACS instrument was adjusted to acquire 20,000 events. Before analysis of amphiphile-treated samples, appropriate voltage and threshold parameter was adjusted for unlabeled-untreated cells. The corresponding signal of unlabeled-untreated cells was set in the lower left quadrant in order to compensate for cellular autofluorescence. Green fluorescence of cFDA-SE stained cells was detected in the FL-1 channel (band pass filter of 530 nm). Acquisition of fluorescence data was accomplished by setting a gate in the forward-angle light scatter (FSC) vs. sideward scatter (SSC) plot, which facilitated discrimination of bacterial cells from other artefacts. Data were acquired and analyzed with the CellQuest Pro software (BD CellQuest™ Pro Version 6.0, Becton-Dickinson, USA) and the WinMDI software program version 2.9 (http://en.bio-soft.net/other/WinMDI).

2.2.7.4. Fluorescence Microscope Analysis

Approximately 10^6 CFU/mL cells of *S. aureus* MTCC 96 and *E. coli* MTCC 433 were treated with varying concentrations (6.0 μM -15 μM) of **C6** and incubated at 37°C and 180 rpm for 3 h. DMSO treated cells incubated under the same conditions were considered as control sample. Following treatment with **C6**, cells were washed and labelled with cFDA-SE and PI as mentioned before, fixed in 2.5% glutaraldehyde and washed twice with sterile PBS. A 10 μl aliquot of the stained sample was spotted on a clean glass slide, air dried and observed under a fluorescence microscope (Eclipse Ti-U, Nikon, USA) with a filter that allowed blue light excitation for cFDA-SE and green light excitation in case of PI stained cells. Images of the control and treated cell were acquired.

2.2.7.5. Effect of Membrane Potential on the Antibacterial Activity of ***Compound 6***

Cells of *S. aureus* MTCC 96 and *E. coli* MTCC 433 were grown overnight in nutrient broth with 0.5% glucose and 20 μM CCCP as described in a previous report (Mangoni et al. 2003). CCCP treated and untreated cells (control) were suspended in sterile PBS (approximately 10^6 CFU/mL each) and incubated with varying concentration of **C6** (9.0 μM and 15 μM) for 6 h at 37°C. At regular time intervals the bactericidal activity of the amphiphile on CCCP-treated and untreated cells was compared by determining the

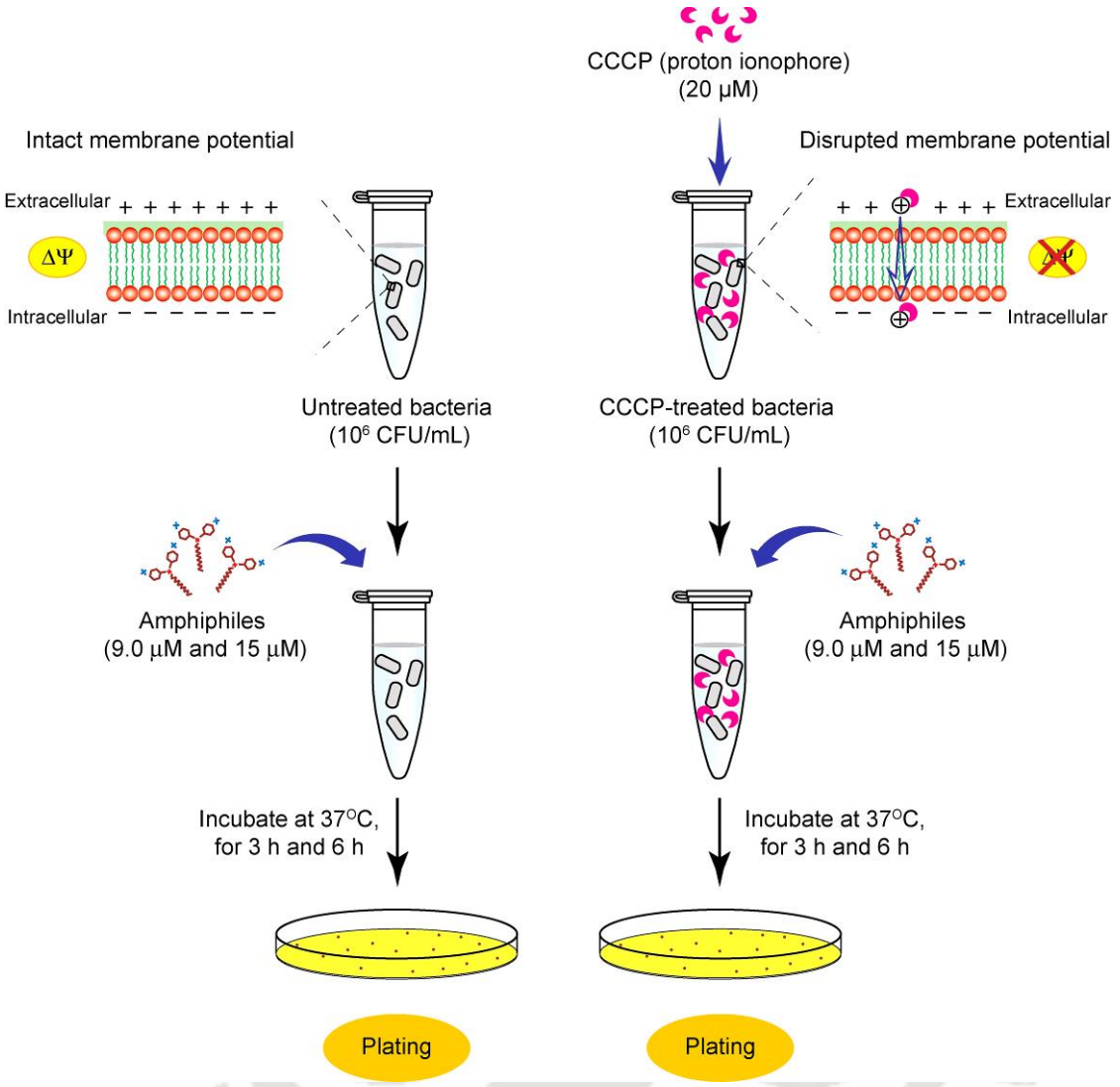

Figure 2.6. Schematic representation of the experimental protocol for CCCP assay.

viable cell count through conventional serial dilution and plating. The scheme of the CCCP assay is illustrated in Figure 2.6.

2.2.7.6. Membrane Depolarization Assay

The ability of **C6** to depolarize the transmembrane potential in target bacteria was determined by a fluorescence-based assay using $DiSC_35$, which is a membrane potential sensitive dye. Cells of *S. aureus* MTCC 96 and *E. coli* MTCC 433 were grown till mid-logarithmic phase (A_{600} = 0.4-0.5). The cells were harvested by centrifugation, washed and resuspended in HEPES buffer (5.0 mM HEPES, 20 mM glucose, pH 7.2) to achieve

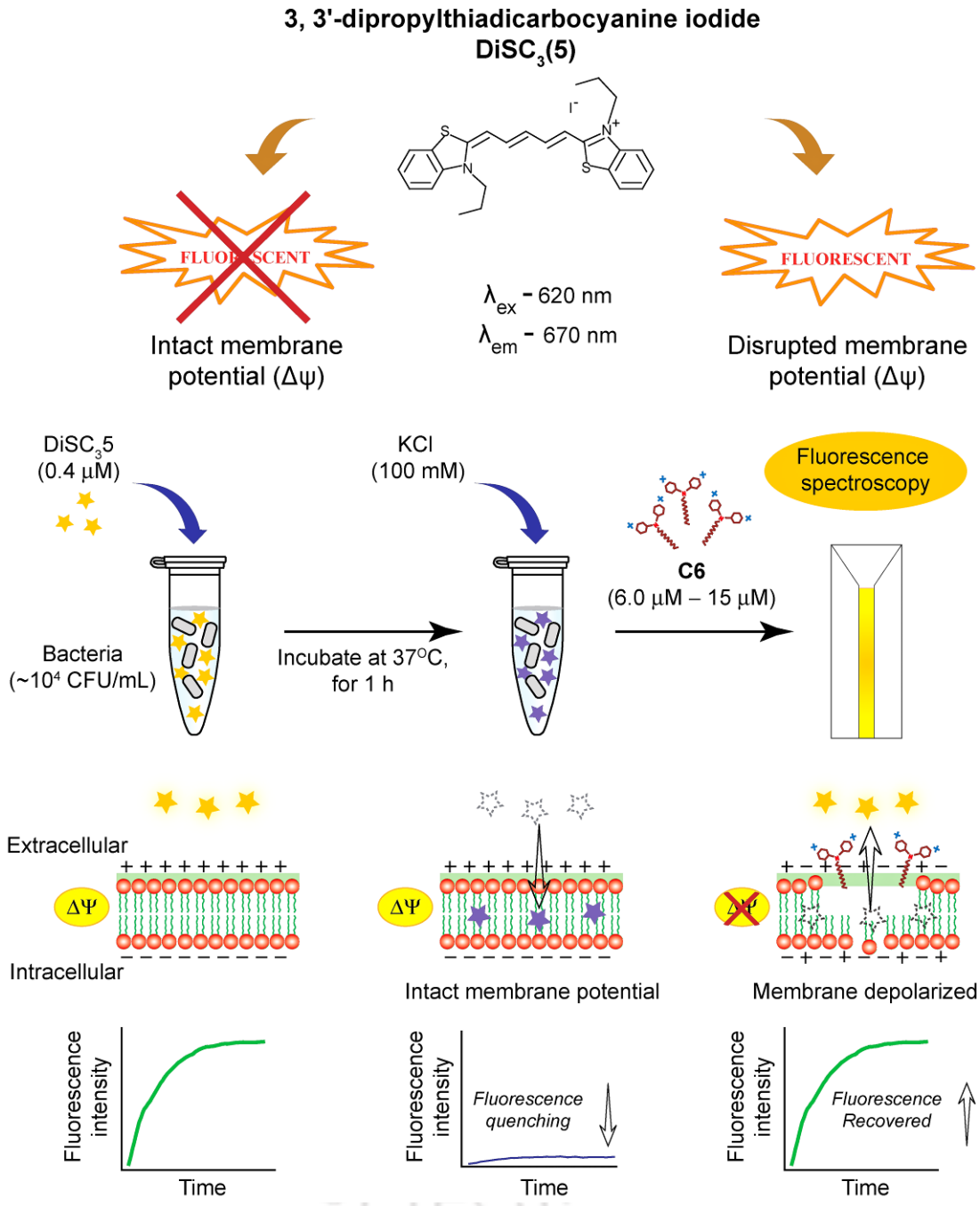

Figure 2.7. Schematic representation of $DiSC_3$5-based membrane depolarization assay.

A_{600} of 0.05. The cell suspensions were incubated with 0.4 µM $DiSC_3$5 for 1 h at 37°C followed by the addition of KCl (final concentration of 100 mM) and further incubated for 15 min (Vooturi et al. 2009). The cell suspension was then placed in a cuvette to which varying concentrations of **C6** (6.0 µM -15 µM) was added and the fluorescence emission

intensity (λ_{Ex} = 622 nm and λ_{Em} = 670 nm) was monitored intermittently in a spectrofluorimeter (FluoroMax-3, HORIBA) with excitation and emission slit width set at 10 nm each. Cells treated with valinomycin (30 μM) were used as positive control. Fluorescence measurements were taken for three independent experimental samples. The $DiSC_35$-based membrane depolarization assay is schematically depicted in Figure 2.7.

2.2.8. Cytotoxic Effect of Amphiphiles on Model Human Cell Lines

A standard MTT assay was performed to ascertain the cytotoxic effect of **C3**, **C4**, **C5** and **C6** on three human cells lines (HeLa, MCF-7 and HT-29). The cells were initially grown in a 25 cm^2 tissue culture flask in Dulbecco's Modified Eagle Medium (DMEM) supplemented with 10% (v/v) fetal bovine serum (FBS), penicillin (100 mg/mL) and streptomycin (100 mg/mL) at 37°C in a CO_2 incubator under a humidified atmosphere of 5% CO_2. For the MTT assay, cells were subsequently seeded onto 96-well tissue culture plates at a density of 10^4 cells per well and incubated with varying concentrations of the amphiphiles made in DMEM, for a period of 24 h in a CO_2 incubator with 5% CO_2. The tested amphiphile concentrations were equivalent to various multiples of the MIC (0.5 ×, 1.0 ×, 2.0 × and 3.0 ×) of the respective amphiphiles against the Gram-positive bacteria *S. aureus* MTCC 96. Control samples (cells treated with DMSO alone) were also incubated in parallel sets. Following incubation, the medium was carefully aspirated and fresh DMEM containing MTT solution was added to the wells. The plates were further incubated for 4 h at 37°C. Subsequently, the supernatant was aspirated and the insoluble formazan product was solubilized in DMSO and its absorbance was measured in a microtiter plate reader (Infinite M200, TECAN, Switzerland) at 550 nm. For every amphiphile, the MTT assay was performed in six sets for each tested concentration. Data analysis and determination of standard deviation were performed with Microsoft Excel 2010 (Microsoft Corporation, USA). In the MTT assay, the absorbance obtained for solvent control samples (cells treated with DMSO alone) was considered to represent 100% cell viability, whereas the absorbance for the amphiphile-treated cells was compared to that for the solvent control cells in order to determine % cell viability.

The IC_{50} values of the amphiphiles (concentration of the amphiphile which leads to 50% reduction in cell viability) for every tested cell line were also determined. Following

MTT assay, the cytotoxic effect of equimolar concentrations of the amphiphiles (40 μM and 60 μM) on the cell lines was also evaluated in a separate set of experiments. For a comparative assessment of the cytotoxic effects exerted by the amphiphiles and to determine the statistical significance of the results obtained in the MTT assay, an analysis of variance (ANOVA) was performed using Sigma plot version 11.0.

The cytotoxic effect of **C6** on human cell lines was also determined by fluorescence microscope analysis. To this end human carcinoma cells (HeLa, MCF-7 and HT-29) were seeded onto 96-well tissue culture plates (approximately 10^4 cells were seeded per well) and grown till 80% confluency in a CO_2 incubator as mentioned before. Subsequently, the cells were incubated with 16 μM of **C6** (equivalent to the MIC against *S. aureus* MTCC 96) made in DMEM, for a period of 24 h in a CO_2 incubator with 5% CO_2. Solvent control samples (cells treated with DMSO alone) were also incubated in parallel wells. For samples representing completely permeabilized cells, separate sets of cells were fixed with 4% paraformaldehyde for 10 min at room temperature followed by treatment with 0.1% Triton X-100 for 10 min. Cells belonging to all the experimental samples (amphiphile-treated cells, solvent control cells and Triton X-100 treated cells) were thoroughly washed with sterile PBS and separate sets of each sample were labelled with 50 mM cFDA-SE and 30 mM PI each for 15 min, respectively. The cells were washed thoroughly with sterile PBS and images of stained cells were captured using a fluorescence microscope (Eclipse Ti-U, Nikon, USA) with a filter that allowed blue light excitation at 445-495 nm for cFDA-SE and green light excitation at 495-570 nm in the case of PI stained cells.

2.3. Results and Discussion

2.3.1. Antibacterial Activity of Synthetic Amphiphiles

The growing menace of drug-resistant pathogenic bacteria in conjunction with a dwindling armory of antibiotics to counter their challenge has spurred a critical need for new antibacterial agents. In this backdrop, low molecular weight synthetic amphiphiles can be envisaged as promising bactericidal agents. Their amphiphilic topology leads to an inherent penchant for membrane insertion in target bacteria, which results in large scale membrane disruption. This mode of action is especially counterproductive to resistance

development since extensive refurbishment of the membrane is conceived as physiologically taxing for the target bacteria. Apart from its profound mode of action, the other benefits of low molecular weight synthetic amphiphiles as antibacterial therapeutic agents are: (a) facile and inexpensive synthesis, (b) the possibility to generate a large library of scaffolds with tailored activity and (c) the likelihood of higher solubility in buffers and biologically relevant fluids as compared to high molecular weight polymeric amphiphiles. In the present study a set of neutral **(C1**, **C3** and **C5)** and cationic amphiphiles **(C2**, **C4** and **C6)** based on pyridine head groups and varying alkyl chain length (octyl and dodecyl) were synthesized and characterized (refer to Appendix of Chapter 2). Their bactericidal activity was screened against Gram-positive and Gram-negative target bacterial strains and a representative result with 100 μg/mL amphiphile concentration is indicated in Figure 2.8. It is evident from the figure that the interaction of target bacterial strains with amphiphiles bearing shorter alkyl chain length (**C1** and **C2**) resulted in only nominal inhibition of growth. However, with increase in the alkyl chain length of the amphiphiles (**C3**, **C4**, **C5** and **C6**), manifestation of bactericidal activity was prominent and the extent of growth inhibition observed for the target bacterial strains was manifold higher compared to the inhibition observed with **C1** and **C2**. Amongst the neutral amphiphiles, the hydrophobicity (log P value) of **C5** was the highest followed by **C3** and **C1**, respectively, (refer to Appendix, Table A2.1). An increase in hydrophobicity of

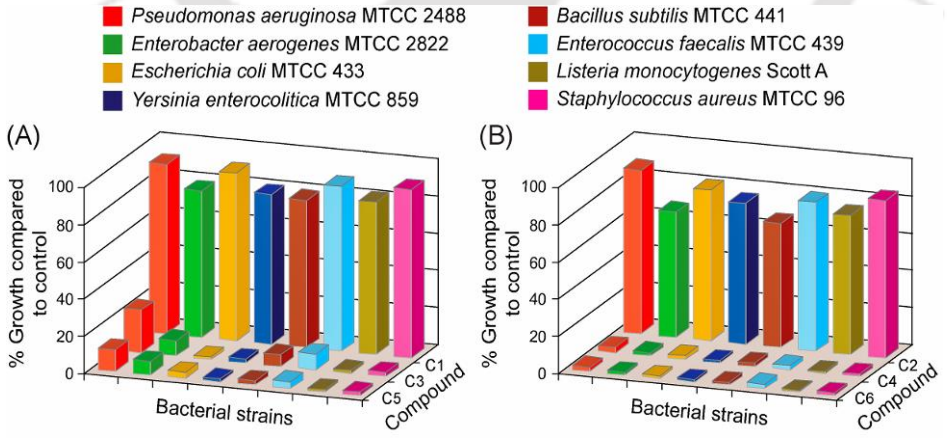

Figure 2.8. Bactericidal activity of (A) neutral (**C1**, **C3** and **C5**) and (B) charged amphiphiles (**C2**, **C4** and **C6**) against target bacterial strains. The target bacteria were interacted with 100 μg/ mL amphiphile for 6 h.

amphiphiles is likely to enhance their insertion into the target cell membrane resulting in enhanced killing of target bacteria (Findlay et al. 2010, Vudumula et al. 2012, Palermo et al. 2009, Kanazawa et al. 1994, Malina and Shai 2005). The cationic amphiphiles **C4** and **C6** exhibited superior bactericidal activity as compared to the neutral amphiphiles **C3** and **C5** (Figure 2.7.). Bacterial cells are considered to be negatively charged, which is attributed to the presence of teichoic acid in Gram-positive bacteria and lipopolysaccharide in Gram-negative bacteria (Weidenmaier and Peschel 2008, Gutsmann and Seydel 2010). Presence of a cationic head group perhaps potentiates the bactericidal activity of amphiphiles by facilitating strong electrostatic interaction with the anionic bacterial cells. Another structural feature of cationic amphiphiles, which apparently contributes to the bactericidal efficacy, is the multiplicity of the head group. It can be observed from Figure 2.1. that **C6**, which bears a double benzylic head group, exhibited superior bactericidal activity as compared to other amphiphiles. Conceivably, an increased positive charge density is likely to promote efficient binding of the amphiphile to the polyanionic bacterial cell surface resulting in heightened bactericidal activity of the amphiphile (Haldar et al. 2005). The high bactericidal activity associated with amphiphiles bearing positive charge, longer alkyl chain and multiple head group was also observed at a lower amphiphile concentration of 50 μg/ mL, with a slightly lesser magnitude of growth inhibition (refer to Appendix, Figure A2.9). Based on the antibacterial activity obtained in the screening experiments, the subsequent experiments were conducted with **C3**, **C4**, **C5** and **C6**.

The MIC and MKC of the antibacterial amphiphiles **(C3**, **C4**, **C5** and **C6)** against selected target bacteria were also determined. The most potent antibacterial activity was observed for **C6** as evident from the low MIC and MKC values in comparison to other amphiphiles (refer to Appendix, Table A2.2). The MIC and MKC of the tested amphiphiles were found to be lower against Gram-positive bacteria like *S. aureus* MTCC 96 and *L. monocytogenes* Scott A, in contrast to the Gram-negative bacteria *E. coli* MTCC 433 and *E. aerogenes* MTCC 2822. This phenomenon perhaps originates from the presence of an outer membrane permeability barrier in Gram-negative bacteria (Bolla et al. 2011, Nikaido 2003). It is significant to mention here that the amphiphile **C6** was potent against *S. aureus* MTCC 96, which is a putative MRSA strain (Vudumula et al. 2012).

2.3.2. Structure-guided Bactericidal Activity

The next endeavor was to pursue a structure-activity study with the amphiphiles **C3**, **C4**, **C5** and **C6** in order to understand the relevance of cationic charge and charge multiplicity in the context of antibacterial activity. Given that amphiphilic compounds trigger membrane damage in bacterial cells (Tang et al. 2006, Rawlinson et al. 2010, Vudumula et al. 2012, Song et al. 2011), experiments were conducted to probe the membrane-directed activity of these structurally diverse amphiphiles. In these experiments, fluorescent probes were selected, which could specifically track bacterial membrane damage and provide a quantitative comparison of the antibacterial activity of the amphiphiles. In the initial experiment, cells of *S. aureus* MTCC 96 and *E. coli* MTCC 433 were labeled with the fluorescent dye cFDA-SE and treated with equimolar concentrations of the amphiphiles (**C3**, **C4**, **C5** and **C6**). cFDA-SE is a membrane permeable dye and following uptake, the ester bond of the dye undergoes cleavage owing to intracellular esterase activity associated with viable cells. As a consequence, accumulation of a highly fluorescent form of the dye ensues in the cell (Hoefel et al. 2003). cFDA-SE labeled cells are suitable in antibacterial assays since the amine reactive fluorophores conjugate with intracellular proteins and thereby reduce passive leakage of the dye from viable cells. The efficacy of a membrane-acting bactericidal agent can be estimated quantitatively by measuring the leakage of the dye from cells as a consequence of membrane damage (Singh et al. 2012). In the present study, it was observed that cFDA-SE leakage from amphiphile-treated cells increased systematically with increasing concentrations of amphiphile, which suggested a dose-dependent effect and this phenomenon was explicitly observed for both the target bacteria (Figure 2.9A-B). Upon comparing the extent of cFDA-SE leakage in amphiphile-treated target cells, a hierarchy in the membrane-disrupting activity of the amphiphiles could be observed, with the highest activity associated with the cationic amphiphile with multiple charge **(C6)**, followed by **C4**, **C5** and **C3**, respectively (Figure 2.8A-B). It can be conceived that charge multiplicity in a cationic amphiphile would promote a multivalent effect resulting in stronger electrostatic interactions and superior adsorption onto the anionic bacterial cell surface (Haldar et al. 2005). This perhaps leads to the superior membrane-directed activity observed for **C6** in the present study. Based on the extent of cFDA leakage in amphiphile-treated cells, it may be mentioned here that the bactericidal

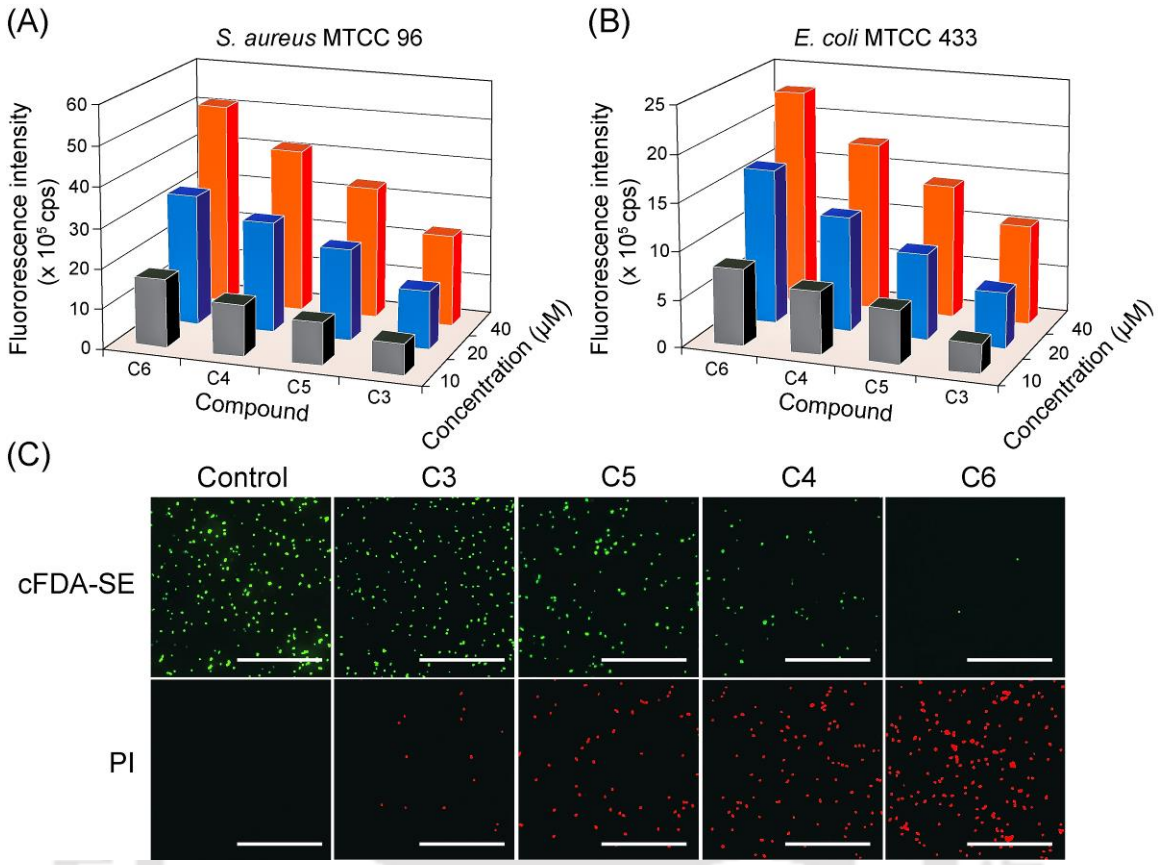

Figure 2.9. Structure-guided bactericidal activity of amphiphiles (**C3**, **C4**, **C5** and **C6**). (A-B) cFDA-SE leakage assay, and (C) fluorescence microscopic images of amphiphile-treated cells of *S. aureus* MTCC 96 labeled with cFDA-SE and PI. Scale bar for all the images is 50 µm.

activity of the amphiphiles was superior against Gram-positive bacteria as compared to the Gram-negative counterpart and this observation was in agreement with the MIC and MKC results (refer to Appendix, Table A2.2). The presence of outer membrane permeability barrier, which is a characteristic feature in Gram-negative bacteria (Bolla et al. 2011, Nikaido 2003) perhaps reduces the uptake of the amphiphile, which results in a lesser extent of cFDA-SE leakage. Evidence for membrane damage in amphiphile-treated target cells was also corroborated through PI uptake assay. PI is a cell-impermeant dye, which is internalized in cells with compromised membrane. Upon uptake the dye subsequently intercalates with nucleic acids to yield a characteristic red fluorescence emission (Virto et al. 2005). The highest uptake of PI was observed in cells treated with **C6** followed by **C4, C5** and **C3**, respectively (refer to Appendix, Figure A2.10). These results further

supported the fact that the extent of membrane damage in target bacteria was largely governed by the cationic charge as well as charge-multiplicity of the amphiphile. Akin to earlier observation in cFDA-SE leakage assay (Figure 2.9A-B), the greater susceptibility of Gram-positive *S. aureus* to amphiphile treatment as compared to Gram-negative *E. coli* was also captured in the PI uptake assay (refer to Appendix, Figure A2.10).

Fluorescence microscope analysis provided additional evidence for the structure-guided antibacterial activity of the amphiphiles. In case of treatment with **C6**, the population of cFDA-SE stained cells of *S. aureus* MTCC 96 was meager while the corresponding PI stained cells were copious (Figure 2.9C), which indicated the superior potential of **C6** to induce membrane damage in target bacteria as compared to the other amphiphiles (**C3**, **C4** and **C5**). Essentially, the trend in the antibacterial activity of the amphiphiles observed through fluorescence microscope analysis was largely consistent with the results obtained in the solution-based fluorescence measurements (Figure. 2.9).

2.3.3. Bactericidal Efficacy and Membrane-directed Activity of ***Compound 6***

A comparative structure-function study identified C**6** as the most potent bactericidal amphiphile. To further validate the bactericidal activity and membrane-targeting mode of action of **C6**, a series of experiments were pursued. Initially, the bactericidal potency of **C6** was ascertained against *S. aureus* MTCC 96 and *E. coli* MTCC 433 cells suspended in sterile PBS (10^6 CFU/mL each). The essential observation was that there was a distinct reduction in the viability of the treated cells and this phenomenon could be correlated with increasing amphiphile concentration, as evident in the steeper slopes of the time-kill curves (Figure 2.9). It was also notable that **C6**-mediated loss of cell viability was more prominent in Gram-positive *S. aureus* as compared to Gram-negative *E. coli* (Figure 2.10), in line with earlier observations. For instance at 15 μM **C6**, which is nearly equivalent to the MIC of the amphiphile against *S. aureus* MTCC 96, a significant reduction in cell viability was observed and the target bacteria was virtually eliminated following 24 h of interaction as the viable cell counts reached below 1.0 Log_{10} CFU (Figure 2.10). In scanning electron microscope (SEM) analysis, untreated cells of *S. aureus* MTCC 96 and *E. coli* MTCC 433 revealed a uniform margin and a morphology characteristic of the respective

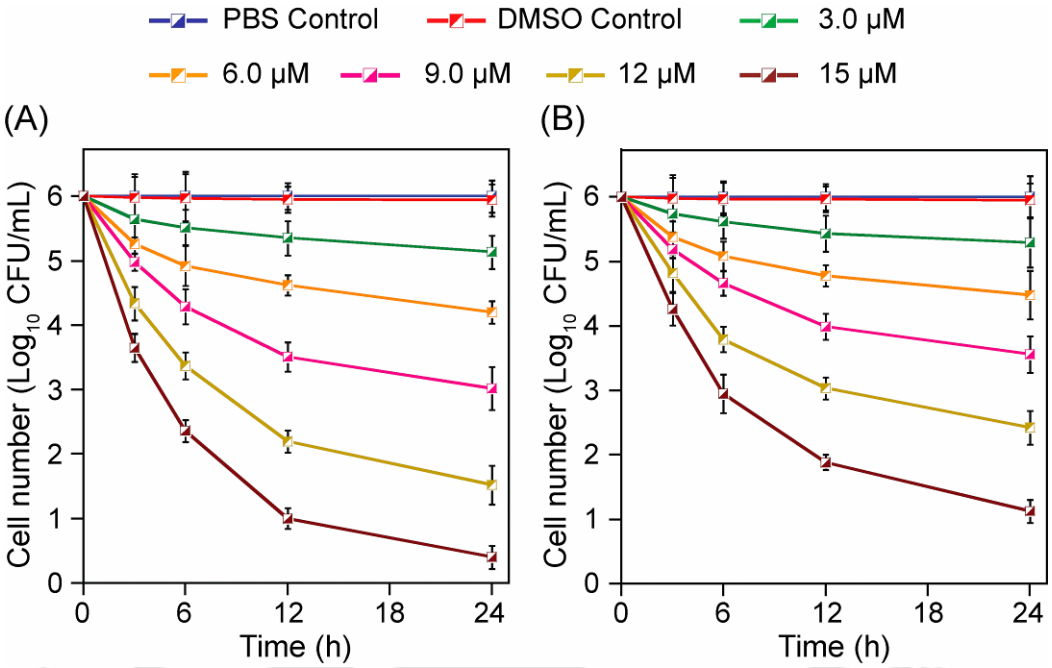

Figure 2.10. Time-kill curves of **C6** against (A) *S. aureus* MTCC 96 and (B) *E. coli* MTCC 433.

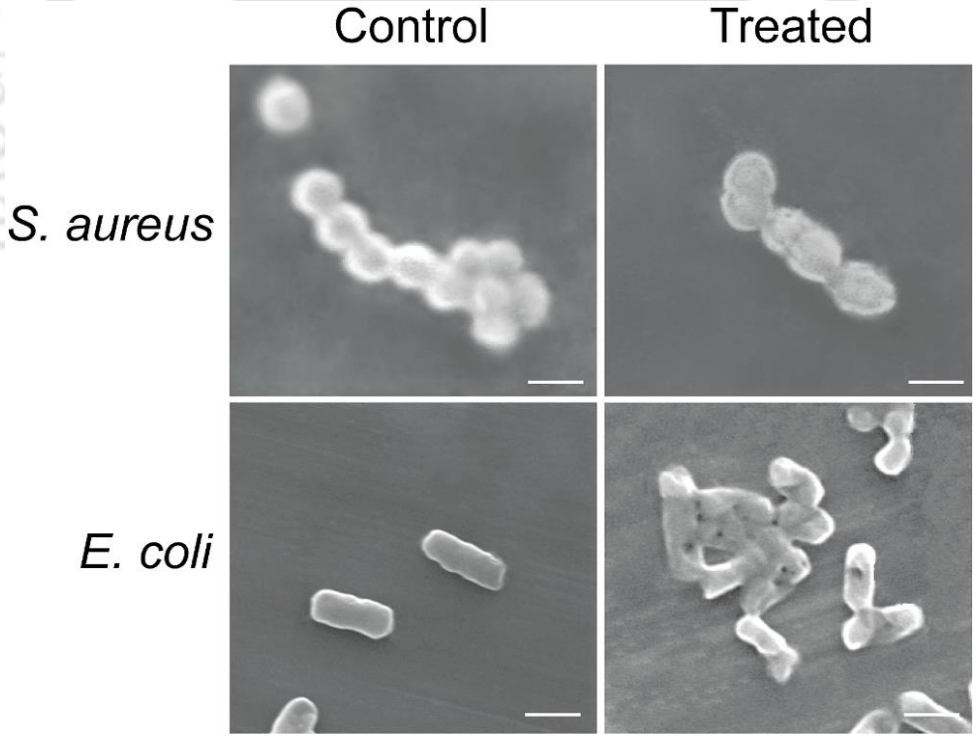

Figure 2.11. Scanning electron microscope images of *S. aureus* MTCC 96 and *E. coli* MTCC 433 cells treated with 50 µM **C6**. Scale bar for the images is 1.0 µm**.**

bacteria. However, cells treated with 50 μM of **C6** displayed a distorted shape and appeared shriveled, which was indicative of membrane damage (Figure 2.11). Flow cytometry analysis was conducted for a quantitative assessment of the bactericidal effect of **C6** on target cells of *S. aureus* MTCC 96 and *E. coli* MTCC 433. As evident in (Figure 2.12), in case of untreated samples (control), the fluorescence histogram and statistical analysis indicated the presence of a large population of viable cells exhibiting strong cFDA-SE fluorescence (marker M1: 97.53% in the case of *S. aureus* MTCC 96 and 91.03% in the case of *E. coli* MTCC 433). Upon treatment with 50 μM of **C6**, there was a distinct shift in the position of the peak, which indicated a discernible reduction in the fluorescence intensity of cFDA-SE for amphiphile-treated cells as compared to control (Figure 2.12). As observed earlier in the structure-function studies, treatment of bacterial cells with **C6** promotes membrane damage and leakage of the fluorescent cFDA-SE dye. As a consequence, the population of cFDA-SE labelled viable cells is reduced significantly (compare marker M1 in histogram statistics of untreated and treated cells), which is

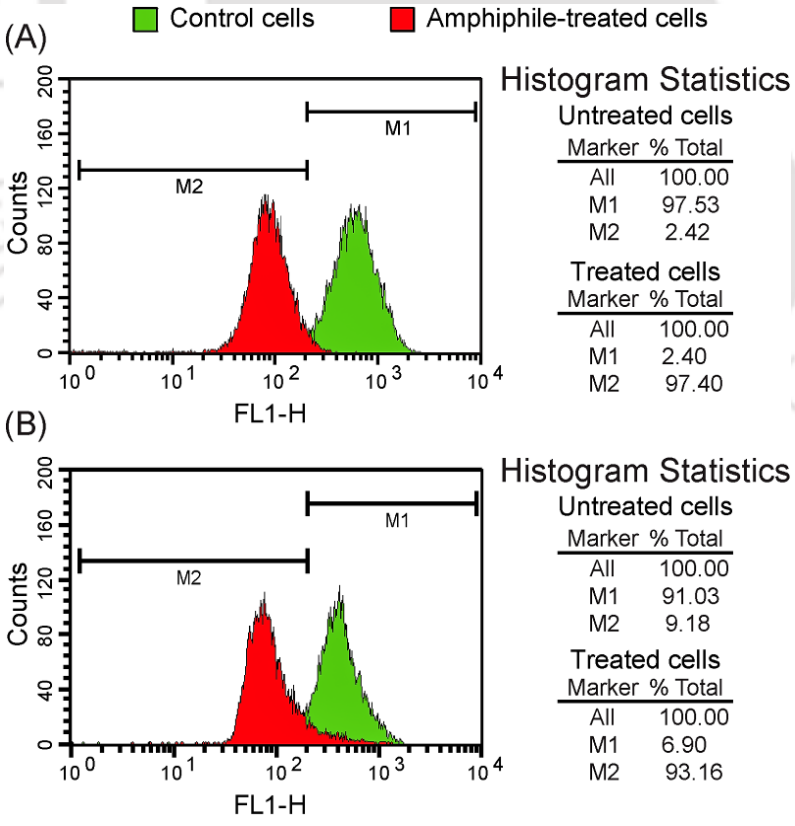

Figure 2.12. Flow cytometry analysis of cFDA-SE labelled cells of (A) *S. aureus* MTCC 96 and (B) *E. coli* MTCC 433 treated with 50 μM of **C6**

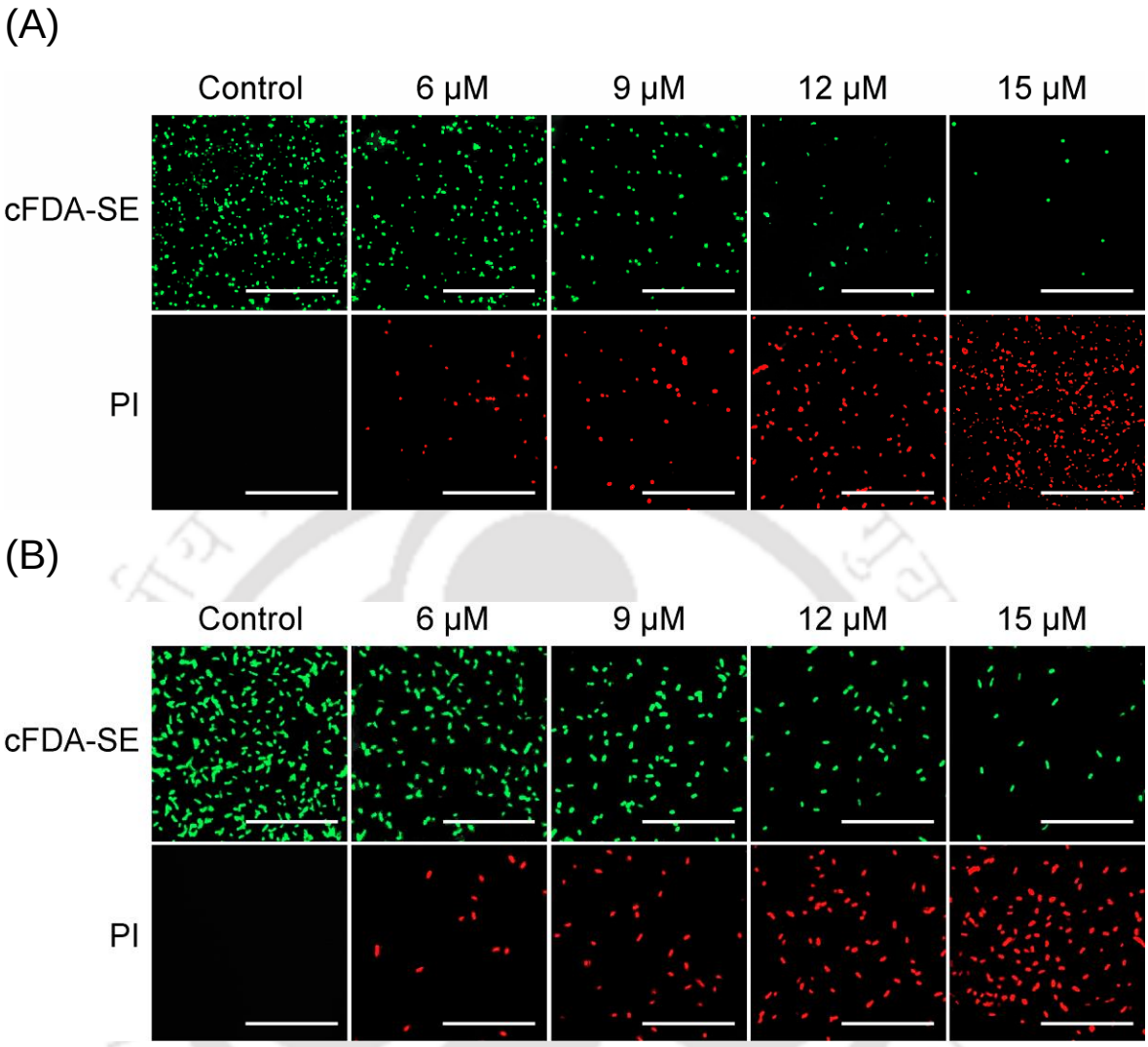

Figure 2.13. Fluorescence microscope images of (A) *S. aureus* MTCC 96 and (B) *E. coli* MTCC 433 cells treated with varying concentrations of **C6**. Scale bar for the images is 50 μm.

captured as a shift in the position of the fluorescence emission peak for **C6**-treated sample (Figure 2.12). A dose-dependent membrane-directed activity of **C6** was also captured in fluorescence microscope analysis, wherein the population of cFDA-SE stained target cells diminished progressively, while the number of PI stained cells increased with a corresponding increase in amphiphile concentration (Figure 2.13).

Based on previous studies it has been acknowledged that that the transmembrane potential ($\Delta\Psi$) in target bacterial cells may influence the activity of membrane-acting

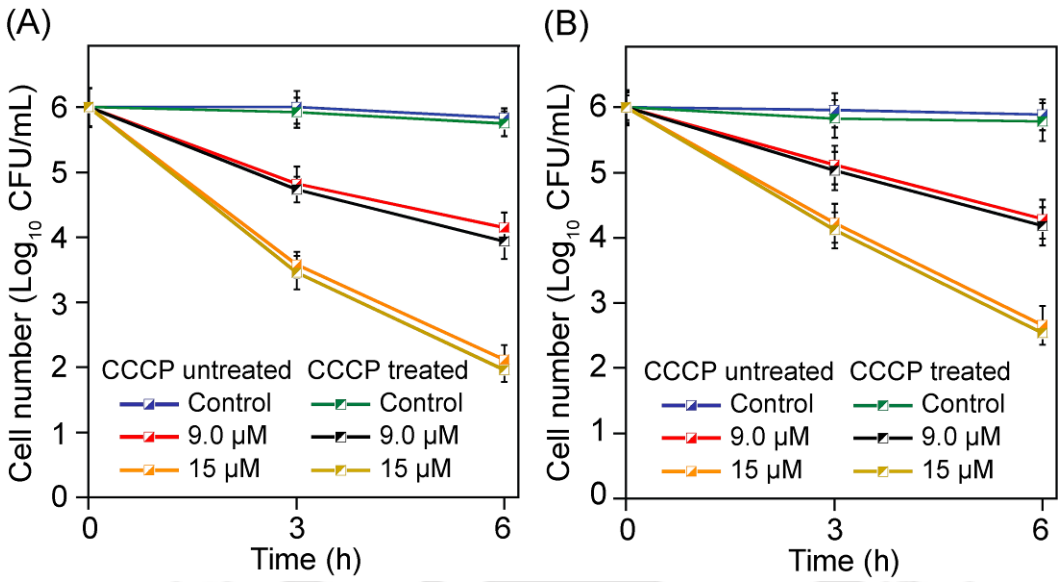

Figure 2.14. Effect of membrane potential on the bactericidal activity of **C6** on (A) *S. aureus* MTCC 96 and (B) *E.coli* MTCC 433.

bactericidal agents (Yeaman and Yount 2003, Breukink and de Kruijff 1999). Thus, to ascertain the effect of membrane potential on the antibacterial activity of **C6**, target cells of *S. aureus* MTCC 96 and *E. coli* MTCC 433 were pre-treated with CCCP, which is a known proton ionophore that can disrupt the proton-motive force (PMF) and depolarize the bacterial membrane. Subsequently, the cells were treated with varying concentrations of **C6**. Control experiments indicated that the cell viability was not affected by CCCP treatment per se as evidenced in the nearly identical viable cell counts present in CCCP-untreated as well as CCCP-treated control samples (Figure 2.14). However, loss in cell viability incurred with time when the cells were treated with **C6** and this phenomenon could be correlated to amphiphile concentration. It is important to mention that in the case of **C6**-treated cells, the loss in cell viability for CCCP-treated and CCCP-untreated cells was equivalent (Figure 2.14), which suggested that the bactericidal activity of **C6** was not affected by CCCP-induced membrane depolarization. Pathogenic bacteria are endowed with various attributes to counter the host-mediated defense mechanism, of which variations in membrane electrochemistry and energetic have been implicated in the case of pathogenic *S. aureus* to evade the action of antimicrobial peptides (Yeaman and Yount 2003). In this backdrop, the mode of action of **C6**, which was found to be independent of the transmembrane potential of bacterial cells holds special therapeutic merit for

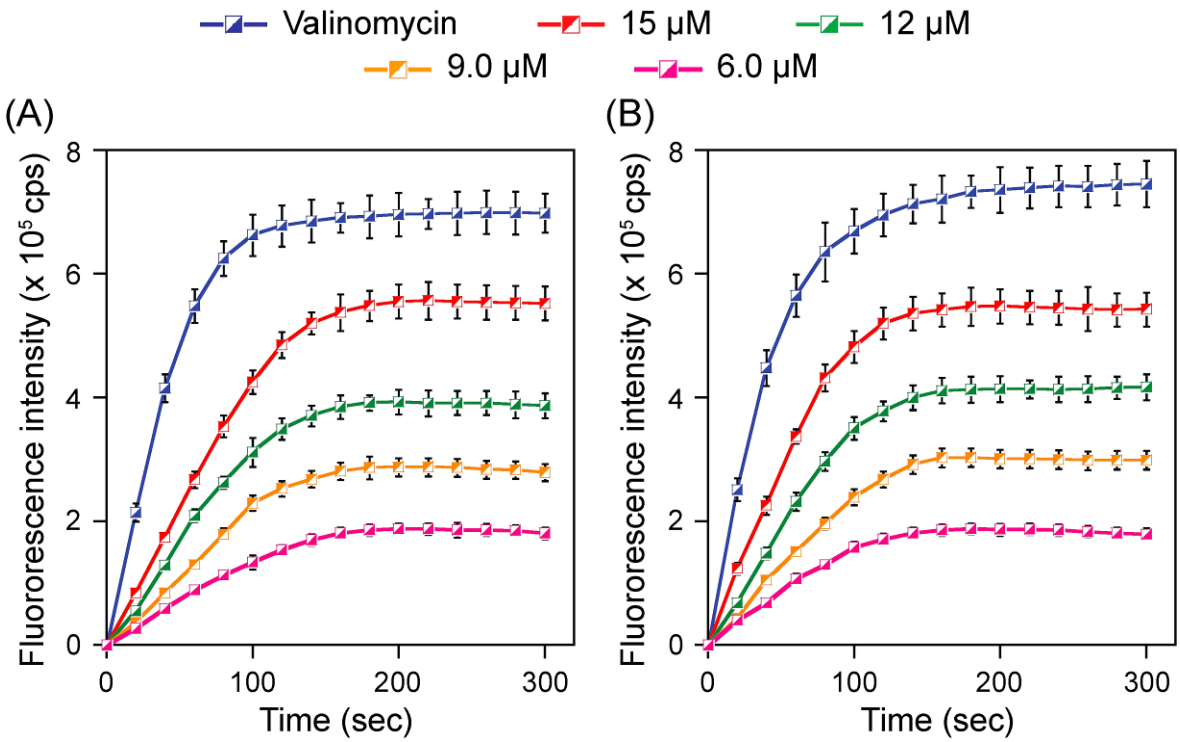

Figure 2.15. DiSC$_3$5-based fluorescence assay to ascertain membrane depolarization in (A) *S. aureus* MTCC 96 and (B) *E. coli* MTCC 433 cells treated with **C6**. Cells treated with 30 µM valinomycin were used as a positive control for the assay.

eradication of pathogenic bacteria, which may display an altered membrane electrochemistry. Given the fact that cytoplasmic membrane depolarization by membrane-acting bactericidal agents has been largely implicated in loss of cell viability (Song et al. 2011, Adhikari et al. 2012), the next endeavor was to ascertain the ability of **C6** to destabilize bacterial membrane potential, for which a fluorescence-based assay was employed using DiSC$_3$5, a membrane potential sensitive probe. As evident from Figure 2.15, treatment of *S. aureus* MTCC 96 and *E. coli* MTCC 433 with various concentrations of **C6** led to dose-dependent enhancement in DiSC$_3$5 fluorescence up to 200 s followed by a plateau, which suggested that the amphiphile could rapidly dissipate the membrane potential in target cells. It was also observed that **C6** could disrupt the transmembrane potential of target bacteria even at concentrations below its MIC against the respective bacteria.

2.3.4. Cytotoxic Effect of Amphiphiles

A fundamental understanding, which emerged from the structure-function studies conducted with the amphiphiles (**C3**, **C4**, **C5** and **C6**) was that the cationic charge density imparted a distinct influence on their bactericidal activity and the amphiphiles triggered large scale membrane-disruption in the target bacteria, a phenomenon, which was also substantiated by the mode of action studies conducted with **C6**. Conceivably, the membrane-directed activity of the amphiphiles are likely to render therapeutic benefits in meeting the challenge of pathogenic bacteria, since a functional membrane is irrefutable for survival of the target bacteria and extensive membrane damage is likely to be counterproductive to the development of resistance (Van Bambeke et al. 2008, Hurdle et al. 2011) However, to rationalize the therapeutic potential of the amphiphiles, it is paramount to ascertain their cytotoxic effect on human cells. Thus the cytotoxic potential of **C3**, **C4**, **C5** and **C6** was ascertained against model human cell lines – HeLa (cervical cancer), MCF-7 (breast cancer) and HT-29 (colon adenocarcinoma) by an MTT assay. Based on the finding that the amphiphiles displayed superior bactericidal activity against Gram-positive bacteria as compared to Gram-negative counterparts, the concentrations of the amphiphiles chosen for the cytotoxicity assay were essentially various multiples of the MIC (0.5×, 1×, 2× and 3×) against the Gram-positive bacteria *S. aureus* MTCC 96. The chosen levels thus rendered a comparative appraisal of the cytotoxic potential of the amphiphiles at bactericidal concentrations relevant for the target bacteria. It was observed that the amphiphiles did not impart any cytotoxic effect on model human cell lines at concentrations equivalent to their respective MICs against *S. aureus* MTCC 96 (Figure 2.16A). This finding was also supported by fluorescence microscope analysis, wherein a large number of cells treated with a concentration of **C6** equivalent to its MIC against *S. aureus* MTCC 96 exhibited intense cFDA-SE fluorescence and were hence viable, akin to the untreated control cells (Figure 2.16B). It was also observed that at concentrations of **C6** equivalent to the MIC against *S. aureus* MTCC 96, the model human cells failed to display PI staining, which indicated the presence of an intact membrane in these cells and an apparent lack of cytotoxic effect of **C6** (Figure 2.16B). Collectively, the MTT assay and fluorescence microscope analysis suggested that at concentrations corresponding to the MIC, the amphiphiles could perhaps be deployed to eliminate the Gram-positive *S. aureus*

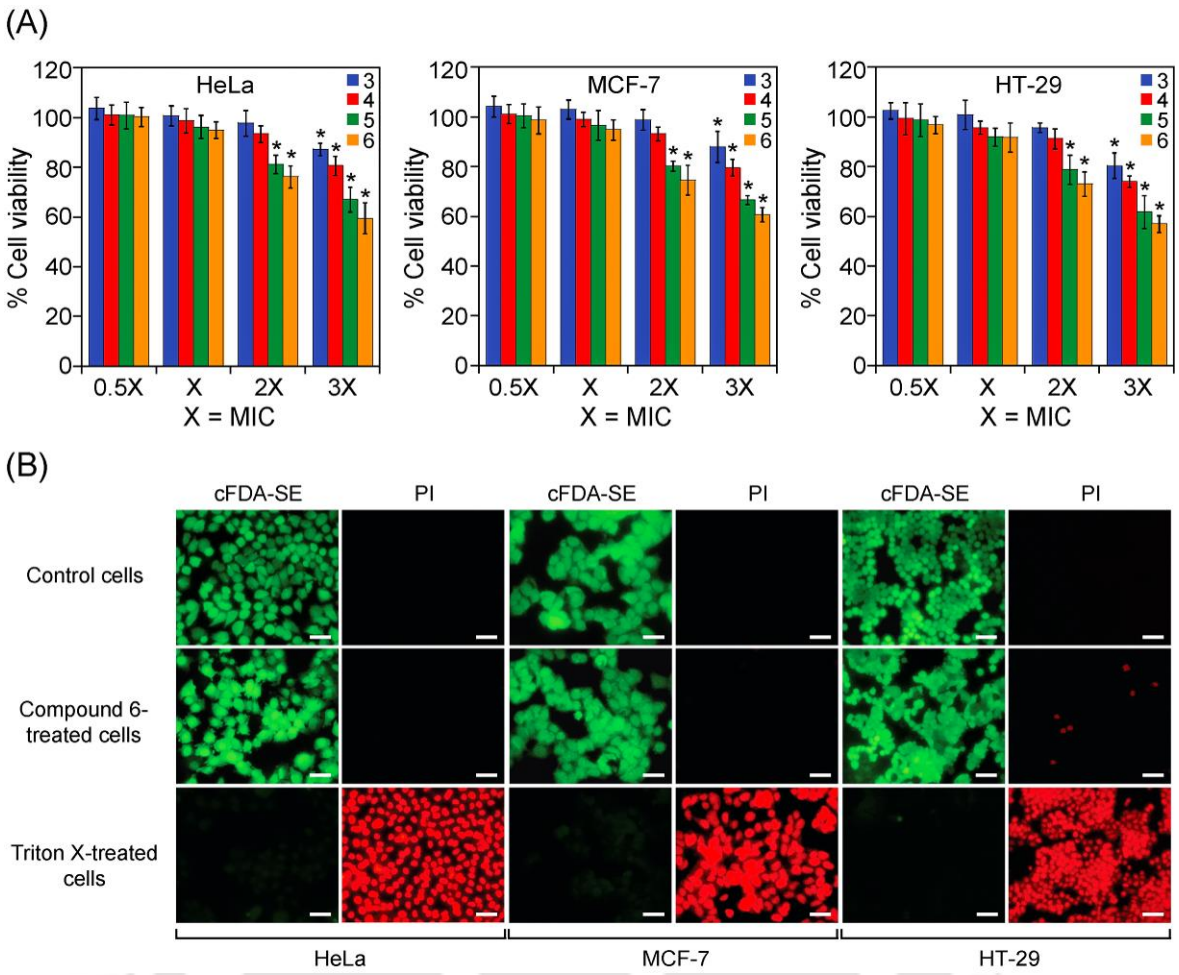

Figure 2.16. (A) MTT assay to determine the cell viability of model human cell lines following treatment with varying concentrations of bactericidal amphiphiles. X indicates an amphiphile concentration equivalent to the MIC against *S. aureus* MTCC 96. Each data point represents mean ± standard deviation from six samples. Statistically significant values derived by ANOVA are indicated by asterisk marks. * indicates *p* value <0.001. (B) Fluorescence microscopic images of model human cell lines treated with 16 µM **C6** (equivalent to the MIC against *S. aureus* MTCC 96) and labeled with cFDA-SE and PI. Scale bar for all the images is 50 µm.

MTCC 96, without the added risk of any unwarranted cytotoxic effect on human cells. Although MIC is considered as one of the major yardsticks to estimate the efficacy of a bactericidal agent, it essentially is a measure of the *in vitro* susceptibility of a microorganism to a given drug. Hence MIC cannot be regarded as an absolute arbitrator for successful *in vivo* mitigation of bacterial infection. The *in vivo* efficacy of a bactericidal

agent is regarded to be governed by several pharmacokinetic and pharmacodynamic considerations such as serum concentration, binding to the plasma protein and tissue distribution (Craig 1998, Mueller et al. 2004). Thus, in order to ensure effective *in vivo* killing concentrations against target pathogens, bactericidal agents are generally used at concentrations in excess of their MIC (Craig 1998, 2003, Wispelwey 2005). However, from a therapeutic perspective, it is critical to ascertain whether the use of a bactericidal agent at concentrations higher than the MIC is liable to gratuitous host cell toxicity. In the present study, this important goal was pursued and the cytotoxic effect of the bactericidal amphiphiles at concentrations exceeding the MIC against *S. aureus* MTCC 96 was ascertained. As evident from Figure 2.16A, at concentrations equivalent to 2× MIC, **C3** and **C4** failed to impart any deleterious effect on cell viability. However, the reduction in the viability of cells treated with **C5** and **C6** at 2× MIC was statistically significant (Figure 2.16A). These findings suggested that for therapeutic interventions, which require amphiphile concentrations higher than the MIC, it would perhaps be judicious to select **C3** and **C4**, as compared to **C5** and **C6**. At the highest tested concentration (3× MIC for *S. aureus* MTCC 96), all the bactericidal amphiphiles exerted cytotoxic effect on the model human cell lines (Figure 2.16A). It was also apparent that the magnitude of cytotoxicity was highest in the case of **C6** followed by **C5**, **C4** and **C3**, respectively. An ANOVA followed by all pairwise multiple comparison (Holm–Sidak method) revealed that at amphiphile concentrations equal to 2× and 3× MIC of *S. aureus* MTCC 96, the % cell viability obtained for **C6** and **C5** was markedly less and this decrease in cell viability was statistically significant for all the tested cell lines, as compared to that obtained for **C4** and **C3** (refer to Appendix, Table A2.3). Based on the IC_{50} values of the bactericidal amphiphiles (Table 2.1) and MTT assay at equimolar amphiphile concentrations (refer to Appendix, Table A2.4) a distinctive hierarchical pattern of cytotoxicity was evident, with **C6** displaying the highest cytotoxic effect on the tested cell lines followed by **C5**, **C4** and **C3**, respectively. It is likely that the charge density of the bactericidal amphiphiles, accessibility of the charge and their conformational flexibility are critical factors, which promote interactions with the human cell membrane and enhance the manifestation of the cytotoxic effect (Palermo et al. 2009, Fischer et al. 2003).

Table 2.1. IC_{50} values of bactericidal amphiphiles.

Synthetic Amphiphile	IC_{50} value (μM) ± standard deviation against human cell lines		
	HeLa	MCF-7	HT-29
C3	100 ± 3.58	100 ± 0.94	98 ± 3.36
C4	86 ± 1.81	86 ± 1.67	82 ± 0.20
C5	80 ± 3.70	80 ± 2.04	80 ± 5.83
C6	50 ± 0.50	50 ± 1.33	50 ± 1.84

Comparison of the structures of the bactericidal amphiphiles (Figure 2.1) indicated that **C6** bears two aromatic rings and displays conformational flexibility due to the presence of two benzylic head groups. These structural features may facilitate appropriate orientation and juxtaposition of the hydrophobic tail of the amphiphile for insertion into the core of the mammalian cell membrane. Further, a superior cationic charge density perhaps contributes for the highest cytotoxicity observed in the case of **C6**, akin to other amphiphilic compounds reported earlier (Fischer et al. 2003, Palermo et al. 2009). On similar lines, the conformational flexibility along with multiple aromatic rings is presumably responsible for the high cytotoxic effect of **C5**. Target cell selectivity of a bactericidal molecule is critical from a therapeutic viewpoint. This selectivity is considered to originate from significant differences in membrane bilayer composition between bacterial and mammalian cells. For instance, bacterial membranes consist of a higher content of negatively charged phospholipids in contrast to mammalian membranes, which are primarily composed of zwitterionic lipids and cholesterol (Tang et al. 2006, Zasloff 2002). The ratio of IC_{50} to MIC is considered to be a rational measure of the potential of an antibacterial agent to curb bacterial growth, without having any deleterious cytotoxic effect on human cells. In the present study, it was observed that the selectivity of the bactericidal amphiphiles was higher in the case of Gram-positive *S. aureus* MTCC 96, with IC_{50}/MIC values ranging from 2.45 to 4.3, as opposed to the Gram-negative *E. coli* MTCC 433, wherein the corresponding IC_{50}/MIC values varied from 0.76 to 1.0 (Table 2.2)

Table 2.2. Selectivity of bactericidal amphiphiles based on IC_{50}/MIC values.

Synthetic Amphiphiles	Selectivity for *S. aureus* MTCC 96 (IC_{50}/MIC)			Selectivity for *E. coli* MTCC 433 (IC_{50}/MIC)		
	HeLa	MCF-7	HT-29	HeLa	MCF-7	HT-29
C3	2.5	2.5	2.45	0.78	0.78	0.76
C4	4.3	4.3	4.1	1.0	1.0	1.0
C5	3.2	3.2	3.2	0.8	0.8	0.8
C6	3.12	3.12	3.12	0.78	0.78	0.78

The observed selectivity was anticipated, given the higher MIC values of the amphiphiles for Gram-negative *E.coli* MTCC 433 (refer to Appendix, Table A2.2).

2.4. Significant Findings

The salient findings of the present study can be enlisted as follows:

1. In the present study, a set of pyridine-based low molecular weight synthetic amphiphiles with varying charge densities and alkyl chain lengths were screened for antibacterial activity and their structure-guided bactericidal potency against target bacteria was determined.
2. The fundamental understanding that emerged from the structure-function studies was that the antibacterial activity of the membrane-acting amphiphiles was strongly influenced by cationic charge multiplicity and hydrophobicity imparted by longer alkyl chain, which is consistent with previous reports on amphiphilic AMP mimics.
3. Fluorescence-based assays in conjunction with microscopic analysis suggested that **C6** was the most potent amphiphile that displayed membrane-disrupting activity.
4. The bactericidal activity of **C6** was independent of the transmembrane potential of the target bacterial strains. However, **C6** could readily depolarize the transmembrane potential in target bacteria.

5. Cytotoxicity assays, which were conducted to rationalize the true therapeutic potential of the bactericidal amphiphiles, suggested that at concentrations equivalent to the MIC against the Gram-positive *S. aureus* MTCC 96, the amphiphiles could possibly eliminate the bacteria without the added risk of any adverse effect on human cells.
6. The amphiphiles exhibited superior antibacterial selectivity in case of Gram-positive *S. aureus* MTCC 96 as compared to the Gram-negative *E.coli* MTCC 433.

Based on the results obtained, the selectivity of the bactericidal amphiphiles per se may be regarded as moderate, which may limit their direct application for *in vivo* elimination of target bacteria. However, given the strong propensity of the amphiphiles to disrupt the bacterial membrane at concentrations well below the MIC, it was envisaged that at low concentrations, which do not render a cytotoxic effect, these amphiphiles can perhaps be safely used as adjuvants to breach the membrane-based barriers, in particular Gram-negative bacteria and enhance the uptake and efficacy of established therapeutic agents such as antibiotics. In the next chapter, the adjuvant potential and the therapeutic prospect of the most efficient bactericidal amphiphile **C6** is demonstrated.

.

Indian Institute of Technology Guwahati

TH-1410_10610607

Chapter 3

Potential Therapeutic Applications of Compound 6

This chapter essentially demonstrates the adjuvant potential of ***Compound 6*** *in enhancing antibiotic-mediated killing of target bacteria.*

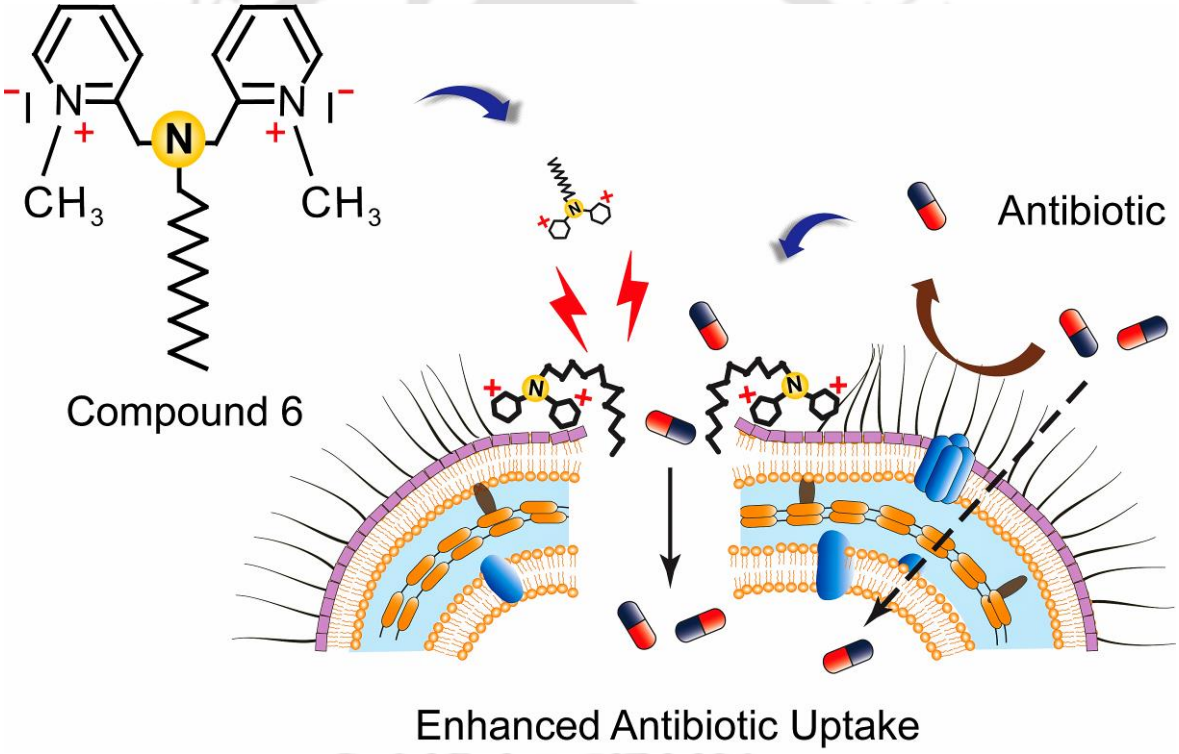

TH-1410_10610607

ABSTRACT

This chapter highlights the application of the amphiphilic **C6** as an adjuvant in potentiating the activity of model therapeutic antibiotics. Initially a fluorescence-based assay employing N-phenyl naphthylamine (NPN) revealed dose-dependent outer membrane permeabilization in target bacterial cells treated with **C6**. Based on the membrane-directed activity of **C6**, it was envisaged that treatment of target bacteria with low and non-toxic concentrations of the amphiphile could infringe the membrane barrier and facilitate enhanced uptake of therapeutic antibiotics in combinatorial assays. A notable increase in the growth inhibition of target bacteria was observed when the cells were subjected to a combined treatment of **C6** and the model antibiotics erythromycin, polymyxin B and ciprofloxacin, as compared to treatment with either **C6** or the antibiotics alone. Interestingly, manifold reduction in the minimum inhibitory concentration (MIC) of the antibiotics was observed in the combination studies, which validated the adjuvant potential of **C6**. With regard to the nature of interaction, a synergistic effect was evident in the studies involving combination of **C6** with erythromycin or polymyxin B, whereas an additive effect manifested in the studies involving **C6** in combination with ciprofloxacin.

Interestingly, **C6** retained its bactericidal activity against model gastrointestinal bacteria even in the complex milieu of simulated gastric fluid (SGF). The lack of resistance development against **C6** in target bacteria captured in the multistep *in vitro* resistance development studies augers well for future therapeutic applications of the bactericidal amphiphile **C6**.

3.1. Introduction

Drug-resistant pathogens are emerging as grave healthcare concern and are a serious scourge to modern medicine. Their unbridled prevalence is thought to be a combined effect of their remarkable endurance and adaptability as well as an unrestrained and arbitrary use of therapeutic antibiotics. Drug-resistant pathogens are armed with a gamut of resistance mechanisms that enable them to counter the action of therapeutic antibiotics as well as outwit host defense parameters (Yeaman and Yount 2003, Wright 2011, Nikaido 2009, Gootz 2010, Fair and Tor 2014). The lack of potent antibacterial agents that are radically different from conventional antibiotics in their mode of action coupled with a critical void in drug discovery programs has exacerbated the problem of tackling drug-resistant pathogens (Silver 2011, Fischbach and Walsh 2009, Nolte 2014). Under these circumstances, membrane-targeting antibacterial agents hold considerable therapeutic potential as the probability of developing resistance against them would essentially demand an extensive revamp of disrupted membrane components, which is physiologically challenging and conceivably unfeasible for the target bacteria (Van Bambeke et al. 2008, Chen et al. 2010, Hurdle et al. 2011). In this context, several membrane-targeting synthetic amphiphilic molecules have been described in the literature that display potent bactericidal activity (Kuroda and DeGrado 2005, Oda et al. 2011, Hoque et al. 2012, Gokel and Negin 2012, Bera et al. 2010, Mitra et al. 2009, Findlay et al. 2010, Vudumula et al. 2012).

It is well established that the membrane of pathogenic bacteria is a formidable shield that hinders the transit of bactericidal agents and thus empowers the bacteria to elude the action of many therapeutic antibiotics. For instance, the outer membrane of Gram-negative bacteria acts a barrier that can prevent effective passage of several antibacterial agents and hydrophobic molecules (Delcour 2009, Nikaido 2003, Bolla et al. 2011). In order to address this issue, a membrane-acting bactericidal agent is again envisaged to be beneficial as it is likely to permeabilize the outer membrane of target bacteria and facilitate superior uptake of a therapeutic antibiotic and thus potentiate its bactericidal efficacy. This premise is also supported by the results emerging from previous studies that demonstrate that membrane-targeting agents could be used to breach the permeability barrier and subsequently render enhanced uptake and higher bactericidal

efficacy of antibiotics (Saha et al. 2008, Atkins et al. 2010, Choi and Lee 2012). The merit of a membrane-acting agent in combinatorial therapy with antibiotics is further enhanced by the fact that it acts as an adjuvant and effectively helps to reduce the dose of antibiotics required to eliminate the target bacteria. This benefit is significant as it is considered that the use of therapeutic antibiotics at lower doses could perhaps curb the evolution of drug resistance (Yeh et al. 2009, Ejim et al. 2011).

Based on the aforementioned rationale and given the potent membrane-directed activity of the synthetic amphiphile **C6**, the adjuvant potential of the amphiphile in enhancing the bactericidal efficacy of model therapeutic antibiotics is investigated in this chapter. In the study presented in this chapter, the therapeutic potential of **C6** is ascertained by evaluating the bactericidal activity of the amphiphile against model gastrointestinal bacteria suspended in simulated gastric fluid (SGF). The *in vitro* resistance development study with the amphiphilic **C6** is also reported in this chapter.

.

3.2. Materials and Methods

3.2.1. Growth Media and Chemicals

Nutrient Broth (NB) and Brain-Heart Infusion (BHI) broth were procured from HiMedia, Mumbai, India. Dimethyl sulfoxide (DMSO) and various salts required to prepare simulated body fluid were obtained from Merck, India. N-2-Hydroxyethyl piperazine-N-2-ethane sulphonic acid (HEPES buffer) was procured from Sisco Research Laboratories SRL, Mumbai, India. Porcine pepsin, 1-N-phenyl-naphthylamine (NPN), erythromycin, polymyxin B, ciprofloxacin, Dulbecco's Modified Eagle Medium (DMEM), trypsin–EDTA and 3-(4, 5-dimethyl-2-thiazolyl)-2, 5- diphenyl-2H-tetrazolium bromide (MTT) were procured from Sigma-Aldrich (USA). Fetal bovine serum (FBS) was procured from PAA Laboratories, USA.

3.2.2. Bacterial Strains and Growth Conditions

The bacterial strains used in the present investigation consisted of Gram-positive *Staphylococcus aureus* MTCC 96 (*S. aureus*), *Listeria monocytogenes* Scott A (*L. monocytogenes*) and Gram-negative *Escherichia coli* MTCC 433 (*E. coli*), *Enterobacter aerogenes* MTCC 2822 (*E. aerogenes*). *E. coli* MTCC 433 and

E. aerogenes MTCC 2822 were grown in NB medium at 37°C and 180 rpm for 12 h whereas *S. aureus* MTCC 96 and *L. monocytogenes* Scott A were propagated in BHI broth at 37°C and 180 rpm for 12 h.

3.2.3. Minimum Inhibitory Concentration (MIC) of Erythromycin, Polymyxin B and Ciprofloxacin

MIC of erythromycin was determined against Gram-negative bacteria *E. coli* MTCC 433 and *E. aerogenes* MTCC 2822 while MIC of polymyxin B was determined against Gram-positive *S. aureus* MTCC 96 and *Listeria monocytogenes* Scott A. MIC of ciprofloxacin was determined against *S. aureus* MTCC 96. A standard protocol was followed for determining the MIC as mentioned in section 2.2.5. Briefly, the target bacterial strains (1% v/v) were inoculated into microtitre wells having 100 µL of the requisite growth medium and grown overnight at 37°C and 130 rpm in presence of varying concentrations of either erythromycin (5.0 µg/mL - 320 µg/mL), polymyxin B (5.0 µg/mL - 320 µg/mL) or ciprofloxacin (1.0 µg/mL - 0.03 µg/mL). Bacterial growth was ascertained by measuring absorbance at 600 nm in a microtitre plate reader (Infinite M200, TECAN, Switzerland). MIC of the antibiotics was recorded as the lowest concentration, which resulted in an absorbance reading of <0.1 at 600 nm (A_{600} = <0.1), indicating lack of cell growth. The MIC values for erythromycin, polymyxin B and ciprofloxacin were calculated from three independent experiments, each having three replicas. Data analysis and calculation of standard deviation was performed with Microsoft Excel 2010 (Microsoft Corporation, USA).

3.2.4. Determination of Membrane Permeabilization by NPN Assay

A stock solution of NPN (500 µM) was made in acetone. Target cells of *E.coli* MTCC 433 were grown in nutrient broth (NB) medium at 37°C in a shaker incubator till mid-logarithmic phase (A_{600} of 0.5). The cells were centrifuged, washed twice with 5.0 mM HEPES buffer (pH 7.4) and resuspended in the same buffer. A 1.0 ml aliquot of target cells was taken in a quartz cuvette to which NPN was added (final concentration of 10 µM). Enhancement in the fluorescence intensity of NPN was measured as a function of time following addition of varying concentrations of **C6** (9.0 µM and 15 µM). As a positive

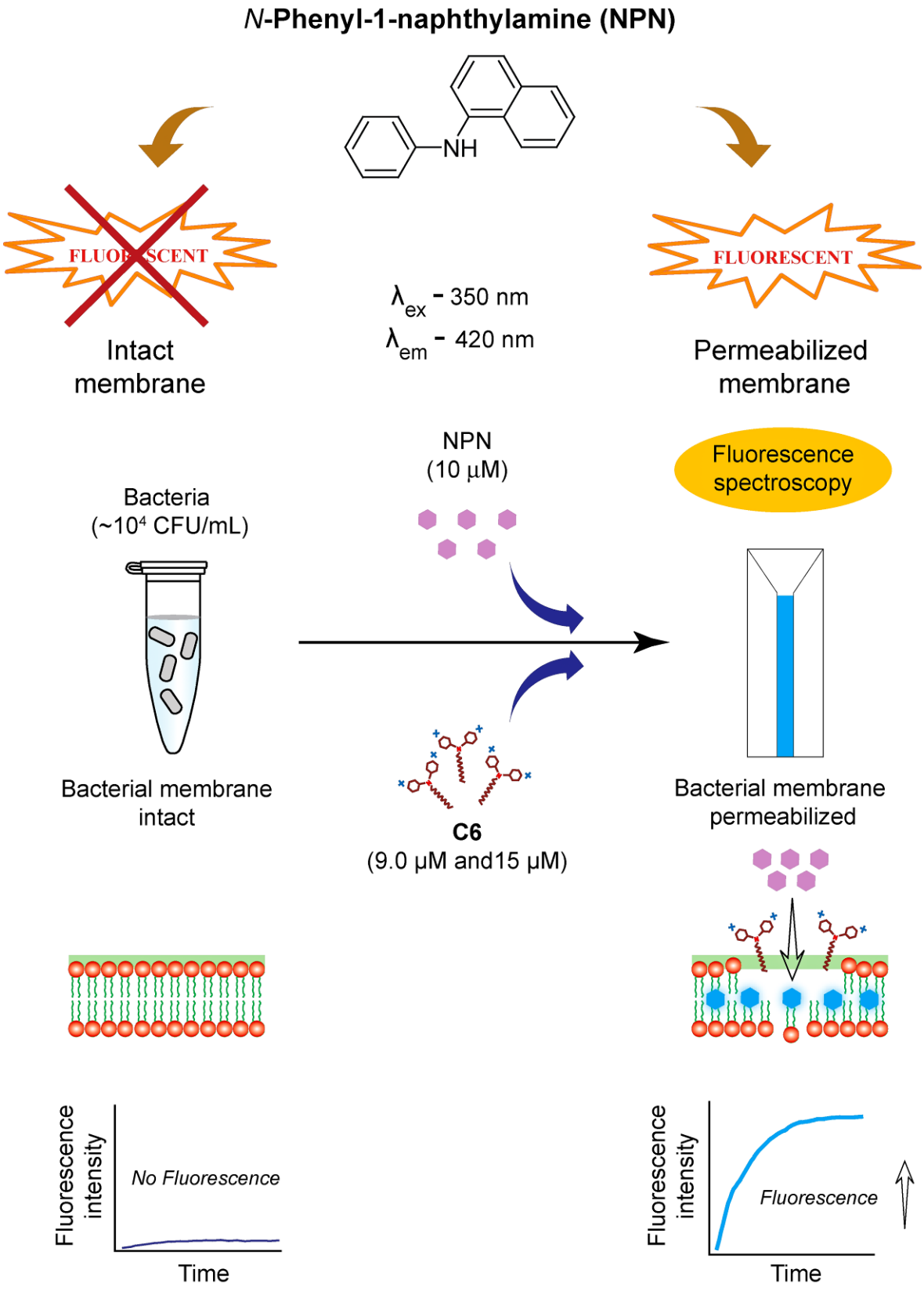

Figure 3.1. Schematic representation of experimental protocol for NPN assay.

control sample, cells treated with polymyxin B (1.0 µg/mL) was included. Fluorescence measurements were taken for three independent samples in a spectrofluorimeter (FluoroMax-3, HORIBA) at an excitation and emission wavelength of 350 nm and 420 nm, respectively. A schematic of the NPN assay is indicated in Figure 3.1.

3.2.5. Bactericidal Activity of Erythromycin, Polymyxin B and Ciprofloxacin in Combination with ***Compound 6***

To determine the potential of **C6** as a therapeutic adjuvant, the bactericidal activity of erythromycin and polymyxin B in combination with the amphiphile was ascertained against Gram-negative bacteria (*E. coli* MTCC 433 and *E. aerogenes* MTCC 2822) and Gram-positive bacteria (*S. aureus* MTCC 96 and *Listeria monocytogenes* Scott A), respectively. Likewise, the antibacterial activity of ciprofloxacin was also determined in combination with **C6** against *S. aureus* MTCC 96. Initially a 10 µL aliquot of bacterial cell suspension (10^6 CFU of the respective target bacteria suspended in sterile PBS) were inoculated in separate sets into sterile microtitre plate wells having requisite growth media (100 µL) incorporated with a serial two fold dilution of either erythromycin (5.0 µg/mL - 320 µg/mL) or polymyxin B (5.0 µg/mL - 320 µg/mL) or ciprofloxacin (1.0 µg/mL - 0.03 µg/mL). For every concentration of erythromycin, polymyxin B or ciprofloxacin, varying concentrations of **C6** was used in combination, depending upon the MIC of the amphiphile for the respective target bacterial strains. Hence, two different sets of increasing **C6** concentrations (5.0 µM, 10 µM, 15 µM and 20 µM against Gram-negative bacteria and 1.5 µM, 3.0 µM, 4.5 µM and 6.0 µM for Gram-positive bacteria) was used in combination with antibiotics. The cells were incubated at 37°C and 180 rpm for 12 h. Bacterial growth was estimated by measuring absorbance at 600 nm in a microtitre plate reader (Infinite M200, TECAN, Switzerland) and expressed as percentage growth inhibition compared to untreated cells (cells grown in the absence of antibiotics and **C6**). In separate sets, the effect of varying concentrations of the antibiotics or **C6** alone on the growth of target bacteria was also ascertained. For every sample, three independent experiments were performed, each having three replicas. Fold decrease in the MIC of erythromycin, polymyxin B and ciprofloxacin in presence of **C6** were compared with that obtained in the absence of **C6**. Data analysis and calculation of standard deviation was

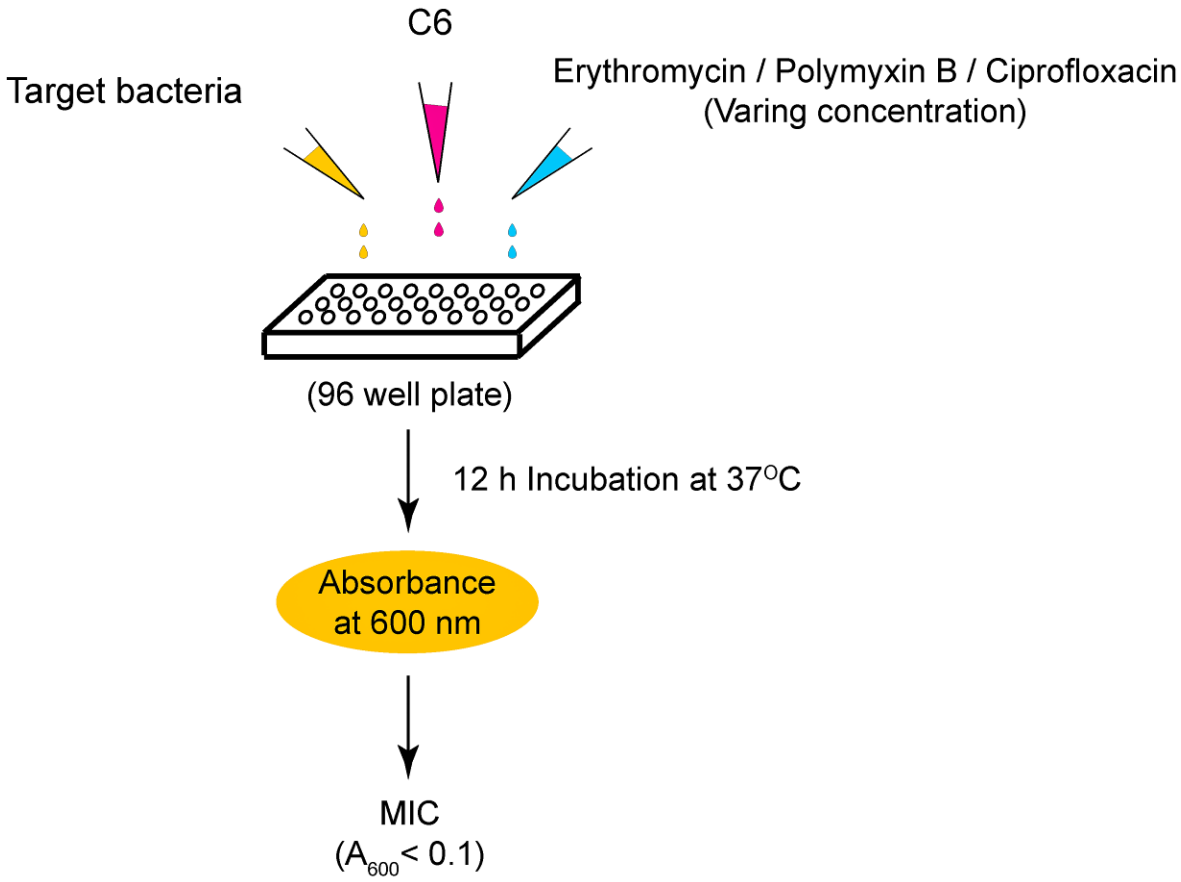

Figure 3.2. Schematic representation of the experimental protocol to study the combination effect of antibiotics and **C6** on target bacterial cells.

performed with Microsoft Excel 2010 (Microsoft Corporation, USA). A schematic representation of the experimental protocol to study the combination effect of antibiotics and **C6** on the target bacterial cells is shown in Figure 3.2.

3.2.6. Determination of Fractional Inhibitory Concentration (FIC) Index

The interaction of **C6** and the antibiotics erythromycin, polymyxin B or ciprofloxacin was quantified and expressed as the fractional inhibitory concentration (FIC) index.

FIC index was determined using the following expression:

$$FIC = \frac{[A]}{MIC_A} + \frac{[B]}{MIC_B}$$

where MIC_A and MIC_B represent the MIC of drug A (erythromycin, polymyxin B or ciprofloxacin) and drug B (**C6**), respectively. [A] and [B] are the MIC of drug A and drug B when used in combination. The interaction was interpreted as synergy (FIC ≤ 0.5), addition (FIC > 0.5 to 1.0), indifference (FIC >1.0 to <4.0) and antagonism (FIC ≥ 4.0) following the method described earlier (Giacometti et al. 2000).

*3.2.7. Antibacterial Activity of **Compound 6** in Simulated Gastric Fluid*

Model gastro-intestinal bacterial strains of *E. coli* MTCC 433 and *L. monocytogenes* Scott A were grown in the respective growth medium overnight under the conditions described previously in section 3.2.2. Cells were harvested by centrifugation from a 1.0 mL aliquot of the overnight grown culture, washed twice in sterile 0.85% saline to remove media ingredients and finally resuspended (10^6 CFU) in simulated gastric fluid (SGF), which was prepared according to the method described earlier (Charteris et al. 1998). The pH of SGF was adjusted to 2.5 with 1.0 N HCl. Subsequently, the cells were treated in SGF in separate sets with varying concentrations of **C6** (5.0 µM, 10 µM, 15 µM and 20 µM) at 37°C for 2 h. The control sample consisted of cells suspended in SGF alone under the same conditions. During incubation, the samples were withdrawn periodically and plated to determine the percentage of viable cells as compared to control (cells suspended in SGF alone). All experiments were performed in triplicates and a one way analysis of variance (ANOVA) was performed using Sigma Plot version 11.0.

*3.2.8. In vitro Resistance Studies with **Compound 6***

Development of spontaneous *in vitro* resistance in *S. aureus* MTCC 96 against **C6** was essentially determined by following a standard method described earlier (Locher et al. 2014, Uday et al. 2014). Briefly, the target bacterial strain was grown in the presence of 2 × MIC - 16 × MIC of **C6**. Enumeration of *S. aureus* MTCC 96 colonies was accomplished on BHI-agar plates following an incubation of 48 h at 37°C. Amongst the

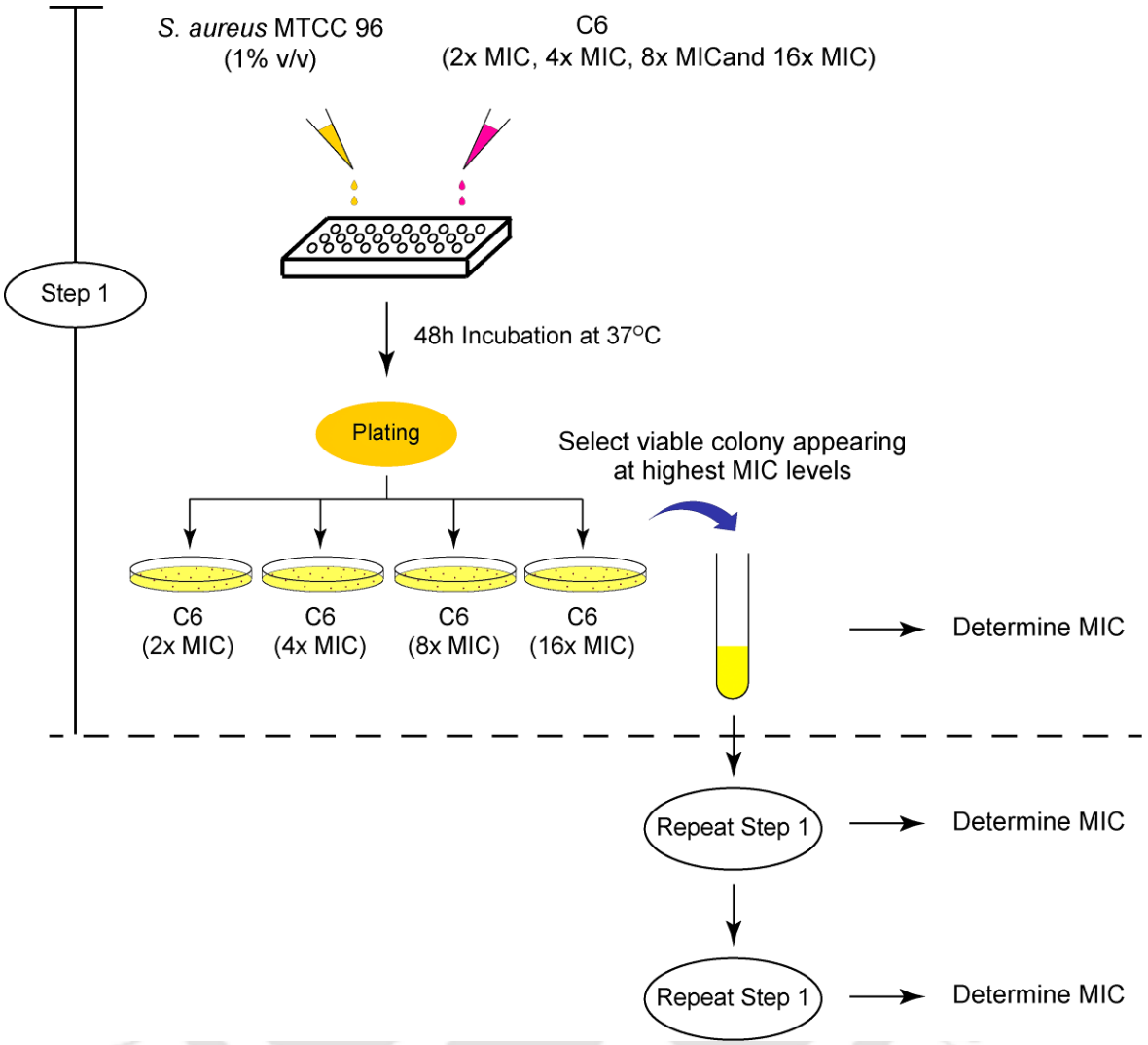

Figure 3.3. Schematic representation of the experimental protocol to study multistep *in vitro* resistance development in presence of **C6**.

samples treated with various MIC levels of **C6**, a viable colony appearing in the plate bearing the highest level of the amphiphile was selected and used to prepare the inoculum for the subsequent resistance selection step and this procedure was repeated for three independent steps. Further, for every step a single colony from the sample treated with the highest concentration of **C6** was isolated and purified by three passages in **C6**-free media and then the MIC of **C6** was determined using a standard method as described in section 2.2.5. A schematic illustration of the experimental steps to ascertain *in vitro* resistance development against **C6** is indicated in Figure 3.3.

3.3. Results and Discussion

*3.3.1. Bactericidal Activity of Antibiotics in Combination with **Compound 6***

Conventional antibiotic-based therapy for elimination of pathogenic bacteria is confronted with formidable challenges. The crux of the problem is the presence of an outer membrane permeability barrier in Gram-negative bacteria (Bolla et al. 2011, Hancock 1997, Nikaido 2003, Delcour 2009), which enables the bacteria to resist the action of therapeutic antibiotics. On the other hand, the cell wall in Gram-positive bacterial strains is predominantly composed of a thick peptidoglycan layer, which forms a strong protective barrier (Weidenmaier and Peschel 2008, Kohler, Weidenmaier, and Peschel 2009). In this regard, bactericidal agents that target the membrane are conceived to be efficient in rendering enhanced uptake of antibiotic, which eventually leads to efficient elimination of the target bacteria (Alakomi et al. 2006, Adhikari et al. 2013, Giacometti et al. 2000, Saha et al. 2008, Gill et al. 2015). Earlier studies with **C6** (highlighted in Chapter 2) revealed that the amphiphile could induce copious membrane disruption in target bacteria. This observation was encouraging and it suggested that **C6** can perhaps contravene the membrane in target bacteria and thereby predispose the cells to the action of certain therapeutic antibiotics.

In an NPN uptake assay, it was observed that treatment of Gram-negative *E. coli* MTCC 433 with **C6** resulted in a time-dependent enhancement of NPN fluorescence followed by a plateau, which suggested outer membrane permeabilization in amphiphile-treated cells (Rawlinson et al. 2010, Helander and Mattila-Sandholm 2000, Singh et al. 2012) and the magnitude of membrane permeabilization could be correlated with amphiphile concentration (Figure 3.4). Interestingly, the NPN uptake assay also suggested that **C6** could permeabilize the outer membrane of Gram-negative *E.coli* MTCC 433 at concentrations manifold below its MIC for the target bacteria. These findings motivated us to explore the possibility of using **C6** at low concentrations in combinatorial experiments in order to breach the membrane barrier in target bacteria and render enhanced bactericidal efficacy of therapeutic antibiotics. To this end, erythromycin, polymyxin B and ciprofloxacin were chosen as model therapeutic antibiotics. Erythromycin is a macrolide that acts on ribosomal 50S subunit and impedes the translocation step of protein synthesis by inhibiting peptidyltransferase reaction. It is a prototype hydrophobic therapeutic

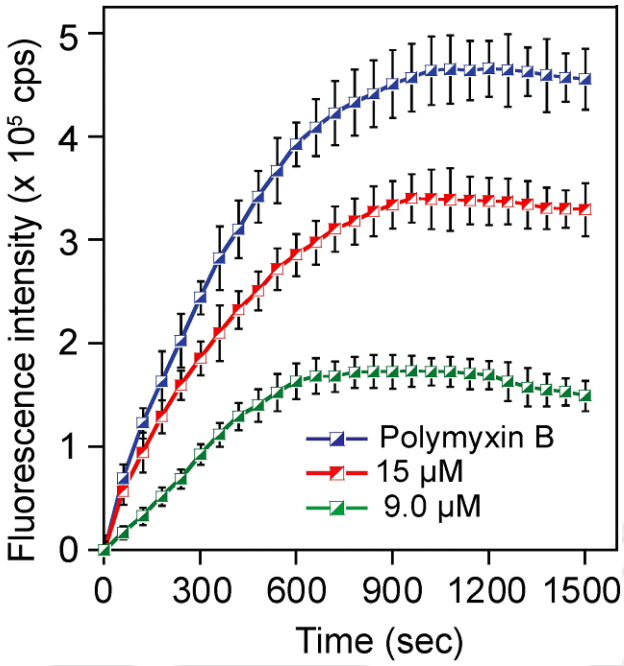

Figure 3.4. NPN uptake assay for the assessment of membrane permeabilization in *E.coli* MTCC 433 cells treated with varying concentrations of **C6**. Cells treated with 1.0 µg/mL polymyxin B were used as positive control.

antibiotic. It has been widely reported that uptake of a hydrophobic antibiotic such as erythromycin may be hindered owing to the presence of the outer membrane permeability barrier in Gram-negative bacteria (Saha et al. 2008, Rawlinson et al. 2010, Choi and Lee 2012, Ulvatne et al. 2001). Ciprofloxacin is a second generation fluoroquinolone, which targets DNA gyrase (topoisomerase II and IV) leading to inhibition of DNA replication and transcription. It has been reported that bacterial strains that possess specific efflux pumps on cell membrane can elude the bactericidal effect of ciprofloxacin (Fair and Tor 2014). Polymyxin B is an amphipathic cationic peptide primarily effective against Gram-negative bacteria and to a much lesser extent, against Gram-positive bacteria, possibly due to the thick peptidoglycan (Vaara 2010).

Table 3.1. Minimum inhibitory concentration (MIC) of erythromycin, polymyxin B and ciprofloxacin against target bacterial strains.

Target Bacteria	Antibiotics		
	Erythromycin MIC (μg/mL) / (μM)	Polymyxin B MIC (μg/mL) / (μM)	Ciprofloxacin MIC (μg/mL) / (μM)
E.coli MTCC 433	80 / 109	ND	ND
E. aerogenes MTCC 2822	80 / 109	ND	ND
S. aureus MTCC 96	ND	160 / 115.5	0.5 /1.3
L. monocytogenes Scott A	ND	320 /231	ND

ND: Not determined

Prior to combination experiments, the MIC of the selected antibiotics was determined against the respective target bacterial strains (Table 3.1). Subsequently combination experiments with **C6** and the antibiotics were pursued. The results of these experiments are described in the following sections:

*3.3.1.1. Antibacterial Activity of Erythromycin in Combination with **Compound 6***

As observed in Figure 3.5, treatment of the Gram-negative target bacteria with varying levels of **C6** alone (5.0 μM - 20 μM) resulted in 11% - 33% growth inhibition in case of *E. coli* MTCC 433 and around 7% - 26% growth inhibition for *E. aerogenes* MTCC 2822. Upon treatment with 10 μg/mL erythromycin alone, growth of the target bacteria was curtailed leading to 34% - 35% growth inhibition. Interestingly, a systematic increase in growth inhibition of the target bacteria was observed when the cells were treated with 10 μg/mL erythromycin in combination with increasing concentrations of **C6** (Figure 3.5). It may be mentioned here that the concentration of **C6** used in these experiments (5.0 μM, 10 μM, 15 μM and 20 μM) was manifold lower than the MIC of **C6** for the respective bacteria. At the highest concentration of **C6** (20 μM), a combinatorial treatment with

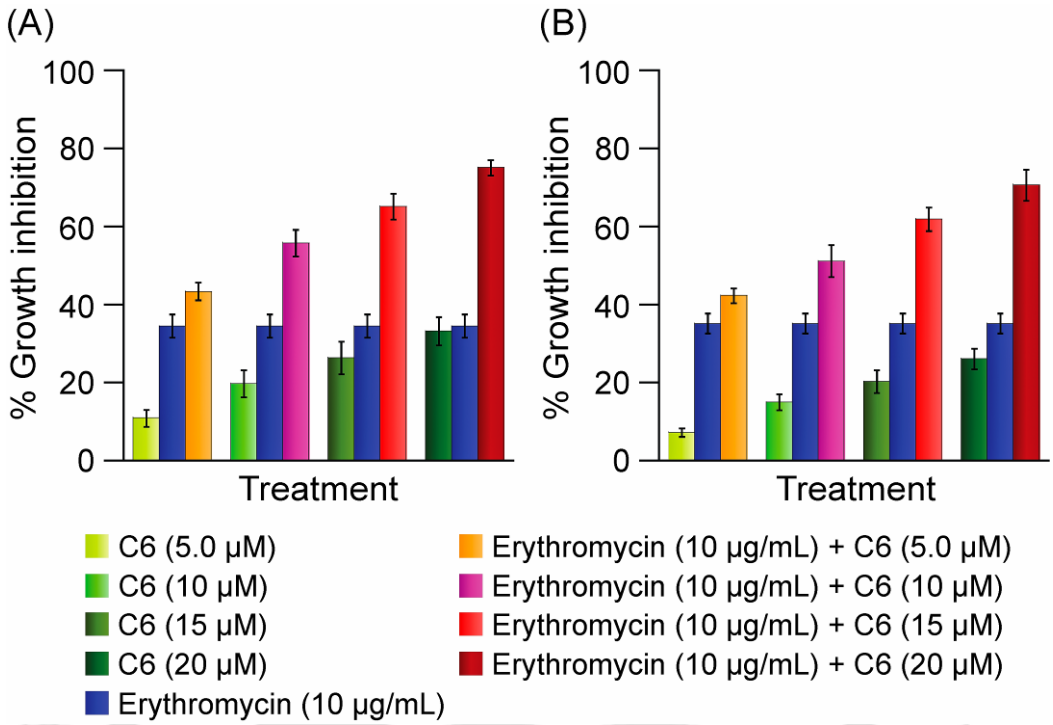

Figure 3.5. Effect of combinatorial treatment of **C6** and erythromycin on the growth of (A) *E. coli* MTCC 433 and (B) *E. aerogenes* MTCC 2822.

Table 3.2. Fold reduction in MIC of erythromycin in combination with **C6** and determination of FIC index.

Target bacteria	C6 (µM)	Fold reduction in MIC of erythromycin	FIC index[a]	Effect[b]
E. coli MTCC 433	5.0	2.0	0.58	A
	10	4.0	0.4	S
	15	4.0	0.48	S
	20	8.0	0.43	S
E. aerogenes MTCC 2822	5.0	0	1.06	I
	10	2.0	0.62	A
	15	2.0	0.68	A
	20	4.0	0.5	S

[a] FIC index was assessed as described in section 3.2.6. [b] A: Addition; S: Synergy.

10 μg/mL erythromycin resulted in considerable growth inhibition for *E.coli* MTCC 433 and *E. aerogenes* MTCC 2822 (Figure 3.5). The superior growth inhibition in case of combination therapy of **C6** and erythromycin was also evident for various other combinations (refer to Appendix, Figure A.3.1). Interestingly, the MIC of erythromycin was reduced when an increasing concentration of **C6** was used in combination treatment. For instance, in the presence of 20 μM of **C6**, the MIC of erythromycin was decreased eight-fold in the case of *E. coli* MTCC 433 and four-fold for *E. aerogenes* MTCC 2822 (Table 3.2). It is plausible that **C6** enhanced the membrane permeability in Gram-negative target bacteria as evident in the NPN uptake assay (Figure 3.4), which perhaps resulted in increased uptake of erythromycin and superior access of internal targets for the antibiotic. At the highest concentration of **C6** (20 μM), a synergistic interaction was evident between the amphiphile and erythromycin based on the FIC index (Table 3.2). The observed synergistic effect is perhaps a combined effect of facilitated access to the cytoplasmic target for erythromycin and concomitant membrane damage induced by **C6** itself.

*3.3.1.2. Antibacterial Activity of Polymyxin B in Combination with **Compound 6***

Polymyxin B is a therapeutic antibiotic used for cell membrane-permeabilization. It is largely known for its potent bactericidal activity against Gram-negative pathogenic bacteria while Gram-positive bacteria are mostly resistant (Zavascki et al. 2007). Based on the strong membrane-targeting activity of **C6**, it was anticipated that this amphiphilic molecule could perhaps be explored to augment the activity of polymyxin B against Gram-positive bacteria. Upon treatment with increasing concentrations of **C6** alone (1.5 μM, 3.0 μM, 4.5 μM and 6.0 μM) the growth inhibition observed for the target bacteria varied from 12% - 36% for *S. aureus* MTCC 96 and 9% - 31% for *L. monocytogenes* Scott A, respectively (Figure 3.6). On the other hand, treatment with 20 μg/mL polymyxin B alone could render around 19% growth inhibition in *S. aureus* MTCC 96 and 8% growth inhibition in case of *L. monocytogenes* Scott A (Figure 3.6). In the combination experiments, the higher growth inhibition of the target bacteria could be readily observed. For instance, treatment with a combination of 6.0 μM **C6** and 20 μg/mL polymyxin B resulted in around 69% and 42.5% growth inhibition in *S. aureus* MTCC 96 and

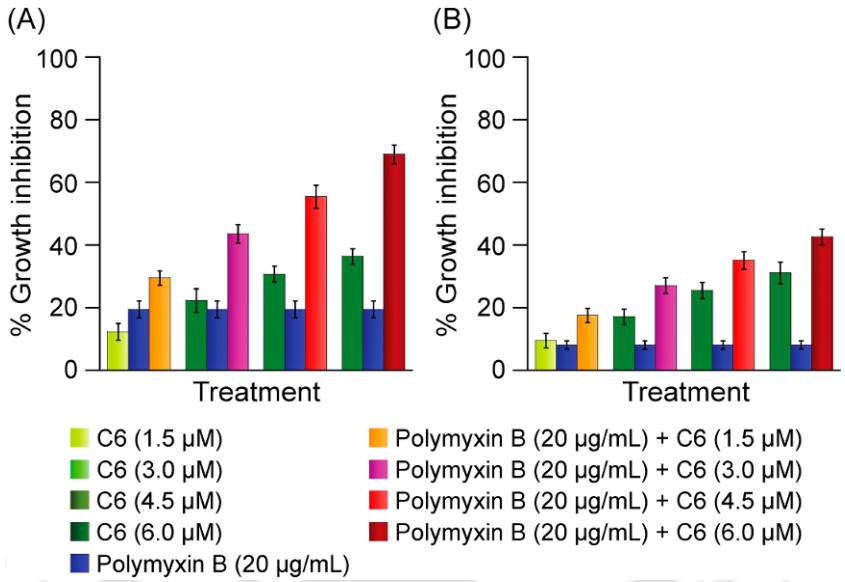

Figure 3.6. Effect of combinatorial treatment of **C6** and polymyxin B on the growth of (A) *S. aureus* MTCC 96 and (B) *L. monocytogenes* Scott A.

Table 3.3. Fold reduction in MIC of polymyxin B in combination with **C6** and determination of FIC index.

Target bacteria	C6 (µM)	Fold reduction in MIC of polymyxin B	FIC index[a]	Effect[b]
S. aureus MTCC 96	1.5	2	0.6	A
	3.0	2	0.68	A
	4.5	4	0.53	A
	6.0	8	0.5	S
L. monocytogenes Scott A	1.5	0	1.1	I
	3.0	2	0.68	A
	4.5	2	0.78	A
	6.0	4	0.63	A

[a] FIC index was assessed as described in section 3.2.6. [b] A: Addition; S: Synergy

L. monocytogenes Scott A, respectively (Figure 3.6). This inhibitory effect was also evident in various other combination experiments (refer to Appendix, Figure A3.2).

In case of *S. aureus* MTCC 96, the MIC of polymyxin B was reduced eightfold in combination with 6.0 µM of **C6** and the nature of interaction was synergistic based on the FIC index (Table 3.3). On the other hand, for *L. monocytogenes* Scott A, the MIC of polymyxin B was reduced fourfold in combination with 6.0 µM of **C6** and the interaction was additive (Table 3.3).

3.3.1.3. Antibacterial Activity of Ciprofloxacin in Combination with ***Compound 6***

Experiments were also conducted to determine the effect of varying concentrations of **C6** on the bactericidal activity of ciprofloxacin. In the presence of varying concentrations of **C6** (1.5 µM, 3.0 µM, 4.5 µM and 6.0 µM) the growth inhibition observed for *S. aureus* MTCC 96 varied from 11%-38% (Figure 3.7). On the other hand, treatment with 0.125 µg/mL ciprofloxacin alone resulted in around 39% growth inhibition for *S. aureus* MTCC 96 (Figure 3.7). Interestingly, in the combination studies, the presence of **C6** promoted ciprofloxacin-mediated inhibition of bacterial growth. For instance, treatment of *S. aureus* MTCC 96 cells with 0.125 µg/mL ciprofloxacin in combination with 6.0 µM **C6** lead to a dramatic 79% growth inhibition (Figure 3.7). This inhibitory effect was also evident in various other combination experiments (refer to Appendix, Figure A3.3).

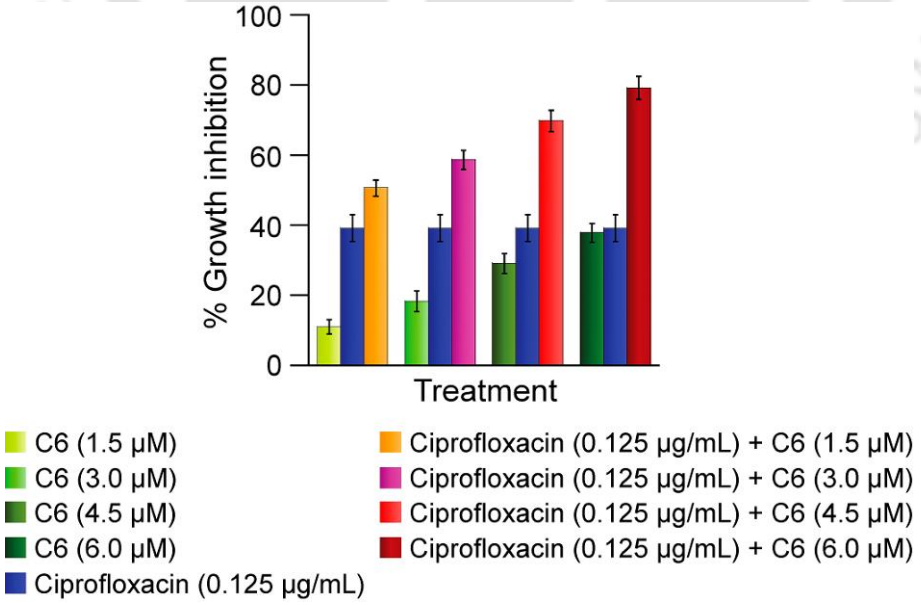

Figure 3.7. Effect of combinatorial treatment of **C6** and ciprofloxacin on the growth of *S. aureus* MTCC 96.

Table 3.4. Fold reduction in MIC of ciprofloxacin in combination treatment with **C6** and determination of fractional inhibitory concentration (FIC) index.

Target bacteria	**Compound 6** (μM)	Folds reduction in MIC of ciprofloxacin	FIC index[a]	Effect[b]
S. aureus MTCC 96	1.5	2	0.6	A
	3.0	2	0.68	A
	4.5	4	0.53	A
	6.0	4	0.63	A

[a] FIC index was assessed as described in section 3.2.6. [b] A: Addition

In presence of 6.0 μM **Compound 6** the MIC of ciprofloxacin against *S. aureus* MTCC 96 reduced fourfold and estimation of FIC index revealed an additive mode of interaction between **C6** and ciprofloxacin (Table 3.4). The combinatorial assays clearly demonstrated that at low concentrations, which do not render any cytotoxic effect, **C6** was able to breach the membrane barrier in target bacteria and emerge as an adjuvant for antibacterial chemotherapy with model antibiotics. From a therapeutic perspective, arbitrary and excessive use of antibiotics to eliminate pathogenic bacteria is detrimental. In this backdrop, the results obtained from the combinatorial assays are significant as they strongly demonstrate the possibility of minimizing the dose of antibiotics to eliminate target bacteria, when the antibiotics are used in combination with **C6**.

*3.3.2. Antibacterial Activity of **Compound 6** in Simulated Gastric Fluid (SGF)*

Elimination of gastrointestinal pathogens is a formidable challenge owing to the innate ability of these pathogens to survive in the harsh acidic environment prevalent in the gastric milieu. Although human gastric fluid is largely considered as a protective barrier against enteric pathogens owing to its acidic pH (Tamplin 2005), several enteric pathogens have acquired mechanisms to counter this and survive in the acidic ambience of the stomach (Foster 1999, 2004, Cotter, Gahan, and Hill 2000, Bavaro 2009, Richard and Foster 2004). Besides, an additional hindrance in the annihilation of acid-resistant pathogenic bacteria is that certain therapeutic antibiotics are rendered inactive in acidic

environment (George and Abraham 2006, Merrell and Camilli 2002, Lamp et al. 1992, Mercier et al. 2002). Given this backdrop, the bactericidal potential of **C6** was determined against model gastrointestinal bacteria *E.coli* MTCC 433 and *L. monocytogenes* Scott A cells suspended in SGF. In these experiments, the cells were treated with varying concentrations of **C6** (5.0 μM, 10 μM, 15 μM and 20 μM) for 2 h, since this duration is considered to be relevant in the context of gastric transit (Gorden and Small 1993). A dose-dependent loss in the viability of **C6**-treated cells was unequivocally observed for both the target bacteria (Figure 3.8A). Further, the viability of cells suspended in SGF alone for 2 h was virtually unaffected (Figure 3.8B), which suggested that the decrease in cell viability for **C6**-treated bacteria was not influenced by pH. It was also observed that the viable cells for both the target bacteria diminished progressively with time upon treatment with 20 μM **C6** in SGF (Figure 3.8B). The ability of **C6** to display bactericidal activity in the acidic pH and even in presence of the proteolytic enzyme pepsin in SGF highlighted the merit of the amphiphile as a potential chemotherapeutic agent against acid-resistant gastrointestinal pathogenic bacteria.

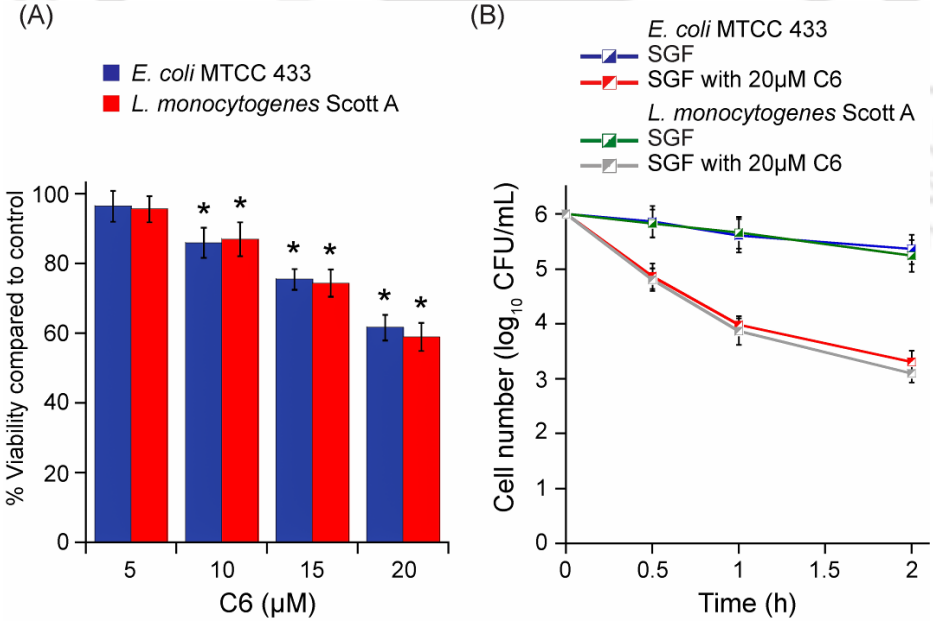

Figure 3.8. (A) Viability of target bacteria treated with **C6** in simulated gastric fluid. Statistically significant values derived by ANOVA are indicated by asterisk marks. * indicates *p* value <0.001. (B) Time-dependent bactericidal activity of 20 μM **C6** on target bacterial cells suspended in simulated gastric fluid.

3.3.3. In vitro Resistance Studies with ***Compound 6***

Drug-resistance is rampant and a natural phenomenon displayed by many pathogenic bacterial strains (Bush et al. 2011, Fair and Tor 2014, Nikaido 2009). It is conceived that on repeated exposure to an antimicrobial agent, bacterial strains have a propensity to acquire resistance. Staphylococcal strains are highly prevalent in hospitals and are considered as menacing nosocomial pathogens that pose significant public health concern (Hawkey and Jones 2009, Otto 2008). This predicament has assumed even more alarming proportions with the emergence of drug-resistant staphylococci (Fair and Tor 2014). Given that membrane-targeting agents are considered to be counterproductive to resistance development and hence hold considerable promise against drug-resistant *S. aureus* (Van Bambeke et al. 2008), it was pertinent to ascertain resistance development against **C6**, which demonstrated potent bactericidal activity against *S. aureus* MTCC 96 (as evident from the results highlighted in Chapter 2). To this end, a multiple step experiment was pursued to determine *in vitro* resistance development in *S. aureus* MTCC 96 cells against **C6**, wherein the cells were treated with the amphiphile for nearly 100 generations (in three steps). Interestingly, in every step the MIC of **C6** against *S. aureus* MTCC 96 was observed to be conserved (Table 3.5), which suggested a lack of resistance development in the target bacteria against the amphiphile.

Table 3.5. Minimum inhibitory concentration (MIC) of **C6** determined against *S. aureus* MTCC 96 in a multistep *in vitro* resistance development experiment.

Test compound	Selection step/Medium	MIC (μM) / OD_{600} ± standard deviation
C6	Step 1/ Agar	16/0.04 ± 0.003
C6	Step 2/ Agar	16/0.028 ± 0.003
C6	Step 3/ Agar	16/0.033 ± 0.006

3.4. Significant Findings

The salient findings of the present study are as follows:

1. The ability of **C6** to permeabilize the membrane barrier in target bacteria was established through NPN-based fluorescence assay.

2. The membrane-directed activity of **C6** was successfully explored in sensitizing target bacteria and thereby enhancing the bactericidal efficacy of the model therapeutic antibiotics erythromycin, polymyxin B and ciprofloxacin.

3. In combinatorial assays with low concentrations of **C6**, a substantial reduction in the MIC of model therapeutic antibiotics against target bacteria could be observed. A synergistic interaction was evident when erythromycin and polymyxin B were used in combination with **C6**, whereas the interaction was additive when ciprofloxacin was deployed in combination with **C6**. Interestingly, the bactericidal activity of **C6** was evident even in a highly acidic and proteolytic environment of the simulated gastric fluid (SGF), which suggested the robust nature of the amphiphile.

4. The therapeutic potential of **C6** was validated as multistep experiments suggested an apparent lack of resistance against the amphiphile in target bacteria.

The profound membrane-directed bactericidal activity of **C6** in conjunction with its adjuvant potential, retention of its activity in the physiological environment such as SGF and a lack of resistance against the amphiphile in target bacteria were encouraging findings in this chapter. These interesting leads were significant motivating factors for exploring the potential of the amphiphilic **C6** in mitigating the challenge of bacterial biofilms. In the following chapter the potential of **C6** as an antibiofilm agent is discussed.

Chapter 4

Antibiofilm Activity of Compound 6

This chapter highlights the antibiofilm activity of ***Compound 6*** *and its ability to potentiate the activity of tobramycin and gentamycin against established biofilms of P. aeruginosa and S. aureus.*

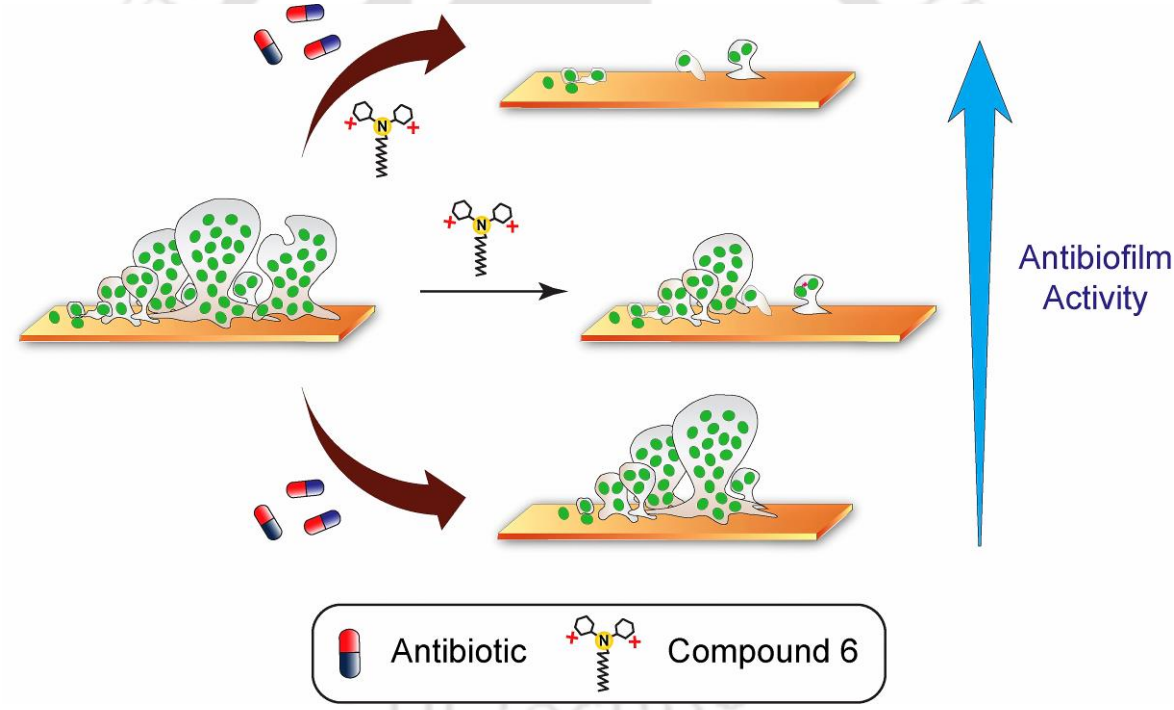

TH-1410_10610607

ABSTRACT

The high prevalence of biofilm-associated infections in conjunction with the remarkable resistance of bacterial biofilms towards therapeutic antibiotics underscores a critical demand for potent antibiofilm agents that can annihilate established biofilms. In present study, the antibiofilm potential of the dipyridinium-based cationic amphiphile (**C6**) was ascertained. A crystal violet assay revealed that **C6** could inhibit the formation of biofilms by *S. aureus* MTCC 96 and *P. aeruginosa* MTCC 2488 and this phenomenon could be correlated with the concentration of the amphiphile. Interestingly, the amphiphilic **C6** could render effective annihilation of established biofilm of *S. aureus* and *P. aeruginosa*, as estimated by MTT, crystal violet and congo red-based colorimetric assays. The efficacy of **C6** in the eradication of pre-formed biofilm was also captured in AFM and FESEM analysis. Additional evidence for **C6**-mediated disintegration of highly structured biofilm network, obliteration of the biofilm matrix and membrane damage in biofilm-associated cells was acquired through fluorescence microscope analysis using dyes such as cFDA-SE, congo red and PI. Interestingly, it was observed that the membrane-directed activity of **C6** could be leveraged to sensitize *P. aeruginosa* MTCC 2488 and *S. aureus* MTCC 96 biofilms to the action of the therapeutic antibiotics tobramycin and gentamycin, respectively. Based on the results, the synthetic amphiphile **C6** emerges as a potent antibiofilm material with therapeutic potential.

4.1. Introduction

Bacterial biofilms comprise a highly organized cluster of cells that exhibit an intrinsic capacity of adhesion to a surface and secrete an extracellular polymeric matrix that shields the embedded cells (Archer et al. 2011, Flemming and Wingender 2010, Kostakioti et al. 2013, Costerton et al. 1999, Donlan and Costerton 2002) Biofilm formation is considered as an alternate lifestyle and a survival strategy, which is adopted by microorganisms in order to deal with stress conditions in a hostile environment such as nutritional deprivation, resistance against the action of antibiotics and evading host immune defenses (Donlan and Costerton 2002, Bordi and de Bentzmann 2011, Hall-Stoodley et al. 2004) Amongst the bacterial strains, the most prevalent and clinically significant biofilm-forming bacteria include *Staphylococcus aureus*, *Staphylococcus epidermidis* and *Pseudomonas aeruginosa* (Otto 2008, Donlan 2009, Singh, Arora, et al. 2012, Mann and Wozniak 2012). Bacterial biofilms are implicated in a phenomenal number of microbial infections (over 80%), which includes periodontitis, endocarditis, cystic fibrosis, conjunctivitis, otitis, urethritis and chronic wound infections (Parsek and Singh 2003, Wagner and Iglewski 2008, Gomez and Prince 2007, James et al. 2008, Lebeaux et al. 2013, Worthington et al. 2012). Furthermore, on the basis of their proclivity to colonize indwelling medical devices such as vascular and urinary catheters, bacterial biofilms have emerged as significant players in device-associated nosocomial infections (Arciola et al. 2012, Hetrick and Schoenfisch 2006, Trautner and Darouiche 2004).

With regard to mitigation of biofilm-associated chronic infections, a particularly formidable challenge is the elimination of matrix-embedded sessile bacteria, which exhibit a remarkable resistance against the action of therapeutic antibiotics (Kostakioti et al. 2013, Hoiby et al. 2010). The extracellular polymeric matrix of biofilms is also regarded as a significant barrier that hinders effective passage of antibiotics (Flemming and Wingender 2010, Kostakioti et al. 2013, Bordi and de Bentzmann 2011, Otto 2008). In addition, metabolically inactive persister cells in biofilm are recalcitrant and defy the action of certain antibiotics, which are known to act essentially on growing cells (Stewart and Costerton 2001, Fux et al. 2005). Owing to the serious healthcare concern associated with bacterial biofilms and the remarkable resistance displayed by biofilms towards known antimicrobial agents, development of small synthetic antibiofilm agents has received

significant impetus (Broderick et al. 2013, Worthington et al. 2012, Geske et al. 2005, Bottcher et al. 2013, Bunders et al. 2011, Slomberg et al. 2013). However, from a clinical standpoint, a bigger challenge is in the mitigation of chronic infections caused by established biofilms, which are highly resistant to the action of common therapeutic antibiotics (Kostakioti et al. 2013). The crux of the problem is in the availability of molecules that can display bactericidal activity in the complex niche of the biofilm matrix and abolish mature biofilms. In this regard, synthetic antibacterial agents that can invade the biofilm matrix, and act on indispensible bacterial targets such as the membrane are promising candidates.

Given this backdrop, it was conceived that the low molecular weight synthetic cationic amphiphile **C6** can perhaps be considered as a potential chemotherapeutic agent as the amphiphile is likely to pervade through the biofilm matrix, gain access to the encased cells based on its innate affinity to interact with anionic bacterial cell surface and eliminate the target cells by triggering extensive membrane damage. Based on this rationale, the potential of **C6** in inhibiting the formation of *S. aureus* MTCC 96 and *P. aeruginosa* MTCC 2488 biofilms is ascertained in this chapter. The ability of **C6** to eradicate *S. aureus* and *P. aeruginosa* biofilms alone as well as in combination with therapeutic antibiotics is also discussed in this chapter.

4.2. Materials and Methods

4.2.1. Growth Media and Chemicals

Nutrient Broth (NB), Brain-Heart Infusion (BHI) broth and crystal violet (CV) dye were procured from HiMedia, Mumbai, India. Dimethyl sulfoxide (DMSO) and glutaraldehyde were obtained from Merck, India. N-2-Hydroxyethyl piperazine-N-2-ethane sulphonic acid (HEPES buffer) was procured from Sisco Research Laboratories SRL, Mumbai, India. 5 (and 6)-carboxyfluorescein diacetate succinimidyl ester (cFDA-SE), propidium iodide (PI), congo red (CR), gentamicin, tobramycin, Dulbecco's Modified Eagle Medium (DMEM), trypsin-EDTA, 3-(4, 5-dimethyl-2-thiazolyl)-2,5- diphenyl-2H-tetrazolium bromide (MTT), paraformaldehyde and Triton X-100 were procured from Sigma-Aldrich. Fetal bovine serum (FBS) was procured from PAA Laboratories, USA.

4.2.2. Bacterial Strains and Growth Conditions

In the present investigation, Gram-positive *S. aureus* MTCC 96 and Gram-negative *P. aeruginosa* MTCC 2488 were chosen as model biofilm forming target bacteria. *S. aureus* and *P. aeruginosa* were grown in Brain-Heart Infusion (BHI) broth and Nutrient Broth (NB), respectively at 37ºC and 180 rpm for 12 h. They were cultured from frozen stocks and propagated in their respective media prior to their use in experiments.

4.2.3. Minimum Inhibitory Concentration (MIC) of Gentamicin and Tobramycin

MIC of gentamicin and tobramycin was determined against *S. aureus* MTCC 96 and *P. aeruginosa* MTCC 2488, respectively. A standard protocol was followed for determining MIC of the antibiotics as described in section 2.2.5. Briefly, the target bacterial strains were inoculated at 1% level in microtitre wells having the specific growth medium and grown overnight at 37ºC and 180 rpm in presence of varying concentrations of either gentamycin (2.0 µg/mL - 512 µg/mL) or tobramycin (0.0625 µg/mL - 160 µg/mL). The growth of the bacterial strains was monitored by measuring absorbance at 600 nm in a microtitre plate reader (Infinite M200, TECAN, Switzerland). MIC of the antibiotics was recorded as the lowest concentration, which resulted in an absorbance reading of <0.1 at 600 nm (A_{600} = <0.1). The MIC values for gentamicin and tobramycin were calculated from three independent experiments, each having three replicas. Data analysis and calculation of standard deviation was performed with Microsoft Excel 2010 (Microsoft Corporation, USA).

*4.2.4. Effect of **Compound 6** on the Growth of S. aureus MTCC 96 and P. aeruginosa MTCC 2488 Biofilm*

Biofilms of *S. aureus* MTCC 96 and *P. aeruginosa* MTCC 2488 were grown sterile in 96 well microtitre plate by following a standard protocol as described earlier (Musken et al. 2010). Biofilm of *S. aureus* MTCC 96 was grown in sterile 96 well microtitre plate in BHI medium incorporated with 0.25% glucose and varying concentrations of **C6** (5.0 µM - 60 µM) in separate sets. Biofilm of *P. aeruginosa* MTCC 2488 was grown in sterile 96 well microtitre plate in NB incorporated with varying concentrations of **C6** (30 µM - 400 µM) in separate sets. After 24 h of biofilm growth in static and humid condition at 37ºC,

the spent media from the microtitre plate wells was gently aspirated and the wells were washed thrice with sterile MilliQ water (200 µl) to remove non-adherent bacteria. The wells were air dried and 1.0% (v/v) crystal violet solution (150 µL) was added to each well and incubated for 45 min to stain the biofilm. The crystal violet stain incorporated by the biofilms was solubilized with 95% ethanol (200 µL) and the biofilm biomass was estimated by transferring the ethanol-solubilized dye solution from each well into fresh well and measuring absorbance at 595 nm in a microtiter plate reader (Infinite M200, TECAN, Switzerland). The minimum biofilm inhibitory concentration ($MBIC_{90}$) of **C6** was defined as the minimum concentration of the amphiphile that resulted in growth inhibition of the target biofilm ($A_{590} < 0.1$). All experiments were performed in triplicates. Data analysis and calculation of standard deviation was performed with Microsoft Excel 2010 (Microsoft Corporation, USA) and a one way analysis of variance (ANOVA) was performed using Sigma Plot.

4.2.5. Antibiofilm Activity of ***Compound 6***

The antibiofilm activity of **C6** was ascertained against *S. aureus* MTCC 96 and *P. aeruginosa* MTCC 2488 biofilms by performing MTT assay, crystal violet staining and congo red binding assay. A schematic representation of these assays is indicated in Figure 4.1. A description of the protocols for these assays is outlined in the following sections:

4.2.5.1. Estimation of Viability by MTT Assay

Biofilms of *S. aureus* MTCC 96 and *P. aeruginosa* MTCC 2488 were grown sterile in 96 well microtitre plate by following a standard protocol as described earlier. For the growth *S. aureus* biofilm, BHI media supplemented with 0.25% glucose was used and for the growth of *P. aeruginosa* biofilm, NB media was used. After 24 h of biofilm growth in static and humid condition at 37ºC, the spent media from the microtitre plate wells was gently aspirated and the biofilms were exposed to fresh growth media having varying concentrations of **C6** (5.0 µM - 60 mM for *S. aureus* biofilm and 30 µM - 400 µM for *P. aeruginosa* biofilm) and incubated for 24 h in a static and humid chamber at 37ºC. Untreated biofilms were also incubated under the same conditions as control. Subsequently, the media was removed from all the samples and the wells were washed

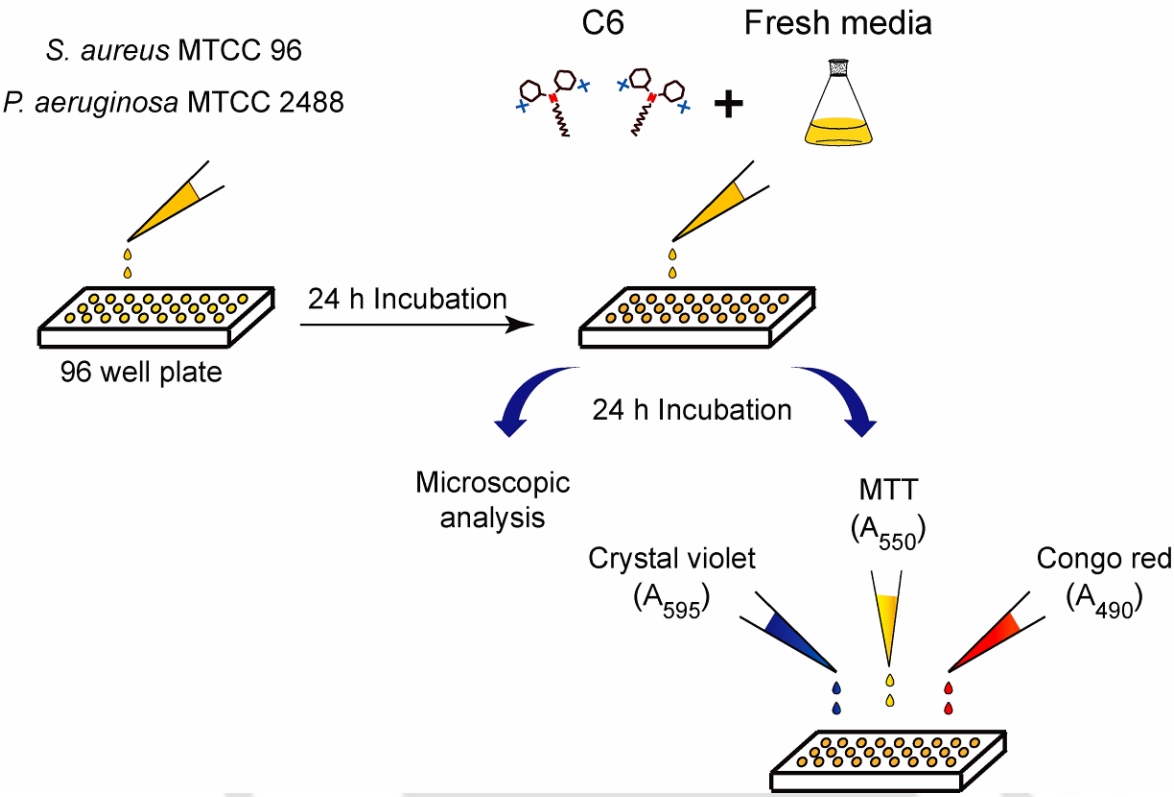

Figure 4.1. Schematic representation of the experimental protocol to study antibiofilm activity of **C6**.

with 200 µL sterile PBS to remove non-adherent planktonic bacterial cells. The wells were air dried and 100 µL of sterile requisite media containing MTT reagent (0.5 mg/mL) was added to each well of the microtiter plate and incubated for 2 h at 37°C. Subsequently, the MTT solution was aspirated and 100 µL of DMSO was immediately added to the wells to solubilize the formazan crystals formed in the wells. Following 15 min incubation at room temperature with brief mixing, the absorbance of the solution was measured at 550 nm using a microtiter plate reader (Infinite M200, TECAN, Switzerland). All experiments were performed in triplicates. Data analysis and calculation of standard deviation was performed with Microsoft Excel 2010 (Microsoft Corporation, USA) and a one way analysis of variance (ANOVA) was performed using Sigma Plot.

4.2.5.2. Estimation of Biofilm Biomass by Crystal Violet Staining

Biofilms of *S. aureus* MTCC 96 and *P. aeruginosa* MTCC 2488 were grown and treated with varying concentrations of **C6** with appropriate controls as described previously in section 4.2.5.1. Subsequently the media was removed and wells were washed with sterile PBS (200 µL) to remove non-adherent bacterial cells. The wells were air dried and 1.0 % (v/v) crystal violet solution (150 µL) was added to each well and incubated for 45 min to stain the biofilm. The crystal violet stain incorporated by biofilms was solubilized with 95 % ethanol (200 µL) and the biofilm biomass was estimated by transferring the ethanol-solubilized dye solution from each well into fresh well and measuring absorbance at 595 nm in a microtiter plate reader (Infinite M200, TECAN, Switzerland). The minimum biofilm eradication concentration ($MBEC_{90}$) of **C6** was defined as the minimum concentration of the amphiphile that resulted in annihilation of the target biofilm ($A_{590} < 0.1$). All experiments were performed in triplicates. Data analysis and calculation of standard deviation was performed with Microsoft Excel 2010 (Microsoft Corporation, USA) and a one way analysis of variance (ANOVA) was performed using Sigma Plot.

4.2.5.3. Estimation of Biofilm Extra-Polymeric Substance (EPS) by Congo Red Binding Assay

Biofilms of *S. aureus* MTCC 96 and *P. aeruginosa* MTCC 2488 were grown and treated with varying concentrations of **C6** with appropriate controls as described previously in section 4.2.5.1. Subsequently the media was removed and wells were washed with sterile PBS (200 µL) to remove non-adherent bacterial cells. The wells were air dried and the biofilm in each well was stained with 1.0 % congo red dye for 1.0 min. The excess dye was aspirated and the bound dye was solubilized in 200 µL of DMSO and its absorbance was measured at 490 nm. All experiments were performed in triplicates. Data analysis and calculation of standard deviation was performed with Microsoft Excel 2010 (Microsoft Corporation, USA) and a one way analysis of variance (ANOVA) was performed using Sigma Plot.

4.2.6. Atomic Force Microscope (AFM) Analysis

Glass cover slips (18 mm x 18 mm) were sterilized by immersion in sodium hypochlorite solution (0.5%) for 2 h and rinsed thoroughly with sterile MilliQ grade water. To initiate biofilm growth on the sterilized glass cover slips, they were then immersed in requisite growth medium (BHI medium supplemented with 0.25% glucose for *S. aureus* MTCC 96 biofilm and NB medium for *P. aeruginosa* MTCC 2488 biofilm) taken in separate sterile 35 mm petriplate and inoculated with the respective bacterial cell suspension (A_{600} = 0.02) and incubated for 24 h at 37ºC in a humid chamber. The glass cover slips with established *S. aureus* and *P. aeruginosa* biofilms were then incubated in fresh requisite medium incorporated with either 30 μM **C6** in case of *S. aureus* biofilm or 200 μM **C6** in case of *P. aeruginosa* biofilm at 37ºC in a humid chamber for 24 h. Subsequently, the media from the petriplate was aspirated and the amphiphile-treated as well as untreated glass cover slips (control biofilms) were washed gently with sterile MilliQ water to remove excess media and air dried. Atomic force microscope images were captured with an Agilent 5500 AFM (Agilent Technologies, Chandler, AZ, USA). Cantilevers made of silicon nitride were used having a resonant frequency of ca. 150 to 250 kHz. Images were acquired in non-contact mode, with 10 μm x 10 μm size at a scan rate of 0.5- 1.0 line/s. Analysis of the topographic images of the surface was accomplished by using the WSxM v5.0 Develop 6.5 image viewer software (Horcas et al. 2007).

4.2.7. Fluorescence Microscope Analysis

Biofilms of *S. aureus* MTCC 96 and *P. aeruginosa* MTCC 2488 were grown in sterile 96 well microtitre plate following the procedure described earlier in section 4.2.5.1. The biofilm samples were then treated with either 30 μM **C6** for 24 h in case of *S. aureus* biofilm or 200 μM **C6** for 24 h in case of *P. aeruginosa* biofilm. Subsequently, untreated biofilm samples (control) as well as **C6**-treated biofilm samples were subjected separately to labeling with cFDA-SE, congo red (CR) and PI in separate sets. cFDA-SE and PI staining of biofilms was accomplished by following a standard procedure described previously (Adhikari et al. 2013). CR staining was pursued by incubating the biofilms with1.0 % congo red dye for 1.0 min as described in section 4.2.4.3. The stained biofilms were then observed under a fluorescence microscope (Eclipse Ti-U, Nikon) with a filter

that allowed blue light excitation for cFDA-SE and green light excitation for PI and CR stained cells. Images of the treated and control biofilms were recorded.

4.2.8. Field Emission Scanning Electron Microscope (FESEM) Analysis

Biofilms of *S. aureus* MTCC 96 and *P. aeruginosa* MTCC 2488 were grown on sterile glass cover slips (18 mm x 18 mm) by following the procedure described earlier in section 4.2.6. The biofilm samples were then treated with either 30 μM **C6** for 24 h in case of *S. aureus* biofilm or 200 μM **C6** for 24 h in case of *P. aeruginosa* biofilm. Subsequently, the amphiphile-treated as well as control biofilm samples (untreated) were washed twice with sterile PBS to remove spent media and finally with sterile MilliQ grade water. The samples were then air-dried in laminar hood, examined in a field emission scanning electron microscope (Zeiss Sigma, USA) and their images were recorded.

4.2.9. Antibiofilm Activity of Gentamicin and Tobramycin in Combination with ***Compound 6***

The antibiofilm activity of gentamicin and tobramycin in combination **C6** was ascertained against *S. aureus* MTCC 96 and *P. aeruginosa* MTCC 2488 biofilms, respectively, by performing crystal violet staining, congo red binding assay and FESEM analysis. A schematic representation of these assays is indicated in Figure 4.2. A description of the protocols for these assays is outlined in the following sections:

4.2.9.1. Estimation of Biofilm Biomass and EPS

Biofilms of *S. aureus* MTCC 96 and *P. aeruginosa* MTCC 2488 were grown in sterile 96 well microtitre plate following a standard method described in section 4.2.5.1. The established *S. aureus* biofilm was subsequently incubated with varying combinations of gentamicin (5.0 μg/mL-30 μg/mL) and **C6** (3.0 μM, 6.0 μM, 9.0 μM, 12 μM and 15 μM) for 24 h at 37^{o}C in a humid chamber. *P. aeruginosa* biofilm was treated with tobramycin (0.08 μg/mL-0.625 μg/mL) in combination with **C6** (10 μM, 20 μM and 30 μM) for 24 h at 37^{o}C in a humid chamber. Subsequently the biofilm biomass and EPS in the samples were determined by crystal violet staining method and congo red binding assay as described in sections 4.2.5.2 and 4.2.5.3, respectively.

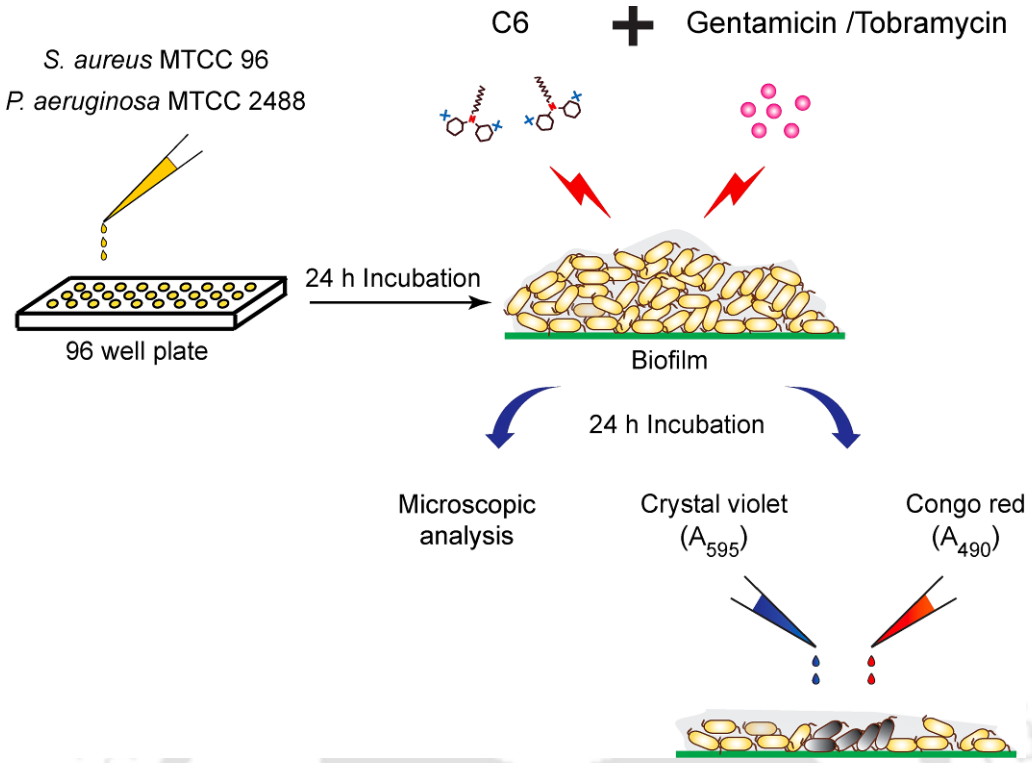

Figure 4.2. Schematic representation of the experimental protocol to study the combined effect of antibiotics and **C6** on target bacterial biofilm.

4.2.9.2. Field Emission Scanning Electron Microscope (FESEM) Analysis

Biofilms of *S. aureus* MTCC 96 and *P. aeruginosa* MTCC 2488 were grown on sterile glass cover slips (18 mm x 18 mm) by following the procedure described earlier in section 4.2.6. The established *S. aureus* and *P. aeruginosa* biofilms were subsequently treated with combinations of gentamicin and **C6** or tobramycin and **C6**, respectively as described in section 4.2.9.1. Subsequently, the untreated biofilm sample (control) and treated biofilm samples were examined in a field emission scanning electron microscope (Zeiss Sigma, USA) and their images were recorded.

*4.2.10. In vitro Cytotoxicity Assay for Combination of **Compound 6** and Tobramycin*

The potential cytotoxic effect of the combination of tobramycin and **C6** used against *P. aeruginosa* biofilm (the concentrations are mentioned in section 4.2.9.1) was ascertained by a standard MTT assay. HeLa cells were cultured in 25 cm^2 tissue culture flask in Dulbecco's Modified Eagle Medium (DMEM) supplemented with 10% (v/v) fetal

bovine serum (FBS), penicillin (100 µg/mL) and streptomycin (100 µg/mL) at 37°C under a humidified atmosphere of 5% CO_2 in an incubator. Subsequently the cells were seeded onto 96-well tissue culture plates at a density of 10^4 cells per well and incubated in separate sets with **C6** (10 µM, 20 µM and 30 µM) or tobramycin (0.08 µg/mL and 0.625 µg/mL) or a combination of **C6** (10 µM, 20 µM and 30 µM) and tobramycin (0.08 µg/mL and 0.625 µg/mL) made in DMEM for a period of 24 h. Untreated cells were also incubated in parallel sets. Following incubation, the media was carefully aspirated and fresh DMEM medium containing MTT solution (0.5 mg/mL) was added to the wells and the plates were further incubated for 4 h at 37ºC. Subsequently, the supernatant was aspirated and the insoluble formazan product was solubilized in DMSO and its absorbance was measured in a microtitre plate reader (Infinite M200, TECAN, Switzerland) at 550 nm. The MTT assay was performed in six sets for each sample. The absorbance obtained for untreated cells was assumed to represent 100% cell viability, and the absorbance for other samples were compared to that obtained for untreated cells in order to determine % cell viability. Data analysis and determination of standard deviation was performed with Microsoft Excel 2010 (Microsoft Corporation, USA).

4.3. Results and Discussion

*4.3.1. Effect of **Compound 6** on the Growth of Biofilm*

Initial interaction of planktonic cells with the surface of a substratum induced by relatively weak forces holds the key for transition from planktonic phase of growth to biofilm (Arciola et al. 2012, Archer et al. 2011, Kostakioti et al. 2013). Given the potent bactericidal activity of **C6**, it was envisaged that the amphiphile was likely to render a dose-dependent killing of planktonic cells at the onset of biofilm formation, which would culminate as a corresponding effect on the extent of biofilm growth. A crystal violet assay clearly revealed a systematic decrease in *S. aureus* MTCC 96 and *P. aeruginosa* MTCC 2488 biofilm growth, which could be correlated with the concentration of **C6** (Figure 4.3). The inhibitory effect of **C6** on *S. aureus* MTCC 96 biofilm could be captured at relatively lower amphiphile concentrations (Figure 4.3A) as compared to that observed in case of *P. aeruginosa* MTCC 96 biofilm (Figure 4.3B). The low MIC of **C6** for *S. aureus* MTCC 96. (16 µM) as opposed to its manifold higher MIC in case of

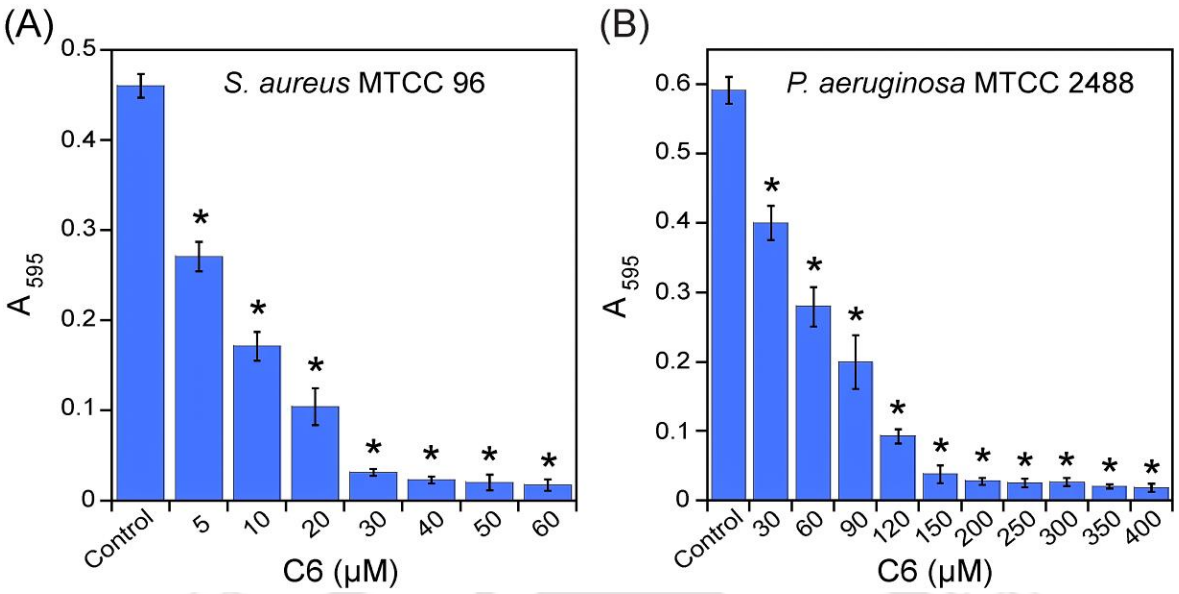

Figure 4.3. Crystal violet assay to ascertain the effect of varying concentrations of **C6** on the growth of (A) *S. aureus* MTCC 96 biofilm and (B) *P. aeruginosa* MTCC 2488 biofilm. Statistically significant values derived by ANOVA are indicated by asterisk marks. * indicates *p* value < 0.001.

Table 4.1. $MBIC_{90}$ and $MBEC_{90}$ values of **C6**, gentamicin and tobramycin.

Test compound	Target Bacteria					
	S. aureus MTCC 96			*P. aeruginosa* MTCC 2488		
	MIC (μM / μg/mL)	$MBIC_{90}$ (μM / μg/mL)	$MBEC_{90}$ (μM / μg/mL)	MIC (μM / μg/mL)	$MBIC_{90}$ (μM / μg/mL)	$MBEC_{90}$ (μM / μg/mL)
C6	16 / 10.42	30 / 19.5	60 / 39	128 / 83.35	200 /130	400 / 260
Gentamicin	32 / 67	64 / 134	128 / 268	ND	ND	ND
Tobramycin	ND	ND	ND	1.34 / 0.625	10.7 / 5.0	21.4 / 10

ND: Not determined

P. aeruginosa MTCC 2488 (128 μM) perhaps accounts for this phenomenon. Based on the crystal violet assay, the $MBIC_{90}$ of **C6** against *S. aureus* MTCC 96 biofilm and *P. aeruginosa* MTCC 2488 was estimated to be 30 μM and 200 μM, respectively (Table 4.1).

4.3.2. Antibiofilm Activity of ***Compound 6***

In the context of antibiofilm therapy, elimination of matrix-entrenched sessile bacteria, which defy the action of common therapeutic antibiotics, is a significant challenge (Kostakioti et al. 2013). The extracellular matrix in biofilms consisting of viscous polymeric substances constitutes a prominent diffusion barrier and has been implicated in sequestration and reduced bioavailability of antibiotics (Flemming and Wingender 2010). Given the high incidence of biofilm-associated chronic infections, antibiofilm agents that can prevail over this matrix-associated barrier and disrupt established biofilms are thus in great demand. Low molecular weight synthetic bactericidal molecules that can penetrate the biofilm matrix and establish contact with the entrenched cells emerge as potential candidates to accomplish this function. Earlier studies on **C6** clearly demonstrated the potent antibacterial activity of the amphiphile and unlike many antibiotics, which act on intracellular targets, **C6** can interact with bacterial cells and induce copious membrane disruption. It was thus envisaged that the cationic **C6** could perhaps be deployed for eradication of preformed biofilms as it is likely to infiltrate through the biofilm matrix, interact with the underlying anionic bacterial cells, and render large-scale membrane damage in cells as conceived in Figure 4.4.

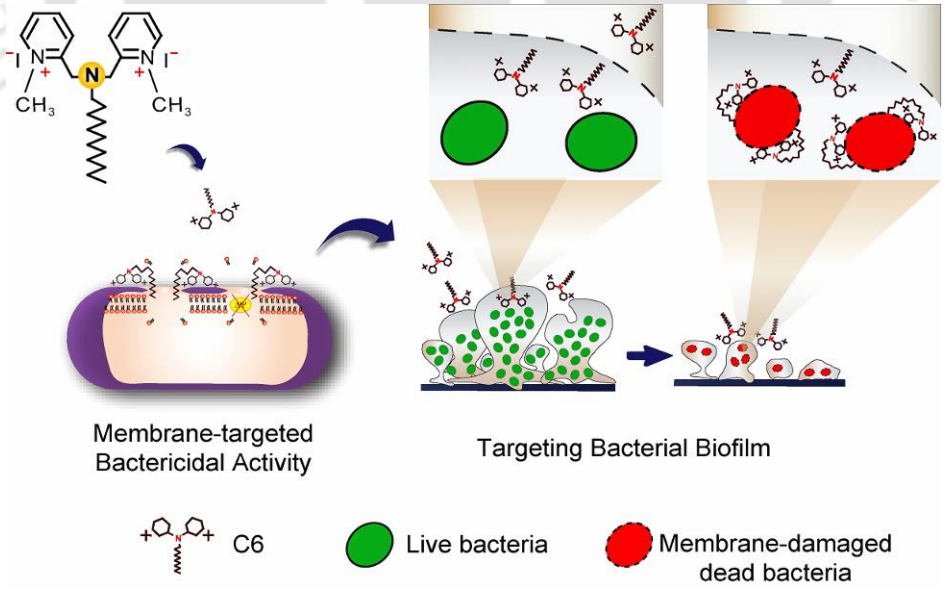

Figure 4.4. Cartoon illustrating the potential antibiofilm activity of the membrane-acting **C6.**

To validate this tenet, bacterial biofilm was grown in microtiter wells and then treated with varying concentrations of **C6**. A standard crystal violet-based colorimetric assay for biofilm biomass suggested a significant eradication of *S. aureus* and *P. aeruginosa* biofilm, which could be correlated with the dose of **C6** (Figure 4.5A-B). It may be mentioned that the concentration of the amphiphile required for elimination of *P. aeruginosa* biofilm was many fold higher compared to *S. aureus* biofilm. This perhaps originates from the intrinsic resistance typically associated with *P. aeruginosa* (Lambert 2002). The concentration-dependent eradication of preformed biofilms of *S. aureus* and *P. aeruginosa* by **C6** was corroborated by an MTT assay (refer to Appendix, Figure A4.1A-B). Annihilation of the established biofilm by **C6** was also validated by a congo red binding assay, which indicated a dose-dependent reduction of biofilm EPS matrix upon treatment with **C6** (refer to Appendix, Figure A4.1C-D). AFM imaging of *S. aureus* and *P. aeruginosa* biofilms was pursued to further ascertain the antibiofilm potential of **C6**. In case of untreated samples (control), compact protrusions and surface corrugations typically associated with dense biofilm architecture were evident in the three-dimensional topographic images (Figure 4.5C-D), amplitude channel, and two- dimensional topographic images (refer to Appendix, Figure A4.2A-B). The average height profiles for untreated *S. aureus* and *P. aeruginosa* biofilms were approximately ~508 nm and ~632 nm, respectively (refer to Appendix, Figure A4.2A-B). AFM images of *S. aureus* and *P. aeruginosa* biofilms treated with 30 μM and 200 μM **C6**, respectively, indicated significant abrasion of the biofilm structure and disaggregation of the cells (Figure 4.5C-D and refer to Appendix, Figure A4.2A-B), corroborated by a dramatic reduction in the average height profile, which was observed to be ~72 nm and ~237 nm for *S. aureus* and *P. aeruginosa* biofilm, respectively (refer to Appendix, Figure A4.2A-B). Fluorescence microscope analysis revealed a dense network of cFDA-SE stained *S. aureus* and *P. aeruginosa* biofilm, indicating the presence of a large number of viable and metabolically active cells in untreated biofilm (Figure 4.5E-F). Interestingly, upon treatment with **C6**, the biofilm architecture was largely disintegrated (Figure 4.5E-F).

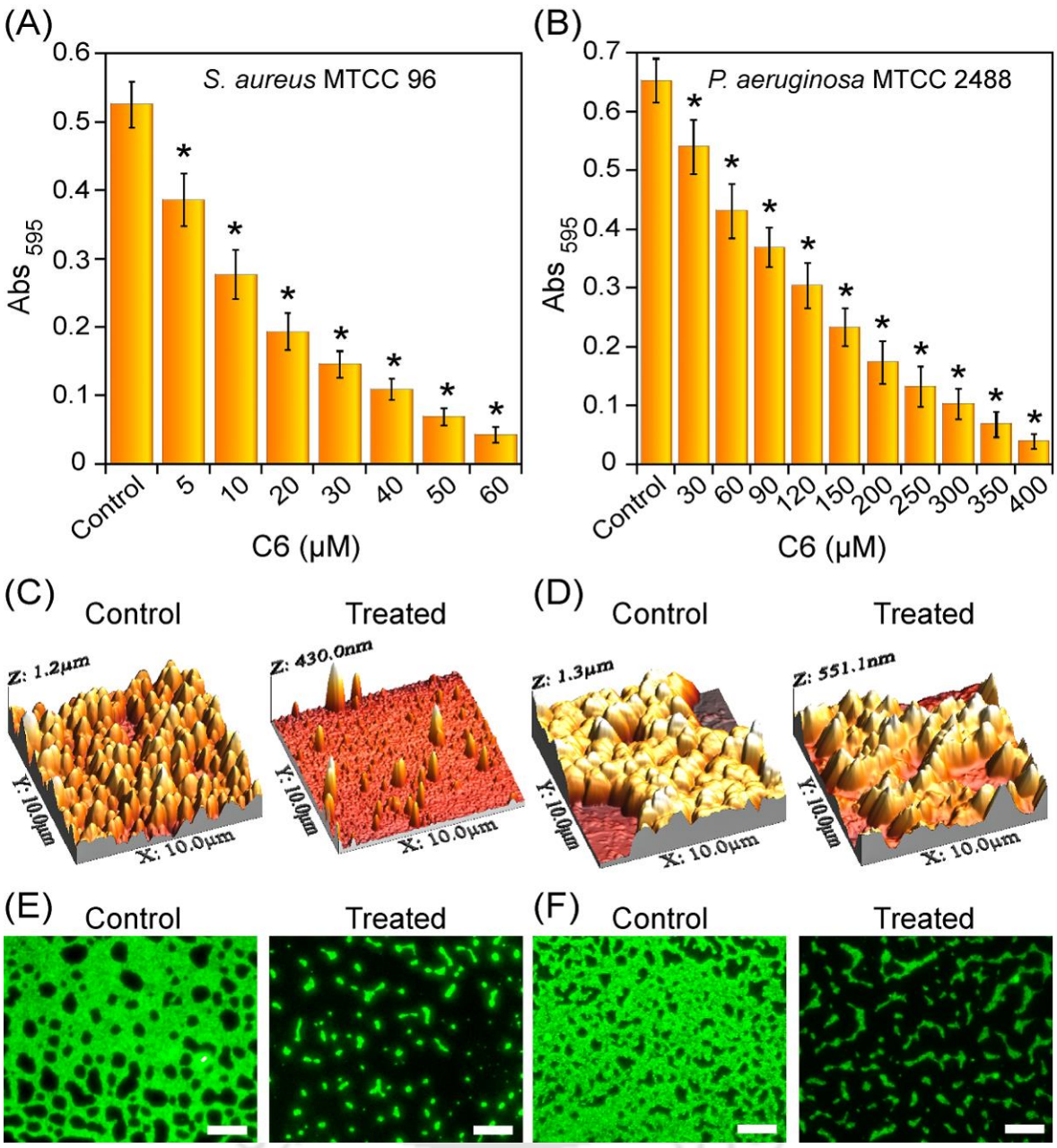

Figure 4.5. Crystal violet assay to assess the antibiofilm activity of **C6** against (A) *S. aureus* MTCC 96 biofilm and (B) *P. aeruginosa* MTCC 2488 biofilm. ∗ indicates the *p* value <0.001 in ANOVA. Three-dimensional topography AFM images of (C) *S. aureus* MTCC 96 biofilm (control and treated with 30 μM **C6**) and (D) *P. aeruginosa* MTCC 2488 biofilm (control and treated with 200 μM **C6**). AFM images are shown for an area of 10 μm × 10 μm. Fluorescence microscope analysis of cFDA-SE labeled (E) *S. aureus* MTCC 96 biofilm (control and treated with 30 μM **C6**) and (F) *P. aeruginosa* MTCC 2488 biofilm (control and treated with 200 μM **C6**). Scale bar for the images is 50 μm.

In FESEM analysis, it was evident that the organized cluster of cells, which is essentially an indication of cell-cell adhesion in case of untreated *S. aureus* biofilm, was severely impaired upon treatment with 30 μM **C6**, wherein the cells apparently lost their characteristic morphology and integrity (Figure 4.6). Eradication of *S. aureus* biofilm by **C6** was also captured through a dramatic reduction in the formation of extracellular EPS as ascertained by congo red staining (Figure 4.6). Furthermore, it was observed that **C6**-treated *S. aureus* biofilm displayed prominent PI staining (Figure 4.6), which suggested that the amphiphile could permeate through the extracellular biofilm matrix to reach the embedded cells and render large-scale membrane damage. Analogous results were also observed in FESEM analysis, congo red staining, and PI staining in the case of *P. aeruginosa* biofilm treated with **C6**. Collectively, the aforementioned results suggested that **C6** could readily pervade through the biofilm matrix, access the encased cells, and display its membrane-directed bactericidal activity even in the complex niche of the matrix, resulting in effective eradication of a preformed biofilm.

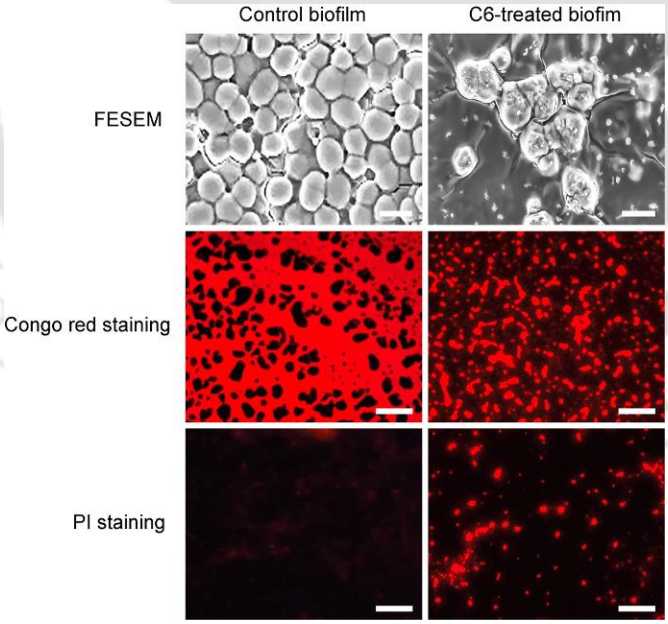

Figure 4.6. Antibiofilm activity of **C6** against *S. aureus* MTCC 96 biofilm assessed by FESEM analysis, congo red staining and PI staining. *S. aureus* biofilm was treated with 30 μM **C6**. Scale bar for FESEM and fluorescence microscope images are 1.0 μm and 50 μm, respectively.

4.3.3. Eradication of Biofilm by Antibiotics in Combination with ***Compound 6***

Bacterial biofilms display a remarkable resistance against conventional antibiotic-mediated therapy as compared to the planktonic cells and are thus largely implicated in chronic and intractable infections (Costerton et al. 1999, Davies 2003, Stewart 2002, Hogan and Kolter 2002, Church et al. 2006). For instance, biofilm of the opportunistic pathogen *Pseudomonas aeruginosa* is known to be associated with chronic lung infection in cystic fibrosis (CF) patients (Wagner and Iglewski 2008, Gomez and Prince 2007). Tobramycin is an aminoglycoside antibiotic, which is often deployed for mitigation of *P. aeruginosa* biofilm (Anderson et al. 2008). However, the presence of an extracellular matrix as a diffusion barrier and limited antibiotic penetration is a major bottleneck in tobramycin-mediated antibiofilm therapy (Tseng et al. 2013, Walters et al. 2003). In the present study, it was observed that **C6** at high concentrations (200 μM) prevailed over the matrix barrier and could eradicate established *P. aeruginosa* biofilm (Figure 4.5B). However, from a therapeutic standpoint, usage of such high concentrations of **C6** to eliminate *P. aeruginosa* biofilm is unsuitable as it may lead to unwarranted host cell toxicity as observed in the results described in Chapter 2 of the thesis. On the basis of its potent membrane-directed bactericidal activity, it was envisaged that **C6** can perhaps be used at low concentrations to sensitize the matrix encased cells of biofilm and render them vulnerable to the action of antibiotics in combination therapy. Combination therapy with bactericidal agents and antibiotics for alleviation of biofilm has been reported in previous studies (Rogers et al. 2010, Kim et al. 2008, Purdy Drew et al. 2009).

To ascertain the potential of combination therapy, treatment of established biofilms of *P. aeruginosa* and *S. aureus* by a combination of **C6** and tobramycin or gentamicin, respectively, was pursued. These antibiotics were chosen based on their known activity against the respective target bacteria (Anderson et al. 2008, Olson et al. 2011). Initially the MIC of **C6**, gentamicin, and tobramycin against the planktonic cells of respective target bacteria were determined (Table 4.1). Determination of the MICs essentially formed the basis for choosing the concentrations of **C6** and the antibiotics in the combination experiments. Treatment of *P. aeruginosa* biofilm with 10 μM - 30 μM **C6** resulted in 5.7%-21.5% eradication of biofilm biomass, respectively (Figure 4.7A-B).When *P. aeruginosa* biofilm was treated with 0.08 μg/mL and 0.625 μg/mL tobramycin,

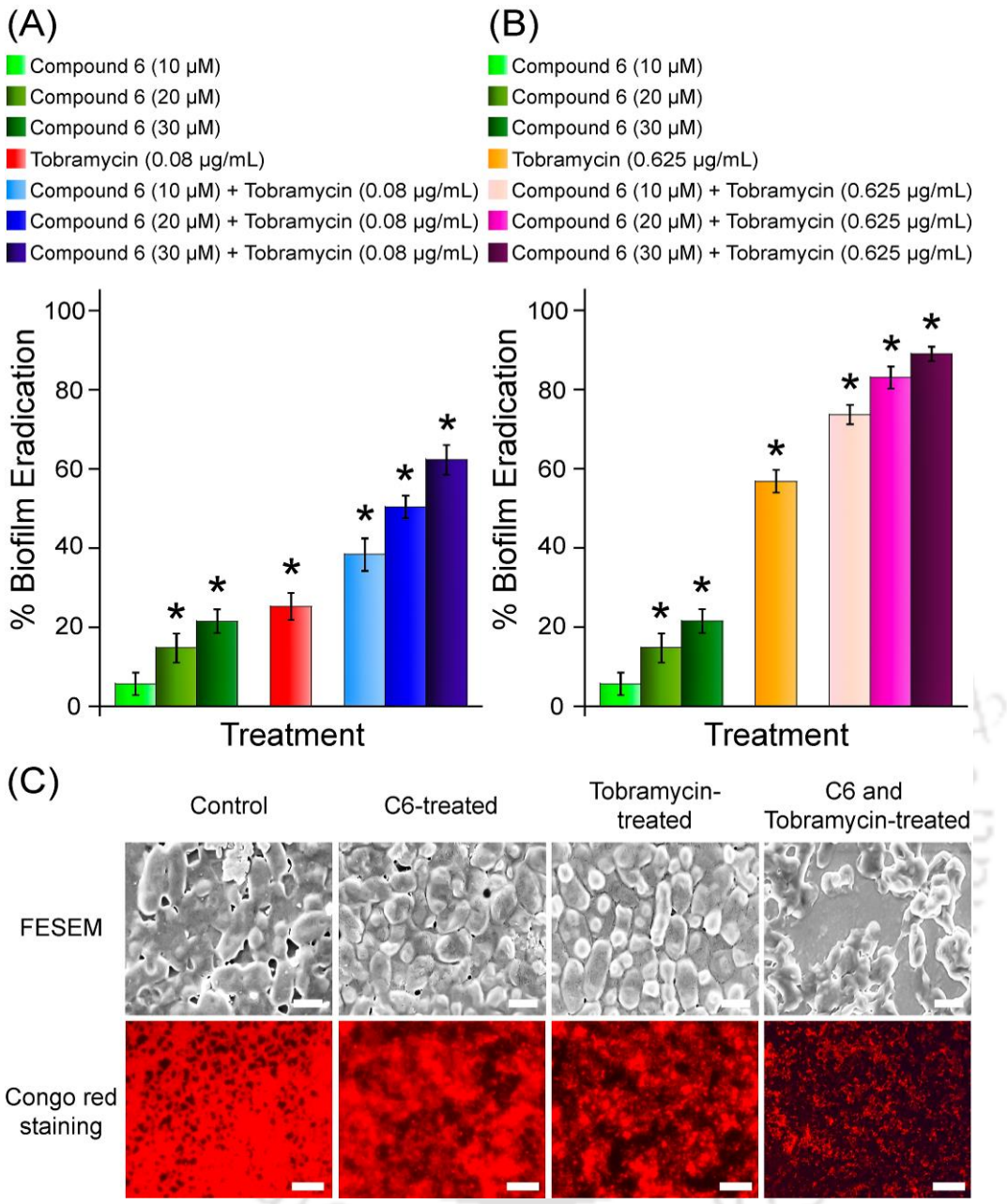

Figure 4.7. Effect of combined treatment of **C6** with (A) 0.08 μg/mL tobramycin and (B) 0.625 μg/mL tobramycin on *P. aeruginosa* MTCC 2488 biofilm measured by crystal violet assay. Statistically significant values derived by ANOVA are indicated by asterisk marks. ∗ indicates *p* value <0.001. (C) Representative FESEM images and congo red stained fluorescence microscope images of *P. aeruginosa* MTCC 2488 biofilm treated with 30 μM **C6**, 0.08 μg/mL tobramycin, and 30 μM **C6** in combination with 0.08 μg/mL tobramycin. Scale bar for FESEM and fluorescence microscope images are 1.0 μm and 50 μm, respectively.

the corresponding eradication of biofilm biomass amounted to 25.3% and 56.8%, respectively (Figure 4.7A-B). Interestingly, in the combinatorial assays, the elimination of biofilm biomass was distinctly higher as compared to treatment with either **C6** or tobramycin alone. For instance, treatment of *P. aeruginosa* biofilm with 0.625 μg/mL tobramycin in combination with **C6** (10 μM, 20 μM, and 30 μM) resulted in 73%, 83%, and 89% eradication of biofilm biomass, respectively (Figure 4.7B). Evidence for superior eradication of *P. aeruginosa* biofilm in combination treatment was captured in FESEM analysis, which suggested extensive disruption of cells and breach of the cell-cell adhesion as well as in congo red staining, which indicated a dramatic reduction in *P. aeruginosa* biofilm EPS (Figure 4.7C). The significant enhancement in *P. aeruginosa* biofilm eradication by using a combination of **C6** and tobramycin was also explicit in fluorescence microscope analysis using cFDA-SE and PI staining, which clearly indicated superior perturbation of the biofilm network in combinatorial assay as opposed to treatment with either the amphiphile or antibiotic alone (refer to Appendix, Figure A4.3). Eradication of *S. aureus* biofilm in the presence of **C6** and gentamicin further substantiated the ability of the amphiphile to abolish biofilm in combination with an antibiotic (refer to Appendix, Figure A4.4). It may be mentioned here that in the combination studies the $MBEC_{90}$ of tobramycin against *P. aeruginosa* biofilm was observed to be 0.625 μg/mL in presence of 30 μM **C6** (Figure 4.7B) as opposed to 10 μg/mL when the antibiotic was used alone (Table 4.1). Likewise, the $MBEC_{90}$ of gentamicin against *S. aureus* biofilm reduced from 128 μg/mL when used alone (Table 4.1) to 20 μg/mL when used in combination with 15 μM **C6** (refer to Appendix, Figure A4.4C).

Interestingly, an MTT assay revealed that at the selected concentrations of **C6** and tobramycin in combination, the viability of HeLa cells was greater than 80% as evident in Figure 4.8. This finding reflects the merit of the amphiphile as an adjuvant in combination therapy for eradication of *P. aeruginosa* biofilm. Furthermore, it offered an opportunity to reduce the levels of tobramycin for effective elimination of *P. aeruginosa* biofilm. This is significant given that the use of tobramycin at high concentrations may lead to gratuitous toxic effects (Lode 1998).

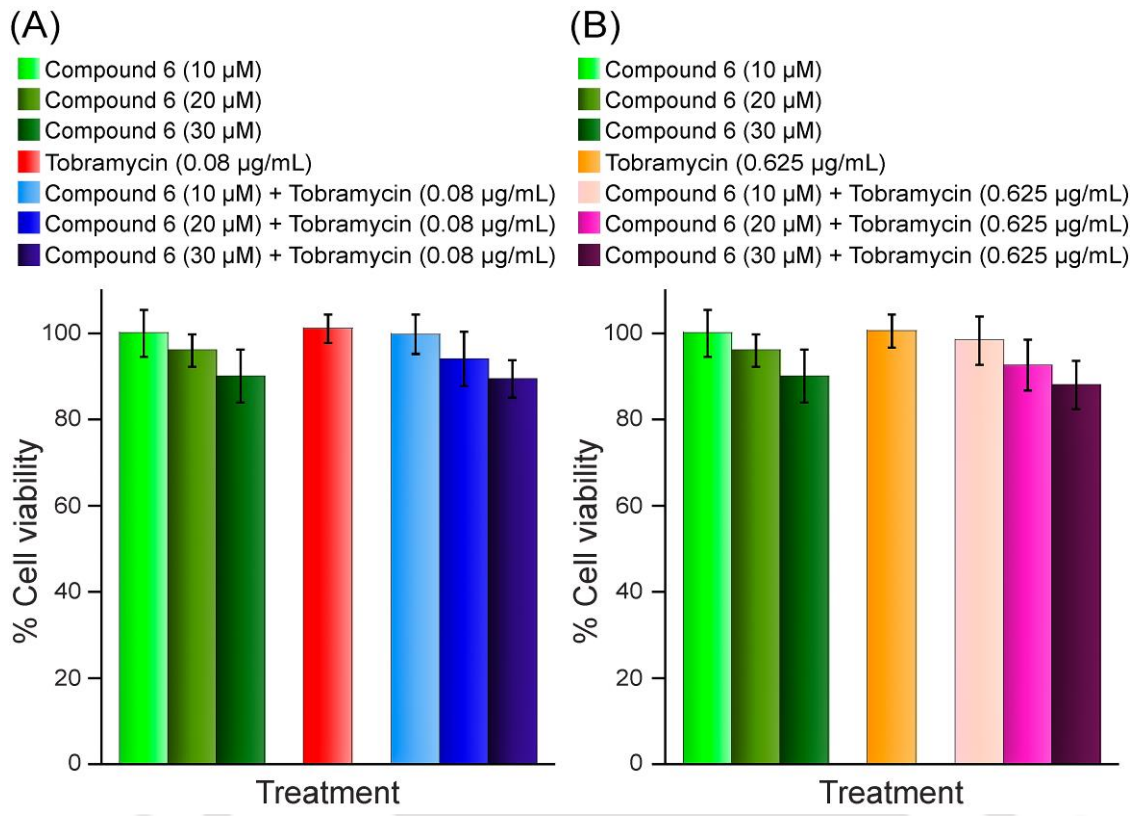

Figure 4.8. MTT-based cytotoxicity assay to determine viability of HeLa cells following treatment with varying concentrations of **C6** or tobramycin or a combination of **C6** with (A) 0.08 μg/mL tobramycin and (B) 0.625 μg/mL tobramycin. Each data point represents mean ± standard deviation from six independent samples.

4.4. Significant Findings

The salient findings of this chapter are as follows:

1. The membrane-acting synthetic amphiphile **C6** could inhibit the formation of *S. aureus* MTCC 96 and *P. aeruginosa* MTCC 2488 biofilms. The amphiphile was observed to be more active against *S. aureus* MTCC 96 biofilm as evident in the lower $MBIC_{90}$ value of 30 μM as opposed to 200 μM in case of *P. aeruginosa* MTCC 2488 biofilm.

2. The amphiphile **C6** could exhibit potent antibiofilm activity even in the complex niche of the biofilm matrix. The antibiofilm activity of **C6** against *S. aureus* MTCC 96 and *P. aeruginosa* MTCC 2488 biofilms could be readily captured through solution-based assays (MTT assay, crystal violet assay and congo red binding assay) and microscopic analysis (AFM and FESEM).

3. The superior antibiofilm potential of **C6** against *S. aureus* MTCC 96 biofilm was evident in the lower $MBEC_{90}$ value of 60 μM as opposed to 400 μM in case of *P. aeruginosa* MTCC 2488 biofilm.

4. The present study also demonstrated that the potent antibacterial synthetic amphiphile **C6** can be employed in combination with low concentrations of therapeutics antibiotics gentamicin or tobramycin to efficiently annihilate established *S. aureus* MTCC 96 biofilm or *P. aeruginosa* MTCC 2488 biofilm.

The menace of bacterial biofilms in the healthcare regime is ominous. The high incidence of life-threatening biofilm-associated chronic infections has triggered a critical demand for antibiofilm therapeutics that can effectively eradicate established biofilms. In this regard, the results obtained in this chapter indicate the promise of the synthetic amphiphile **C6** as an antibiofilm agent. However, a key factor, which is likely to impact the potential of **C6** as an antibiofilm agent is the development of an effective delivery system that can ensure sustained release of the amphiphile. In this direction, development of a nanocarrier for entrapment and controlled release of potentially therapeutic antibacterial amphiphiles can be conceived as a rational approach. Hence, in the subsequent chapter, generation of a human serum albumin (HSA)-based biocompatible nanocarrier for efficient delivery of **C6** and its activity on established *S. aureus* biofilm is discussed.

TH-1410_10610607

Chapter 5

Antibiofilm Activity of Compound 6-loaded Human Serum Albumin Nanocarrier (C6-HNC)

*This chapter describes the development of **Compound 6**-loaded HSA nanocarrier (C6-HNC) and its application in eradication of S. aureus biofilm.*

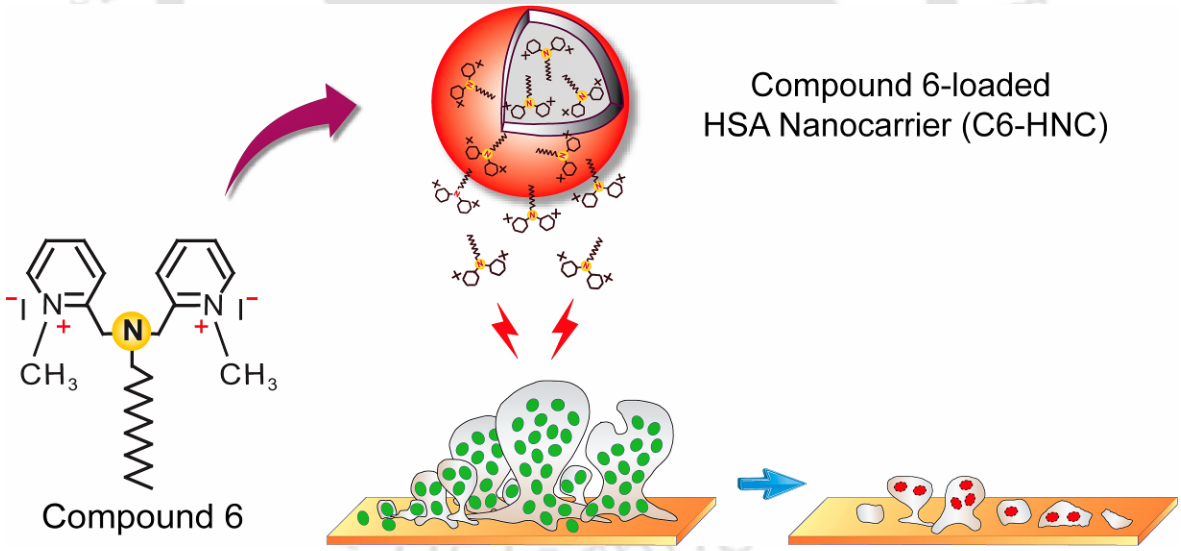

TH-1410_10610607

ABSTRACT

The present study highlights the development of human serum albumin (HSA)-based nanocarrier (HNC) for sustained release of the bactericidal amphiphile **C6** and its application in eradication of *S. aureus* MTCC 96 biofilm. HSA nanoparticles (HNPs) were prepared by a desolvation method and subsequently used to generate **C6**-loaded HSA nanocarrier (**C6**-HNC). The payload nanocarrier was characterized by UV-visible spectroscopy, TEM and FT-IR analysis. The loading capacity (LC) and the amount of encapsulated **C6** in HNC were estimated to be around 8.2% and 125 μM, respectively. *In vitro* release kinetics studies indicated a sustained release of **C6** from the nanocarrier at physiological pH, while the release was comparatively rapid in acidic pH. The bactericidal activity of **C6**-HNC could be captured in time-kill curves, TEM analysis and membrane-depolarization assay. An important highlight of the study is the demonstration of the application potential of the nanocarrier in device-associated antibiofilm therapy, which is illustrated through abolition of *S. aureus* MTCC 96 biofilm from the surface of Foley's urinary catheter. Furthermore, *in vitro* cytotoxic assay on cultured human cell lines indicated the non-toxic nature of **C6**-HNC. Based on its biocompatibility and potent antibiofilm activity, it is envisaged that the amphiphile-loaded nanocarrier may hold significant potential in antibiofilm therapy.

TH-1410_10610607

5.1. Introduction

The high incidence of bacterial biofilm-associated infections coupled with their formidable resistance to therapeutic antibiotics is a burgeoning healthcare issue of serious concern. This irrefutable crisis has fuelled a pressing need for potent antibiofilm therapeutics. The profound implication of bacterial biofilm is reflected in the fact that approximately 80% of all microbial infections are caused by biofilms (Chambers and Deleo 2009). Bacterial biofilms are widely considered to be refractory towards conventional therapeutic antibiotics and this defiance can perhaps be attributed to the presence of an extracellular polymeric matrix, which may assume the role of a barrier and hinder diffusion of antibiotics (Flemming and Wingender 2010, Kostakioti et al. 2013, Bordi and de Bentzmann 2011, Otto 2008, Jones et al. 2001). Further, elevated levels of metal ions and a highly acidic pH associated with the biofilm matrix may lead to inactivation of antibiotics (Kostakioti et al. 2013, Jones et al. 2001). Literature reports also suggest that persister cells in biofilm can display an innate resistance towards antibiotics, which specifically act upon metabolically active cells (Stewart and Costerton 2001, Lewis 2008, Costerton et al. 2007).

Owing to the growing concern of biofilms in modern healthcare and the inherent resistance displayed by biofilms towards conventional therapeutic agents such as antibiotics, potent antibiofilm agents are in premium demand. Conceivably, synthetic antibacterial agents that can penetrate the biofilm matrix, and act on indispensible bacterial targets such as the membrane are potential candidates, which can be explored for antibiofilm therapy. The results obtained in the previous study (Chapter 4) seem to suggest that the synthetic amphiphile **C6** fulfills this rational and emerges as a promising antibiofilm agent based on its membrane-targeting activity, antibiofilm potential and adjuvant trait, which potentiated the action of the antibiotics tobramycin and gentamicin in combination against *S. aureus* MTCC 96 biofilm

In order to harness the true potential of **C6** as an antibiofilm agent, the development of a robust and biocompatible delivery system that can render sustained release of the bactericidal amphiphile would be critical. In this context, generation of nanoscale materials as antibiofilm agents can be a viable option. Super paramagnetic iron oxide nanoparticles (SPIONs) in combination with metabolic stimuli (fructose) have been shown to exhibit

high antibiofilm activity against MRSA and Gram-negative *E.coli* and *Pseudomonas* (Durmus et al. 2013). In another study, gold nanoparticle-polythiophene composite was used as a potent membrane-targeting bactericidal agent against biofilm (Adhikari et al. 2013). Studies have also demonstrated the use of nitric oxide releasing polymer-bearing nanocomposites that render efficient dispersion of biofilm matrix (Slomberg et al. 2013). Amongst various options for developing nanocarriers as reservoirs for delivery of antibiofilm agents, protein-based nanocarriers are particularly suitable owing to their high permeation and retention effect, biocompatibility and biodegradability (Shimanovich et al. 2014, Elzoghby et al. 2012b) In this regard, nanocarriers made from human serum albumin hold considerable therapeutic potential since they are biodegradable, non-antigenic and can facilitate encapsulation of high levels of payload (Elzoghby et al. 2012a, Kratz 2008).

Based on the aforementioned rationale, the present study demonstrates the development of **C6**-loaded human serum albumin (HSA)-based non-toxic nanocarrier that renders sustained release of the bactericidal payload and retains the antibiofilm activity of the amphiphile in the complex niche of the biofilm matrix. Application of the developed nanocarrier in eradication of an established biofilm from the surface a model urinary catheter is also illustrated in this study.

5.2. Materials and Methods

5.2.1. Growth Media and Chemicals

Nutrient Broth (NB), Brain-Heart Infusion (BHI) and crystal violet (CV) dye broth were procured from HiMedia, Mumbai, India. Dimethyl sulfoxide (DMSO), absolute ethanol and glutaraldehyde were obtained from Merck, India. N-2-Hydroxyethyl piperazine-N-2-ethane sulphonic acid (HEPES buffer) was procured from Sisco Research Laboratories SRL, Mumbai, India. 5 (and 6)-carboxyfluorescein diacetate succinimidyl ester (cFDA-SE), propidium iodide (PI), human serum albumin (HSA, Fraction V, purity 96−99%), valinomycin, Dulbecco's Modified Eagle Medium (DMEM), trypsin-EDTA, 3-(4,5-dimethyl-2-thiazolyl)-2,5- diphenyl-2H-tetrazolium bromide (MTT), paraformaldehyde and Triton X-100 were procured from Sigma-Aldrich. Fetal bovine serum (FBS) was procured from PAA Laboratories, USA. Foley's urinary catheter was procured from Sisco Latex Pvt. Ltd. (India).

5.2.2. Bacterial Strains and Growth Conditions

In the present investigation the Gram-positive bacterial strains *S. aureus* MTCC 96 and *L. monocytogenes* Scott A and Gram-negative bacterial strains *E. coli* MTCC 433 and *E. aerogenes* MTCC 2822 were used. *S. aureus* MTCC 96 and *L. monocytogenes* Scott A were cultured in BHI broth at 37°C and 180 rpm for 12 h whereas, *E. coli* MTCC 433 and *E. aerogenes* MTCC 2822 were propagated in NB at 37°C and 180 rpm for 12 h. All the bacterial strains were grown from frozen stocks and sub-cultured prior to their use in experiments.

5.2.3. Generation of HSA Nanoparticle (HNP)

HSA nanoparticles (HNPs) were prepared essentially based on the desolvation process described earlier (Langer et al. 2003). Briefly, 100 mg HSA was dissolved in 2.0 ml of sterile MilliQ water (adjusted to pH 8.2). To generate HNPs, this solution was subjected to desolvation by drop wise addition of 8.0 ml of ethanol at a flow rate of 1.0 ml/min under constant stirring condition (500 rpm) at room temperature. Following desolvation, 100 µL of 8.0% glutaraldehyde was added to the suspension in order to stabilize the nanoparticles by cross-linking. The resulting nanoparticle suspension was further stirred for 24 h at room temperature to complete the cross-linking process. Purification of HNPs from residual albumin and glutaraldehyde was achieved by five consecutive cycles of centrifugation (20,000 × g, 8 min for each cycle) with intermittent resuspension of the pellet in original volume of sterile MilliQ water (adjusted to pH 8.2) by using an ultrasonication bath for 5 min. The purified HNPs recovered from the final washing step were subjected to freeze-drying in a lyophilizer and stored in 4^{o}C till further use. The yield (*Ynp*) of HNPs was calculated as follows:

$$Y_{np} = \frac{W_{Total\ HSA} - W_{Free\ HSA}}{W_{Total\ HSA}} \times 100\ \%$$

where, $W_{Total\ HSA}$ is the total amount of HSA, which was ascertained by Bradford reagent (Sigma-Aldrich, USA) following manufacturer instructions and $W_{Free\ HSA}$ is the amount of non-desolvated free HSA. To obtain a measure of the non-desolvated free HSA, the

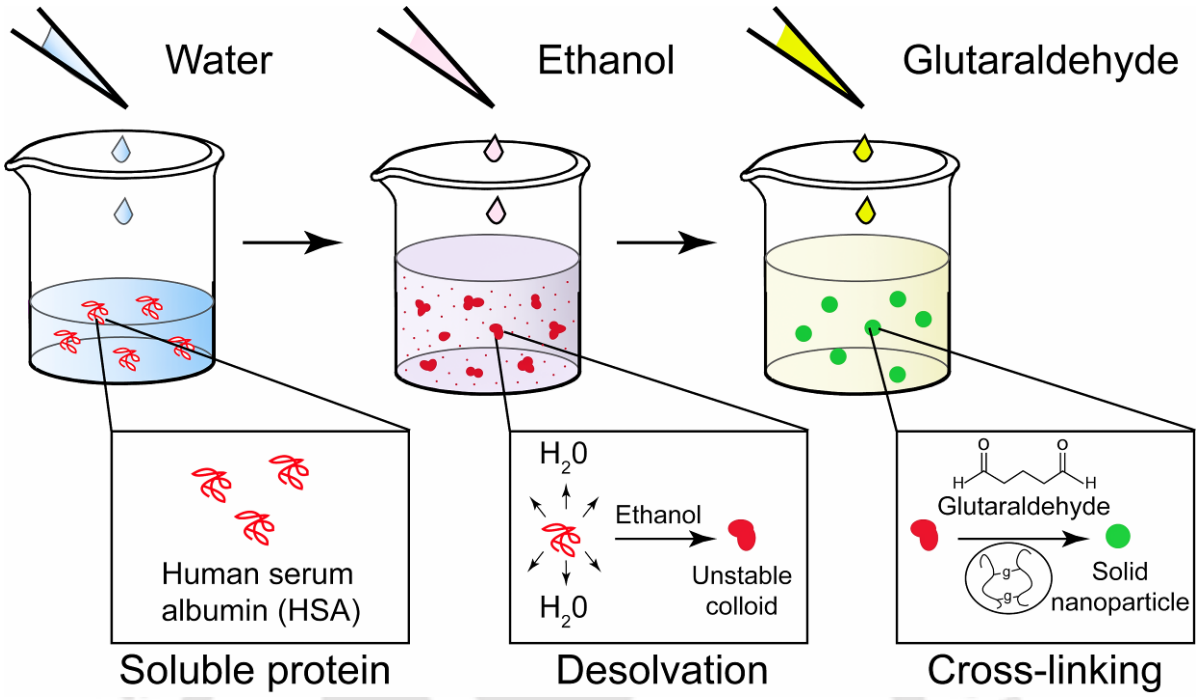

Figure 5.1. Schematic representation of the experimental protocol to prepare HSA nanoparticles.

nanoparticles were separated by centrifugation at 16,000 × g for 20 min at room temperature immediately after the desolvation process. An aliquot of the supernatant was then diluted with sterile MilliQ water and the amount of HSA protein in the supernatant was determined by Bradford reagent (Sigma-Aldrich, USA) following manufacturer instructions. A schematic representation of the protocol used to prepare HNPs is depicted in Figure 5.1.

*5.2.4. Preparation of **Compound 6**-loaded HSA Nanocarrier (C6-HNC)*

For generation of **C6**-loaded HSA nanocarrier (**C6**-HNC), HNPs (1.0 mg/ mL in sterile MilliQ water, pH titrated to 8.2) were interacted overnight with varying concentrations of **C6** (5.0 µM - 800 µM) on a rocker at room temperature. Following incubation, the solution was centrifuged at 10, 000 × g for 5 min. The pellet representing **C6**-HNC was resuspended in sterile MilliQ water (pH titrated to 8.2). A schematic illustration of the preparation of C6-HNC is shown in Figure. 5.2.

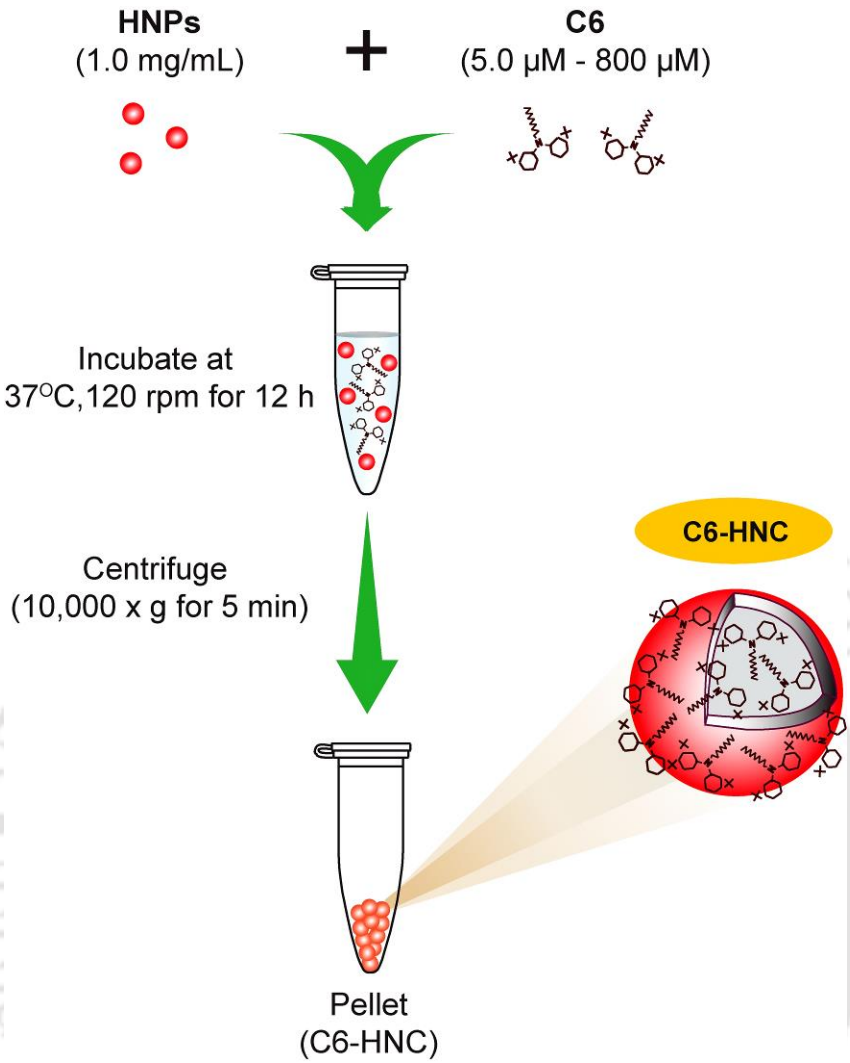

Figure 5.2. Schematic representation of th eexperimental protocol to prepare **Compound 6**-loaded HSA nanocarrier (C6-HNC).

5.2.5. Characterization of HNP and C6-HNC

Characterization of HNPs and C6-HNC was accomplished by the following methods:

5.2.5.1. Microscopic Analysis

A representative aliquot of HNPs was added on a clean sterile cover slip. The sample was then air-dried in a laminar hood and examined in a field emission scanning electron microscope (Zeiss Sigma, USA). Separate aliquots of HNPs and **C6**-HNC (2.0 µl each) were also spotted on carbon coated TEM grid (Pacific Grid, USA), air-dried in laminar hood and examined in a transmission electron microscope (Jeol JEM 2100, Japan)

operating at 200 kV and their images were recorded. Based on the TEM images of HNPs, the particle size was determined using ImageJ software (http://rsb.info.nih.gov/ij).

5.2.5.2. UV-visible Spectroscopy

Representative samples of as prepared HNPs and **C6**-HNC were subjected to UV-visible spectroscopy (Varian Cary 100, Varian Medical Systems, Inc., Palo Alto, CA) in scanning mode in a wavelength range of 200-500 nm. The absorption spectra of HSA and **C6** were also acquired for reference. For each sample, UV-visible spectra were recorded from multiple sets.

5.2.5.3. Fourier Transform Infrared (FT-IR) Spectroscopy

FT-IR spectra of HSA, **C6**, HNPs and **C6**-HNC were recorded in KBr pellets at 4.0 cm^{-1} resolution in an infrared spectrometer (Spectrum One, Perkin-Elmer). Eight scans were performed for every sample in the range of 4000 cm^{-1} to 500 cm^{-1}. A background spectrum for pure KBr was also measured.

*5.2.6. Loading capacity (LC) and Encapsulation of **Compound 6***

Prior to preparation of **C6**-HNC, UV-visible spectra of varying concentrations of **C6** (2.5 μM - 25 μM) was recorded at 265 nm in a spectrophotometer and a standard curve was generated for quantification of **C6**, which was subsequently used for estimation of loading capacity (LC) and amount of encapsulated **C6**. For estimation of LC, HNPs (1.0 mg/mL in sterile MilliQ water) were interacted with varying concentrations of **C6** (5.0 μM - 800 μM) for 12 h on a rocker at room temperature. Following incubation, the solution was centrifuged at 10,000 × g for 5 min. The pellet, which represents **C6**-HNC was resuspended in sterile MilliQ water. The concentration of free **C6** in the supernatant was determined using the previously generated calibration curve for the amphiphile. The loading capacity (LC) of HNPs was calculated as follows:

$$LC = \frac{W_{Total\ compound\ 6} - W_{Free\ compound\ 6}}{W_{np}} \times 100\ \%$$

where $W_{Total\ \textbf{Compound 6}}$ is the total amount of **C6** used for preparing C6-HNC, $W_{Free\ \textbf{Compound 6}}$ is the amount of free **C6** recovered after formation of **C6**-HNC and W_{np} is the weight of HSA nanoparticle.

*5.2.7. In vitro Release Kinetics of **Compound 6** from C6-HNC*

C6-HNC loaded with 125 µM of **C6** was dispersed in separate sets in 1.0 mL of 10 mM HEPES buffer (pH 7.4) and 100 mM citrate buffer (pH 3.0), respectively. The samples were incubated in an orbital shaker at 120 rpm at 37°C. At specific time intervals (1 h, 3 h, 6 h, 12 h, 24 h, 48 h and 72 h) the samples were withdrawn and centrifuged at 10,000 × g for 5 min. The supernatant from various samples were transferred into a fresh microcentrifuge tube, and UV-visible absorbance of the solutions was measured at 265 nm in a spectrophotometer. The absorbance value at 265 nm and a previously generated calibration curve for **C6** was used to measure the quantity of **C6** released from **C6**-HNC at specific time periods and expressed as % cumulative release. A schematic representation of the experimental protocol to study *in vitro* release kinetics of **C6** is depicted in Figure 5.3.

5.2.8. Antibacterial Activity of C6-HNC

The bactericidal activity of **C6**-HNC was ascertained by the following methods:

5.2.8.1. Time-kill Curve

Target cells of *S. aureus* MTCC 96 and *E. coli* MTCC 433 (10^6 CFU/mL each) suspended in sterile PBS were incubated with separate sets of **C6**-HNC (representing 5.0 µM, 10 µM, 15 µM, 20 µM, 25 µM and 30 µM **C6**) at 37°C and 180 rpm. Following incubation, the viable cell numbers (Log_{10} CFU/mL) were determined for every sample at regular intervals (3 h, 6 h, 12 h and 24 h) by serial dilution and plating. The viable cell count was also determined at the specified intervals for cells suspended in sterile PBS as well as cells treated with HNPs alone.

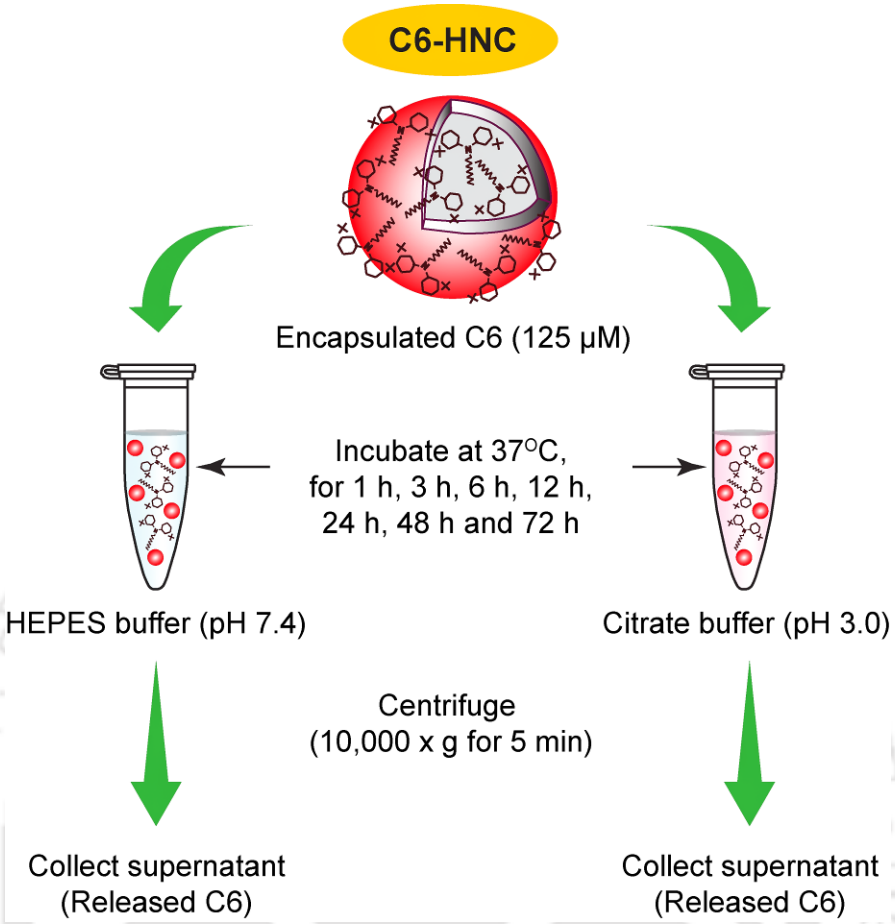

Figure 5.3. Schematic representation of the experimental protocol for *in vitro* release kinetics of **Compound 6** from C6-HNC.

5.2.8.2. Transmission Electron Microscope (TEM) Analysis

Target cells of *S. aureus* MTCC 96 (approximately 10^6 CFU/mL suspended in sterile PBS) was treated with **C6**-HNC (corresponding to 30 µM of **C6**) for 6 h. In a parallel set, the target bacterial cells were also treated with HNPS alone for 6 h. A 2.0 µL aliquot of cells treated with HNPs and **C6**-HNC were spotted on separate carbon coated TEM grid (Pacific Grid, USA) and air-dried in laminar hood. The samples were subsequently subjected to TEM analysis (Jeol JEM 2100, Japan) and their images were recorded.

5.2.8.3. Membrane Depolarization Assay

Cells of *S. aureus* MTCC 96 and *E. coli* MTCC 433 were grown till mid-logarithmic phase (A_{600} = 0.4-0.5). The cells were harvested by centrifugation, washed and resuspended in

HEPES buffer (5.0 mM HEPES, 20 mM glucose, pH 7.2) to achieve a cell suspension of desired concentration (A_{600} of 0.05). The cell suspensions were incubated with 0.4 µM $DiSC_35$ for 1 h at 37°C followed by the addition of KCl (final concentration of 100 mM) and further incubated for 15 min. The cell suspension was then placed in a cuvette with diluted **C6**-HNC samples representing various working concentrations of **C6** (15 µM, 20 µM and 25 µM). The fluorescence emission intensity of the samples (λ_{Ex} = 622 nm and λ_{Em} = 670 nm) were then monitored in short time intervals in a spectrofluorimeter (FluoroMax-3, HORIBA) with excitation and emission slit width set at 10 nm each. Cells treated with valinomycin (30 µM) and HNPs were used as positive and negative controls, respectively. Fluorescence measurements were taken for three independent experimental samples.

5.2.9. Antibacterial Activity of C6 following In vitro Release from C6-HNC

C6-HNC (corresponding to 125 µM **C6** concentration) was dispersed in 500 µl of 10 mM HEPES buffer (pH 7.4) and incubated in an orbital shaker at 120 rpm at 37°C for 48 h to facilitate maximum *in vitro* release of **C6**. The target bacteria, which included Gram-positive *S. aureus* MTCC 96 and *L. monocytogenes* Scott A and Gram-negative *E. coli* MTCC 433 and *E. aerogenes* MTCC 2822 were inoculated in fresh requisite growth media incorporated with varying concentrations of *in vitro* released **C6** (15.0 µM, 30 µM and 45 µM) at 37°C and 130 rpm for 24 h. The growth of **C6**-treated cells was monitored by measuring absorbance at 600 nm in a spectrophotometer (Cary 300, Varian) and was expressed as percentage killing compared to control (untreated cells). A schematic representation of the experimental protocol used to ascertain antibacterial activity of **C6** following *in vitro* release from **C6**-HNC is depicted in Figure 5.4.

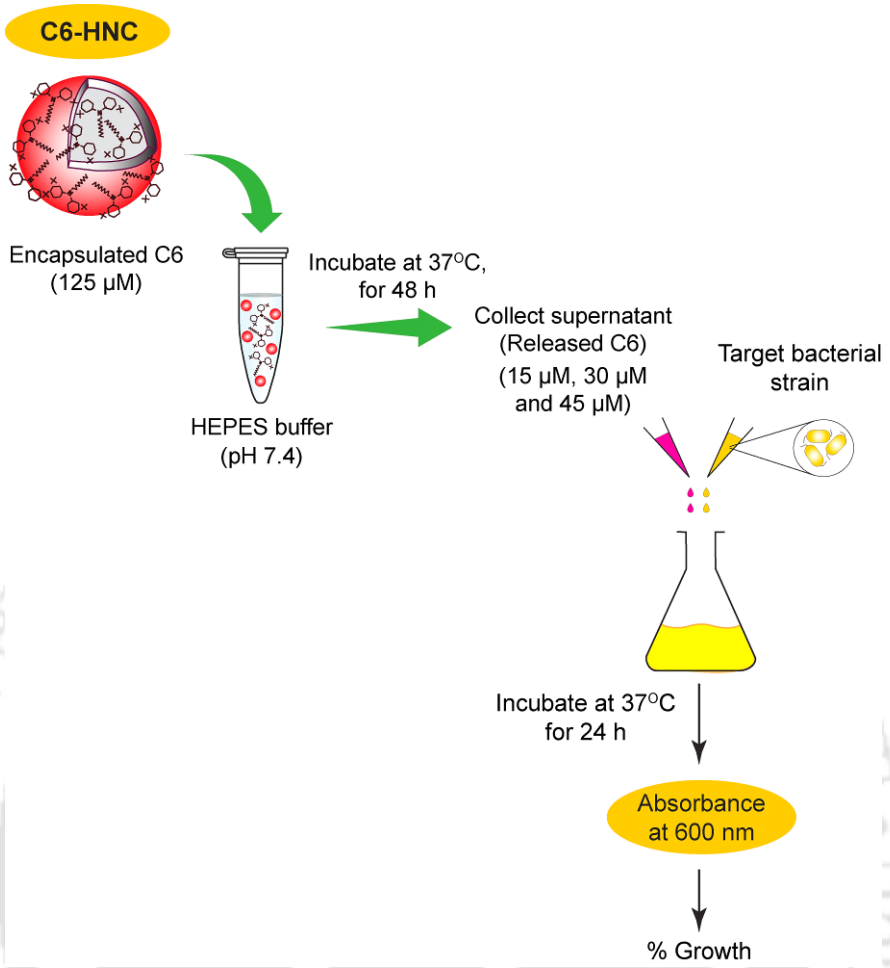

Figure 5.4. Schematic representation of the experimental protocol for screening antibacterial activity of **C6** following *in vitro* release from **C6**-HNC.

5.2.10. Antibiofilm Activity of C6-HNC

Biofilm of *S. aureus* MTCC 96 was grown in a sterile 96 well microtiter plate following a standard procedure described earlier in section 4.2.4 of Chapter 4 and treated in separate sets with various samples of **C6**-HNC (corresponding to 5.0 µM, 10 µM, 15 µM, 20 µM, 25 µM, 30 µM, and 45 µM of **C6**) for 24 h. In a parallel control experiment *S. aureus* MTCC 96 biofilm was also treated with HNPs alone. Following incubation, the wells were washed with sterile PBS and an MTT-based viability assay was performed for both **C6**-HNC-treated and HNP-treated samples by following the protocol mentioned earlier in section 4.2.5.1 of Chapter 4.

5.2.11. Eradication of Biofilm from Foley's Urinary Catheter Surface

The potential of **C6** and **C6**-HNC to eradicate catheter-associated biofilm was determined by a quantitative MTT assay. Biofilm of *S. aureus* MTCC 96 was grown over Foley's urinary catheter by incubating 1.0 cm × 0.5 cm segmented pieces of the catheter in a sterile tissue culture petridish (35 mm diameter) containing BHI broth with 0.25% glucose and the bacterial cell suspension (~10^7 CFU/mL) for 24 h in static and humid conditions under 37°C. Following incubation, catheter segments colonized with *S. aureus* MTCC 96 biofilm were recovered aseptically and rinsed gently with sterile PBS to remove unbound bacterial cells. The catheters were then transferred to separate sterile tissue culture petridish containing fresh media incorporated with varying concentrations of either **C6** or **C6**-HNC (corresponding to 5.0 μM, 10 μM, 15 μM, 20 μM, 25 μM, 30 μM and 45 μM **C6**) and incubated for 24 h. Subsequently, the catheter segments were harvested, gently rinsed in sterile PBS, and further incubated in fresh sterile BHI media containing MTT reagent (0.5 mg/mL). After incubation for 4 h at 37°C, the samples were washed thrice with sterile PBS to remove all traces of MTT. The purple colored formazan crystals were dissolved in DMSO for 15 min with brief mixing, and the absorbance of a 100 μL aliquot was measured at 550 nm using a microtiter plate reader (Infinite M200, TECAN, Switzerland). Each assay was performed in triplicate, and the results were expressed as the mean of three independent experiments. A schematic representation of the experimental protocol followed to determine the antibiofilm activity of **C6**-HNC on Foley's urinary catheter surface is indicated in Figure 5.5.

In order to prepare catheter specimens with bacterial biofilm for FESEM analysis, segments of the catheter were incubated into separate tubes containing 1.0 mL of BHI broth with 0.25% glucose and the bacterial cell inoculum (~10^7 CFU/mL *S. aureus* MTCC 96) for 24 h in static and humid condition under 37°C. Subsequently, the catheter segments with pre-grown *S. aureus* MTCC 96 biofilm were incubated in separate sets in fresh requisite media incorporated with 30 μM **C6** or **C6**-HNC (representing 30 μM **C6**) for 24 h. Following treatment, the catheter segments were gently removed, rinsed with sterile MilliQ water, and fixed with 2.5% glutaraldehyde for 1 h at room temperature followed by further rinsing with sterile MilliQ water and drying. Samples representing the bare catheter segment (devoid of any biofilm growth) and the untreated catheter segment

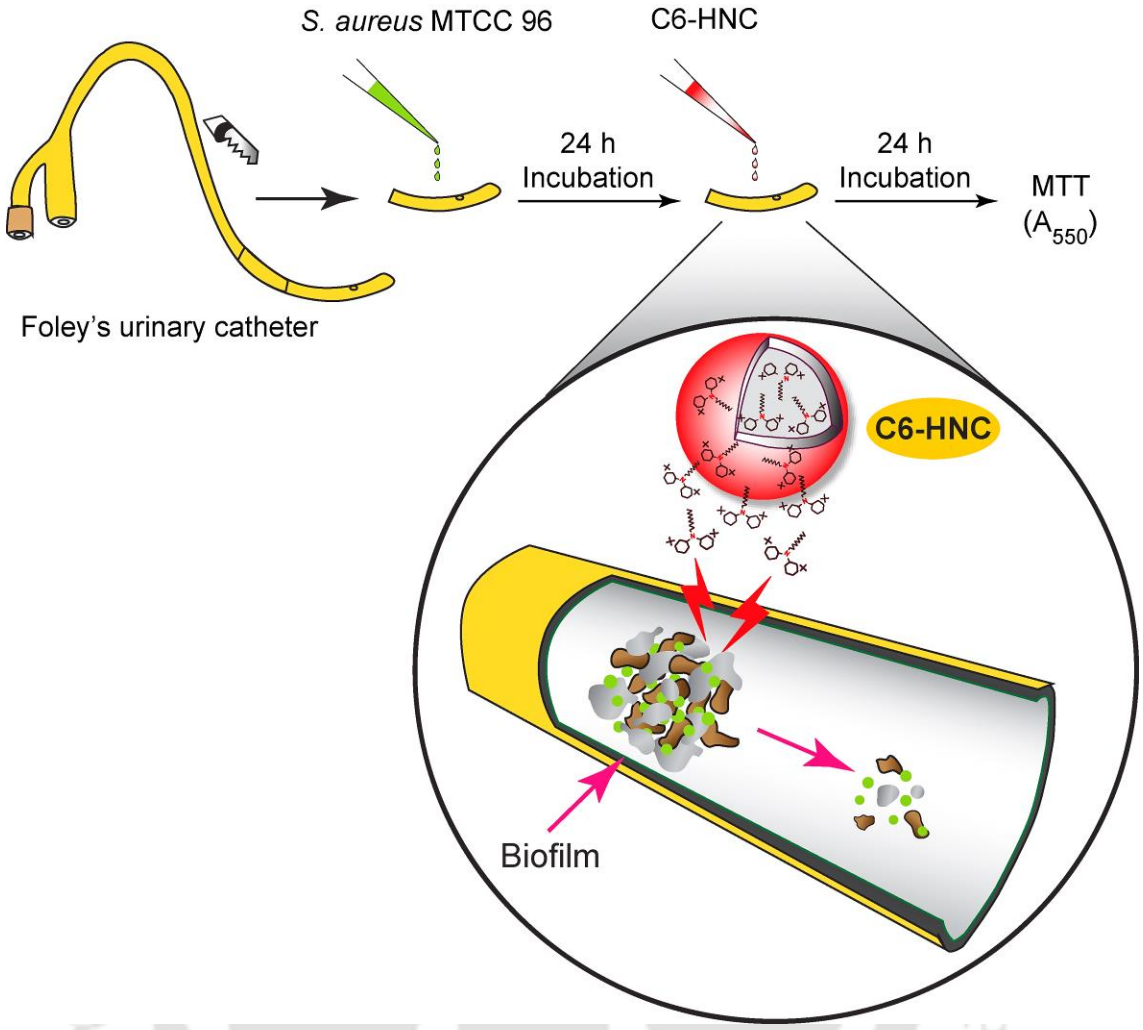

Figure 5.5. Schematic representation of the experimental protocol to study the antibiofilm activity of **C6**-HNC on Foley's urinary catheter surface.

with established *S. aureus* MTCC 96 biofilm were also fixed similarly. Subsequently, all the processed catheter segments were examined in a field emission scanning electron microscope (Zeiss Sigma) and their images were recorded.

5.2.12. Cytotoxic Effect of C6-HNC

The cytotoxic effect of C6-HNC was ascertained by the following methods:

5.2.12.1. MTT Assay

Cytotoxicity of **C6**-HNC was assessed *in vitro* against HeLa cell line by a standard MTT-based colorimetric assay following the manufacturer's instructions (Sigma-Aldrich). The

cells were initially grown in a 25 cm^2 tissue culture flask in Dulbecco's Modified Eagle Medium (DMEM) supplemented with 10% (v/v) fetal bovine serum (FBS), penicillin (100 μg/mL), and streptomycin (100 μg/mL) at 37°C under a humidified atmosphere of 5.0% CO_2 in an incubator. The cells were subsequently seeded onto 96-well tissue culture plates at a density of 10^4 cells per well and incubated with **C6**-HNC (corresponding to 5.0 μM, 10 μM, 15 μM, 20 μM, 25 μM, 30 μM, and 45 μM **C6**) for a period of 24 h. Untreated cells and cells treated with HNPs were also incubated in parallel sets. Following incubation, the media was carefully aspirated and fresh DMEM medium containing MTT solution was added to the wells and the plates were incubated for 4 h at 37°C. Subsequently, the supernatant was aspirated and the insoluble formazan product was solubilized in DMSO and its absorbance was measured in a microtiter plate reader (Infinite M200, TECAN, Switzerland) at 550 nm. The MTT assay was performed in six sets for each sample. The absorbance obtained for untreated cells was assumed to represent 100% cell viability, and the absorbance for other samples was compared to that obtained for untreated cells in order to determine % cell viability. Data analysis and determination of standard deviation were performed with Microsoft Excel 2010 (Microsoft Corporation).

5.2.12.2. Fluorescence Microscope Analysis

HeLa cells were seeded onto 96 well tissue culture plates (approximately 10^4 cells per well) and propagated in a CO_2 incubator as mentioned before to achieve 80% confluency. Subsequently, the cells were incubated with 30 μM of **C6**-HNC made in DMEM for a period of 24 h. HeLa cells treated with HNPs alone (control samples) were also incubated in separate wells. In parallel sets, HeLa cells were fixed with 4% paraformaldehyde for 10 min at room temperature followed by treatment with 0.1% Triton X-100 for 10 min to achieve permeabilization of the cells. Cells belonging to all the experimental samples (HNP-treated cells, **C6**-HNC-treated cells, and Triton X-100 treated cells) were thoroughly washed with sterile PBS and labeled in separate sets with either 50 μM cFDA-SE or 30 μM PI each for 15 min, respectively. The cells were subsequently washed with sterile PBS, and images of the cells were captured using a fluorescence microscope (Eclipse Ti-U, Nikon) with a filter that allowed blue light excitation for cFDA-SE and green light excitation in the case of PI stained cells.

5.3. Results and Discussion

*5.3.1. **Compound 6**-loaded HSA Nanocarrier (C6-HNC)*

The results of the previous chapter (Chapter 4) clearly highlighted that the antibiofilm potential of the synthetic amphiphile **C6** was quite promising. However, to explore the therapeutic prospect of **C6** as an antibiofilm agent, generation of a delivery vehicle that ensures sustained release of the bactericidal payload would be critical. In this regard, it was conceived that development of a **C6**-loaded nanocarrier, which can permeate the biofilm matrix is likely to render a sustained and localized release of the amphiphile, leading to effective eradication of the biofilm. However, it was imperative to ensure that the nanocarrier itself was nontoxic and suitable for potential therapeutic applications. Given this rationale, a human serum albumin (HSA)-based nanocarrier for **C6** was developed, based on the biocompatible nature and extensive use of this serum protein as a nanocarrier in biomedical applications (Kratz 2008, Elzoghby et al. 2012a). Following a well-established desolvation process (Langer et al. 2003), HSA nanoparticles (HNPs) were obtained in high yield of nearly 80% as measured by Bradford assay. FESEM and TEM analysis revealed characteristic spherical-shaped HNPs with an average particle size of 220 nm (Figure 5.6A-C). **C6**-HNC was prepared by incubating pre-formed HNPs with varying concentrations of **C6** in order to facilitate uptake of the amphiphile. UV-visible spectra of **C6**-HNC revealed an absorbance peak at 265 nm, which suggested the presence of **C6** in HSA nanocarrier (Figure 5.6D). TEM analysis of **C6**-HNC indicated aggregates of nanoparticles (Figure 5.6E) perhaps due to strong hydrophobic interactions. Loading of HNPs with **C6** was further corroborated by FT-IR spectroscopic analysis of **C6**-HNC, wherein characteristic stretching frequencies of the HSA protein as well as **C6** was conserved (Figure 5.6F).

5.3.2. Loading Parameters and In vitro Release Kinetics

Prior to estimating the amphiphile loading capacity (LC) of HNPs, a concentration-dependent UV-visible absorption spectra of **C6** was measured (Figure 5.7A), which yielded a linear calibration plot (Refer to Appendix, Figure A5.1). The loading capacity (LC) of HNPs exhibited a progressive increase with increment in the concentration of **C6** and a saturation effect was observed at around 600 μM of the amphiphile (Figure 5.7B).

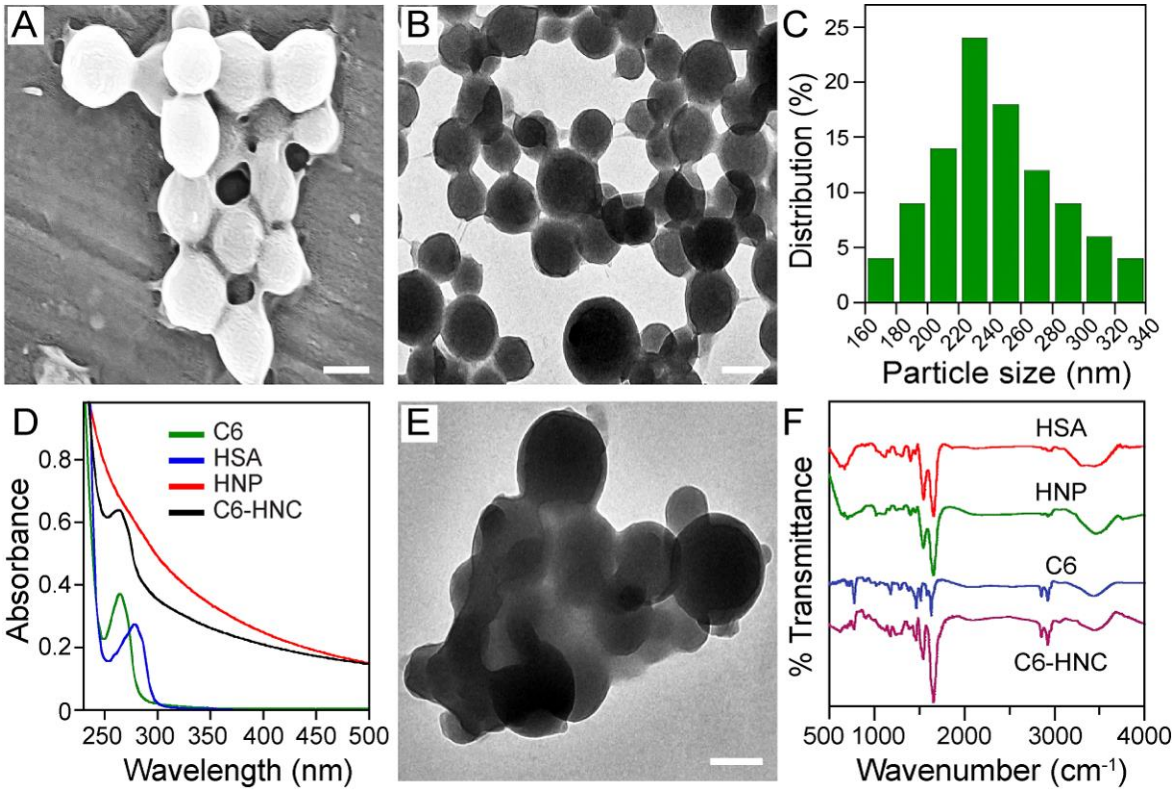

Figure 5.6. (A) FESEM image of HSA nanoparticles (HNPs). (B) TEM image of HNPs. (C) Determination of particle size of HNPs using ImageJ software (http://rsb.info.nih.gov/ij). Characterization of **C6**-loaded HSA nanocarrier (**C6**-HNC) by (D) UV-visible absorbance spectroscopy, (E) TEM analysis and (F) FT-IR analysis. The scale bar for the images in panel A, B, and E is 200 nm.

At the highest concentration of **C6** (800 μM), the LC of HNPs and the amount of encapsulated **C6** was estimated to be around 8.2% and 125 μM, respectively (Figure 5.7B). In order to evaluate the therapeutic potential of **C6**-loaded HSA nanocarrier, studies on the *in vitro* release of **C6** from the payload nanocarrier was pertinent. The *in vivo* efficacy of a bactericidal molecule is generally influenced by its serum concentration and binding to plasma protein and tissue and thus it is a common practice to employ antibacterials at concentrations exceeding their MIC for effective *in vivo* elimination of target bacteria (Craig 1998, 2003, Mueller et al. 2004, Wispelwey 2005). Based on this premise, the *in vitro* release kinetics of **C6** was studied with **C6**-HNC loaded with a high concentration of **C6** (125 μM). At a physiological pH of 7.4, a slow release of the amphiphile from

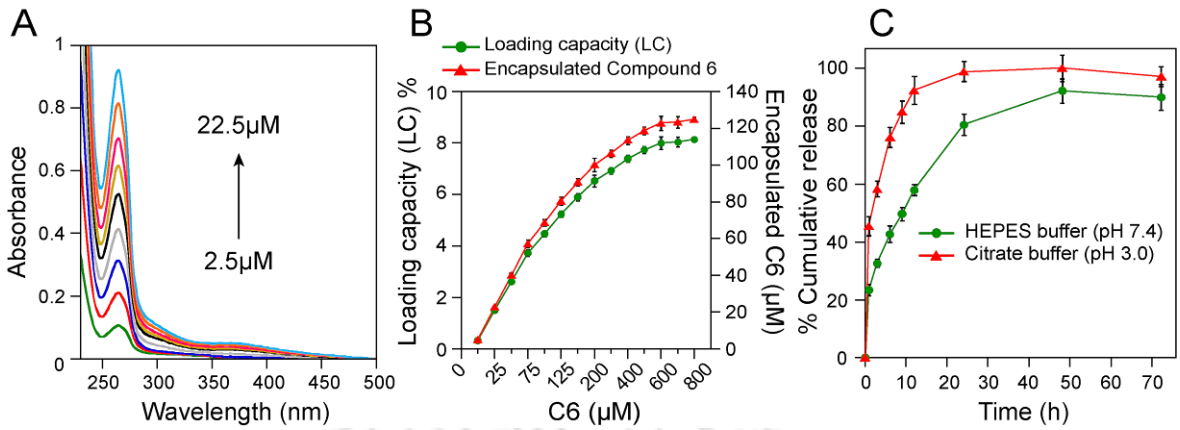

Figure 5.7. (A) UV-visible absorption spectra of varying concentrations of **C6**. (B) Loading capacity (LC) and amount of encapsulation of **C6** in HSA nanoparticles. (C) *In vitro* release kinetics of **C6** from **C6**-HNC incubated in 10 mM HEPES buffer (pH 7.4) and 100 mM citrate buffer (pH 3.0).

C6-HNC was observed, with around 60% release following 12 h of incubation (Figure 5.7C). Subsequently, there was a progressive increase in the release of **C6** with the estimated cumulative release reaching a plateau of around 92% after 48 h. In acidic pH (pH 3.0), release of **C6** from the nanocarrier was rapid, as compared to the profile observed at pH 7.4 (Figure 5.7C).

5.3.3. Bactericidal Activity of C6-HNC

Following successful encapsulation and *in vitro* release of **C6** from the HSA-based nanocarrier, it was pertinent to ascertain whether the loaded amphiphile retained its characteristic bactericidal activity upon encapsulation. To pursue this goal, *S. aureus* MTCC 96 was selected as a model Gram-positive target bacteria. As a Gram-negative bacterium, *E. coli* MTCC 433 was used as a target in lieu of *P. aeruginosa* MTCC 2488. This was based on the lower MIC of **C6** against *E. coli* MTCC 433 (64 μM or 41.68 μg/mL) (Refer to Appendix, Table A2.2) as compared to the MIC against *P. aeruginosa* MTCC 2488 (Refer to Chapter 4, Table A4.1). Moreover, given the higher concentration of **C6** required for annihilation of *P. aeruginosa*, therapeutic usage of **C6**-HNC against this target bacterium warrants circumspection as high concentration of the amphiphile may bear cytotoxic implications (Refer to Chapter 2, Section 2.3.3). A dose-dependent reduction of bacterial cell viability was observed upon treatment with **C6**-HNC

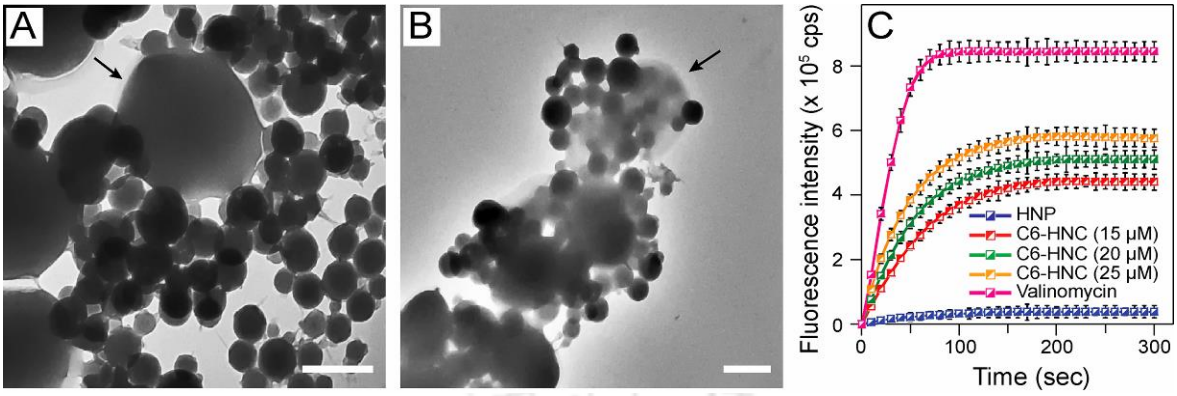

Figure 5.8. TEM images of *S. aureus* MTCC 96 cells treated with (A) HNPs and (B) **C6**-HNC. Arrow in panel A indicates a typical spherical shaped *S. aureus* cell surrounded by a cluster of smaller size HNPs in the vicinity. Arrow in panel B indicates disintegration and loss of electron density in *S. aureus* cell treated with **C6**-HNC. Scale bar for the TEM images is 0.2 µm. (C) $DiSC_35$-based membrane depolarization assay for *S. aureus* MTCC 96 cells treated with **C6**-HNC. Cells treated with 30 µM valinomycin were used as positive control in the assay.

as evident from the time-kill curves (Refer to Appendix, Figure A5.2A-B). TEM analysis suggested that HNPs alone were devoid of any antibacterial activity as evident from the retention of the distinctive spherical morphology in *S. aureus* cells, which were bound by a cluster of smaller size HNPs (Figure 5.8A). Interestingly, upon treatment with **C6**-HNC significant morphological distortion and leakage of cellular contents, which resulted in loss of electron density in the target bacterial cells was apparent (Figure 5.8B). **C6**-HNC could also render a rapid and dose-dependent membrane depolarization in *S. aureus* MTCC 96 and *E. coli* MTCC 433 cells (Figure 5.8C and refer to Appendix, Figure A5.3), which is an archetypal activity associated **C6** (Refer to Chapter 2, Section 2.3.2). The antibacterial activity of **C6**-HNC is presumably the consequence of release of the payload (**C6**) from the nanocarrier. To verify this phenomenon, the antibacterial activity of released **C6** was also ascertained. In these experiments, **C6**-HNC (loaded with 125 µM **C6**) was subjected to the conditions that favor *in vitro* release of the payload in 10 mM HEPES buffer (pH 7.4) for 48 h (the experimental conditions were essentially similar to that described in section 5.2.10). Subsequently, the recovered supernatant was diluted to achieve a **C6** concentration of 15 µM, 30 µM, and 45 µM in separate sets and their antibacterial activity was tested against representative Gram-positive and Gram-negative bacteria.

A concentration-dependent killing was observed for all the target bacterial strains (Refer to Appendix, Figure A5.4). It may be mentioned that among the target bacterial strains, **C6** was most potent against *S. aureus* MTCC 96, which is a presumptive MRSA strain (Vudumula et al. 2012).

*5.3.4. Antibiofilm Activity of **Compound 6**-loaded HSA Nanocarrier (C6-HNC)*

The potent bactericidal activity exhibited by **C6**-HNC against *S. aureus* MTCC 96 suggested that the amphiphile-loaded nanocarrier could perhaps be deployed for eradication of biofilm formed by this bacterium. Interestingly, an MTT-based colorimetric assay revealed a systematic and prominent loss in the viability of *S. aureus* biofilm-associated cells upon treatment with increasing concentrations of **C6**-HNC (Figure 5.9A). FESEM analysis of untreated as well as HNP-treated *S. aureus* MTCC 96 biofilm revealed a cluster of cells displaying the typical spherical morphology and prominent cell-cell adhesion associated with biofilm formation (Figure 5.9B, panels i-ii). It was also noted that in the case of HNP-treated *S. aureus* MTCC 96 biofilm, a bunch of smaller size HNPs adhering on to the biofilm were discernible (Figure 5.9B, panel ii). Interestingly, FESEM analysis could capture the antibiofilm activity of **C6**-HNC as a significant disruption of *S. aureus* MTCC 96 biofilm was conspicuous in the form of gross morphological perturbation of cells and breach of the typical cell-cell adhesion (Figure 5.9B, panel iii). These findings suggested that **C6**-loaded HSA nanocarrier could infiltrate the *S. aureus* biofilm matrix to establish contact with the underlying cells, and the antibiofilm activity of the nanocarrier is perhaps accounted by the release of the bactericidal payload (**C6**) and its resultant action on biofilm-associated cells.

5.3.5. Eradication of Catheter-associated Biofilm

Intravascular and urinary catheters are the most commonly used implantable medical devices. They are highly vulnerable to colonization by bacterial biofilm that display remarkable resistance to antibiotic-mediated therapy leading to the development of persistent catheter-associated infections (Costerton et al. 1999, Donlan and Costerton 2002, Stewart and Costerton 2001, Noimark et al. 2009). Although a number of prudent strategies based on surface coating with antibacterials have been proposed to

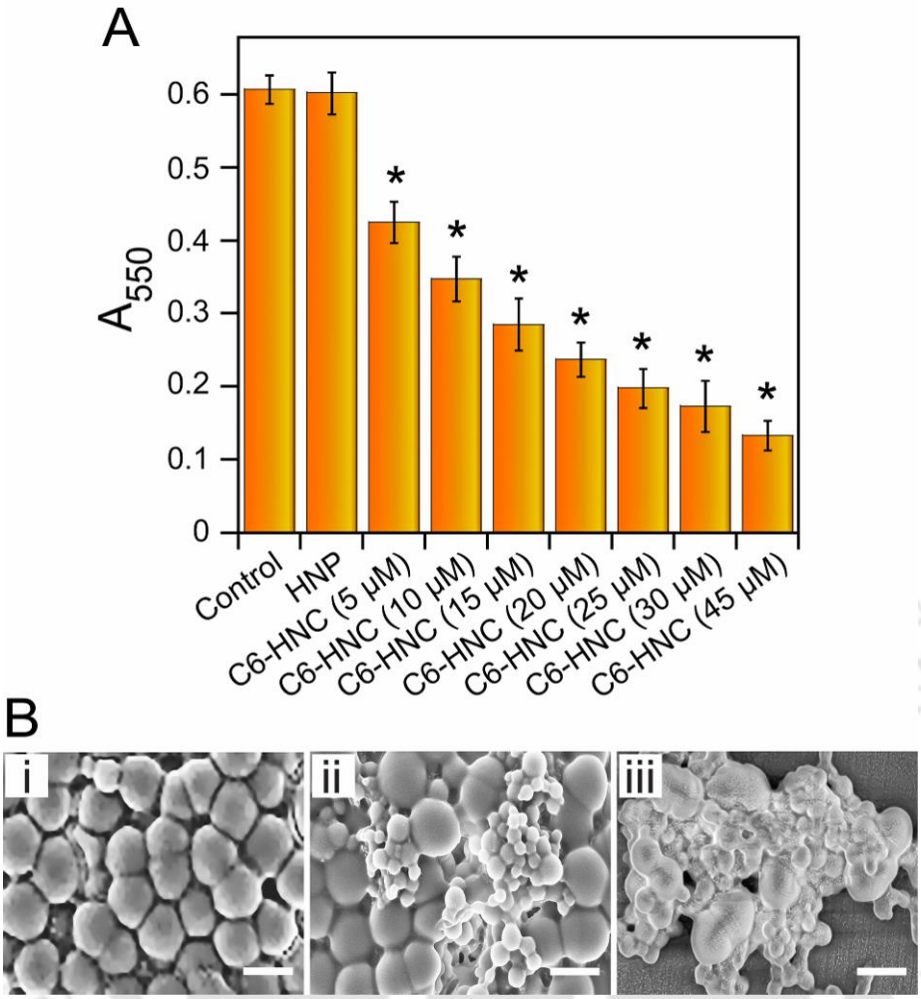

Figure 5.9. (A) MTT assay to determine the effect of **C6**-HNC on the viability of *S. aureus* MTCC 96 biofilm. The concentrations of **C6** in **C6**-HNC samples are indicated in parentheses. Statistically significant values derived by ANOVA are indicated by asterisk marks. ∗ indicates *p* value <0.001. (B) FESEM images of (i) untreated *S. aureus* MTCC 96 biofilm and *S. aureus* MTCC 96 biofilm treated with (ii) HNPs and (iii) **C6**-HNC (corresponding to 30 μM **C6** concentration). Scale bar for the images is 1.0 μm.

prevent biofilm formation on catheters (Hetrick and Schoenfisch 2006, Gutierrez-Gonzalez and Boto 2010, Furno et al. 2004), eradication of catheter-associated biofilm infection remains a serious therapeutic challenge and underscores the critical need of bactericidal agents that can abolish established biofilms from a catheter surface. The significant bactericidal activity of **C6** on preformed biofilms suggested that the amphiphile can perhaps be deployed for eradication of catheter-associated biofilm.

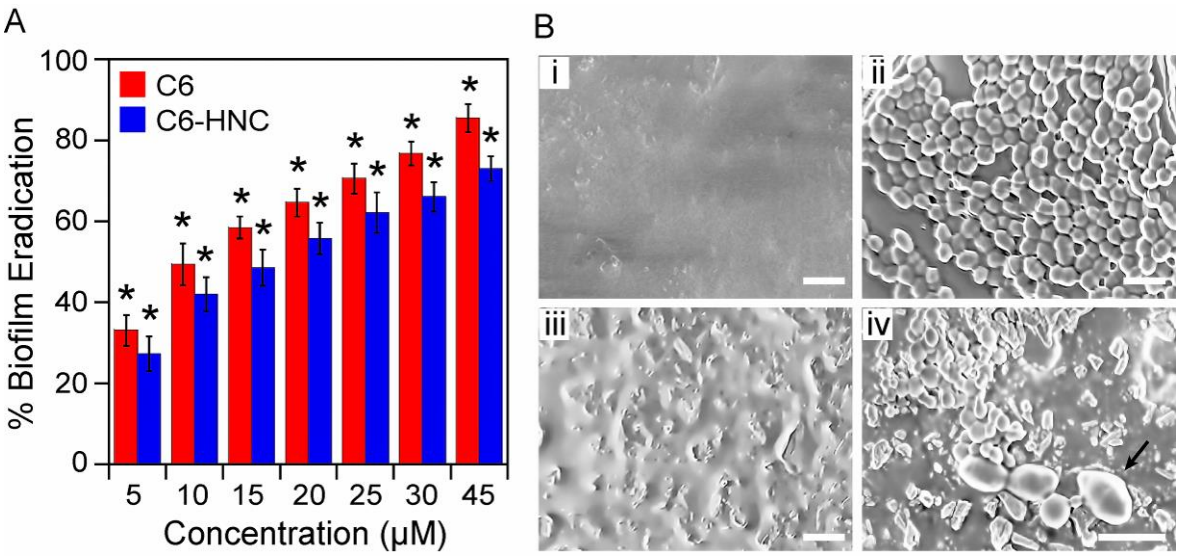

Figure 5.10. (A) MTT assay to ascertain eradication of *S. aureus* MTCC 96 biofilm from the surface of a Foley's urinary catheter treated with **C6** and **C6**-HNC. (B) FESEM images of Foley's urinary catheter segments indicating (i) bare catheter surface, (ii) untreated *S. aureus* MTCC 96 biofilm, (iii) *S. aureus* MTCC 96 biofilm treated with 30 μM **C6**, and (iv) *S. aureus* MTCC 96 biofilm treated with **C6**-HNC (corresponding to 30 μM **C6**). The arrow in panel iv indicates a damaged cell. The scale bar for the FESEM images is 2.0 μm.

To this end, *S. aureus* MTCC 96 was chosen as a model biofilm forming target bacteria and grown on Foley's urinary catheter, given the propensity of *S. aureus* to adhere to the catheter surface and its relevance in catheter-associated urinary tract infections (Muder et al. 2006). Interestingly, an MTT assay indicated a significant dose-dependent annihilation of *S. aureus* biofilm from the surface of the catheter upon treatment with **C6** as well as **C6**-HNC albeit to a marginally lesser extent (Figure 5.10A). Obliteration of *S. aureus* MTCC 96 biofilm from the surface of the catheter is likely to be a function of the local concentration of the bactericidal amphiphile available at the abiotic surface. In case of treatment with **C6**, the amphiphile is readily accessible for its action on the biofilm, whereas in case of **C6**-HNC, release of the amphiphile from the nanocarrier is a prerequisite for its subsequent action on established biofilm. This may account for the slightly higher eradication of *S. aureus* MTCC 96 biofilm from the surface of the catheter treated with **C6** as against treatment with **C6**-HNC. FESEM analysis provided additional evidence for antibiofilm activity of **C6** as well as **C6**-HNC on the catheter surface.

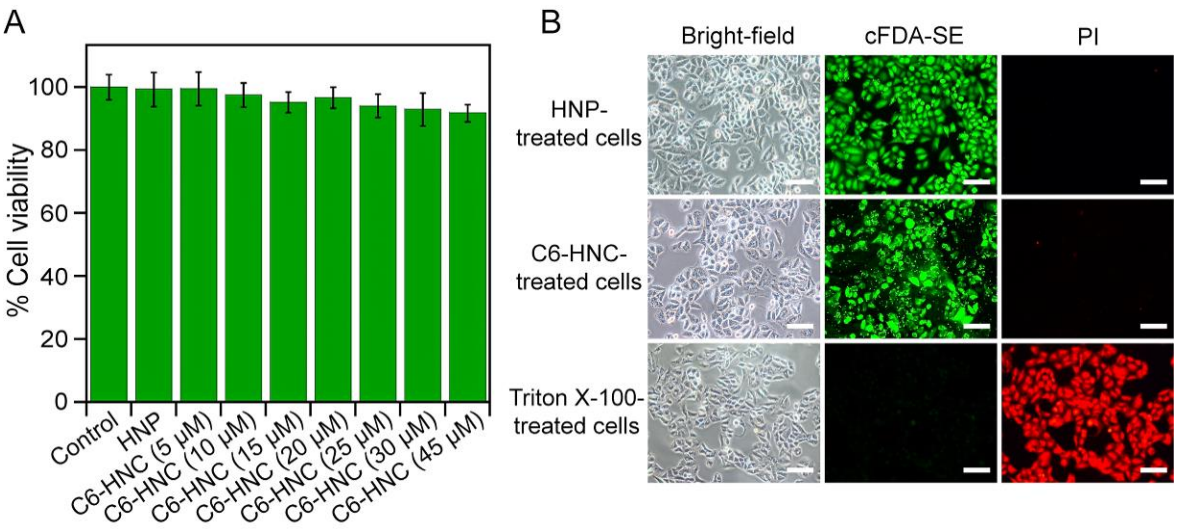

Figure 5.11. (A) MTT-based assay to determine the cytotoxic effect of **C6**-HNC on HeLa cells. The concentrations of **C6** in **C6**-HNC are mentioned in parentheses. (B) Fluorescence microscope images of HNP-treated, **C6**-HNC-treated, and Triton X-100-treated HeLa cells. The scale bar for the images is 50 μm.

In case of untreated sample, densely packed adherent cells of *S. aureus* MTCC 96 typically associated with biofilm architecture were noticeable on the surface of Foley's urinary catheter (Figure 5.10B, panel ii). Exposure of the biofilm-colonized catheter to **C6** resulted in a remarkable eradication of *S. aureus* MTCC 96 biofilm from the surface of the catheter (Figure 5.10B, panel iii). Elimination of *S. aureus* MTCC 96 biofilm from the catheter surface was also conspicuous in case of **C6**-HNC treatment, wherein disintegration of the biofilm network and loss of typical cell morphology was evident (Figure 5.10B, panel iv). Collectively, the findings of these experiments highlighted the potential of the amphiphile **C6** and **C6**-loaded HSA nanocarrier to annihilate established *S. aureus* biofilm from a clinically relevant surface.

5.3.6. Cytotoxic Effect of C6-HNC

With regard to potential therapeutic application of **C6**-loaded HSA nanocarrier for eradication of established *S. aureus* biofilm from a catheter surface, it is critical that the payload nanocarrier should not render any deleterious cytotoxic effect on host cells. To this end, HeLa cells were chosen as model human cells to ascertain the cytotoxic effect of **C6**-HNC. Interestingly, an MTT-based assay revealed that the amphiphile-loaded

nanocarrier did not perturb the metabolic activity and viability of HeLa cells (Figure 5.11A) even at concentrations (30 μM and 45 μM **C6**), which rendered effective eradication of *S. aureus* MTCC 96 biofilm from the catheter surface (Figure 5.10A). Fluorescence microscope analysis of HeLa cells treated with **C6**-HNC (30 μM) revealed the presence of a large number of cFDA-SE stained cells, suggesting that the cells were viable (Figure 5.11B). Furthermore, HeLa cells treated with either HNPs or **C6**-HNC failed to exhibit any PI staining, which suggested the lack of any membrane damage. Collectively, MTT assay and fluorescence microscope analysis indicated the nontoxic nature of **C6**-loaded HSA nanocarrier and highlighted the potential of the developed nanocarrier in device-associated antibiofilm therapy.

5.4. Significant Findings

The salient findings of this chapter are as follows:

1. A **C6**-loaded human serum albumin (HSA)-based nanocarrier was generated and characterized by microscopic and spectroscopic techniques.
2. At the highest concentration of **C6** (800 μM), the loading capacity of HNPs and the amount of encapsulated **C6** was observed to be around 8.2% and 125 μM, respectively.
3. At a physiological pH of 7.4, a sustained release of the bactericidal payload (**C6**) from **C6**-HNC was observed, whereas in acidic pH (pH 3.0), release of **C6** from the nanocarrier was rapid, as compared to the profile observed at pH 7.4.
4. **C6**-HNC displayed potent membrane-directed bactericidal activity as well as antibiofilm activity.
5. Interestingly, both **C6** as well as **C6**-HNC could effectively eradiate *S. aureus* MTCC 96 biofilm from the surface of a Foley' urinary catheter.
6. **C6**-HNC was non-toxic to cultured HeLa cells at concentrations, which rendered significant eradication of *S. aureus* MTCC 96 biofilm from the catheter surface.

Significant Findings

The collective results obtained from Chapters 2-5 of the present investigation clearly highlight the therapeutic potential of the dipyridinium-based cationic amphiphile (**C6**). Although the results point out the high bactericidal activity associated with the amphiphile and how this activity could be explored in adjuvant and antibiofilm applications, the potential cytotoxic implications of the amphiphile as detailed in Chapter 2 may limit the scope of this molecule as an antibacterial therapeutic when higher levels of the amphiphile are required to eliminate the target bacteria. An interesting and radical approach to prevail over this impediment is to judiciously tweak the structure of a bactericidal amphiphile so as to enhance its affinity manifold towards target bacteria as opposed to host cells. This design principle would then ensure high target cell selectivity, minimize gratuitous host cell toxicity and thereby augment the therapeutic potential of the molecule. Based on the aforementioned tenet, the subsequent chapter of this thesis describes the generation of a Zn(II) complex of the neutral pyridine-based synthetic amphiphile **C5**. Interestingly, this complexation enables the new amphiphile (referred to as **C5**-Zn) to have strong interactions with metal reactive groups (MRGs) in bacterial cell envelope, which is leveraged in a remarkable enhancement in the membrane-directed bactericidal activity of the amphiphile.

Chapter 6

Zinc Complex of a Neutral Pyridine-based Amphiphile as a Potent Bactericidal Agent

This chapter presents a rational drug design approach rendered by a zinc-triggered remarkable enhancement in the bactericidal potency and therapeutic index of a neutral pyridine-based amphiphile.

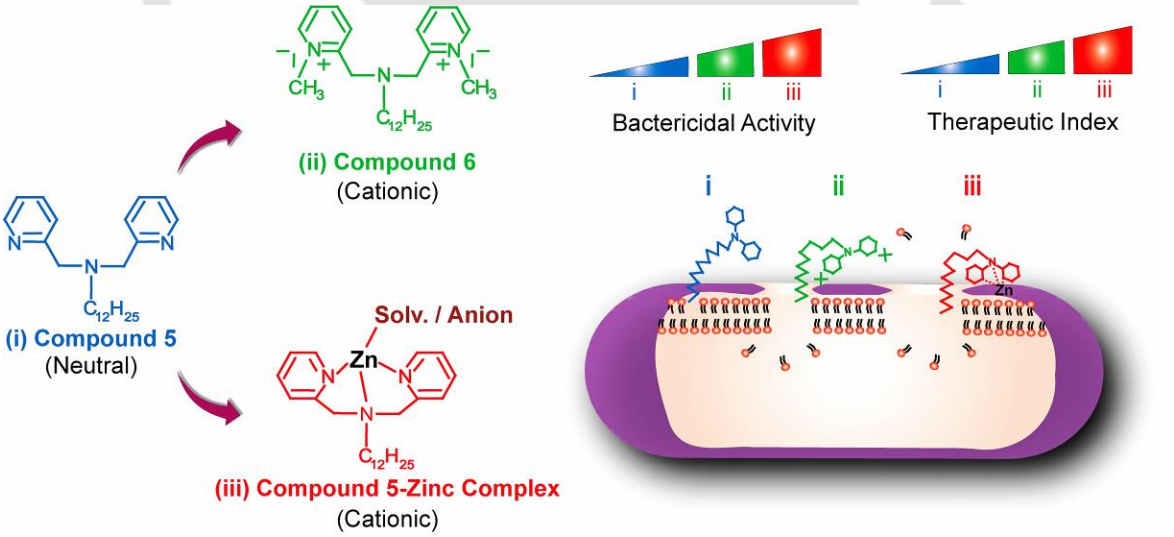

TH-1410_10610607

ABSTRACT

The present study describes the generation of a potent amphiphilic bactericidal material tailored to leverage interactions with metal reactive groups (MRGs) present in bacterial cell surface envelope. Complexation of Zn(II) with a neutral pyridine-based synthetic amphiphile (**C5**) generated the cationic **C5**-Zn, which exhibited manifold higher membrane-directed bactericidal activity as compared to the neutral amphiphile **C5** or the cationic amphiphile bearing two pyridinium head groups (**C6**). The enhanced bactericidal activity of **C5**-Zn complex was also evident in FESEM, AFM and TEM analysis. The relevance of MRGs in **C5**-Zn-bacteria interactions was verified by amphiphile-bacteria binding studies and metal protection assays performed with Mg(II), which provided a distinct shield against **C5**-Zn mediated killing of target bacterial cells. **C5**-Zn displayed bactericidal activity in simulated gastric fluid (SGF) and the enhanced membrane-directed bactericidal activity of **C5**-Zn could be harnessed in adjuvant application to increase the efficacy of erythromycin. Given the relevance of Zn(II) in *S. aureus* biofilm formation and the propensity of **C5** to bind Zn(II) and generate the highly potent **C5**-Zn, the amphiphile **C5** could be deployed as a potential pro-drug to prevent *S. aureus* MTCC 96 biofilm formation. Further **C5**-Zn was a highly potent antibiofilm agent, which could render significant eradication of *S. aureus* biofilm. Based on the lack of resistance in target bacteria coupled with a favorable therapeutic index (IC_{50}/MIC) and non-toxic nature, **C5**-Zn holds significant implications as a potential antibacterial therapeutic material.

6.1. Introduction

The prevalence of antibiotic-resistant pathogenic bacteria coupled with a critical dearth of new therapeutic agents to counter their challenge is a contemporary healthcare problem (Fischbach and Walsh 2009, Nikaido 2009, Gootz 2010, Morar and Wright 2010, Davies and Davies 2010, Fair and Tor 2014). This predicament demands a radical approach in order to develop antibacterial agents that can act on irrefutable cellular targets and be counterproductive to resistance development. In this context, antibacterials that target the membrane are considered as viable candidates, since the probability of developing resistance against such molecules would necessitate extensive overhaul of membrane components and thus impose a physiologically insurmountable task on the target bacteria (Hurdle et al. 2011, Silver 2011, Adhikari et al. 2013). To this end, synthetic amphiphiles, which mimic the bactericidal activity of membrane-acting antimicrobial peptides (AMPs) are considered as promising antibacterial agents (Findlay et al., 2010, Gokel and Negin 2012). The interesting prospect of synthetic amphiphiles as antibacterial materials is also validated by literature reports, which describe the synthesis and bactericidal activity of diverse AMP-mimicking amphiphilic scaffolds (Vudumula et al. 2012, Paslay et al. 2012, Palermo and Kuroda 2009, LaDow et al. 2011, Zimmermann et al. 2013).

Structural descriptors that impart an overriding influence on the bactericidal activity of synthetic amphiphiles are well known. Initial interaction with the anionic bacterial cell surface is generally mediated by the cationic charge of the molecule, while the hydrophobic moiety of the amphiphile renders subsequent insertion into the membrane leading to extensive membrane disruption and cell death (Findlay et al. 2010, Vudumula et al. 2012, Song et al. 2011). Functional groups that render key attributes to synthetic amphiphiles such as cationic charge, charge density and hydrophobicity have been implicated in their bactericidal activity (Vudumula et al. 2012, Paslay et al. 2012, Palermo and Kuroda 2009, LaDow et al. 2011, Kuroda and DeGrado 2005, Palermo et al. 2009). Based on the fundamental understanding of the structure-activity relationship reported in previous studies, there is considerable scope to adopt a rational approach and select appropriate functional groups as building blocks in order to impart high bactericidal activity to synthetic amphiphiles. In order to realize the therapeutic potential of bactericidal synthetic amphiphiles, it is imperative that the amphiphile is biocompatible and non-toxic

to host cells at concentrations relevant to *in vivo* elimination of the target bacteria. To fulfill these criteria, a viable approach during synthesis of the amphiphile is to select functional groups that ensure high bactericidal activity of the molecule and prevent host cell toxicity. Previous studies have illustrated that the cationic charge and hydrophobicity of synthetic amphiphiles, which hold key to their bactericidal activity can also have considerable effect on the manifestation of host cell toxicity. A judicious balance between cationic attribute and hydrophobicity is thus essential to render high antibacterial activity and curtail cytotoxic effects (Song et al. 2011). It is also proposed that modulation of the cationic group, hydrophobicity and conformational flexibility is likely to augment the antibacterial selectivity of amphiphilic molecules (Palermo and Kuroda 2009, Palermo et al. 2009, Oda et al. 2011, Fischer et al. 2003) and thus enhance their therapeutic potential.

Bacterial cells are negatively charged and this attribute originates from the presence of teichoic acid or lipopolysaccharide (Weidenmaier and Peschel 2008, Gutsmann and Seydel 2010, French et al. 2013). It is thus envisaged that rendering a cationic charge to a synthetic amphiphile is likely to promote strong interactions with the anionic bacterial cells and augment the antibacterial selectivity of the molecule. In this endeavour, deployment of a metal ion to impart cationic charge to an amphiphile can be a radical approach, as anionic metal-reactive groups (MRGs) ubiquitous in bacterial envelope (French et al. 2013, Kern et al. 2010) is likely to sustain a strong interaction and significantly enhance the affinity of the amphiphile for target bacterial cells, leading to superior bactericidal activity and antibacterial selectivity.

Based on aforementioned rationale, generation of the zinc complex of a neutral pyridine-based amphiphile (**C5**-Zn) and demonstration of its heightened membrane-directed bactericidal activity is discussed in this chapter. The application of the membrane-targeting amphiphile **C5**-Zn as an adjuvant to enhance the efficacy of the therapeutic antibiotic erythromycin is illustrated. The study demonstrates the pro-drug potential of **C5**-Zn realized through complexation of zinc and generation of a potent bactericidal material thereof and this phenomenon also rendered the application of the amphiphilic material as a potent bactericidal and antibiofilm agent. The non-toxic nature and antibacterial selectivity of **C5**-Zn achieved through metal complexation highlights the merit of the amphiphilic material as a potentially therapeutic antibacterial agent.

6.2. Materials and Methods

6.2.1. Growth Media and Chemicals

Brain-Heart Infusion (BHI) Broth, Nutrient Broth (NB) and crystal violet (CV) were purchased from HiMedia, Mumbai, India. Dimethyl sulfoxide (DMSO), and absolute ethanol were procured from Merck, Mumbai, India. Magnesium chloride salt and N-2-Hydroxyethyl Piperazine N-2 Ethane Sulphonic acid (HEPES Buffer) was procured from Sisco Research Laboratories SRL, Mumbai, India. 5 (and 6)-carboxyfluorescein diacetate succinimidyl ester (cFDA-SE), propidium iodide (PI), 3,3'-dipropylthiadicarbocyanine iodide $DiSC_3(5)$, 1-N-phenyl-naphthylamine (NPN), congo red (CR), 3-(4,5-dimethyl-2-thiazolyl)-2,5-diphenyl-2H-tetrazolium bromide (MTT), Dulbecco's Modified Eagle Medium (DMEM), trypsin–EDTA, valinomycin, polymyxin B, erythromycin and zinc perchlorate were procured from Sigma Aldrich Chemicals, USA. Fetal bovine serum (FBS) was procured from PAA Laboratories, USA.

6.2.2. Synthetic Amphiphile

In the present study, the pyridine-based synthetic amphiphiles **C5** and **C6** and the Zn(II) complex of **C5** referred to as **C5**-Zn were used. The general structures of **C5**, **C6** and **C5**-Zn are shown in Figure. 6.1.

6.2.3. Compound 5-Zinc Complex

Initially a 50 mM stock solution of $Zn(ClO_4)_2$ was prepared in sterile MilliQ water. **C5**-Zn was allowed to form by adding equimolar concentration of $Zn(ClO_4)_2$ to a solution of **C5** (10 mM in DMSO) followed by continuous stirring at room temperature overnight. Formation of **C5**-Zn was ascertained by ESI-MS using an Agilent Technologies 6520 Accurate Mass Spectrometer. FT-IR spectra of **C5**-Zn were recorded in KBr pellets at 4 cm^{-1} resolution in an infrared spectrometer (Perkin-Elmer Spectrum One). Eight scans were performed for every sample in the range of 4000 cm^{-1} to 450 cm^{-1}. A background spectrum for pure KBr was also measured.

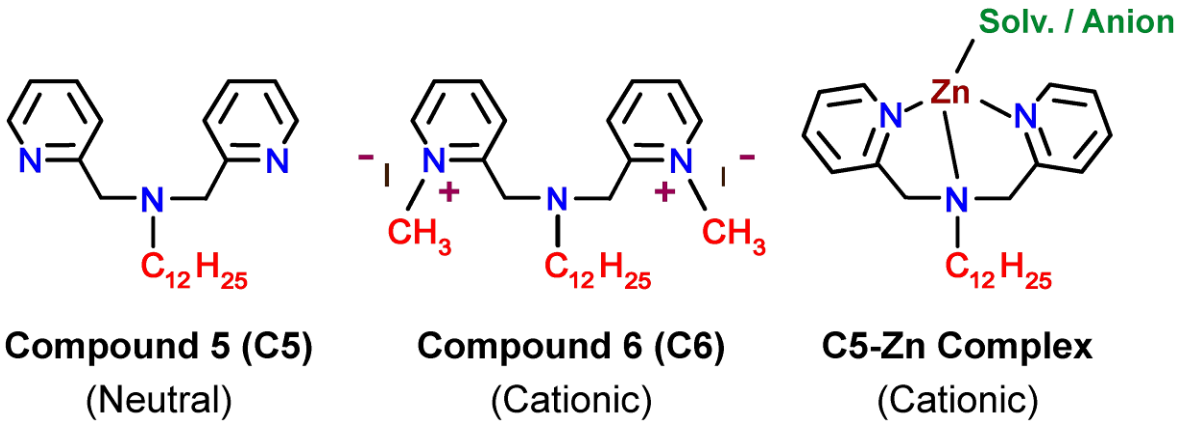

Compound 5 (C5) (Neutral) **Compound 6 (C6)** (Cationic) **C5-Zn Complex** (Cationic)

Figure 6.1. Structure of synthetic amphiphiles used in the present study.

6.2.4. Apparent Binding Constant for Formation of C5-Zn

To determine binding stoichiometry and binding affinity of zinc towards **C5** at room temperature (at 298 K), UV-visible titration spectra was pursued. A 25 µM solution of **C5** prepared in buffered methanol (4:1 methanol: water) solvent was titrated with $Zn(ClO_4)_2$ solution so that the effective Zn(II) concentration was varied between 0-1250 µM. UV-visible absorption spectra was recorded in a Cary UV-100 spectrophotometer (Varian, USA) using 10 mm path length cuvette in the range of 200-500 nm wavelength. The apparent binding constant for the formation of **C5**-Zn was determined using modified Benesi-Hildebrand (B-H) plot (Benesi and Hildebrand 1949) and the following equation:

$$1/ (A - A_0) = 1/ \{K (A_{max} - A_0) C\} + 1/ (A_{max} - A_0)$$

Where A_0 is the absorbance of **C5** at absorbance maximum (λ = 262 nm), A is the observed absorbance at that particular wavelength in the presence of a certain concentration of the metal ion (C), A_{max} is the maximum absorbance value that was obtained at λ = 262 nm during titration with varying Zn(II) concentrations. The apparent binding constant K (M^{-1}) was determined from the slope of the linear plot and C is the concentration of Zn(II) added during titration studies.

6.2.5. Bacterial Strains and Growth Conditions

The target bacterial strains used in the present study included Gram-positive *S. aureus* MTCC 96 and *L. monocytogenes* Scott A and Gram-negative *E. coli* MTCC 433 and *E. aerogenes* MTCC 2822. *S. aureus* MTCC 96 and *L. monocytogenes* Scott A were propagated in BHI broth at 37°C and 180 rpm for 12 h. *E. coli* MTCC 433 and *E. aerogenes* MTCC 2822 were grown in NB medium at 37°C and 180 rpm for 12 h. All the bacterial strains were grown from frozen stocks and sub-cultured prior to their use in experiments.

*6.2.6. Minimum Inhibitory Concentration (MIC) of **C5**-Zn*

MIC of **C5**-Zn was ascertained against Gram-positive bacteria *S. aureus* MTCC 96 and *L. monocytogenes* Scott A and Gram-negative bacteria *E. coli* MTCC 433 and *E. aerogenes* MTCC 2822. The bacterial strains were inoculated at 1% level in microtitre wells (approximately 5×10^5 CFU/well) having 100 µL of the specific growth medium and propagated overnight at 37°C and 180 rpm in presence of varying concentrations of **C5**-Zn. The growth of the bacterial strains was verified by measuring absorbance at 600 nm in a microtitre plate reader (Infinite M200, TECAN, Switzerland). MIC of **C5**-Zn was defined as the minimum amphiphile concentration that resulted in growth inhibition of the target bacteria (A_{600}<0.1). The MIC values were determined from six independent experiments and expressed as average values.

6.2.7. Antibacterial Activity of Amphiphiles

The bactericidal activity of amphiphiles was determined by the following experiments:

6.2.7.1. Field Emission Scanning Electron Microscope (FESEM) Analysis

Overnight grown cells of *S. aureus* MTCC 96 and *E. coli* MTCC 433 were collected by centrifugation, washed twice with sterile PBS and resuspended in the same. Approximately 10^6 CFU/ mL cells were treated with $Zn(ClO_4)_2$, **C5** and **C5**-Zn (6.0 µM each) for 6 h at 37°C. Control samples consisted of untreated cells incubated in sterile PBS for the same period. Treated as well as untreated cells were washed twice with sterile PBS and fixed in 2.5% glutaraldehyde for 90 mins at 4°C. Following fixation, cells were washed and

resuspended in sterile MilliQ grade water. A 10 µL aliquot of each sample was spotted on separate aluminium foil covered glass stubs and air dried in a laminar hood. Subsequently, the samples were coated with gold plasmon and examined in a field emission scanning electron microscope (Zeiss Sigma, USA) and their images were recorded.

6.2.7.2. Atomic Force Microscope (AFM) Analysis

Samples of untreated cells (control) and cells treated with $Zn(ClO_4)_2$, **C5** and **C5**-Zn (6.0 µM each) for 6 h at 37ºC were prepared by following the procedure described in section 6.2.7.1. Treated as well as untreated cells were washed twice with sterile PBS and a 10 µL aliquot of each sample was spotted on sterile glass cover slips (18 mm x 18 mm) and air-dried in laminar hood. Atomic force microscope images were captured with an Agilent 5500 AFM (Agilent Technologies, Chandler, AZ, USA). Cantilevers made of silicon nitride were used having a resonant frequency of ca. 150 to 250 kHz. Images were acquired in non-contact mode, with 10 µm x 10 µm area at a scan rate of 0.5- 1.0 line/s. Analysis of the topographic images of the surface was accomplished by using the WSxM v5.0 Develop 6.5 image viewer software (Horcas et al. 2007).

6.2.7.3. Transmission Electron Microscope (TEM) Analysis

Samples of untreated cells (control) and cells treated with $Zn(ClO_4)_2$, **C5** and **C5**-Zn (6.0 µM each) for 6 h at 37ºC were prepared by following the procedure described in section 6.2.7.1. Treated as well as untreated cells were washed twice with sterile PBS and a 2.0 µL aliquot of each sample was spotted on carbon coated TEM grid (Pacific Grid, USA) and air-dried in laminar hood. The samples were then subjected to TEM analysis (Jeol JEM 2100, Japan) operating at 200 kV and their images were recorded.

6.2.7.4. cFDA- SE Leakage Assay

Target cells of *S. aureus* MTCC 96 and *E. coli* MTCC 433 were labelled with cFDA-SE following the method described in section 2.2.6.1. cFDA-SE labelled target cells resuspended in 1.0 mL of sterile PBS and treated with **C5**, **C6** and **C5**-Zn (6.0 µM each) at 37ºC and 180 rpm for 6 h. In case of control sample, only DMSO was added to cFDA-SE labelled cells and incubated under the same conditions without amphiphile. Leakage of

cFDA from cells was determined by measuring fluorescence of the cell free supernatant at an excitation wavelength of 488 nm and emission wavelength of 518 nm in a spectrofluorimeter (LS-55 Perkin-Elmer, USA). The fluorescence measurements were recorded after subtracting the fluorescence of effluxed dye from control samples. Fluorescence measurements were recorded from three independent experimental samples.

6.2.7.5. Propidium Iodide (PI) Uptake Assay

A stock solution of PI (1.5 mM) was prepared in sterile MilliQ water. Target cells of *S. aureus* MTCC 96 and *E. coli* MTCC 433 were harvested from overnight grown cultures and resuspended in sterile PBS. Cells (approximately 10^6 CFU/ mL) were treated with **C5**, **C6** and **C5**-Zn (6.0 µM each) at 37ºC and 180 rpm for 6 h. Cells incubated in DMSO under the same conditions without amphiphile was included as control. Following incubation, cells were washed with sterile PBS, resuspended in the same and incubated with PI (final concentration of 30 µM) for 30 min at 37°C in a circulating water bath incubator (Amersham, USA). Subsequently, the cells were centrifuged and washed with sterile PBS to remove excess dye, resuspended in PBS and fluorescence was measured in a spectrofluorimeter (LS-55 Perkin-Elmer, USA) at an excitation wavelength of 535 nm and emission wavelength of 617 nm. The values obtained for untreated cells were subtracted from all experimental values. Fluorescence measurements were acquired for three independent samples.

6.2.7.6. Fluorescence Microscope Analysis

Cells of *S. aureus* MTCC 96 and *E. coli* MTCC 433 suspended in sterile PBS (approximately 10^6 CFU/ mL) were treated with **C5**, **C6** and **C5**-Zn (6.0 µM each) at 37ºC and 180 rpm for 6 h. In case of control sample, DMSO was added to the cells and incubated under the same conditions. For comparison, cells treated with 6.0 µM $Zn(ClO_4)_2$ at 37ºC and 180 rpm for 6 h were also included. Subsequently, cells were washed twice with sterile PBS to remove unbound amphiphile or $Zn(ClO_4)_2$ and labelled with cFDA-SE and PI as described in section 2.2.6.1 and section 6.2.7.5, respectively. The stained samples were fixed in 2.5% glutaraldehyde and washed twice with sterile PBS. A 10 µl aliquot of the stained sample was spotted on a clean glass slide, air dried and observed under

fluorescence microscope (Eclipse Ti-U, Nikon, USA) with a filter that allowed blue light excitation at for cFDA-SE and green light excitation in case of PI stained cells. The images of the cells were recorded.

6.2.7.7. Flow Cytometry Analysis

The effect of $Zn(ClO_4)_2$, **C5**, **C6** and **C5**-Zn on the viability of *S. aureus* MTCC 96 and *E. coli* MTCC 433 was studied by flow cytometry (FCM), which was performed on a FACS Calibur flow cytometer (Becton-Dickinson Immunocytometry Systems, San Jose, CA, USA) equipped with a 15-mW, 488-nm, air-cooled argon ion laser. The target bacterial cells were pre-labelled with cFDA-SE following the protocol mentioned earlier in section 2.2.6.1 and treated in separate sets with $Zn(ClO_4)_2$, **C5**, **C6** and **C5**-Zn (6.0 µM each) for 6 h at 37°C in a circulating water bath incubator (Amersham, USA). Following treatment, the cells were analysed along with unlabelled-untreated cells as well as labelled-untreated cells (control). For FCM analysis, approximately 10^6 cells per ml were analyzed at a low flow rate setting (150-500 cells per second) and the FACS instrument was adjusted to acquire 50,000 fluorescent events. Appropriate voltage and threshold parameter were adjusted for unlabeled-untreated cells. The corresponding signal of unlabeled-untreated cells was set in the lower left quadrant in order to compensate for cellular autofluorescence. All the signals were collected in logarithmic mode. Green fluorescence of cFDA-SE stained cells was detected in the FL-1 channel (band pass filter of 530 nm). Acquisition of fluorescence data was accomplished by setting a gate in the forward-angle light scatter (FSC) vs. sideward scatter (SSC) plot, which facilitated discrimination of bacterial cells from other artefacts. Data were acquired and analyzed with the CellQuest Pro software (BD CellQuestTM Pro Version 6.0, Becton-Dickinson, USA) and the WinMDI software program WinMDI ver 2.9 (http://en.bio-soft.net/other/WinMDI). The data was analysed with the aid of statistical tables

6.2.7.8. Membrane Depolarization Assay

Cells of *S. aureus* MTCC 96 and *E. coli* MTCC 433 were grown till mid-logarithmic phase (OD_{600} = 0.4-0.5). The cells were harvested by centrifugation, washed and resuspended in the same buffer solution (5.0 mM HEPES, 5.0 mM glucose, pH 7.4) to an OD_{600} of 0.05 and incubated with 0.4 µM $DiSC_35$ for 1h at 37°C followed by 15 min incubation in 100 mM KCl. Subsequently the cell suspensions (1.0 mL) in separate sets were placed in a cuvette to which $Zn(ClO_4)_2$, **C5**, **C6** and **C5**-Zn (6.0 µM each) was added and the fluorescence emission intensity (λ_{Ex} = 622 nm and λ_{Em} = 670 nm) was monitored in short time intervals in a spectrofluorimeter (LS-55 Perkin-Elmer, USA) with excitation and emission slit width of 10 nm each. Valinomycin (30 µM) treated cells and DMSO treated cells were included as positive control and negative control samples, respectively. Fluorescence measurements were taken for three independent experimental samples.

6.2.7.9. Outer Membrane Permeabilization Assay

A stock solution of NPN (500 µM) was made in acetone. Initially, target cells of *E. coli* MTCC 433 were grown in NB at 37°C in a shaker incubator till mid-log phase (A_{600} of 0.5). The cells were centrifuged, washed twice with 5.0 mM HEPES buffer (pH 7.4) and resuspended in the same buffer. NPN was added (at a final concentration of 10 µM) to 1.0 ml aliquot of target cells, which was interacted in separate cuvettes with $Zn(ClO_4)_2$, **C5**, **C6** and **C5**-Zn (6.0 µM each). Enhancement in the fluorescence intensity of NPN was measured at regular intervals in a spectrofluorimeter (LS-55 Perkin-Elmer, USA) at an excitation and emission wavelength of 350 nm and 420 nm, respectively. Polymixin B (1.0 µg/mL) treated cells and DMSO treated cells were used as positive control and negative control samples, respectively. Fluorescence measurements were taken for three independent samples.

6.2.8. Binding of C6 and C5-Zn with Bacterial Cells

UV-visible spectra of varying concentrations of **C6** were recorded at 265 nm in a spectrophotometer and a calibration plot was generated for quantification of **C6** as described earlier in section 5.2.7. For quantification of **C5**-Zn, a concentration-dependent calibration plot for zinc was generated using atomic absorption spectrophotometer

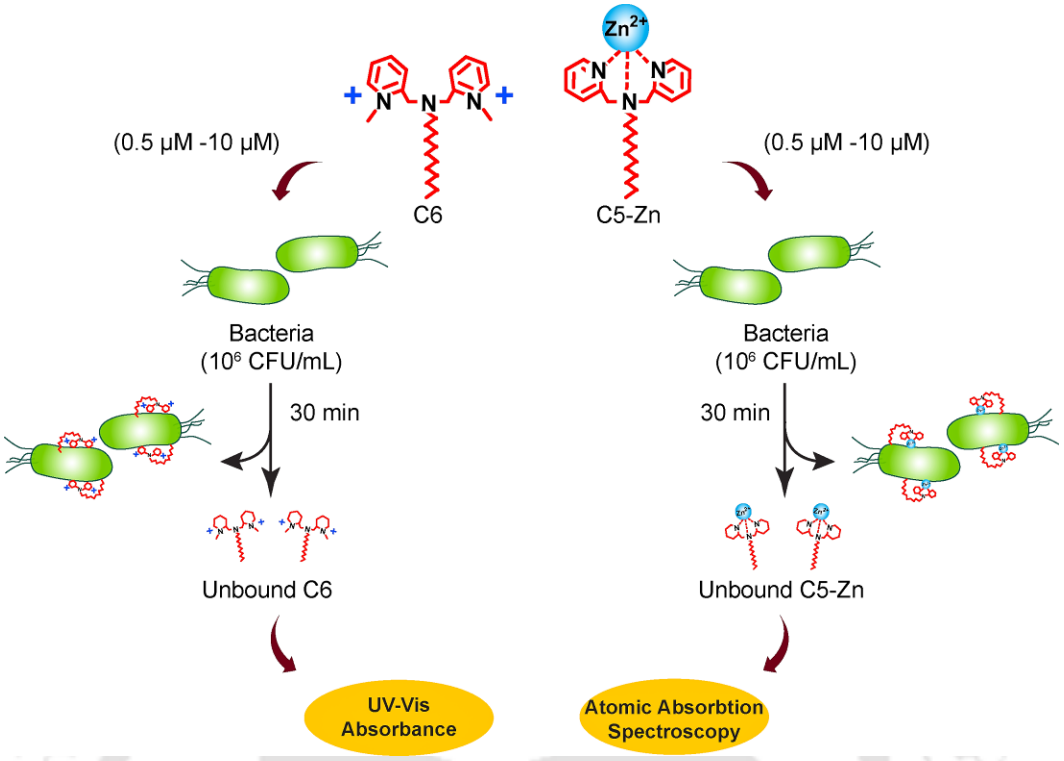

Figure 6.2. Schematic representation of the experimental protocol for determining cell-bound **C6** and **C5**-Zn.

(AA240, Varian, Netherlands) prior to actual sample scanning. To ascertain binding of amphiphiles onto bacterial cells, varying concentrations of **C6** and **C5**-Zn (0.5 µM -10 µM each) was added to *S. aureus* MTCC 96 and *E. coli* MTCC 433 cells (10^6 CFU/mL each) suspended in sterile 0.85% saline and incubated at 37°C and 180 rpm. Following 30 min of incubation, cells were separated by centrifugation and unbound **C6** and **C5**-Zn in the cell free supernatant was ascertained by UV-visible and atomic absorption spectroscopy, respectively. Following spectroscopic measurements, quantification of unbound **C6** and **C5**-Zn was accomplished using the previously generated calibration plots. The concentration of bound amphiphile was ascertained from the difference of initial amphiphile concentration used to interact with bacterial cells and the concentration of unbound amphiphile. A plot of bound amphiphile (**C6** and **C5**-Zn) as a function of initial amphiphile concentration and a Scatchard plot (Bound/free versus Bound) were generated The slope of the respective Scatchard plot was used to calculate the dissociation constant (K_d) of **C6** and **C5**-Zn. A schematic illustration of the experimental protocol used to

determine cell-bound **C6** and **C5**-Zn is indicated in Figure 6.2.

6.2.9. Effect of Mg(II) on the Bactericidal Activity of C5-Zn

E. coli MTCC 433 cells were grown overnight in Nutrient Broth (NB). An aliquot of the grown cells (A_{600} = 0.2) were added in separate sets to 25 mL of fresh NB supplemented with varying concentrations of Mg(II) (0.1 mM, 1.0 mM, 5.0 mM and 10 mM). In these experiments, $MgCl_2$ was used as a source of Mg(II). The cell suspensions were grown in a shaker incubator at 37ºC and 180 rpm. Following 1 h of incubation, 32 µM of **C5**-Zn was added to one set of cells. Growth of *E. coli* MTCC 433 cells in all the samples (untreated cells and cells treated with **C5**-Zn) was monitored by measuring absorbance (A_{600}) at regular intervals. For comparison, growth of cells in NB alone as well as cells grown in NB for 1 h without Mg(II) supplementation followed by treatment with 32 µM of **C5**-Zn were also measured.

6.2.10. Bactericidal Activity of C5-Zn in Simulated Gastric Fluid (SGF)

Cells of *E. coli* MTCC 433 and *L. monocytogenes* Scott A were grown overnight. The cells were washed twice with sterile 0.85% saline to remove media ingredients and were resuspended (approximately 10^6 CFU of each target bacteria) in simulated gastric fluid (SGF), which was prepared according to the method described earlier.(Charteris et al. 1998) The pH of SGF was adjusted to 2.5 with 1.0 N HCl. Subsequently, the cells were treated in SGF with various concentrations of **C5**-Zn (5.0 µM, 10 µM, 15 µM and 20 µM) at 37ºC for 2 h. The control sample consisted of cells suspended in SGF alone. The samples were plated periodically and the results were expressed as percentage viability of cells as compared to control (cells suspended in SGF alone). All experiments were performed in triplicates. Data analysis and calculation of standard deviation was performed with Microsoft Excel 2010 (Microsoft Corporation, USA). A one way analysis of variance (ANOVA) was performed using Sigma Plot.

6.2.11. Application of C5-Zn as an Adjuvant in Combination with Erythromycin

To ascertain the adjuvant activity of **C5**-Zn, a 10 µL aliquot of *E. coli* MTCC 433 cell suspension (10^6 CFU suspended in sterile PBS) was inoculated onto sterile 96 well microtitre plate wells having 100 µL specific growth media incorporated in separate sets with a range of erythromycin (5.0 µg/mL, 10 µg/mL, 15 µg/mL and 20 µg/mL). For every concentration of erythromycin, varying concentrations of **C5**-Zn was used in combination (2.5 µM, 5.0 µM, 7.5 µM and 10 µM). The cells were incubated at 37°C and 180 rpm for 6 h. Bacterial cell growth was estimated by measuring absorbance at 600 nm in a microtitre plate reader (Infinite M200, TECAN, Switzerland) and expressed as percentage growth inhibition compared to untreated cells. The growth of target bacterial cells treated with either varying concentrations of erythromycin or **C5**-Zn was also measured. All experiments were performed in triplicates. Data analysis and calculation of standard deviation was performed with Microsoft Excel 2010 (Microsoft Corporation, USA). The fold decrease in the MIC of erythromycin for **C5**-Zn treated cells was determined. The fractional inhibitory concentration (FIC) index of **C5**-Zn and the nature of interaction between **C5**-Zn and erythromycin was also determined based on a method described previously in section 3.2.6.

6.2.12. Pro-drug Potential of C5 in Presence of Zn(II)

S. aureus MTCC 96 and *E. coli* MTCC 433 cells were grown overnight and an aliquot of the grown cells were added in separate sets to 25 mL of fresh growth media supplemented with 50 µM and 250 µM of Zn(II), respectively. In these experiments, $Zn(ClO_4)_2$ was used as a source of Zn(II). The cell suspensions were grown in a shaker incubator at 37°C and 180 rpm. Following 3 h of incubation, 10 µM and 50 µM of **C5** were added to the growing cells of *S. aureus* MTCC 96 and *E. coli* MTCC 433, respectively. Growth of the target bacterial cells in all the samples was monitored by measuring absorbance (A_{600}) at regular intervals. For comparison, growth of *S. aureus* MTCC 96 and *E. coli* MTCC 433 cells in media only and media supplemented with either 50 µM Zn(II) (in case of *S. aureus* MTCC 96) or 250 µM Zn(II) (in case of *E. coli* MTCC 433) was also measured. Furthermore, growth of the target bacterial cells in media for 3 h without Zn(II) supplementation followed by treatment with either **C5** or **C5**-Zn (10 µM each in case of *S. aureus*

MTCC 96 and 50 µM each in case of *E. coli* MTCC 433) were also measured. All experiments were performed in triplicates. Data analysis and calculation of standard deviation was performed with Microsoft Excel 2010 (Microsoft Corporation, USA).

The pro-drug effect of **C5** in presence of Zn(II) was also evaluated by cFDA-SE leakage assay. Labeling of target bacteria with cFDA-SE was accomplished by following a standard protocol as described in section 2.2.6.1. Approximately 10^6 CFU/mL cFDA-SE labelled cells of *S. aureus* MTCC 96 and *E. coli* MTCC 433 (taken in 5.0 mM HEPES buffer, pH 7.4) were interacted in separate sets with 10 µM Zn(II). In these experiments, $Zn(ClO_4)_2$ was used as a source of Zn(II). The cell suspensions were incubated under shaking conditions at 37°C. Following 1h incubation, 10 µM **C5** was added to one set of cell suspension. Leakage of cFDA from cells was determined at regular intervals by measuring fluorescence of the cell free supernatant at an excitation wavelength of 488 nm and emission wavelength of 518 nm in a spectrofluorimeter (LS-55 Perkin-Elmer, USA). For comparison, leakage of cFDA from cells treated with either 10 µM Zn(II) or 10 µM **C5**-Zn was also measured. Furthermore, leakage of cFDA from cells incubated for 1h in 5.0 mM HEPES buffer devoid of Zn(II) supplementation followed by addition of 10 µM **C5** was also measured. All experiments were performed in triplicates. Data analysis and calculation of standard deviation was performed with Microsoft Excel 2010 (Microsoft Corporation, USA).

6.2.13. Application of C5-Zn as an Antibiofilm Agent

The antibiofilm activity of the amphiphiles was evaluated by performing the following experiments:

6.2.13.1. Microtitre Well Assay for Determination of Biofilm Eradication

S. aureus MTCC 96 biofilm was grown sterile in 96 well microtitre plate by following a standard protocol described earlier in section 4.2.4. For the growth *S. aureus* biofilm, BHI media supplemented with 0.25% glucose was used. In a parallel set, *S. aureus* biofilm was also grown in BHI media having 0.25% glucose and supplemented with 50 µM Zn(II). In these experiments, $Zn(ClO_4)_2$ was used as a source of Zn(II). Following 24 h of biofilm growth in static and humid condition at 37°C, the spent media from the microtitre

plate wells was aspirated and the biofilm was incubated in fresh growth media in separate sets having varying concentrations of **C5**, **C6** and **C5**-Zn (8.0 μM - 256 μM each) for 24 h in a static and humid chamber at 37ºC. *S. aureus* biofilm grown in BHI media with 0.25% glucose and supplemented with 50 μM Zn(II) in the absence of any amphiphile was considered as the control sample. Following incubation, the growth media was removed from all the samples and the wells were washed with sterile PBS (200 μL) to remove any non-adherent planktonic bacterial cells and air dried for 45 min. Subsequently, for one set of samples crystal violet staining was performed to estimate biofilm biomass by following the method described earlier in section 4.2.5.2. The minimum biofilm eradication concentration ($MBEC_{90}$) for the amphiphiles alone or in combination with 50 μM Zn(II) was determined as the concentration, which resulted in 90% reduction in biofilm biomass as compared to untreated control sample. All the experiments were performed in triplicates and a one way analysis of variance (ANOVA) was performed using Sigma Plot.

In another set of sample, estimation of biofilm extra-polymeric substance (EPS) was accomplished by congo red binding assay following the method described earlier in section 4.2.5.3. All experiments were performed in triplicates and a one way analysis of variance (ANOVA) was performed using Sigma Plot.

6.2.13.2. Fluorescence Microscope Analysis

Biofilm of *S. aureus* MTCC 96 was grown in microtitre plate wells as described above and treated in separate sets with **C5**, **C6**, **C5**-Zn (16 μM each) or 16 μM **C5** in presence of 50 μM Zn(II). An appropriate control sample as described in the previous section was also included. Subsequently, the biofilm in each well were washed twice with sterile PBS to remove unbound amphiphile and stained in separate sets with 50 μM cFDA-SE or 1% congo red. The stained samples were washed twice with sterile PBS to remove unbound dye, air dried and observed under fluorescence microscope (Eclipse Ti-U, Nikon, USA) with a filter that allowed blue light excitation for cFDA-SE and green light excitation in case of CR stained cells. Fluorescence images of control and amphiphile-treated biofilms were recorded.

6.2.13.3. Microtitre Well Assay for Determination of Biofilm Inhibition

Biofilm of *S. aureus* MTCC 96 was grown in sterile 96 well microtitre plate in BHI medium incorporated with 0.25% glucose and varying concentrations of **C5**, **C6** or **C5**-Zn (8.0 µM and 16 µM each). In a separate set of experiment, *S. aureus* MTCC 96 biofilm was grown in sterile 96 well microtitre plate in BHI medium incorporated with 0.25% glucose and varying concentrations of **C5** (8.0 µM and 16 µM) and Zn(II). In these experiments, the ratio of C5:Zn(II) was varied (1:2, 1:4 and 1:6). Following 24 h of biofilm growth, biofilm biomass was estimated by crystal violet staining as mentioned before. The results were expressed as percentage biofilm biomass compared to control. The minimum biofilm inhibition concentration ($MBIC_{90}$) for the amphiphiles alone or in combination with Zn(II) was determined as the concentration, which resulted in 90% inhibition of biofilm growth as compared to untreated control sample. All the experiments were performed in triplicates and a one way analysis of variance (ANOVA) was performed using Sigma Plot.

6.2.14. In vitro Resistance Studies

The *in vitro* resistance of *S. aureus* MTCC 96 against **C5**, **C6** and **C5**-Zn was determined in a multistep experiment following a method described earlier (Locher et al. 2014). The concentrations of the amphiphiles used in these experiments corresponded to 2 × MIC-16 × MIC against the target bacteria. Enumeration of *S. aureus* MTCC 96 colonies was accomplished on BHI-agar plates following an incubation period of 48 h at 37°C. All experiments were performed in triplicates. Data analysis and calculation of standard deviation was performed with Microsoft Excel 2010 (Microsoft Corporation, USA).

6.2.15. Cytotoxicity Assay

The cytotoxic effect of **C5**, **C6** and **C5**-Zn was tested on human cervical carcinoma (HeLa) cell lines by an MTT assay following the manufacturer instruction (Sigma-Aldrich, MO, USA). HeLa cells were initially propagated in 25 cm^2 tissue culture flask in Dulbecco's Modified Eagle Medium (DMEM) supplemented with 10% FBS**,** penicillin (100 µg/mL) and streptomycin (100 µg/mL) at 37°C in a CO_2 incubator under a humidified atmosphere of 5% CO_2. The cells were subsequently seeded in 96 well plates (10^4 cells/well) and varying concentrations of each amphiphile (8.0 µM, 16 µM, 32 µM, 64 µM, 96 µM and

128 µM) made in DMEM were added to the cells in separate sets and incubated for 24 h under 5% CO_2 at 37°C. Control samples (cells treated with DMSO alone) and cells treated with equimolar concentrations of Zn(II) were also included in parallel sets and incubated under the same conditions. Following incubation, the media was aspirated and fresh DMEM containing MTT solution was added to the wells and incubated for 4 h at 37°C. Subsequently, the supernatant was removed and the insoluble formazan product was solubilized in DMSO and its absorbance was measured in a microtitre plate reader (Infinite M200, TECAN, Switzerland) at 550 nm. MTT assay was performed in six sets for each sample. Data analysis and determination of standard deviation was performed with Microsoft Excel 2010 (Microsoft Corporation, USA). The absorbance obtained for solvent control samples (cells treated with DMSO alone) was considered to represent 100% cell viability, whereas the absorbance for treated cells were compared to the solvent control cells to determine % cell viability.

6.3. Results and Discussion

6.3.1. Bactericidal Activity of C5-Zn

In the present study, the initial endeavor was to ascertain the antibacterial activity of **C5**-Zn. For a comparative appraisal of bactericidal activity, **C5** and the previously characterized cationic amphiphile bearing two pyridinium head groups (**C6)** were selected (Figure 6.1). To generate **C5**-Zn, the neutral pyridine-based amphiphile **C5** was selected owing to the presence of three nitrogen atoms in the amphiphile (Figure 6.1.), which would render facile complexation with a biocompatible and physiologically relevant metal ion such as Zn(II). As compared to **C5**, the conformational flexibility of **C5**-Zn is likely to be reduced upon complexation with Zn(II), which in turn, may diminish the risk of host cell toxicity (Fischer et al. 2003). Importantly, it was envisaged that the fourth coordination site of zinc in **C5**-Zn would offer an additional opportunity to promote strong and selective interactions with the accessible metal-reactive phosphate groups typically present in wall teichoic acid (WTA) and lipopolysaccharide (LPS) of bacterial cells (French et al. 2013) and thereby provide a conduit to achieve a prominent gain-in-function in terms binding affinity to target bacteria and bactericidal activity as conceived in Figure 6.3.

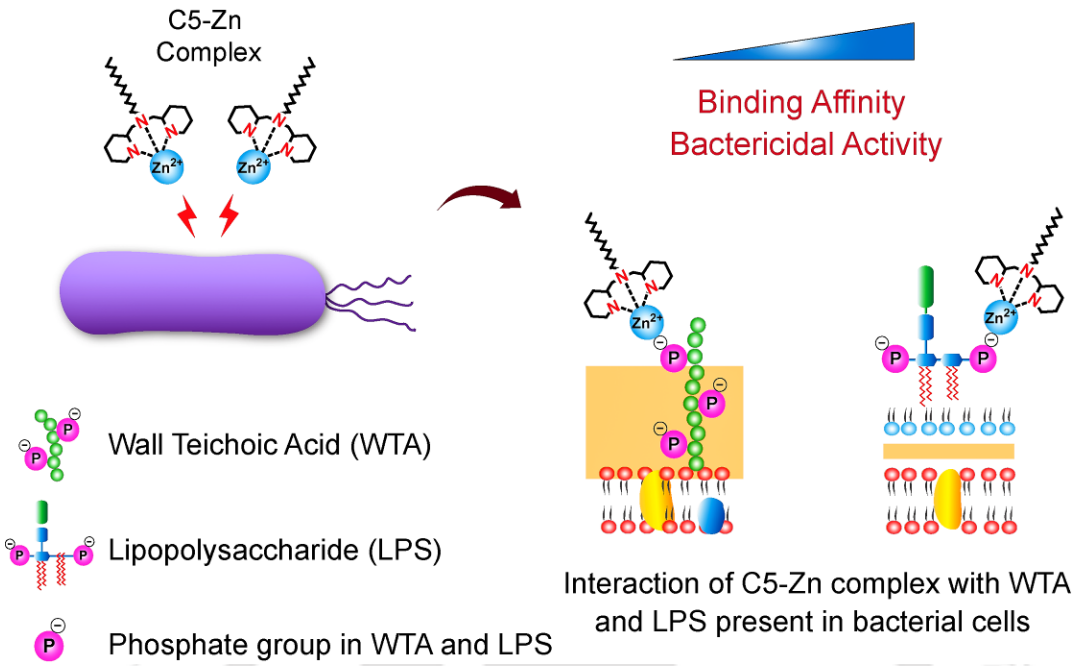

Figure 6.3. Cartoon illustrating the propensity of **compound 5**-zinc complex (**C5**-Zn) to interact with metal-reactive groups (MRGs) in bacteria, which may lead to heightened bactericidal potency.

Based on the aforementioned premise, **C5**-Zn was generated and evidence for formation of Zn(II) complex was acquired through ESI-MS and FTIR analysis (Refer to Appendix, Figure A6.1 and A6.2). Job's plot suggested a 1:1 binding stoichiometry, while a Benesi-Hildebrand plot indicated the association constant (K_a) of **C5** for Zn(II) to be 2.4 x 10^4 M^{-1} (Refer to Appendix, Figure A6.3). Evidence for zinc-triggered enhancement in the bactericidal activity was captured in the lowest MIC observed for **C5**-Zn as compared to **C5** and **C6** (Table 6.1). The MIC of the tested amphiphiles was observed to be lower against Gram-positive bacteria *S. aureus* MTCC 96 and *L. monocytogenes* Scott A as compared to the Gram-negative bacteria *E.coli* MTCC 433 and *E. aerogenes* MTCC 2822 (Table 6.1), which can perhaps be attributed to the presence of an outer membrane permeability barrier in Gram-negative bacteria (Nikaido 2003, Bolla et al. 2011).

The higher antibacterial activity of **C5**-Zn was further corroborated by FESEM analysis. In case of untreated (control) and Zn(II)-treated samples, the characteristic shape and morphology of the target bacteria cells was distinct (Figure 6.4). In case of **C5**-treated sample, the cells appeared irregular in shape providing primary indications of cellular

Table 6.1. Minimum inhibitory concentration (MIC) of **C5**, **C6** and **C5**-Zn against target bacteria

Target Bacteria	MIC of Amphiphiles		
	C5	**C6**	**C5**-Zn
Staphylococcus aureus MTCC 96	25 µM	16 µM	8.0 µM
Listeria monocytogenes Scott A	25 µM	16 µM	8.0 µM
Escherichia coli MTCC 433	100 µM	64 µM	32 µM
Enterobacter aerogenes MTCC 2822	128 µM	80 µM	64 µM

damage. Interestingly, FESEM analysis revealed a profound perturbation of cell shape and integrity in bacteria treated with **C5**-Zn as compared to **C5**, which clearly suggested that the bactericidal potency of **C5** was perhaps enhanced upon complexation with Zn(II) (Figure 6.4). The antibacterial activity of **C5**-Zn was also ascertained by AFM imaging of *S. aureus* MTCC 96 cells. In case of untreated (control), Zn(II)-treated and **C5**-treated samples, the three-dimensional topographic images of *S. aureus* MTCC 96 cells revealed a similar pattern of surface corrugations and comparable average height profiles (Figure 6.5). In contrast, AFM images of *S. aureus* MTCC 96 cells treated with equimolar concentration of **C5**-Zn indicated significant obliteration of the surface corrugations, which suggested cellular damage (Figure 6.5). A remarkable reduction in the average height profile for *S. aureus* MTCC 96 cells (~ 187 nm) further corroborated the enhanced antibacterial activity of **C5**-Zn. TEM analysis also indicated the heightened bactericidal activity of **C5**-Zn as compared to **C5** (Refer to Appendix, Figure A6.4).

.

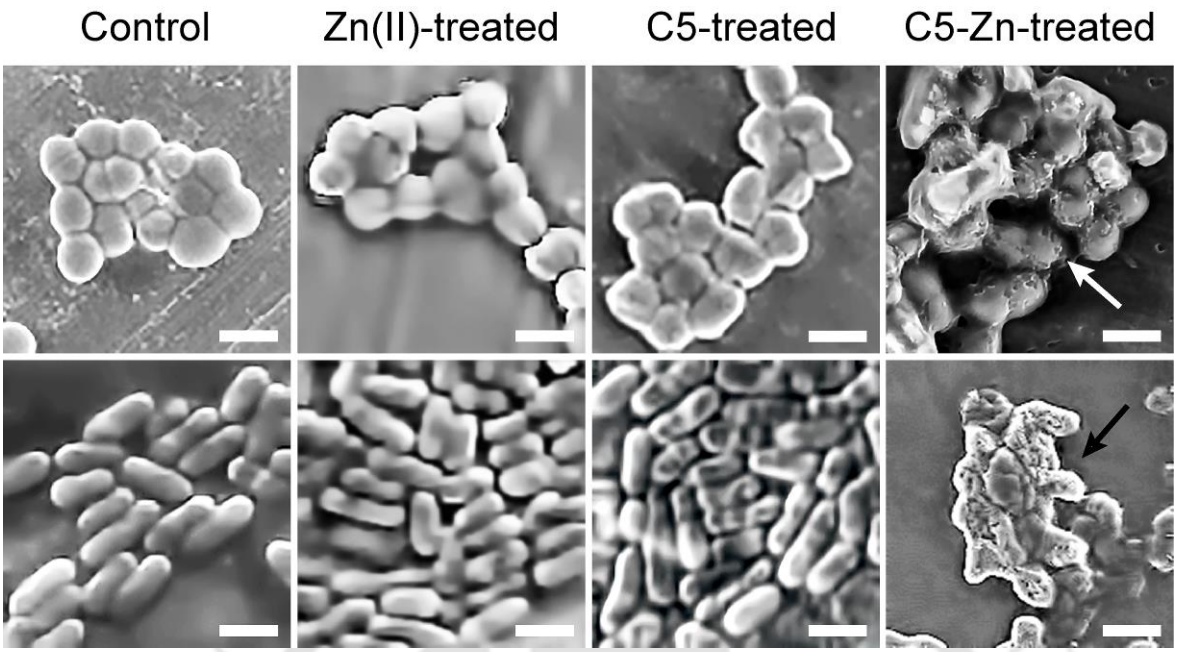

Figure 6.4. FESEM images of *S. aureus* MTCC 96 and *E. coli* MTCC 433 cells treated with Zn(II), **C5** and **C5**-Zn (6.0 µM each). Scale bar for the images is 1.0 µm. Arrow in the panel for **C5**-Zn treated samples indicates damaged cells.

6.3.2. Membrane-targeting Bactericidal Activity of C5-Zn

Synthetic amphiphiles are known to exhibit membrane-directed bactericidal activity (Vudumula et al. 2012, Findlay et al. 2010, Song et al. 2011). Hence a comparative assessment of the membrane-directed activity of **C5**, **C6** and **C5**-Zn was performed using the fluorescent probes cFDA-SE and PI, which can track bacterial membrane damage (Hoefel et al. 2003, Virto et al. 2005). Interestingly, rendering a cationic charge to **C5** through complexation with Zn(II) translated into a remarkable upsurge in the membrane-directed bactericidal activity of **C5**-Zn vis-à-vis the neutral **C5** and cationic **C6**, as evident in cFDA-SE leakage and PI uptake assays (Figure 6.6A and refer to Appendix, Figure A6.5A). Fluorescence microscope analysis revealed a striking decrease in the number of cFDA-SE stained cells of target bacteria treated with **C5**-Zn and provided evidence for heightened membrane-directed activity associated with **C5**-Zn as compared to **C5** and **C6** (Figure 6.6B and refer to Appendix, Figure A6.5B). These results were also supported by the presence of a large number of PI stained cells observed in case of treatment with **C5**-Zn, indicating copious membrane damage in contrast to untreated (control) and Zn(II)-treated cells as well as cells treated with **C5** or **C6** (Figure 6.6B and

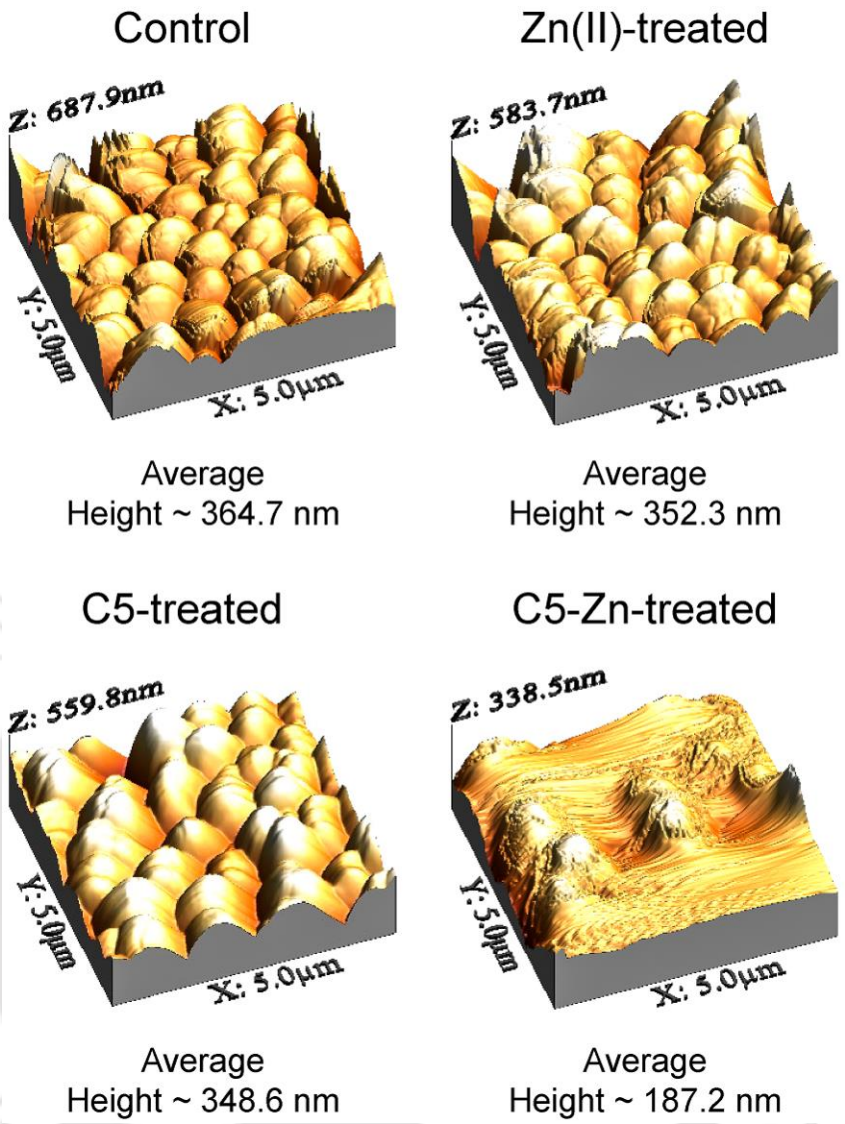

Figure 6.5. AFM analysis indicating three dimensional topography images of *S. aureus* MTCC 96 cells treated with Zn(II), **C5** and **C5**-Zn (6.0 µM each). AFM images are shown for an area of 10 µm x 10 µm.

refer to Appendix, Figure A6.5B). Evidence for enhanced membrane-targeting activity of **C5**-Zn was also acquired through flow cytometry of cFDA-SE labelled target cells. In case of untreated (control) as well as Zn(II)-treated cells, statistical analysis of the histogram (Marker M1) revealed the presence of a large number of viable cells (Figure 6.6C and refer to Appendix, Figure A6.5C). However, a significant shift in the position of the cFDA fluorescence peak was recorded in case of **C5**-Zn treated cells and the magnitude of the

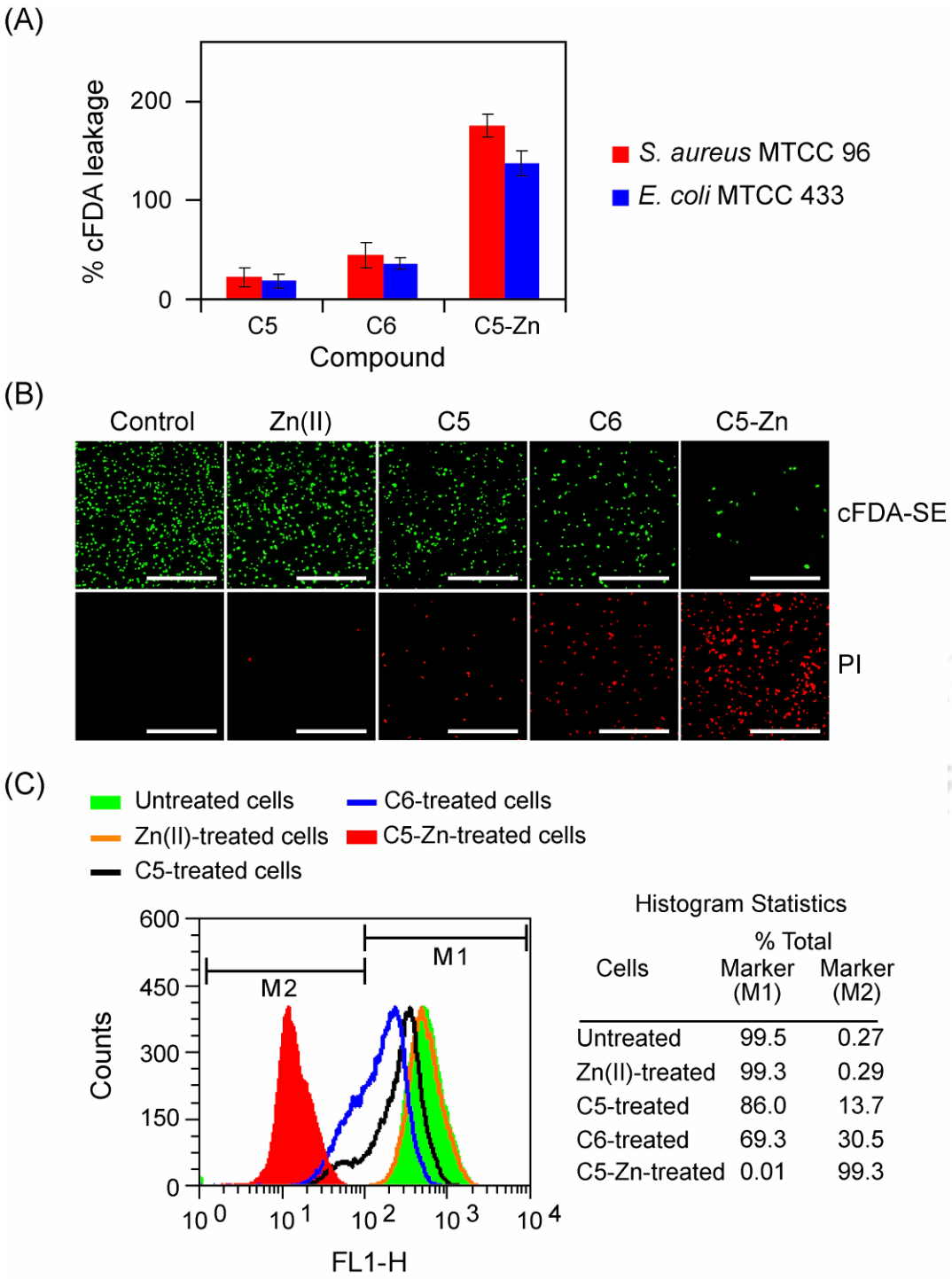

Figure 6.6. (A) cFDA-SE leakage assay for target bacterial cells treated with amphiphiles (6.0 µM each). (B) Fluorescence microscope analysis of *S. aureus* MTCC 96 cells treated with Zn(II) and amphiphiles (6.0 µM each for 6 h). Scale bar for the images is 50 µm. (C) Flow cytometry analysis of cFDA-SE labelled cells of *S. aureus* MTCC 96 treated with Zn(II) and the amphiphiles (6.0 µM each for 6 h).

shift was considerably higher than **C5** or **C6**-treated cells (Figure 6.6C and refer to Appendix, Figure A6.5C). Presumably, the extent of membrane damage and subsequent leakage of cFDA-SE dye from target cells is comparatively higher in case of **C5**-Zn treated cells. As a result, the population of cFDA-SE labelled viable cells diminished significantly, which is captured in the prominent shift of the position of the fluorescence emission peak for **C5**-Zn-treated cells (Figure 6.6C and refer to Appendix, Figure A6.5C).

It is recognized that membrane-targeting antibacterial agents can destabilize the membrane potential (Ψ) in target cells (Breukink and de Kruijff 1999, Adhikari et al. 2012). In order to ascertain the effect of **C5**-Zn on the membrane potential of bacterial cells, a fluorescence-based assay with $DiSC_35$ was pursued. It was observed that treatment of *S. aureus* MTCC 96 and *E.coli* MTCC 433 with 6.0 μM **C5**-Zn resulted in a striking enhancement in $DiSC_35$ fluorescence till around 200 sec followed by a plateau thereof, which suggested that the amphiphile could readily dispel the transmembrane potential in target cells (Figure 6.7). It is important to mention that **C5**-Zn could significantly perturb the transmembrane potential of target bacteria at concentrations below its MIC against the target bacteria. At equimolar concentrations (6.0 μM), **C5**-Zn rendered rapid and manifold higher dissipation of the transmembrane potential in target cells as compared to **C5** and **C6** (Figure 6.7). Furthermore, increased uptake of the hydrophobic fluorophore NPN by *E.coli* MTCC 433 cells treated with **C5**-Zn as compared to **C5** and **C6** suggested higher outer membrane-permeabilizing activity for **C5**-Zn (Figure 6.8). The significant membrane-permeabilizing activity of **C5**-Zn as captured in the NPN assay reiterated the antibacterial potency of the amphiphile given that the outer membrane of Gram-negative bacteria is widely acknowledged as a defiant permeability barrier against bactericidal agents (Nikaido 2003, Bolla et al. 2011).

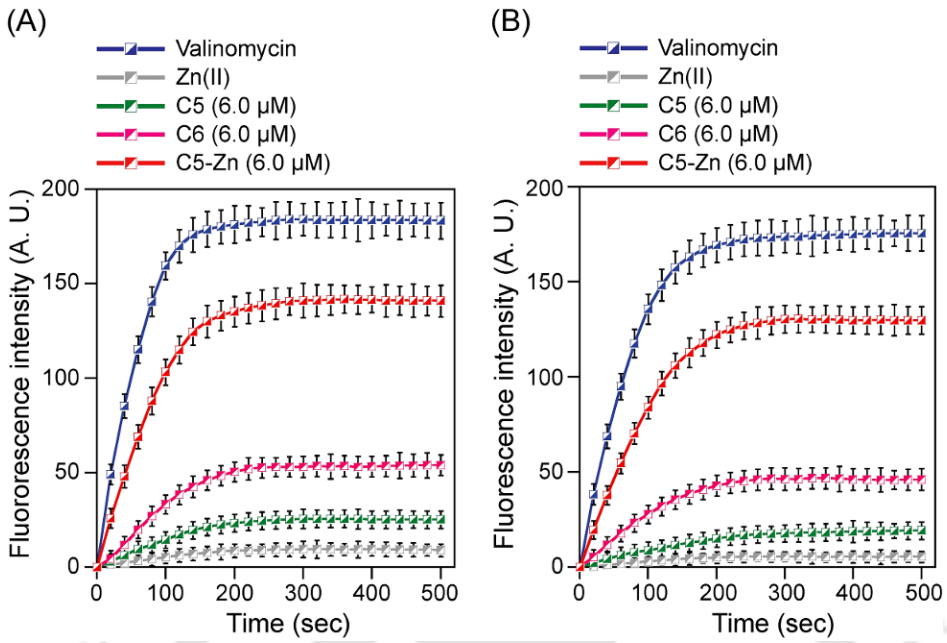

Figure 6.7. $DiSC_35$-based membrane depolarization assay for (A) *S. aureus* MTCC 96 and (B) *E. coli* MTCC 433 cells treated with Zn(II) and amphiphiles. Cells treated with 30 μM valinomycin were used as positive control in the assay.

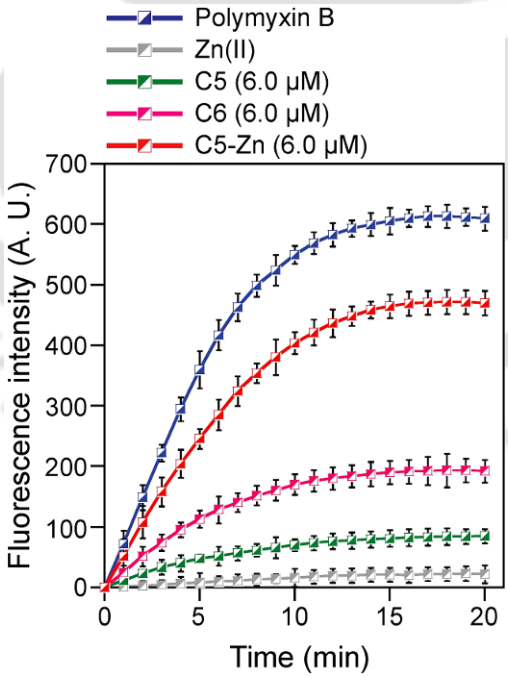

Figure 6.8. NPN-based outer membrane permeabilization assay for *E. coli* MTCC 433 cells treated with Zn(II) and amphiphiles. Cells treated with 1.0 μg/mL polymyxin B were used as positive control in the assay.

6.3.3. Binding Affinity and Effect of Mg(II) on the Growth of E. coli cells treated with C5-Zn

Interestingly, **C5**-Zn displayed radically higher bactericidal activity than **C6**, despite their equivalent cationic charge. Acquisition of this heightened function in **C5**-Zn is perhaps driven by the fourth coordination site of Zn(II), which may facilitate strong and stable interaction with anionic metal-reactive groups (MRGs) that are known to be present in bacterial cell envelope (French et al. 2013). It is also envisaged that the resultant strong interaction with MRGs is likely to enhance the binding affinity of **C5**-Zn towards bacterial cells. To this end, a distinctly higher binding affinity (lower K_d values) of **C5**-Zn (Figure 6.9A) as compared to **C6** (Refer to Appendix, Figure A6.6) implied the presence of an enduring interaction of **C5**-Zn with bacterial cells, which is perhaps leveraged in the high bactericidal activity of **C5**-Zn.

In order to validate the role of MRGs in promoting strong binding of **C5**-Zn to bacterial cells, a protection assay was conducted in presence of surplus divalent cation so as to render a competitive inhibition to binding and subsequent activity of **C5**-Zn against target bacteria. For the protection assay, Mg(II), which is known to bind strongly to MRGs (French et al. 2013, Kern et al. 2010) and is likely to impede **C5**-Zn-bacteria interactions was chosen. Interestingly, presence of surplus Mg(II) in the medium (5.0 mM and 10 mM) provided a shield to *E.coli* MTCC 433 cells against **C5**-Zn-mediated killing, while this protection waned away with decrease in Mg(II) concentration (Figure 6.9B). Conceivably, the presence of high levels of Mg(II) could compete with **C5**-Zn for binding with MRGs on bacterial cells. As a consequence, the quantum of cell-bound **C5**-Zn was effectively reduced and a protective effect was manifested with regard to cell viability. Collectively, these experiments reiterated the plausible relevance of MRGs in **C5**-Zn-bacteria interactions.

6.3.4. Antibacterial Activity of C5-Zn in Simulated Gastric Fluid (SGF)

It is widely acknowledged that during gastro-intestinal transit, pathogenic bacteria can endure the harsh acidic milieu prevalent in the stomach (Foster 2004). Moreover, annihilation of such acid-resistant pathogenic bacteria is hindered by the fact that certain

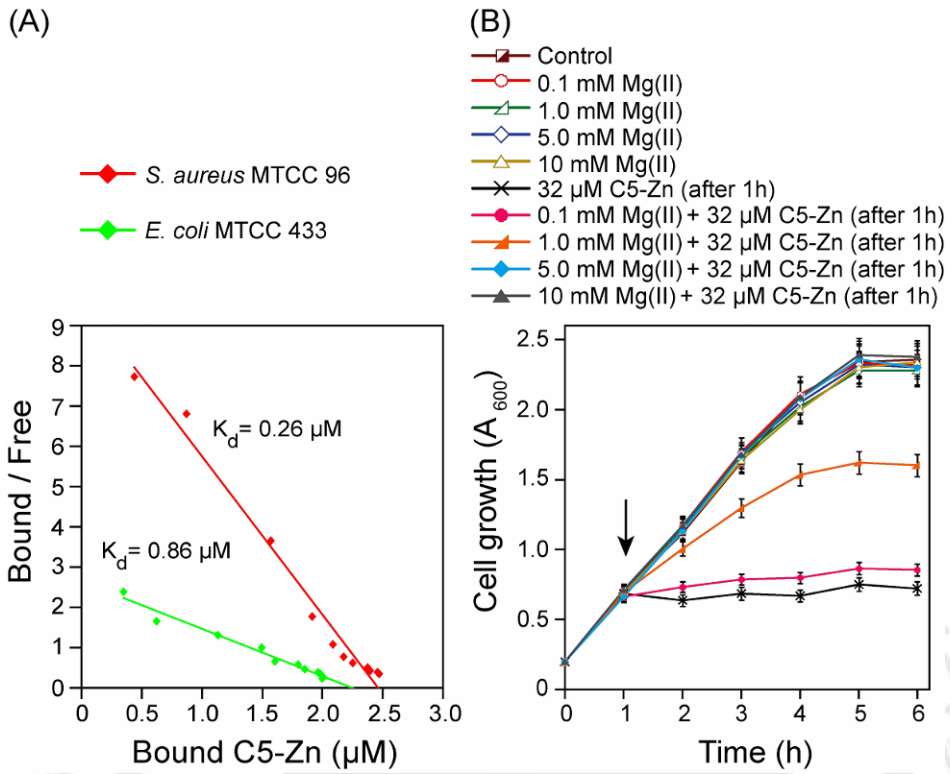

Figure 6.9. (A) Scatchard plot to determine binding affinity of **C5**-Zn for target bacteria. (B) Effect of Mg(II) on the growth of *E. coli* MTCC 433 treated with **C5**-Zn.

antibiotics are rendered inactive in the highly acidic environment (Lamp et al. 1992, Mercier et al. 2002). Given the remarkable antibacterial activity of **C5**-Zn and its promise as a therapeutic antibacterial, it was worthwhile to ascertain whether the amphiphile exhibited bactericidal activity in the gastric environment. To pursue this goal, the antibacterial activity of **C5**-Zn was tested against *E.coli* MTCC 433 and *L. monocytogenes* Scott A cells suspended in SGF. Interestingly, exposure of target bacterial cells to 20 μM **C5**-Zn in SGF resulted in considerable reduction in the viability of the cells, with the final cell number being less than 3.0 $\log_{10}$ CFU/mL following 2 h treatment (Figure 6.10A). It may be mentioned here that the pH of SGF was 2.5 and there was only a marginal decrease in viability for cells incubated in SGF alone for 2 h (Figure 6.10A), which suggested that the reduction in viability of **C5**-Zn-treated target bacteria could be largely attributed to the bactericidal activity of the amphiphile and not to the highly acidic pH of SGF per se. Further, the decrease in the viability of target cells could also be correlated to the concentration of **C5**-Zn in SGF (Figure 6.10B). Conservation of

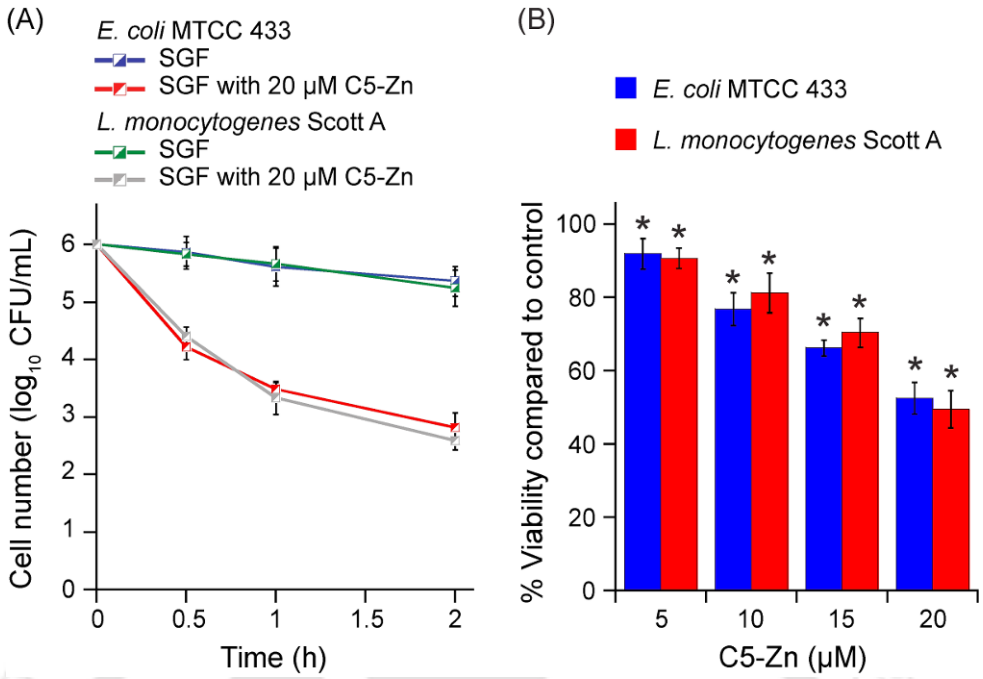

Figure 6.10. (A) Time-dependent effect of **C5**-Zn treatment on *E. coli* MTCC 433 and *L. monocytogenes* Scott A cells in simulated gastric fluid (SGF). (B) Dose-dependent effect of **C5**-Zn on the viability of target bacterial cells incubated in simulated gastric fluid (SGF). * indicates p value < 0.001 in ANOVA.

the potent bactericidal activity of **C5**-Zn in a highly acidic environment and even in the presence of a gastric enzyme such as pepsin present in SGF is a desirable attribute that enhances the therapeutic potential of **C5**-Zn. In future it would be pertinent to corroborate these findings in *in vivo* infection models.

6.3.5. Application of C5-Zn as an Adjuvant to Enhance the Activity of Erythromycin

The presence of an outer membrane permeability barrier in Gram-negative bacteria is a bottleneck to conventional antibiotic-based therapy (Nikaido 2003, Bolla et al. 2011). In this regard, bactericidal agents that can permeabilize the outer membrane can be explored as a viable option to render enhanced uptake of antibiotic (Adhikari et al. 2013, Uday et al. 2014). The high membrane-permeabilizing activity of **C5**-Zn (Figure 6.8) suggested that the amphiphile is likely to contravene the outer membrane barrier in Gram-negative bacteria and function as an adjuvant for antibiotic-mediated therapy. In the present study, treatment with varying concentrations of **C5**-Zn (2.5 μM – 10 μM) resulted in a

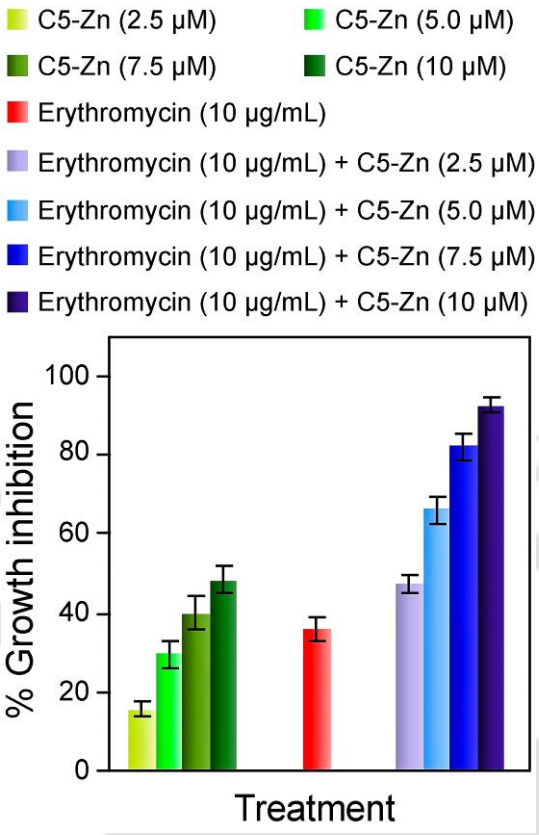

Figure 6.11. Effect of combined treatment of **C5**-Zn and erythromycin on the growth of *E. coli* MTCC 433.

Table 6.2. Fold reduction in MIC of erythromycin in combination with **C5**-Zn and determination of fractional inhibitory concentration (FIC) index.

Indicator strain	**C5**-Zn (µM)	Folds reduction in MIC of Erythromycin	FIC index[a]	Effect[b]
E. coli MTCC 433	2.5	4.0	0.32	S
	5.0	4.0	0.40	S
	7.5	8.0	0.35	S
	10	16.0	0.37	S

[a] Fractional inhibitory concentration (FIC) index was assessed as described in the section 3.2.6. [b] An FIC index of ≤ 0.5 is considered as synergism, FIC index of > 0.5-1.0 indicates additive effect, FIC index > 1.0 - < 4.0 represents indifference and FIC index of ≥ 4.0 indicates antagonism. S: Synergism.

dose-dependent growth inhibition, whereas treatment with 10 µg/mL erythromycin alone resulted in approximately 40% growth inhibition for *E. coli* MTCC 433 (Figure 6.11). However, superior growth inhibition of *E.coli* MTCC 433 was recorded when **C5**-Zn was used in conjunction with erythromycin as opposed to **C5**-Zn or the antibiotic alone (Figure 6.11 and refer to Appendix, Figure A6.7). It may be noted that the concentration of **C5**-Zn used in the combination experiments (2.5 µM – 10 µM) was lower than the MIC of the amphiphile for *E. coli* MTCC 433 (Table 6.1). It is also significant to mention that in presence of 10 µM of **C5**-Zn, the MIC for erythromycin was reduced sixteen-fold and a synergistic interaction ensued between **C5**-Zn and erythromycin (Table 6.2). In the light of growing concerns regarding excessive use of antibiotics, this is noteworthy as **C5**-Zn facilitated target cell elimination at low antibiotic concentration.

6.3.6. Pro-drug Potential of C5 in Presence of Zn(II)

Based on the finding that complexation of Zn(II) with **C5** lead to the manifestation of profound bactericidal activity, it was conceived that **C5** could perhaps be deployed as a potential pro-drug in a media containing surplus Zn(II). This tenet was validated as addition of 10 µM **C5** after 3 h of growth in Zn(II)-supplemented media rendered a dramatic bactericidal effect on *S. aureus* MTCC 96 cells, on par with 10 µM **C5**-Zn (Figure 6.12A and refer to Appendix, Figure A6.8A). An important observation in these experiments was that the viability of target bacterial cells diminished with immediate effect following addition of **C5** after 3 h of cell growth in Zn(II)-supplemented media. This phenomenon suggested that complexation of Zn(II) by **C5** and its subsequent transformation into a highly potent **C5**-Zn in the media was facile and rapid. This premise was also captured in the striking increase in cFDA-SE leakage from cells exposed to Zn(II) for 1 h followed by addition of **C5** as opposed to cells incubated for 1 h in a buffer devoid of Zn(II) and then treated with **C5** (Figure 6.12B and refer to Appendix, Figure A6.8B). Collectively, the findings of these experiments bear interesting therapeutic nuances. For instance, it is known that the presence of Zn(II) has a critical physiological role in the formation of *S. aureus* biofilm (Conrady et al. 2008, Conrady et al. 2013). In this regard, **C5** can perhaps be deployed to sequester Zn(II) and thereby hinder the process of *S. aureus* biofilm formation. Further, sequestration of Zn(II) by **C5** may also lead to

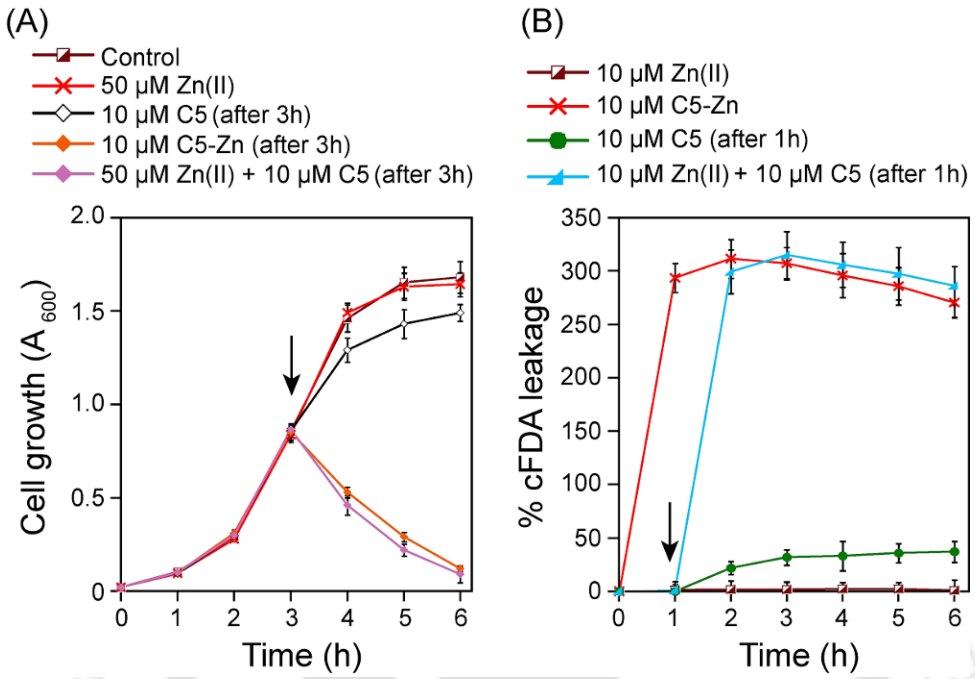

Figure 6.12. (A) Effect of addition of **C5** on *S. aureus* MTCC 96 cells grown in presence of 50 μM Zn(II). Arrow indicates the time of addition of **C5** or **C5**-Zn. (B) cFDA-SE leakage assay in *S. aureus* MTCC 96 cells incubated in 5.0 mM HEPES buffer in presence of 10 μM Zn(II) followed by addition of **C5**. Arrow indicates the time of addition of **C5**.

generation of the potent antibacterial amphiphile **C5**-Zn, which could then effectively eliminate the target cells in the biofilm.

6.3.7. Application of C5-Zn as an Antibiofilm Agent

It was conceived that the amphiphilic **C5**-Zn could perhaps be explored as an antibiofilm agent as low molecular weight amphiphiles are likely to pervade through the biofilm matrix and target the underlying cells (Uday et al. 2014). To this end, a crystal violet assay revealed that **C5**-Zn rendered a dose-dependent eradication of *S. aureus* biofilm and displayed higher antibiofilm activity than **C5** and **C6** (Figure 6.13A, Table 6.3). Superior annihilation of *S. aureus* MTCC 96 biofilm by **C5**-Zn as compared to **C5** and **C6** was also substantiated by a congo red binding assay, which indicated a dose-dependent reduction of biofilm EPS matrix following treatment with the amphiphile (Figure 6.13B). The superior antibiofilm activity of **C5**-Zn as compared to **C5** and **C6** was also captured in fluorescence microscope analysis using cFDA-SE and congo red staining, which clearly indicated

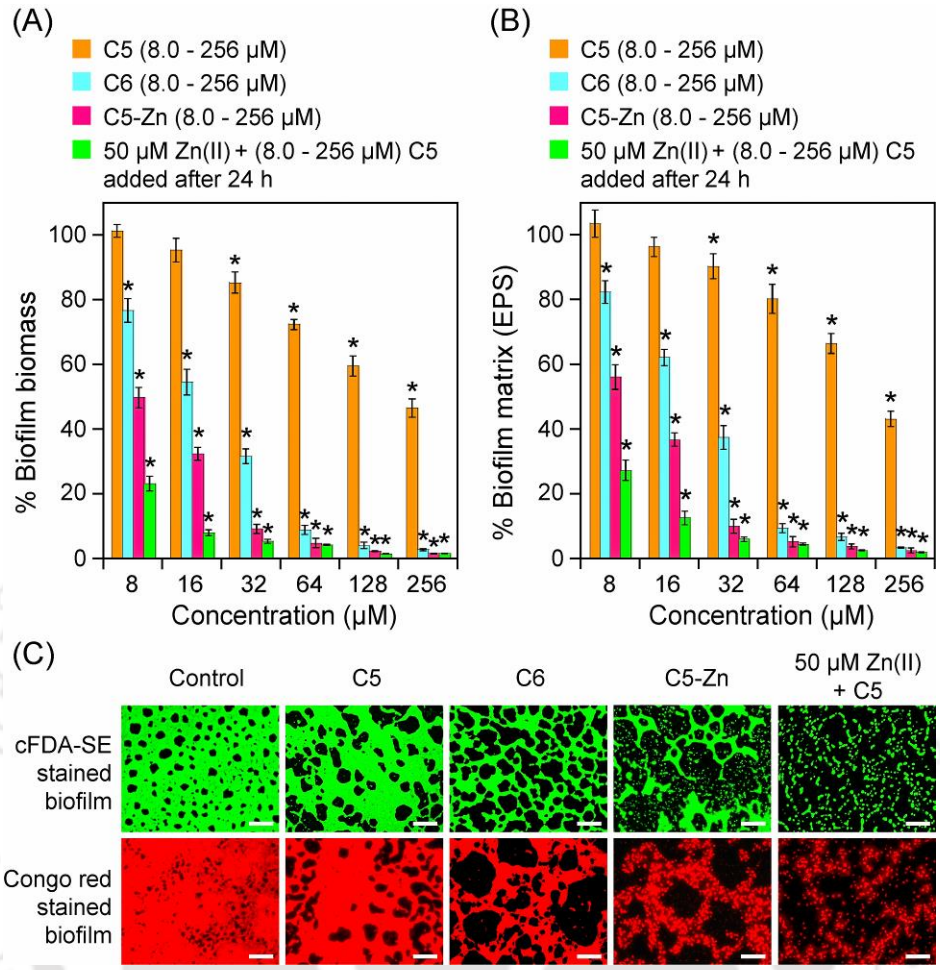

Figure 6.13. (A) Crystal violet assay to assess the antibiofilm activity of amphiphiles against *S. aureus* MTCC 96 biofilm. * indicates *p* value < 0.001 in ANOVA. (B) Congo red assay to assess reduction in *S. aureus* MTCC 96 biofilm matrix associated extra-polymeric substance (EPS) upon treatment with amphiphiles. * indicates *p* value < 0.001 in ANOVA. (C) Fluorescence microscope analysis of *S. aureus* MTCC 96 biofilm treated with amphiphiles. cFDA-SE and congo red were used to stain viable cells and biofilm matrix associated EPS, respectively. Scale bar for the images is 50 μm.

greater disintegration of the biofilm network and reduction of biofilm EPS in **C5**-Zn treated samples (Figure 6.13C).

It is established that zinc is critical for cell-cell contact in staphylococci biofilm (Conrady et al. 2013, Conrady et al. 2008). Based on the propensity of **C5** to bind Zn(II), it was envisaged that **C5** can perhaps sequester Zn(II) and hinder cell-cell

Table 6.3. Minimum biofilm eradication concentration ($MBEC_{90}$) of **C5**, **C6**, **C5**-Zn and **C5** supplemented with Zn(II) against *S. aureus* MTCC 96 biofilm.

Amphiphiles	$MBEC_{90}$ against *S. aureus* MTCC 96 biofilm
C5	> 256 µM
C6	64 µM
C5-Zn	32 µM
C5+ 50 µM Zn(II)	16 µM

contact in *S. aureus* biofilm grown in zinc-supplemented media. This may in turn predispose the biofilm cells to the action of the highly potent bactericidal material **C5**-Zn formed in the media as a consequence of complexation of Zn(II) by **C5**, resulting in effective biofilm eradication. Manifestation of this dual effect was captured in the crystal violet and congo red assays as well as in fluorescence microscope analysis, which indicated superior eradication of *S. aureus* biofilm in Zn(II)-supplemented media in presence of **C5** as compared to treatment with **C5**, **C6** or **C5**-Zn (Figure 6.13A-C).

Interestingly, the pro-drug potential of **C5** in presence of Zn(II) could also be harnessed in preventing *S. aureus* MTCC 96 biofilm formation, wherein the inhibition observed with **C5** in presence of excess Zn(II) (1:2, 1:4 and 1:6) was higher than **C5**, **C6** or **C5**-Zn (Figure 6.14, Table 6.4). Thus, the aforementioned experiments demonstrated that amphiphile-mediated Zn(II) chelation and the resultant generation of a bactericidal material (**C5**-Zn) may represent a potential therapeutic approach for combating *S. aureus* biofilm-related infections, wherein Zn(II) is known to assume a central role in biofilm formation.

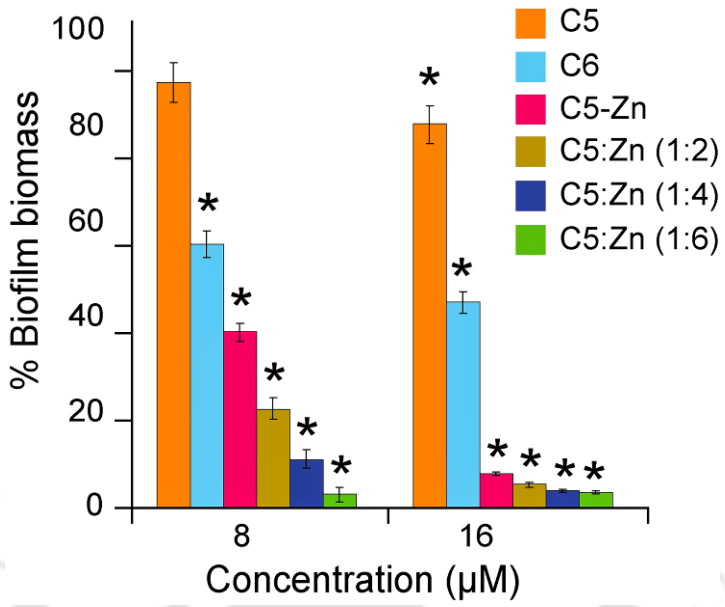

Figure 6.14. Effect of **C5** on *S. aureus* MTCC 96 biofilm grown in a media supplemented with varying levels of zinc. The ratio of **C5**: Zn(II) chosen in the experiments is indicated. Amphiphile concentrations used in the experiments were 8.0 μM and 16 μM. * indicates *p* value < 0.001 in ANOVA.

Table 6.4. Minimum biofilm inhibitory concentration ($MBIC_{90}$) of **C5**, **C6**, **C5**-Zn and **C5** supplemented with Zn(II) in various ratios against *S. aureus* MTCC 96 biofilm.

Amphiphiles	$MBIC_{90}$ against *S. aureus* MTCC 96 biofilm
C5	256 μM
C6	32 μM
C5-Zn	16 μM
C5+ Zn(II) (1:2)	16 μM
C5+ Zn(II) (1:4)	8.0 μM
C5+ Zn(II) (1:6)	8.0 μM

6.3.8. In vitro Resistance, Cytotoxic Effect and Antibacterial Selectivity of C5-Zn

The potent bactericidal activity, adjuvant potential and antibiofilm activity of **C5**-Zn indicated the therapeutic potential of the amphiphile as an antibacterial material. However, just as therapeutic antibiotics are rendered ineffective when the target bacteria develop resistance, a key factor that could determine the efficacy of **C5**-Zn as an antibacterial agent is the likelihood of resistance development against the amphiphile. To this end, a multiple step experiment was conducted to determine resistance development in *S. aureus* MTCC 96 cells. Interestingly, the merit of **C5**-Zn as a potentially therapeutic antibacterial was reinforced in these experiments, which indicated consistent MIC of **C5**-Zn against *S. aureus* MTCC 96 in consecutive steps and thus suggested a lack of resistance development in target bacteria, akin to **C5** and **C6** (Table 6.5).

In the context of potential therapeutic application of **C5**-Zn, it is imperative that the amphiphile should not display unwarranted cytotoxic effect on human cells. It is widely acknowledged that pharmacokinetic and pharmacodynamic factors such as serum concentration, interactions with plasma protein and tissue distribution are the determining factors for the *in vivo* efficiency of an antibacterial (Mueller et al. Derendorf 2004). This premise necessitates the use of antibacterials at concentrations higher than

Table 6.5. MIC of amphiphiles determined against *S. aureus* MTCC 96 in a multistep resistance development experiment.

Test compound	Selection step/Medium	MIC (μM) / OD_{600} ± standard deviation
C5	Step 1/ Agar	25 / 0.062 ± 0.005
C5	Step 2/ Agar	25 / 0.04 ± 0.004
C5	Step 3/ Agar	25 / 0.06 ± 0.007
C6	Step 1/ Agar	16 / 0.04 ± 0.003
C6	Step 2/ Agar	16 / 0.028 ± 0.003
C6	Step 3/ Agar	16 / 0.033 ± 0.006
C5-Zn	Step 1/ Agar	8.0 / 0.017 ± 0.002
C5-Zn	Step 2/ Agar	8.0 / 0.022 ± 0.006
C5-Zn	Step 3/ Agar	8.0 / 0.031 ± 0.004

the MIC in order to ensure the requisite killing concentrations for *in vivo* elimination of the target pathogen (Wispelwey 2005, Craig 2003). Hence, in order to assess the true therapeutic potential of an antibacterial agent, it is critical to ascertain whether the bactericidal agent is likely to render any cytotoxic effect at concentrations higher than MIC. Based on this tenet, the cytotoxic effect of **C5**-Zn at concentrations manifold higher than its MIC against *S. aureus* MTCC 96 was determined by a standard MTT assay. Interestingly it was observed that the viability of cultured HeLa cells was as high as 80% in presence of 64 μM of **C5**-Zn (equivalent to 8 × MIC against *S. aureus* MTCC 96) as compared to only 50% in case of equivalent levels of **C6** (Figure 6.15). This observation is noteworthy as it suggested that for effective *in vivo* elimination of target bacteria, **C5**-Zn can perhaps be deployed at high concentrations without the concomitant risk of host cell toxicity.

From a therapeutic perspective it is desirable that an antibacterial agent displays high selectivity. Membrane-acting cationic amphiphiles are likely to exhibit high antibacterial selectivity as bacterial membranes bear a higher content of negatively charged phospholipids in contrast to mammalian membranes wherein zwitterionic lipids and cholesterol are present in high proportions (Zasloff 2002). Despite equivalent cationic charge, the toxicity of **C5**-Zn was manifold lower than **C6** (Figure 6.15). On comparison of the structures (Figure 6.1), it is apparent that **C6** consists of two aromatic rings and displays conformational flexibility, whereas in case of **C5**-Zn complexation with zinc likely leads to chelation-driven reduced flexibility of the head groups, which perhaps accounts for the reduced cytotoxicity of the molecule (Fischer et al. 2003). The therapeutic index (IC_{50}/MIC) of a bactericidal agent is largely regarded as a measure of its antibacterial selectivity. The cationic **C5**-Zn exhibited three-fold higher antibacterial selectivity (IC_{50}/MIC) than **C5** and **C6** (Table 6.6), likely originating from the complexation with Zn(II) that renders enduring interactions of **C5**-Zn with MRGs associated with bacterial cells (French et al. 2013). This enhanced therapeutic index of **C5**-Zn is particularly significant, which suggested that *in vivo* deployment of **C5**-Zn as an antibacterial material can perhaps render selective elimination of the target pathogen without an associated risk of high host cell toxicity.

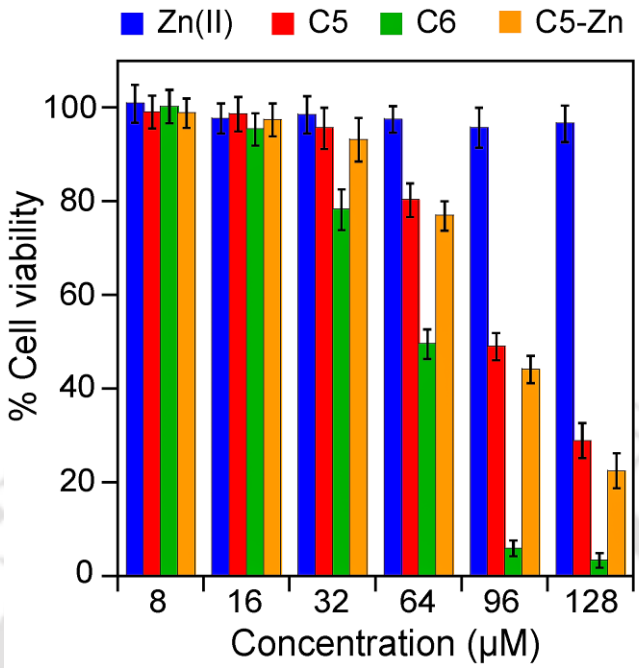

Figure 6.15. MTT-based assay to ascertain *in vitro* cytotoxicity of **C5**, **C6** and **C5**-Zn on the viability of cultured HeLa cells. Each data point represents mean ± SD values from six independent samples.

Table 6.6. Therapeutic index of amphiphiles based on selectivity for *S. aureus* MTCC 96 determined by IC_{50}/MIC values.

Amphiphiles	IC_{50} against HeLa cells (μM)	MIC against *S. aureus* MTCC 96 (μM)	Selectivity for *S. aureus* MTCC 96 (IC_{50} / MIC)
C5	80	25	3.2
C6	50	16	3.125
C5-Zn	75	8.0	9.375

6.4. Significant Findings

The salient findings of the present study are as follows:

1. The radical design principle realized through complexation of Zn(II) with a pyridine-based synthetic amphiphile (**C5**) enables the generated molecule (**C5**-Zn) to have strong interactions with metal reactive groups (MRGs) in bacterial cell envelope and this acquired capability is leveraged in a remarkable enhancement in the membrane-directed bactericidal activity of the molecule.

2. The Zn(II)-mediated heightened membrane-directed activity of the amphiphile (**C5**-Zn) could be harnessed in adjuvant applications to increase the potency of a common therapeutic antibiotic such as erythromycin.

3. Interestingly, the propensity of Zn(II)-complexation by the amphiphile could be exploited in a pro-drug regime for generation of the potent bactericidal amphiphile **C5**-Zn in a zinc-rich media.

4. Given the germane role of Zn(II) in the formation of *S. aureus* biofilm, the Zn(II)-mediated pro-drug potential of the amphiphile **C5** coupled with the manifestation of high bactericidal activity in the resultant **C5**-Zn following Zn(II)-complexation by **C5**, could be garnered in elimination of *S. aureus* biofilm and thus demonstrated an important healthcare application of the newly developed amphiphilic material.

5. Further, the therapeutic potential of the amphiphilic **C5**-Zn was validated as experiments suggested an apparent lack of resistance against the amphiphile in target bacteria and retention of its bactericidal activity in the physiological environment such as simulated gastric fluid.

6. From a therapeutic perspective, the non-toxic nature of **C5**-Zn even at concentrations manifold higher than its MIC is significant as it suggested that the antibacterial material can perhaps be employed at high concentrations to ensure effective *in vivo* elimination of target bacteria without an added risk of host cell toxicity.

Significant Findings

7. A prominent gain-in-function, which was achieved through the radical drug design approach presented herein, is the significant increase in the therapeutic index of **C5**-Zn as compared to the metal-free amphiphile (**C5**) or the cationic amphiphile bearing two pyridinium head groups (**C6**).

TH-1410_10610607

SUMMARY AND FUTURE PERSPECTIVE

TH-1410_10610607

TH-1410_10610607

SUMMARY AND FUTURE PERSPECTIVE

In the age of rampant antibiotic-resistance, the present study on pyridine-based synthetic amphiphiles augers well in addressing a very important and contemporary global healthcare problem. The study is an illustration of the use of prudent synthetic drug design and medicinal chemistry to generate synthetic amphiphiles with high bactericidal activity and therapeutic potential. The significant leads, which emerged from the study and the future prospect of the findings is discussed in the following section:

1. The discovery of efficient bactericidal scaffolds is critical in order to mitigate the daunting challenge of drug-resistant pathogenic bacteria. The present investigation, which reports pyridine-based synthetic amphiphiles as potent bactericidal agents, is an effort in this direction. The low molecular weight synthetic amphiphiles used in the present study are likely to provide beneficial therapeutic attributes such as higher solubility in buffers and biologically relevant fluids, efficient passage through membranes and superior tissue distribution. Enriched with the fundamental understanding on how the structures of the amphiphiles influence the bactericidal activity, cytotoxicity and selectivity, it is envisaged that the activity of these amphiphiles can be fine-tuned to generate safer therapeutic agents in future in order to combat the emerging drug-resistant pathogens.

2. The cationic amphiphile referred to as **C6** in the present study displayed potent membrane-directed activity. It is envisioned that this amphiphile may thwart the probability of resistance development in target pathogens and thus holds interesting prospect in antibacterial therapy against drug-resistant pathogens. Based on this tenet, a viable and an important therapeutic application of **C6** could be demonstrated where the amphiphile at very low concentrations, which is non-toxic, prevailed over the membrane-based barrier and sensitized Gram-negative target bacteria to the therapeutic antibiotic erythromycin. This case in point indicates the possibility of deploying the amphiphile as an adjuvant in future for antibiotic-mediated antibacterial therapy.

3. From a therapeutic perspective, the potent antibiofilm activity displayed by the synthetic amphiphile **C6** augers well in addressing the significant clinical challenge of treating chronic infections caused by antibiotic-resistant biofilms. Given the profound membrane-directed activity of the amphiphile, an interesting prospect in future would be would be to exploit the amphiphile as a surface-active bactericidal agent and prevent the formation of biofilms, which is a major challenge in the treatment of nosocomial infections.

4. Development of a biocompatible amphiphile-loaded nanocarrier that displayed antibiofilm activity on a clinically relevant surface and eradicate established biofilm from a model catheter highlights the potential of the developed nanocarrier in device-associated antibiofilm therapy. In future, it would be interesting to employ the amphiphile-loaded nanocarrier in conjunction with appropriate materials chemistry to develop a surface active coating for catheters that enables controlled-release of the amphiphile and prevents colonization of such implants by biofilms.

5. Complexation of Zn(II) with a neutral pyridine-based synthetic amphiphile (**C5**) generated a radical bactericidal amphiphile referred to as **C5**-Zn, which was empowered to have strong interactions with metal reactive groups (MRGs) in bacterial cell envelope. This metal-driven functionality is leveraged in a remarkable enhancement in the membrane-directed bactericidal activity of the molecule. Interestingly, this Zn(II)-complexation mechanism could be exploited in a pro-drug regime for generation of a potent bactericidal material in a zinc-rich media. Further, given the germane role of Zn(II) in *S. aureus* biofilm formation, the present study revealed that acquisition of high bactericidal activity by the amphiphile following Zn(II)-complexation could be garnered in elimination of *S. aureus* biofilm and thus demonstrated an important healthcare application of the amphiphilic material. An apparent lack of resistance against **C5**-Zn in target bacteria, retention of its bactericidal activity in the physiological milieu such as simulated gastric fluid and the non-toxic nature of **C5**-Zn even at concentrations manifold higher than its MIC enhance the therapeutic prospect of the amphiphile for future *in vivo*

applications.The results obtained in the present study are encouraging and they provide a fundamental guideline to the research community who are working at the interface of chemistry, biology and materials science and are motivated to build an armory of potent synthetic molecules that display high bactericidal activity, low toxicity and emerge as therapeutic agents against antibiotic-resistant bacteria. A schematic illustration of the salient findings emerging from the chapters of the present investigation is indicated in the cartoon shown in **Scheme 2**.

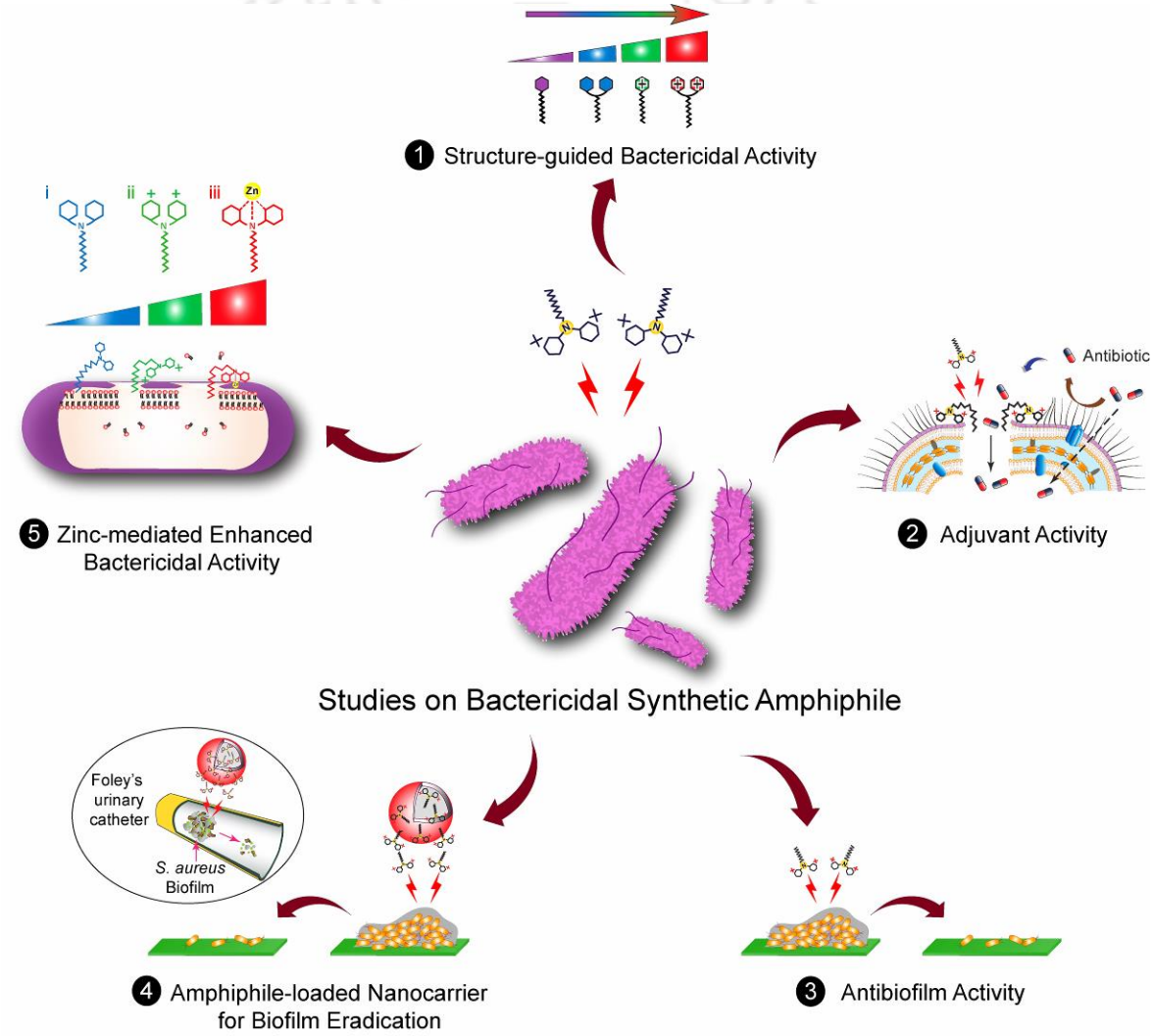

Scheme 2. Schematic representation of significant findings of the present investigation.

TH-1410_10610607

BIBLIOGRAPHY

TH-1410_10610607

TH-1410_10610607

Bibliography

Adhikari, M. D.; Das, G.; Ramesh, A. Retention of nisin activity at elevated pH in an organic acid complex and gold nanoparticle composite. *Chem. Commun*. **2012**, *48*, 8928-8930.

Adhikari, M. D.; Goswami, S.; Panda, B. R.; Chattopadhyay, A.; Ramesh, A. Membrane-directed high bactericidal activity of (gold nanoparticle)-polythiophene composite for niche applications against pathogenic bacteria. *Adv. Healthc. Mater*. **2013**, *2*, 599-606.

Alakomi, H. L.; Paananen, A.; Suihko, M. L.; Helander, I. M.; Saarela, M. Weakening effect of cell permeabilizers on gram-negative bacteria causing biodeterioration. *Appl. Environ. Microbiol*. **2006**, *72*, 4695-4703.

Alekshun, M. N.; Levy, S. B. Molecular mechanisms of antibacterial multidrug resistance. *Cell* **2007**, *128*, 1037-1050.

Allesen-Holm, M.; Barken, K. B.; Yang, L.; Klausen, M.; Webb, J. S.; Kjelleberg, S.; Molin, S.; Givskov, M.; Tolker-Nielsen, T. A characterization of DNA release in *Pseudomonas aeruginosa* cultures and biofilms. *Mol. Microbiol*. **2006**, *59*, 1114-1128.

Almeida Da Silva, P. E.; Palomino, J. C. Molecular basis and mechanisms of drug resistance in *Mycobacterium tuberculosis*: classical and new drugs. *J. Antimicrob. Chemother*. **2011**, *66*, 1417-1430.

Anderson, G. G.; Moreau-Marquis, S.; Stanton, B. A.; O'Toole, G. A. *In vitro* analysis of tobramycin-treated *Pseudomonas aeruginosa* biofilms on cystic fibrosis-derived airway epithelial cells. *Infect. Immun*. **2008**, *76*, 1423-1433.

Archer, N. K.; Mazaitis, M. J.; Costerton, J. W.; Leid, J. G.; Powers, M. E.; Shirtliff, M. E. *Staphylococcus aureus* biofilms: properties, regulation, and roles in human disease. *Virulence* **2011**, *2*, 445-459.

Arciola, C. R.; Campoccia, D.; Speziale, P.; Montanaro, L.; Costerton, J. W. Biofilm formation in Staphylococcus implant infections. A review of molecular mechanisms and implications for biofilm-resistant materials. *Biomaterials* **2012**, *33*, 5967-5982.

Atkins, J. L.; Patel, M. B.; Cusumano, Z.; Gokel, G. W. Enhancement of antimicrobial activity by synthetic ion channel synergy. *Chem. Commun*. **2010**, *46*, 8166-8167.

Avrahami, D.; Shai, Y. Conjugation of a magainin analogue with lipophilic acids controls hydrophobicity, solution assembly, and cell selectivity. *Biochemistry* **2002**, *41*, 2254-2263.

Baussanne, I.; Bussiere, A.; Halder, S.; Ganem-Elbaz, C.; Ouberai, M.; Riou, M.; Paris, J. M.; Ennifar, E.; Mingeot-Leclercq, M. P.; Decout, J. L. Synthesis and antimicrobial evaluation of amphiphilic neamine derivatives. *J. Med. Chem*. **2010**, *53*, 119-127.

Bavaro, M. F. Escherichia coli O157: what every internist and gastroenterologist should know. *Curr. Gastroenterol Rep*. **2009**, *11*, 301-306.

Benesi, H. A.; Hildebrand, J. H. A Spectrophotometric Investigation of the Interaction of Iodine with Aromatic Hydrocarbons. *J. Am. Chem. Soc.* **1949**, *71*, 2703-2707.

Bera, S.; Zhanel, G. G.; Schweizer, F. Antibacterial activities of aminoglycoside antibiotics-derived cationic amphiphiles. Polyol-modified neomycin B-, kanamycin A-, amikacin-, and neamine-based amphiphiles with potent broad spectrum antibacterial activity. *J. Med. Chem*. **2010**, *53*, 3626-3631.

Blair, J. M.; Webber, M. A.; Baylay, A. J.; Ogbolu, D. O.; Piddock, L. J. Molecular mechanisms of antibiotic resistance. *Nat. Rev. Microbiol*. **2015**, *13*, 42-51.

Bolla, J. M.; Alibert-Franco, S.; Handzlik, J.; Chevalier, J.; Mahamoud, A.; Boyer, G.; Kiec-Kononowicz, K.; Pages, J. M. Strategies for bypassing the membrane barrier in multidrug resistant Gram-negative bacteria. *FEBS Lett*. **2011**, *585*, 1682-1690.

Bordi, C.; de Bentzmann, S. Hacking into bacterial biofilms: a new therapeutic challenge. *Ann. Intensive Care* **2011**, *1*, 19.

Bottcher, T.; Kolodkin-Gal, I.; Kolter, R.; Losick, R.; Clardy, J. Synthesis and activity of biomimetic biofilm disruptors. *J. Am. Chem. Soc*. **2013**, *135*, 2927-2930.

Bowdish, D. M.; Davidson, D. J.; Lau, Y. E.; Lee, K.; Scott, M. G.; Hancock, R. E. Impact of LL-37 on anti-infective immunity. *J. Leukoc. Biol*. **2005**, *77*, 451-459.

Brahmachari, S.; Debnath, S.; Dutta, S.; Das, P. K. Pyridinium based amphiphilic hydrogelators as potential antibacterial agents. *Beilstein J. Org. Chem*. **2010**, *6*, 859-868.

Breukink, E.; de Kruijff, B. The lantibiotic nisin, a special case or not? *Biochim. Biophys. Acta* **1999**, *1462*, 223-234.

Broderick, A. H.; Breitbach, A. S.; Frei, R.; Blackwell, H. E.; Lynn, D. M. Surface-mediated release of a small-molecule modulator of bacterial biofilm formation: a non-bactericidal approach to inhibiting biofilm formation in *Pseudomonas aeruginosa*. *Adv. Healthc. Mater*. **2013**, *2*, 993-1000.

Brogden, K. A. Antimicrobial peptides: pore formers or metabolic inhibitors in bacteria? *Nat. Rev. Microbiol*. **2005**, *3*, 238-250.

Bunders, C.; Cavanagh, J.; Melander, C. Flustramine inspired synthesis and biological evaluation of pyrroloindoline triazole amides as novel inhibitors of bacterial biofilms. *Org. Biomol. Chem*. **2011**, *9*, 5476-5481.

Burton, E.; Gawande, P. V.; Yakandawala, N.; LoVetri, K.; Zhanel, G. G.; Romeo, T.; Friesen, A. D.; Madhyastha, S. Antibiofilm activity of GlmU enzyme inhibitors against catheter-associated uropathogens. *Antimicrob. Agents Chemother*. **2006**, *50*, 1835-1840.

Bush, K.; Courvalin, P.; Dantas, G.; Davies, J.; Eisenstein, B.; Huovinen, P.; Jacoby, G. A.; Kishony, R.; Kreiswirth, B. N.; Kutter, E.; Lerner, S. A.; Levy, S.; Lewis, K.; Lomovskaya, O.; Miller, J. H.; Mobashery, S.; Piddock, L. J.; Projan, S.; Thomas, C. M.; Tomasz, A.; Tulkens, P. M.; Walsh, T. R.; Watson, J. D.; Witkowski, J.; Witte, W.; Wright, G.; Yeh, P.; Zgurskaya, H. I. Tackling antibiotic resistance. *Nat. Rev. Microbiol*. **2011**, *9*, 894-896.

Chambers, H. F.; Deleo, F. R. Waves of resistance: *Staphylococcus aureus* in the antibiotic era. *Nat. Rev. Microbiol*. **2009**, *7*, 629-641.

Chan, B. C.; Ip, M.; Lau, C. B.; Lui, S. L.; Jolivalt, C.; Ganem-Elbaz, C.; Litaudon, M.; Reiner, N. E.; Gong, H.; See, R. H.; Fung, K. P.; Leung, P. C. Synergistic effects of baicalein with ciprofloxacin against NorA over-expressed methicillin-resistant *Staphylococcus aureus* (MRSA) and inhibition of MRSA pyruvate kinase. *J. Ethnopharmacol*. **2011**, *137*, 767-773.

Charteris, W. P.; Kelly, P. M.; Morelli, L.; Collins, J. K. Development and application of an *in vitro* methodology to determine the transit tolerance of potentially probiotic *Lactobacillus* and *Bifidobacterium* species in the upper human gastrointestinal tract. *J. Appl. Microbiol*. **1998**, *84*, 759-768.

Chen, C.; Pan, F.; Zhang, S.; Hu, J.; Cao, M.; Wang, J.; Xu, H.; Zhao, X.; Lu, J. R. Antibacterial activities of short designer peptides: a link between propensity for nanostructuring and capacity for membrane destabilization. *Biomacromolecules* **2010**, *11*, 402-411.

Choi, H.; Lee, D. G. Antimicrobial peptide pleurocidin synergizes with antibiotics through hydroxyl radical formation and membrane damage, and exerts antibiofilm activity. *Biochim. Biophys. Acta* **2012**, *1820*, 1831-1838.

Church, D.; Elsayed, S.; Reid, O.; Winston, B.; Lindsay, R. Burn wound infections. *Clin. Microbiol. Rev*. **2006**, *19*, 403-434.

Collin, F.; Karkare, S.; Maxwell, A. Exploiting bacterial DNA gyrase as a drug target: current state and perspectives. *Appl. Microbiol. Biotechnol*. **2011**, *92*, 479-497.

Conrady, D. G.; Brescia, C. C.; Horii, K.; Weiss, A. A.; Hassett, D. J.; Herr, A. B. A zinc-dependent adhesion module is responsible for intercellular adhesion in staphylococcal biofilms. *Proc. Natl. Acad. Sci. U S A.* **2008**, *105*, 19456-19461.

Conrady, D. G.; Wilson, J. J.; Herr, A. B. Structural basis for Zn2+-dependent intercellular adhesion in staphylococcal biofilms. *Proc. Natl. Acad. Sci. U S A.* **2013**, *110*, E202-211.

Costerton, J. W.; Montanaro, L.; Arciola, C. R. Bacterial communications in implant infections: a target for an intelligence war. *Int. J. Artif. Organs*. **2007**, *30*, 757-763.

Costerton, J. W.; Stewart, P. S.; Greenberg, E. P. Bacterial biofilms: a common cause of persistent infections. *Science* **1999**, *284*, 1318-1322.

Cotter, P. D.; Gahan, C. G.; Hill, C. Analysis of the role of the *Listeria monocytogenes* F0F1 -AtPase operon in the acid tolerance response. *Int. J. Food Microbiol*. **2000**, *60*, 137-146.

Craig, W. A. Pharmacokinetic/pharmacodynamic parameters: rationale for antibacterial dosing of mice and men. *Clin. Infect. Dis*. **1998**, *26*, 1-10; quiz 11-12.

Craig, W. A. Basic pharmacodynamics of antibacterials with clinical applications to the use of beta-lactams, glycopeptides, and linezolid. *Infect. Dis. Clin. North Am*. **2003**, *17*, 479-501.

Cusumano, C. K.; Pinkner, J. S.; Han, Z.; Greene, S. E.; Ford, B. A.; Crowley, J. R.; Henderson, J. P.; Janetka, J. W.; Hultgren, S. J. Treatment and prevention of urinary tract infection with orally active FimH inhibitors. *Sci. Transl. Med*. **2011**, *3*, 109ra115.

Danhorn, T.; Fuqua, C. Biofilm formation by plant-associated bacteria. *Annu. Rev. Microbiol*. **2007**, *61*, 401-422.

Davies, D. Understanding biofilm resistance to antibacterial agents. *Nat. Rev. Drug Discov*. **2003**, *2*, 114-122.

Davies, J.; Davies, D. Origins and evolution of antibiotic resistance. *Microbiol. Mol. Biol. Rev*. **2010**, *74*, 417-433.

Debnath, S.; Shome, A.; Das, D.; Das, P. K. Hydrogelation through self-assembly of fmoc-peptide functionalized cationic amphiphiles: potent antibacterial agent. *J. Phys. Chem. B* **2010**, *114*, 4407-4415.

Delcour, A. H. Outer membrane permeability and antibiotic resistance. *Biochim. Biophys. Acta* **2009**, *1794*, 808-816.

Diemond-Hernandez, B.; Solorzano-Santos, F.; Leanos-Miranda, B.; Peregrino-Bejarano, L.; Miranda-Novales, G. Production of icaADBC-encoded polysaccharide intercellular adhesin and therapeutic failure in pediatric patients with Staphylococcal device-related infections. *BMC Infect. Dis*. **2010**, *10*, 68.

Donlan, R. M. Biofilms and device-associated infections. *Emerg. Infect. Dis*. **2001**, *7*, 277-281.

Donlan, R. M. Preventing biofilms of clinically relevant organisms using bacteriophage. *Trends Microbiol*. **2009**, *17*, 66-72.

Donlan, R. M.; Costerton, J. W. Biofilms: survival mechanisms of clinically relevant microorganisms. *Clin. Microbiol. Rev*. **2002**, *15*, 167-193.

Duong, H. T. T.; Adnan, N. N. M.; Barraud, N.; Basuki, J. S.; Kutty, S. K.; Jung, K.; Kumar, N.; Davis, T. P.; Boyer, C. Functional gold nanoparticles for the storage and controlled release of nitric oxide: applications in biofilm dispersal and intracellular delivery. *J. Mater. Chem. B* **2014**, *2*, 5003-5011.

Durmus, N. G.; Taylor, E. N.; Kummer, K. M.; Webster, T. J. Enhanced efficacy of superparamagnetic iron oxide nanoparticles against antibiotic-resistant biofilms in the presence of metabolites. *Adv. Mater*. **2013**, *25*, 5706-5713.

Dutta, S.; Shome, A.; Kar, T.; Das, P. K. Counterion-induced modulation in the antimicrobial activity and biocompatibility of amphiphilic hydrogelators: influence of in-situ-synthesized Ag-nanoparticle on the bactericidal property. *Langmuir* **2011**, *27*, 5000-5008.

Dymond, M. K.; Attard, G. S. Cationic type I amphiphiles as modulators of membrane curvature elastic stress *in vivo*. *Langmuir* **2008**, *24*, 11743-11751.

Ejim, L.; Farha, M. A.; Falconer, S. B.; Wildenhain, J.; Coombes, B. K.; Tyers, M.; Brown, E. D.; Wright, G. D. Combinations of antibiotics and nonantibiotic drugs enhance antimicrobial efficacy. *Nat. Chem. Biol*. **2011**, *7*, 348-350.

Elzoghby, A. O.; Samy, W. M.; Elgindy, N. A. Albumin-based nanoparticles as potential controlled release drug delivery systems. *J. Control Release* **2012a**, *157*, 168-182.

Elzoghby, A. O.; Samy, W. M.; Elgindy, N. A. Protein-based nanocarriers as promising drug and gene delivery systems. *J. Control Release* **2012b**, *161*, 38-49.

Epand, R. F.; Pollard, J. E.; Wright, J. O.; Savage, P. B.; Epand, R. M. Depolarization, bacterial membrane composition, and the antimicrobial action of ceragenins. *Antimicrob. Agents Chemother*. **2010**, *54*, 3708-3713.

Fair, R. J.; Tor, Y. Antibiotics and bacterial resistance in the 21st century. *Perspect. Medicin. Chem*. **2014**, *6*, 25-64.

Fernandes, P. Antibacterial discovery and development--the failure of success? *Nat. Biotechnol*. **2006**, *24*, 1497-1503.

Fernández Fuentes, M. Á.; Ortega Morente, E.; Abriouel, H.; Pérez Pulido, R.; Gálvez, A. Antimicrobial resistance determinants in antibiotic and biocide-resistant gram-negative bacteria from organic foods. *Food Control*. **2014**, *37*, 9-14.

Fernandez, L.; Hancock, R. E. Adaptive and mutational resistance: role of porins and efflux pumps in drug resistance. *Clin. Microbiol. Rev*. **2012**, *25*, 661-681.

Findlay, B.; Zhanel, G. G.; Schweizer, F. Cationic amphiphiles, a new generation of antimicrobials inspired by the natural antimicrobial peptide scaffold. *Antimicrob. Agents Chemother*. **2010**, *54*, 4049-4058.

Fischbach, M. A.; Walsh, C. T. Antibiotics for emerging pathogens. *Science* **2009**, *325*, 1089-1093.

Fischer, D.; Li, Y.; Ahlemeyer, B.; Krieglstein, J.; Kissel, T. *In vitro* cytotoxicity testing of polycations: influence of polymer structure on cell viability and hemolysis. *Biomaterials* **2003**, *24*, 1121-1131.

Flemming, H. C.; Wingender, J. The biofilm matrix. *Nat. Rev. Microbiol*. **2010**, *8*, 623-633.

Foster, J. W. When protons attack: microbial strategies of acid adaptation. *Curr. Opin. Microbiol*. **1999**, *2*, 170-174.

Foster, J. W. *Escherichia coli* acid resistance: tales of an amateur acidophile. *Nat. Rev. Microbiol*. **2004**, *2*, 898-907.

Foxman, B. The epidemiology of urinary tract infection. *Nat. Rev. Urol*. **2010**, *7*, 653-660.

French, S.; Puddephatt, D.; Habash, M.; Glasauer, S. The dynamic nature of bacterial surfaces: implications for metal-membrane interaction. *Crit. Rev. Microbiol*. **2013**, *39*, 196-217.

Furno, F.; Morley, K. S.; Wong, B.; Sharp, B. L.; Arnold, P. L.; Howdle, S. M.; Bayston, R.; Brown, P. D.; Winship, P. D.; Reid, H. J. Silver nanoparticles and polymeric medical devices: a new approach to prevention of infection? *J. Antimicrob. Chemother*. **2004**, *54*, 1019-1024.

Fux, C. A.; Costerton, J. W.; Stewart, P. S.; Stoodley, P. Survival strategies of infectious biofilms. *Trends Microbiol*. **2005**, *13*, 34-40.

Geilich, B. M.; Webster, T. J. Reduced adhesion of *Staphylococcus aureus* to ZnO/PVC nanocomposites. *Int. J. Nanomedicine* **2013**, *8*, 1177-1184.

Geske, G. D.; Wezeman, R. J.; Siegel, A. P.; Blackwell, H. E. Small molecule inhibitors of bacterial quorum sensing and biofilm formation. *J. Am. Chem. Soc*. **2005**, *127*, 12762-12763.

Giacometti, A.; Cirioni, O.; Del Prete, M. S.; Paggi, A. M.; D'Errico, M. M.; Scalise, G. Combination studies between polycationic peptides and clinically used antibiotics against Gram-positive and Gram-negative bacteria. *Peptides* **2000**, *21*, 1155-1160.

Gill, E. E.; Franco, O. L.; Hancock, R. E. Antibiotic adjuvants: diverse strategies for controlling drug-resistant pathogens. *Chem. Biol. Drug Des*. **2015**, *85*, 56-78.

Glukhov, E.; Stark, M.; Burrows, L. L.; Deber, C. M. Basis for selectivity of cationic antimicrobial peptides for bacterial versus mammalian membranes. *J. Biol. Chem*. **2005**, *280*, 33960-33967.

Gokel, G. W.; Negin, S. Synthetic membrane active amphiphiles. *Adv. Drug Deliv. Rev*. **2012**, *64*, 784-796.

Gomez, M. I.; Prince, A. Opportunistic infections in lung disease: Pseudomonas infections in cystic fibrosis. *Curr. Opin. Pharmacol*. **2007**, *7*, 244-251.

Gootz, T. D. The global problem of antibiotic resistance. *Crit. Rev. Immunol*. **2010**, *30*, 79-93.

Gorden, J.; Small, P. L. Acid resistance in enteric bacteria. *Infect. Immun*. **1993**, *61*, 364-367.

Govan, J. R.; Deretic, V. Microbial pathogenesis in cystic fibrosis: mucoid *Pseudomonas aeruginosa* and Burkholderia cepacia. *Microbiol. Rev*. **1996**, *60*, 539-574.

Grumezescu, A. M.; Ghitulica, C. D.; Voicu, G.; Huang, K. S.; Yang, C. H.; Ficai, A.; Vasile, B. S.; Grumezescu, V.; Bleotu, C.; Chifiriuc, M. C. New silica nanostructure for the improved delivery of topical antibiotics used in the treatment of staphylococcal cutaneous infections. *Int. J. Pharm*. **2014**, *463*, 170-176.

Gutierrez-Gonzalez, R.; Boto, G. R. Do antibiotic-impregnated catheters prevent infection in CSF diversion procedures? Review of the literature. *J. Infect*. **2010**, *61*, 9-20.

Gutsmann, T.; Seydel, U. Impact of the glycostructure of amphiphilic membrane components on the function of the outer membrane of Gram-negative bacteria as a matrix for incorporated channels and a target for antimicrobial peptides or proteins. *Eur. J. Cell Biol*. **2010**, *89*, 11-23.

Gwynn, M. N.; Portnoy, A.; Rittenhouse, S. F.; Payne, D. J. Challenges of antibacterial discovery revisited. *Ann. N. Y. Acad. Sci*. **2010**, *1213*, 5-19.

Haldar, J.; Kondaiah, P.; Bhattacharya, S. Synthesis and antibacterial properties of novel hydrolyzable cationic amphiphiles. Incorporation of multiple head groups leads to impressive antibacterial activity. *J. Med. Chem*. **2005**, *48*, 3823-3831.

Hall-Stoodley, L.; Costerton, J. W.; Stoodley, P. Bacterial biofilms: from the natural environment to infectious diseases. *Nat. Rev. Microbiol*. **2004**, *2*, 95-108.

Hancock, R. E. The bacterial outer membrane as a drug barrier. *Trends Microbiol*. **1997a**, *5*, 37-42.

Hancock, R. E. Peptide antibiotics. *Lancet* **1997b**, *349*, 418-422.

Hancock, R. E.; Chapple, D. S. Peptide antibiotics. *Antimicrob. Agents Chemother*. **1999**, *43*, 1317-1323.

Hancock, R. E.; Sahl, H. G. Antimicrobial and host-defense peptides as new anti-infective therapeutic strategies. *Nat. Biotechnol*. **2006**, *24*, 1551-1557.

Hawkey, P. M.; Jones, A. M. The changing epidemiology of resistance. *J. Antimicrob. Chemother*. **2009**, *64 Suppl 1*, i3-10.

He, J.; Soderling, E.; Osterblad, M.; Vallittu, P. K.; Lassila, L. V. Synthesis of methacrylate monomers with antibacterial effects against *S. mutans*. *Molecules* **2011**, *16*, 9755-9763.

Helander, I. M.; Mattila-Sandholm, T. Fluorometric assessment of gram-negative bacterial permeabilization. *J. Appl. Microbiol*. **2000**, *88*, 213-219.

Hetrick, E. M.; Schoenfisch, M. H. Reducing implant-related infections: active release strategies. *Chem. Soc. Rev*. **2006**, *35*, 780-789.

Hoefel, D.; Grooby, W. L.; Monis, P. T.; Andrews, S.; Saint, C. P. A comparative study of carboxyfluorescein diacetate and carboxyfluorescein diacetate succinimidyl ester as indicators of bacterial activity. *J. Microbiol. Methods* **2003**, *52*, 379-388.

Hogan, D.; Kolter, R. Why are bacteria refractory to antimicrobials? *Curr. Opin. Microbiol*. **2002**, *5*, 472-477.

Hoiby, N.; Bjarnsholt, T.; Givskov, M.; Molin, S.; Ciofu, O. Antibiotic resistance of bacterial biofilms. *Int. J. Antimicrob. Agents* **2010**, *35*, 322-332.

Hoque, J.; Akkapeddi, P.; Yarlagadda, V.; Uppu, D. S.; Kumar, P.; Haldar, J. Cleavable cationic antibacterial amphiphiles: synthesis, mechanism of action, and cytotoxicities. *Langmuir* **2012**, *28*, 12225-12234.

Horcas, I.; Fernandez, R.; Gomez-Rodriguez, J. M.; Colchero, J.; Gomez-Herrero, J.; Baro, A. M. WSXM: a software for scanning probe microscopy and a tool for nanotechnology. *Rev. Sci. Instrum.* **2007**, *78*, 013705.

Huh, A. J.; Kwon, Y. J. "Nanoantibiotics": a new paradigm for treating infectious diseases using nanomaterials in the antibiotics resistant era. *J. Control Release* **2011**, *156*, 128-145.

Hurdle, J. G.; O'Neill, A. J.; Chopra, I.; Lee, R. E. Targeting bacterial membrane function: an underexploited mechanism for treating persistent infections. *Nat. Rev. Microbiol.* **2011**, *9*, 62-75.

Incani, V.; Omar, A.; Prosperi-Porta, G.; Nadworny, P. Ag5IO6: novel antibiofilm activity of a silver compound with application to medical devices. *Int. J. Antimicrob. Agents*. **2015**, *45*, 586-593.

Izano, E. A.; Sadovskaya, I.; Wang, H.; Vinogradov, E.; Ragunath, C.; Ramasubbu, N.; Jabbouri, S.; Perry, M. B.; Kaplan, J. B. Poly-N-acetylglucosamine mediates biofilm formation and detergent resistance in *Aggregatibacter actinomycetemcomitans*. *Microb. Pathog.* **2008**, *44*, 52-60.

James, G. A.; Swogger, E.; Wolcott, R.; Pulcini, E.; Secor, P.; Sestrich, J.; Costerton, J. W.; Stewart, P. S. Biofilms in chronic wounds. *Wound Repair Regen.* **2008**, *16*, 37-44.

Jennings, M. C.; Ator, L. E.; Paniak, T. J.; Minbiole, K. P.; Wuest, W. M. Biofilm-eradicating properties of quaternary ammonium amphiphiles: simple mimics of antimicrobial peptides. *Chembiochem.* **2014**, *15*, 2211-2215.

Jiang, P.; Li, J.; Han, F.; Duan, G.; Lu, X.; Gu, Y.; Yu, W. Antibiofilm activity of an exopolysaccharide from marine bacterium Vibrio sp. QY101. *PLoS One* **2011**, *6*, e18514.

Jiang, Z.; Vasil, A. I.; Hale, J. D.; Hancock, R. E.; Vasil, M. L.; Hodges, R. S. Effects of net charge and the number of positively charged residues on the biological activity of amphipathic alpha-helical cationic antimicrobial peptides. *Biopolymers* **2008**, *90*, 369-383.

Jones, S. M.; Morgan, M.; Humphrey, T. J.; Lappin-Scott, H. Effect of vancomycin and rifampicin on meticillin-resistant *Staphylococcus aureus* biofilms. *Lancet* **2001**, *357*, 40-41.

Kafshgari, M. H.; Cavallaro, A.; Delalat, B.; Harding, F. J.; McInnes, S. J.; Makila, E.; Salonen, J.; Vasilev, K.; Voelcker, N. H. Nitric oxide-releasing porous silicon nanoparticles. *Nanoscale Res. Lett.* **2014**, *9*, 333.

Kanazawa, A.; Ikeda, T.; Endo, T. Synthesis and antimicrobial activity of dimethyl- and trimethyl-substituted phosphonium salts with alkyl chains of various lengths. *Antimicrob. Agents Chemother*. **1994**, *38*, 945-952.

Kaplan, J. B.; Velliyagounder, K.; Ragunath, C.; Rohde, H.; Mack, D.; Knobloch, J. K.; Ramasubbu, N. Genes involved in the synthesis and degradation of matrix polysaccharide in *Actinobacillus actinomycetemcomitans* and *Actinobacillus pleuropneumoniae* biofilms. *J Bacteriol*. **2004**, *186*, 8213-8220.

Kaye, K. S.; Kaye, D. Multidrug-resistant Pathogens: Mechanisms of Resistance and Epidemiology. *Curr. Infect. Dis. Rep*. **2000**, *2*, 391-398.

Kern, T.; Giffard, M.; Hediger, S.; Amoroso, A.; Giustini, C.; Bui, N. K.; Joris, B.; Bougault, C.; Vollmer, W.; Simorre, J. P. Dynamics characterization of fully hydrated bacterial cell walls by solid-state NMR: evidence for cooperative binding of metal ions. *J. Am. Chem. Soc*. **2010**, *132*, 10911-10919.

Kim, J.; Pitts, B.; Stewart, P. S.; Camper, A.; Yoon, J. Comparison of the antimicrobial effects of chlorine, silver ion, and tobramycin on biofilm. *Antimicrob. Agents Chemother*. **2008**, *52*, 1446-1453.

Klocek, G.; Schulthess, T.; Shai, Y.; Seelig, J. Thermodynamics of melittin binding to lipid bilayers. Aggregation and pore formation. *Biochemistry* **2009**, *48*, 2586-2596.

Koch, C.; Hoiby, N. Pathogenesis of cystic fibrosis. *Lancet* **1993**, *341*, 1065-1069.

Kohanski, M. A.; Dwyer, D. J.; Collins, J. J. How antibiotics kill bacteria: from targets to networks. *Nat. Rev. Microbiol*. **2010**, *8*, 423-435.

Kohler, T.; Weidenmaier, C.; Peschel, A. Wall teichoic acid protects *Staphylococcus aureus* against antimicrobial fatty acids from human skin. *J. Bacteriol*. **2009**, *191*, 4482-4484.

Kolodkin-Gal, I.; Cao, S.; Chai, L.; Bottcher, T.; Kolter, R.; Clardy, J.; Losick, R. A self-produced trigger for biofilm disassembly that targets exopolysaccharide. *Cell* **2012**, *149*, 684-692.

Kostakioti, M.; Hadjifrangiskou, M.; Hultgren, S. J. Bacterial biofilms: development, dispersal, and therapeutic strategies in the dawn of the postantibiotic era. *Cold Spring Harb. Perspect. Med*. **2013**, *3*, a010306.

Kratz, F. Albumin as a drug carrier: design of prodrugs, drug conjugates and nanoparticles. *J. Control Release*. **2008**, *132*, 171-183.

Kumar, S.; Varela, M. F. Molecular mechanisms of bacterial resistance to antimicrobial agents. *chemotherapy* **2013**, *14*, 18.

Kuramitsu, H. K.; Wang, B. Y. The whole is greater than the sum of its parts: dental plaque bacterial interactions can affect the virulence properties of cariogenic *Streptococcus mutans*. *Am. J. Dent*. **2011**, *24*, 153-154.

Kuroda, K.; DeGrado, W. F. Amphiphilic polymethacrylate derivatives as antimicrobial agents. *J. Am. Chem. Soc*. **2005**, *127*, 4128-4129.

LaDow, J. E.; Warnock, D. C.; Hamill, K. M.; Simmons, K. L.; Davis, R. W.; Schwantes, C. R.; Flaherty, D. C.; Willcox, J. A.; Wilson-Henjum, K.; Caran, K. L.; Minbiole, K. P.; Seifert, K. Bicephalic amphiphile architecture affects antibacterial activity. *Eur. J. Med. Chem*. **2011**, *46*, 4219-4226.

Lambert, P. A. Mechanisms of antibiotic resistance in *Pseudomonas aeruginosa*. *J. R. Soc. Med*. **2002**, *95 Suppl 41*, 22-26.

Lamp, K. C.; Rybak, M. J.; Bailey, E. M.; Kaatz, G. W. *In vitro* pharmacodynamic effects of concentration, pH, and growth phase on serum bactericidal activities of daptomycin and vancomycin. *Antimicrob. Agents Chemother*. **1992**, *36*, 2709-2714.

Lange, R. P.; Locher, H. H.; Wyss, P. C.; Then, R. L. The targets of currently used antibacterial agents: lessons for drug discovery. *Curr. Pharm. Des*. **2007**, *13*, 3140-3154.

Langer, K.; Balthasar, S.; Vogel, V.; Dinauer, N.; von Briesen, H.; Schubert, D. Optimization of the preparation process for human serum albumin (HSA) nanoparticles. *Int. J. Pharm*. **2003**, *257*, 169-180.

Lavigne, J. P.; Sotto, A.; Nicolas-Chanoine, M. H.; Bouziges, N.; Bourg, G.; Davin-Regli, A.; Pages, J. M. Membrane permeability, a pivotal function involved in antibiotic resistance and virulence in *Enterobacter aerogenes* clinical isolates. *Clin. Microbiol. Infect*. **2012**, *18*, 539-545.

Lebeaux, D.; Chauhan, A.; Rendueles, O.; Beloin, C. From *in vitro* to *in vivo* Models of Bacterial Biofilm-Related Infections. *Pathogens* **2013**, *2*, 288-356.

Leevy, W. M.; Gammon, S. T.; Levchenko, T.; Daranciang, D. D.; Murillo, O.; Torchilin, V.; Piwnica-Worms, D.; Huettner, J. E.; Gokel, G. W. Structure-activity relationships, kinetics, selectivity, and mechanistic studies of synthetic hydraphile channels in bacterial and mammalian cells. *Org. Biomol. Chem*. **2005**, *3*, 3544-3550.

Lewis, K. Multidrug tolerance of biofilms and persister cells. *Curr. Top. Microbiol. Immunol*. **2008**, *322*, 107-131.

Lewis, K. Platforms for antibiotic discovery. *Nat. Rev. Drug Discov*. **2013**, *12*, 371-387.

Li, L.; Li, Z.; Guo, N.; Jin, J.; Du, R.; Liang, J.; Wu, X.; Wang, X.; Liu, M.; Jin, Q.; Yu, L. Synergistic activity of 1-(1-naphthylmethyl)-piperazine with ciprofloxacin against clinically resistant *Staphylococcus aureus*, as determined by different methods. *Lett. Appl. Microbiol.* **2011**, *52*, 372-378.

Li, X. Z.; Nikaido, H. Efflux-mediated drug resistance in bacteria: an update. *Drugs* **2009**, *69*, 1555-1623.

Lindstedt, M.; Allenmark, S.; Thompson, R. A.; Edebo, L. Antimicrobial activity of betaine esters, quaternary ammonium amphiphiles which spontaneously hydrolyze into nontoxic components. *Antimicrob. Agents Chemother*. **1990**, *34*, 1949-1954.

Locher, H. H.; Caspers, P.; Bruyere, T.; Schroeder, S.; Pfaff, P.; Knezevic, A.; Keck, W.; Ritz, D. Investigations of the mode of action and resistance development of cadazolid, a new antibiotic for treatment of *Clostridium difficile* infections. *Antimicrob. Agents Chemother*. **2014**, *58*, 901-908.

Lode, H. Tobramycin: a review of therapeutic uses and dosing schedules. *Curr. Ther. Res.* **1998**, *59*, 420-453.

Lowery, C. A.; Park, J.; Gloeckner, C.; Meijler, M. M.; Mueller, R. S.; Boshoff, H. I.; Ulrich, R. L.; Barry, C. E., 3rd; Bartlett, D. H.; Kravchenko, V. V.; Kaufmann, G. F.; Janda, K. D. Defining the mode of action of tetramic acid antibacterials derived from *Pseudomonas aeruginosa* quorum sensing signals. *J. Am. Chem. Soc*. **2009**, *131*, 14473-14479.

Lowy, F. D. Antimicrobial resistance: the example of *Staphylococcus aureus*. *J. Clin. Invest*. **2003**, *111*, 1265-1273.

Lv, J.; Qian, Y.; Liu, T.; Wang, Y. Synthesis and evaluation of amphiphilic cationic quinine-derived for antibacterial activity against methicillin-resistant *Staphylococcus aureus*. *Bioorg. Med. Chem. Lett*. **2007**, *17*, 4102-4106.

Madsen, J. S.; Burmolle, M.; Hansen, L. H.; Sorensen, S. J. The interconnection between biofilm formation and horizontal gene transfer. *FEMS Immunol. Med. Microbiol*. **2012**, *65*, 183-195.

Mah, T. F.; O'Toole, G. A. Mechanisms of biofilm resistance to antimicrobial agents. *Trends Microbiol*. **2001**, *9*, 34-39.

Malina, A.; Shai, Y. Conjugation of fatty acids with different lengths modulates the antibacterial and antifungal activity of a cationic biologically inactive peptide. *Biochem. J*. **2005**, *390*, 695-702.

Mangoni, M. L.; Papo, N.; Mignogna, G.; Andreu, D.; Shai, Y.; Barra, D.; Simmaco, M. Ranacyclins, a new family of short cyclic antimicrobial peptides: biological function, mode of action, and parameters involved in target specificity. *Biochemistry* **2003**, *42*, 14023-14035.

Mann, E. E.; Wozniak, D. J. Pseudomonas biofilm matrix composition and niche biology. *FEMS Microbiol. Rev*. **2012**, *36*, 893-916.

Marafino, J. N.; Gallagher, T. M.; Barragan, J.; Volkers, B. L.; LaDow, J. E.; Bonifer, K.; Fitzgerald, G.; Floyd, J. L.; McKenna, K.; Minahan, N. T.; Walsh, B.; Seifert, K.; Caran, K. L. Colloidal and antibacterial properties of novel triple-headed, double-tailed amphiphiles: Exploring structure-activity relationships and synergistic mixtures. *Bioorg. Med. Chem*. **2015**,

Marr, A. K.; Gooderham, W. J.; Hancock, R. E. Antibacterial peptides for therapeutic use: obstacles and realistic outlook. *Curr. Opin. Pharmacol*. **2006**, *6*, 468-472.

Mather, A. E.; Reid, S. W.; Maskell, D. J.; Parkhill, J.; Fookes, M. C.; Harris, S. R.; Brown, D. J.; Coia, J. E.; Mulvey, M. R.; Gilmour, M. W.; Petrovska, L.; de Pinna, E.; Kuroda, M.; Akiba, M.; Izumiya, H.; Connor, T. R.; Suchard, M. A.; Lemey, P.; Mellor, D. J.; Haydon, D. T.; Thomson, N. R. Distinguishable epidemics of multidrug-resistant *Salmonella Typhimurium* DT104 in different hosts. *Science* **2013**, *341*, 1514-1517.

Matsuzaki, K.; Mitani, Y.; Akada, K. Y.; Murase, O.; Yoneyama, S.; Zasloff, M.; Miyajima, K. Mechanism of synergism between antimicrobial peptides magainin 2 and PGLa. *Biochemistry* **1998**, *37*, 15144-15153.

McCoy, L. S.; Xie, Y.; Tor, Y. Antibiotics that target protein synthesis. *Wiley Interdiscip. Rev. RNA*. **2011**, *2*, 209-232.

Mejias Carpio, I. E.; Santos, C. M.; Wei, X.; Rodrigues, D. F. Toxicity of a polymer-graphene oxide composite against bacterial planktonic cells, biofilms, and mammalian cells. *Nanoscale* **2012**, *4*, 4746-4756.

Mercier, R. C.; Stumpo, C.; Rybak, M. J. Effect of growth phase and pH on the *in vitro* activity of a new glycopeptide, oritavancin (LY333328), against *Staphylococcus aureus* and *Enterococcus faecium*. *J. Antimicrob. Chemother*. **2002**, *50*, 19-24.

Meyers, S. R.; Juhn, F. S.; Griset, A. P.; Luman, N. R.; Grinstaff, M. W. Anionic amphiphilic dendrimers as antibacterial agents. *J. Am. Chem. Soc*. **2008**, *130*, 14444-14445.

Miller, K. A.; Suresh Kumar, E. V.; Wood, S. J.; Cromer, J. R.; Datta, A.; David, S. A. Lipopolysaccharide sequestrants: structural correlates of activity and toxicity in novel acylhomospermines. *J. Med. Chem*. **2005**, *48*, 2589-2599.

Mintzer, M. A.; Dane, E. L.; O'Toole, G. A.; Grinstaff, M. W. Exploiting dendrimer multivalency to combat emerging and re-emerging infectious diseases. *Mol. Pharm*. **2012**, *9*, 342-354.

Mitra, R. N.; Shome, A.; Paul, P.; Das, P. K. Antimicrobial activity, biocompatibility and hydrogelation ability of dipeptide-based amphiphiles. *Org. Biomol. Chem*. **2009**, *7*, 94-102.

Moghimi, S. M.; Hunter, A. C.; Murray, J. C. Nanomedicine: current status and future prospects. *FASEB J*. **2005**, *19*, 311-330.

Molin, S.; Tolker-Nielsen, T. Gene transfer occurs with enhanced efficiency in biofilms and induces enhanced stabilisation of the biofilm structure. *Curr. Opin. Biotechnol*. **2003**, *14*, 255-261.

Morar, M.; Wright, G. D. The genomic enzymology of antibiotic resistance. *Annu. Rev. Genet*. **2010**, *44*, 25-51.

Mowery, B. P.; Lee, S. E.; Kissounko, D. A.; Epand, R. F.; Epand, R. M.; Weisblum, B.; Stahl, S. S.; Gellman, S. H. Mimicry of antimicrobial host-defense peptides by random copolymers. *J. Am. Chem. Soc*. **2007**, *129*, 15474-15476.

Muder, R. R.; Brennen, C.; Rihs, J. D.; Wagener, M. M.; Obman, A.; Stout, J. E.; Yu, V. L. Isolation of *Staphylococcus aureus* from the urinary tract: association of isolation with symptomatic urinary tract infection and subsequent staphylococcal bacteremia. *Clin. Infect. Dis*. **2006**, *42*, 46-50.

Mueller, M.; de la Pena, A.; Derendorf, H. Issues in pharmacokinetics and pharmacodynamics of anti-infective agents: kill curves versus MIC. *Antimicrob. Agents Chemother*. **2004**, *48*, 369-377.

Murray, E. J.; Crowley, R. C.; Truman, A.; Clarke, S. R.; Cottam, J. A.; Jadhav, G. P.; Steele, V. R.; O'Shea, P.; Lindholm, C.; Cockayne, A.; Chhabra, S. R.; Chan, W. C.; Williams, P. Targeting *Staphylococcus aureus* quorum sensing with nonpeptidic small molecule inhibitors. *J. Med. Chem*. **2014**, *57*, 2813-2819.

Musken, M.; Di Fiore, S.; Romling, U.; Haussler, S. A 96-well-plate-based optical method for the quantitative and qualitative evaluation of *Pseudomonas aeruginosa* biofilm formation and its application to susceptibility testing. *Nat. Protoc*. **2010**, *5*, 1460-1469.

Naghmouchi, K.; Drider, D.; Baah, J.; Teather, R. Nisin A and Polymyxin B as Synergistic Inhibitors of Gram-positive and Gram-negative Bacteria. *Probiotics Antimicrob. Proteins* **2010**, *2*, 98-103.

Nikaido, H. Molecular basis of bacterial outer membrane permeability revisited. *Microbiol. Mol. Biol. Rev*. **2003**, *67*, 593-656.

Nikaido, H. Multidrug resistance in bacteria. *Annu. Rev. Biochem*. **2009**, *78*, 119-146.

Noimark, S.; Dunnill, C. W.; Wilson, M.; Parkin, I. P. The role of surfaces in catheter-associated infections. *Chem. Soc. Rev*. **2009**, *38*, 3435-3448.

Nolte, O. Antimicrobial resistance in the 21st century: a multifaceted challenge. *Protein Pept. Lett*. **2014**, *21*, 330-335.

Oda, Y.; Kanaoka, S.; Sato, T.; Aoshima, S.; Kuroda, K. Block versus random amphiphilic copolymers as antibacterial agents. *Biomacromolecules* **2011**, *12*, 3581-3591.

Olson, K. M.; Starks, C. M.; Williams, R. B.; O'Neil-Johnson, M.; Huang, Z.; Ellis, M.; Reilly, J. E.; Eldridge, G. R. Novel pentadecenyl tetrazole enhances susceptibility of methicillin-resistant *Staphylococcus aureus* biofilms to gentamicin. *Antimicrob. Agents Chemother*. **2011**, *55*, 3691-3695.

Ooi, N.; Miller, K.; Randall, C.; Rhys-Williams, W.; Love, W.; Chopra, I. XF-70 and XF-73, novel antibacterial agents active against slow-growing and non-dividing cultures of *Staphylococcus aureus* including biofilms. *J. Antimicrob. Chemother*. **2010**, *65*, 72-78.

Otto, M. Staphylococcal biofilms. *Curr. Top. Microbiol. Immunol*. **2008**, *322*, 207-228.

Otto, M. *Staphylococcus epidermidis*--the 'accidental' pathogen. *Nat. Rev. Microbiol*. **2009**, *7*, 555-567.

Pag, U.; Oedenkoven, M.; Sass, V.; Shai, Y.; Shamova, O.; Antcheva, N.; Tossi, A.; Sahl, H. G. Analysis of *in vitro* activities and modes of action of synthetic antimicrobial peptides derived from an alpha-helical 'sequence template'. *J. Antimicrob. Chemother*. **2008**, *61*, 341-352.

Palermo, E. F.; Kuroda, K. Chemical structure of cationic groups in amphiphilic polymethacrylates modulates the antimicrobial and hemolytic activities. *Biomacromolecules* **2009**, *10*, 1416-1428.

Palermo, E. F.; Sovadinova, I.; Kuroda, K. Structural determinants of antimicrobial activity and biocompatibility in membrane-disrupting methacrylamide random copolymers. *Biomacromolecules* **2009**, *10*, 3098-3107.

Palmer, A. C.; Kishony, R. Opposing effects of target overexpression reveal drug mechanisms. *Nat. Commun*. **2014**, *5*, 4296.

Paniak, T. J.; Jennings, M. C.; Shanahan, P. C.; Joyce, M. D.; Santiago, C. N.; Wuest, W. M.; Minbiole, K. P. The antimicrobial activity of mono-, bis-, tris-, and tetracationic amphiphiles derived from simple polyamine platforms. *Bioorg. Med. Chem. Lett*. **2014**, *24*, 5824-5828.

Parsek, M. R.; Singh, P. K. Bacterial biofilms: an emerging link to disease pathogenesis. *Annu. Rev. Microbiol*. **2003**, *57*, 677-701.

Parsek, M. R.; Tolker-Nielsen, T. Pattern formation in *Pseudomonas aeruginosa* biofilms. *Curr. Opin. Microbiol*. **2008**, *11*, 560-566.

Paslay, L. C.; Abel, B. A.; Brown, T. D.; Koul, V.; Choudhary, V.; McCormick, C. L.; Morgan, S. E. Antimicrobial poly(methacrylamide) derivatives prepared via aqueous RAFT polymerization exhibit biocidal efficiency dependent upon cation structure. *Biomacromolecules* **2012**, *13*, 2472-2482.

Patch, J. A.; Barron, A. E. Helical peptoid mimics of magainin-2 amide. *J. Am. Chem. Soc*. **2003**, *125*, 12092-12093.

Patti, J. M.; Allen, B. L.; McGavin, M. J.; Hook, M. MSCRAMM-mediated adherence of microorganisms to host tissues. *Annu. Rev. Microbiol*. **1994**, *48*, 585-617.

Periasamy, S.; Joo, H. S.; Duong, A. C.; Bach, T. H.; Tan, V. Y.; Chatterjee, S. S.; Cheung, G. Y.; Otto, M. How *Staphylococcus aureus* biofilms develop their characteristic structure. *Proc. Natl. Acad. Sci. U S A*. **2012**, *109*, 1281-1286.

Piers, K. L.; Brown, M. H.; Hancock, R. E. Improvement of outer membrane-permeabilizing and lipopolysaccharide-binding activities of an antimicrobial cationic peptide by C-terminal modification. *Antimicrob. Agents Chemother*. **1994**, *38*, 2311-2316.

Piletska, E. V.; Stavroulakis, G.; Larcombe, L. D.; Whitcombe, M. J.; Sharma, A.; Primrose, S.; Robinson, G. K.; Piletsky, S. A. Passive control of quorum sensing: prevention of *Pseudomonas aeruginosa* biofilm formation by imprinted polymers. *Biomacromolecules* **2011**, *12*, 1067-1071.

Pinto-Alphandary, H.; Andremont, A.; Couvreur, P. Targeted delivery of antibiotics using liposomes and nanoparticles: research and applications. *Int. J. Antimicrob. Agents* **2000**, *13*, 155-168.

Pompilio, A.; Scocchi, M.; Pomponio, S.; Guida, F.; Di Primio, A.; Fiscarelli, E.; Gennaro, R.; Di Bonaventura, G. Antibacterial and anti-biofilm effects of cathelicidin peptides against pathogens isolated from cystic fibrosis patients. *Peptides* **2011**, *32*, 1807-1814.

Purdy Drew, K. R.; Sanders, L. K.; Culumber, Z. W.; Zribi, O.; Wong, G. C. Cationic amphiphiles increase activity of aminoglycoside antibiotic tobramycin in the presence of airway polyelectrolytes. *J. Am. Chem. Soc*. **2009**, *131*, 486-493.

Rawlinson, L. A.; Ryan, S. M.; Mantovani, G.; Syrett, J. A.; Haddleton, D. M.; Brayden, D. J. Antibacterial effects of poly(2-(dimethylamino ethyl)methacrylate) against selected gram-positive and gram-negative bacteria. *Biomacromolecules* **2010**, *11*, 443-453.

Richard, H.; Foster, J. W. *Escherichia coli* glutamate- and arginine-dependent acid resistance systems increase internal pH and reverse transmembrane potential. *J. Bacteriol*. **2004**, *186*, 6032-6041.

Risbud, M. V.; Hardikar, A. A.; Bhat, S. V.; Bhonde, R. R. pH-sensitive freeze-dried chitosan-polyvinyl pyrrolidone hydrogels as controlled release system for antibiotic delivery. *J. Control Release*. **2000**, *68*, 23-30.

Rogers, S. A.; Huigens, R. W., 3rd; Cavanagh, J.; Melander, C. Synergistic effects between conventional antibiotics and 2-aminoimidazole-derived antibiofilm agents. *Antimicrob. Agents Chemother*. **2010**, *54*, 2112-2118.

Roy, S.; Das, P. K. Antibacterial hydrogels of amino acid-based cationic amphiphiles. *Biotechnol. Bioeng*. **2008**, *100*, 756-764.

Saha, S.; Savage, P. B.; Bal, M. Enhancement of the efficacy of erythromycin in multiple antibiotic-resistant gram-negative bacterial pathogens. *J. Appl. Microbiol*. **2008**, *105*, 822-828.

Shai, Y. Mode of action of membrane active antimicrobial peptides. *Biopolymers* **2002**, *66*, 236-248.

Shanks, R. M.; Sargent, J. L.; Martinez, R. M.; Graber, M. L.; O'Toole, G. A. Catheter lock solutions influence staphylococcal biofilm formation on abiotic surfaces. *Nephrol. Dial. Transplant*. **2006**, *21*, 2247-2255.

Shimanovich, U.; Bernardes, G. J.; Knowles, T. P.; Cavaco-Paulo, A. Protein micro- and nano-capsules for biomedical applications. *Chem. Soc. Rev*. **2014**, *43*, 1361-1371.

Silver, L. L. Challenges of antibacterial discovery. *Clin. Microbiol. Rev*. **2011**, *24*, 71-109.

Singh, A. K.; Mukherjee, S.; Adhikari, M. D.; Ramesh, A. Fluorescence-Based Comparative Evaluation of Bactericidal Potency and Food Application Potential of

Anti-listerial Bacteriocin Produced by Lactic Acid Bacteria Isolated from Indigenous Samples. *Probiotics Antimicrob. Proteins* **2012**, *4*, 122-132.

Singh, P. K.; Schaefer, A. L.; Parsek, M. R.; Moninger, T. O.; Welsh, M. J.; Greenberg, E. P. Quorum-sensing signals indicate that cystic fibrosis lungs are infected with bacterial biofilms. *Nature* **2000**, *407*, 762-764.

Singh, R.; Ray, P.; Das, A.; Sharma, M. Penetration of antibiotics through *Staphylococcus aureus* and *Staphylococcus epidermidis* biofilms. *J. Antimicrob Chemother*. **2010**, *65*, 1955-1958.

Singh, V.; Arora, V.; Alam, M. J.; Garey, K. W. Inhibition of biofilm formation by esomeprazole in *Pseudomonas aeruginosa* and *Staphylococcus aureus*. *Antimicrob. Agents Chemother*. **2012**, *56*, 4360-4364.

Slomberg, D. L.; Lu, Y.; Broadnax, A. D.; Hunter, R. A.; Carpenter, A. W.; Schoenfisch, M. H. Role of size and shape on biofilm eradication for nitric oxide-releasing silica nanoparticles. *ACS Appl. Mater. Interfaces* **2013**, *5*, 9322-9329.

Song, A.; Walker, S. G.; Parker, K. A.; Sampson, N. S. Antibacterial studies of cationic polymers with alternating, random, and uniform backbones. *ACS Chem. Biol*. **2011**, *6*, 590-599.

Speziale, P.; Pietrocola, G.; Rindi, S.; Provenzano, M.; Provenza, G.; Di Poto, A.; Visai, L.; Arciola, C. R. Structural and functional role of *Staphylococcus aureus* surface components recognizing adhesive matrix molecules of the host. *Future Microbiol*. **2009**, *4*, 1337-1352.

Stewart, P. S. Mechanisms of antibiotic resistance in bacterial biofilms. *Int. J. Med. Microbiol*. **2002**, *292*, 107-113.

Stewart, P. S.; Costerton, J. W. Antibiotic resistance of bacteria in biofilms. *Lancet* **2001**, *358*, 135-138.

Stone, P. W. Economic burden of healthcare-associated infections: an American perspective. *Expert Rev. Pharmacoecon. Outcomes Res*. **2009**, *9*, 417-422.

Sugandhi, E. W.; Macri, R. V.; Williams, A. A.; Kite, B. L.; Slebodnick, C.; Falkinham, J. O., 3rd; Esker, A. R.; Gandour, R. D. Synthesis, critical micelle concentrations, and antimycobacterial properties of homologous, dendritic amphiphiles. Probing intrinsic activity and the "cutoff" effect. *J. Med. Chem*. **2007**, *50*, 1645-1650.

Sun, J.; Deng, Z.; Yan, A. Bacterial multidrug efflux pumps: mechanisms, physiology and pharmacological exploitations. *Biochem. Biophys. Res. Commun*. **2014**, *453*, 254-267.

Sutherland, I. W.; Hughes, K. A.; Skillman, L. C.; Tait, K. The interaction of phage and biofilms. *FEMS Microbiol. Lett*. **2004**, *232*, 1-6.

Taglietti, A.; Arciola, C. R.; D'Agostino, A.; Dacarro, G.; Montanaro, L.; Campoccia, D.; Cucca, L.; Vercellino, M.; Poggi, A.; Pallavicini, P.; Visai, L. Antibiofilm activity

of a monolayer of silver nanoparticles anchored to an amino-silanized glass surface. *Biomaterials* **2014**, *35*, 1779-1788.

Tamplin, M. L. Inactivation of *Escherichia coli* O157:H7 in simulated human gastric fluid. *Appl. Environ. Microbiol*. **2005**, *71*, 320-325.

Tang, H.; Doerksen, R. J.; Jones, T. V.; Klein, M. L.; Tew, G. N. Biomimetic facially amphiphilic antibacterial oligomers with conformationally stiff backbones. *Chem. Biol*. **2006**, *13*, 427-435.

Tew, G. N.; Liu, D.; Chen, B.; Doerksen, R. J.; Kaplan, J.; Carroll, P. J.; Klein, M. L.; DeGrado, W. F. De novo design of biomimetic antimicrobial polymers. *Proc. Natl. Acad. Sci. U S A.* **2002**, *99*, 5110-5114.

Thompson, R. J.; Bobay, B. G.; Stowe, S. D.; Olson, A. L.; Peng, L.; Su, Z.; Actis, L. A.; Melander, C.; Cavanagh, J. Identification of BfmR, a response regulator involved in biofilm development, as a target for a 2-Aminoimidazole-based antibiofilm agent. *Biochemistry* **2012**, *51*, 9776-9778.

Toprak, E.; Veres, A.; Michel, J. B.; Chait, R.; Hartl, D. L.; Kishony, R. Evolutionary paths to antibiotic resistance under dynamically sustained drug selection. *Nat. Genet.* **2012**, *44*, 101-105.

Trautner, B. W.; Darouiche, R. O. Catheter-associated infections: pathogenesis affects prevention. *Arch. Intern. Med*. **2004**, *164*, 842-850.

Tseng, B. S.; Zhang, W.; Harrison, J. J.; Quach, T. P.; Song, J. L.; Penterman, J.; Singh, P. K.; Chopp, D. L.; Packman, A. I.; Parsek, M. R. The extracellular matrix protects *Pseudomonas aeruginosa* biofilms by limiting the penetration of tobramycin. *Environ. Microbiol*. **2013**, *15*, 2865-2878.

Uday, S. P.; Thiyagarajan, D.; Goswami, S.; Adhikari, M. D.; Das, G.; Ramesh, A. Amphiphile-mediated enhanced antibiotic efficacy and development of a payload nanocarrier for effective killing of pathogenic bacteria. *J. Mater. Chem. B.* **2014**, *2*, 5818-5827.

Ulvatne, H.; Karoliussen, S.; Stiberg, T.; Rekdal, O.; Svendsen, J. S. Short antibacterial peptides and erythromycin act synergically against *Escherichia coli*. *J. Antimicrob. Chemother*. **2001**, *48*, 203-208.

Unger, T.; Oren, Z.; Shai, Y. The Effect of Cyclization of Magainin 2 and Melittin Analogues on Structure, Function, and Model Membrane Interactions: Implication to Their Mode of Action. *Biochemistry* **2001**, *40*, 6388-6397.

Vaara, M. Polymyxins and their novel derivatives. *Curr. Opin. Microbiol*. **2010**, *13*, 574-581.

Van Bambeke, F.; Mingeot-Leclercq, M. P.; Struelens, M. J.; Tulkens, P. M. The bacterial envelope as a target for novel anti-MRSA antibiotics. *Trends Pharmacol. Sci*. **2008**, *29*, 124-134.

van Meer, G.; de Kroon, A. I. Lipid map of the mammalian cell. *J. Cell. Sci*. **2011**, *124*, 5-8.

Verdurmen, W. P.; Bovee-Geurts, P. H.; Wadhwani, P.; Ulrich, A. S.; Hallbrink, M.; van Kuppevelt, T. H.; Brock, R. Preferential uptake of L- versus D-amino acid cell-penetrating peptides in a cell type-dependent manner. *Chem. Biol*. **2011**, *18*, 1000-1010.

Virto, R.; Manas, P.; Alvarez, I.; Condon, S.; Raso, J. Membrane damage and microbial inactivation by chlorine in the absence and presence of a chlorine-demanding substrate. *Appl. Environ. Microbiol*. **2005**, *71*, 5022-5028.

Vooturi, S. K.; Cheung, C. M.; Rybak, M. J.; Firestine, S. M. Design, synthesis, and structure-activity relationships of benzophenone-based tetraamides as novel antibacterial agents. *J. Med. Chem*. **2009**, *52*, 5020-5031.

Vudumula, U.; Adhikari, M. D.; Ojha, B.; Goswami, S.; Das, G.; Ramesh, A. Tuning the bactericidal repertoire and potency of quinoline-based amphiphiles for enhanced killing of pathogenic bacteria. *RSC Adv*. **2012**, *2*, 3864-3871.

Wagner, V. E.; Iglewski, B. H. *P. aeruginosa* Biofilms in CF Infection. *Clin. Rev. Allergy Immunol*. **2008**, *35*, 124-134.

Walters, M. C., 3rd; Roe, F.; Bugnicourt, A.; Franklin, M. J.; Stewart, P. S. Contributions of antibiotic penetration, oxygen limitation, and low metabolic activity to tolerance of *Pseudomonas aeruginosa* biofilms to ciprofloxacin and tobramycin. *Antimicrob. Agents Chemother*. **2003**, *47*, 317-323.

Wassenaar, T. M.; Ussery, D.; Nielsen, L. N.; Ingmer, H. Review and phylogenetic analysis of qac genes that reduce susceptibility to quaternary ammonium compounds in *Staphylococcus species*. *Eur. J. Microbiol. Immunol (Bp)*. **2015**, *5*, 44-61.

Weidenmaier, C.; Peschel, A. Teichoic acids and related cell-wall glycopolymers in Gram-positive physiology and host interactions. *Nat. Rev. Microbiol*. **2008**, *6*, 276-287.

Westerhoff, H. V.; Zasloff, M.; Rosner, J. L.; Hendler, R. W.; De Waal, A.; Vaz Gomes, A.; Jongsma, P. M.; Riethorst, A.; Juretic, D. Functional synergism of the magainins PGLa and magainin-2 in *Escherichia coli*, tumor cells and liposomes. *Eur. J. Biochem*. **1995**, *228*, 257-264.

Whitchurch, C. B.; Tolker-Nielsen, T.; Ragas, P. C.; Mattick, J. S. Extracellular DNA required for bacterial biofilm formation. *Science* **2002**, *295*, 1487.

Widanapathirana, L.; Zhao, Y. Effects of amphiphile topology on the aggregation of oligocholates in lipid membranes: macrocyclic versus linear amphiphiles. *Langmuir* **2012**, *28*, 8165-8173.

Wilson, D. N. Ribosome-targeting antibiotics and mechanisms of bacterial resistance. *Nat. Rev. Microbiol*. **2014**, *12*, 35-48.

Wimley, W. C. Describing the mechanism of antimicrobial peptide action with the interfacial activity model. *ACS Chem. Biol*. **2010**, *5*, 905-917.

Wiradharma, N.; Khoe, U.; Hauser, C. A.; Seow, S. V.; Zhang, S.; Yang, Y. Y. Synthetic cationic amphiphilic alpha-helical peptides as antimicrobial agents. *Biomaterials* **2011**, *32*, 2204-2212.

Wispelwey, B. Clinical implications of pharmacokinetics and pharmacodynamics of fluoroquinolones. *Clin. Infect. Dis*. **2005**, *41 Suppl 2*, S127-135.

Worthington, R. J.; Richards, J. J.; Melander, C. Small molecule control of bacterial biofilms. *Org. Biomol. Chem*. **2012**, *10*, 7457-7474.

Wright, G. D. Bacterial resistance to antibiotics: enzymatic degradation and modification. *Adv. Drug Deliv. Rev*. **2005**, *57*, 1451-1470.

Wright, G. D. Molecular mechanisms of antibiotic resistance. *Chem. Commun*. **2011**, *47*, 4055-4061.

Yang, L.; Gordon, V. D.; Mishra, A.; Som, A.; Purdy, K. R.; Davis, M. A.; Tew, G. N.; Wong, G. C. Synthetic antimicrobial oligomers induce a composition-dependent topological transition in membranes. *J. Am. Chem. Soc*. **2007**, *129*, 12141-12147.

Yeaman, M. R.; Yount, N. Y. Mechanisms of antimicrobial peptide action and resistance. *Pharmacol. Rev*. **2003**, *55*, 27-55.

Yeh, P. J.; Hegreness, M. J.; Aiden, A. P.; Kishony, R. Drug interactions and the evolution of antibiotic resistance. *Nat. Rev. Microbiol*. **2009**, *7*, 460-466.

Zasloff, M. Antimicrobial peptides of multicellular organisms. *Nature* **2002**, *415*, 389-395.

Zavascki, A. P.; Goldani, L. Z.; Li, J.; Nation, R. L. Polymyxin B for the treatment of multidrug-resistant pathogens: a critical review. *J. Antimicrob. Chemother*. **2007**, *60*, 1206-1215.

Zhang, L.; Dhillon, P.; Yan, H.; Farmer, S.; Hancock, R. E. Interactions of bacterial cationic peptide antibiotics with outer and cytoplasmic membranes of *Pseudomonas aeruginosa*. *Antimicrob. Agents Chemother*. **2000**, *44*, 3317-3321.

Zhang, L.; Pornpattananangku, D.; Hu, C. M.; Huang, C. M. Development of nanoparticles for antimicrobial drug delivery. *Curr. Med. Chem*. **2010**, *17*, 585-594.

Zhao, T.; Liu, Y. N-acetylcysteine inhibit biofilms produced by *Pseudomonas aeruginosa*. *BMC Microbiol*. **2010**, *10*, 140.

Zhong, Z.; Yan, J.; Zhao, Y. Cholic acid-derived facial amphiphiles with different ionic characteristics. *Langmuir* **2005**, *21*, 6235-6239.

Zimmermann, L.; Bussiere, A.; Ouberai, M.; Baussanne, I.; Jolivalt, C.; Mingeot-Leclercq, M. P.; Decout, J. L. Tuning the antibacterial activity of amphiphilic neamine derivatives and comparison to paromamine homologues. *J. Med. Chem*. **2013**, *56*, 7691-7705.

TH-1410_10610607

APPENDIX

TH-1410_10610607

TH-1410_10610607

APPENDIX

A2.1 Synthesis of Amphiphiles

The control **Compound 1** and **Compound 2** were synthesized as per scheme shown in Figure 2.2.

Compound 3 *[N-((pyridin-2-yl)methyl)dodecan-1-amine]*

100 mg of 2-pyridinealdehyde was refluxed with 190 mg (1.1 eqv.) of dodecylamine in methanol to afford the Schiff base N-((pyridin-2-yl)methylene)dodecan-1-amine in 70% yield. The Schiff base was reduced by gradual addition of 0.75 equivalent of $NaBH_4$ in its methanolic solution to obtain N-((pyridin-2-yl)methyl)dodecan-1-amine or **compound 3**. Crude product was purified by column chromatography with 62% yield.

Compound 4 *[N-((methylpyridinium-2-yl)methyl)dodecan-1-amine]*

Compound 3 was methylated by refluxing it in presence of 1.5 eqv. of methyl iodide in dioxane solvent to obtain the desired product N-((methylpyridinium-2-yl)methyl)dodecan-1-amine or **compound 4**. Crude product was purified by column chromatography with 49% yield.

Compound 5 *[N,N-bis((pyridin-2-yl)methyl) dodecan-1-amine]*

Compound 5 was synthesized from compound 3 by refluxing it with 1.2 equivalent of 1-chloromethyl (pyridine hydrochloride) in the presence of K_2CO_3 in CH_3CN for 48 hours. Crude product was purified by column chromatography with 59% yield.

Compound 6 *[N,N-bis((methylpyridinium-2-yl)methyl) dodecan-1-amine]*

Compound 6 was synthesized from **compound 5** by refluxing it with 3 equivalent of methyl iodide. The crude product was purified with column chromatography with 23% yield.

A2.2 Characterization of Amphiphiles

A2.2.1.Characterization of Compound 3

^{1}H NMR [400 MHz, $CDCl_3$, δ (ppm)]: 8.553 (1H, d, J=0.013), 7.640 (1H, t, J=0.020), 7.305 (1H, d, J=0.020), 7.158 (1H, t, J=0.013), 3.906 (2H, s), 2.651 (2H, t, J=0.019), 1.255 (20H, m), 0.0879 (3H, t, J=0.017), ^{13}C NMR [100 MHz, $CDCl_3$, $SiMe_4$, δ (ppm)]: 159.826, 149.294, 136.841, 122.379, 121.952, 55.258, 49.729, 31.974, 30.121, 29.686, 29.625, 29.404, 27.413, 22.738 14.158. ESI-MS (positive mode, m/z). Calcd for $C_{18}H_{33}N_2$: 276.26. Found: 277.26 ($M + H^+$).

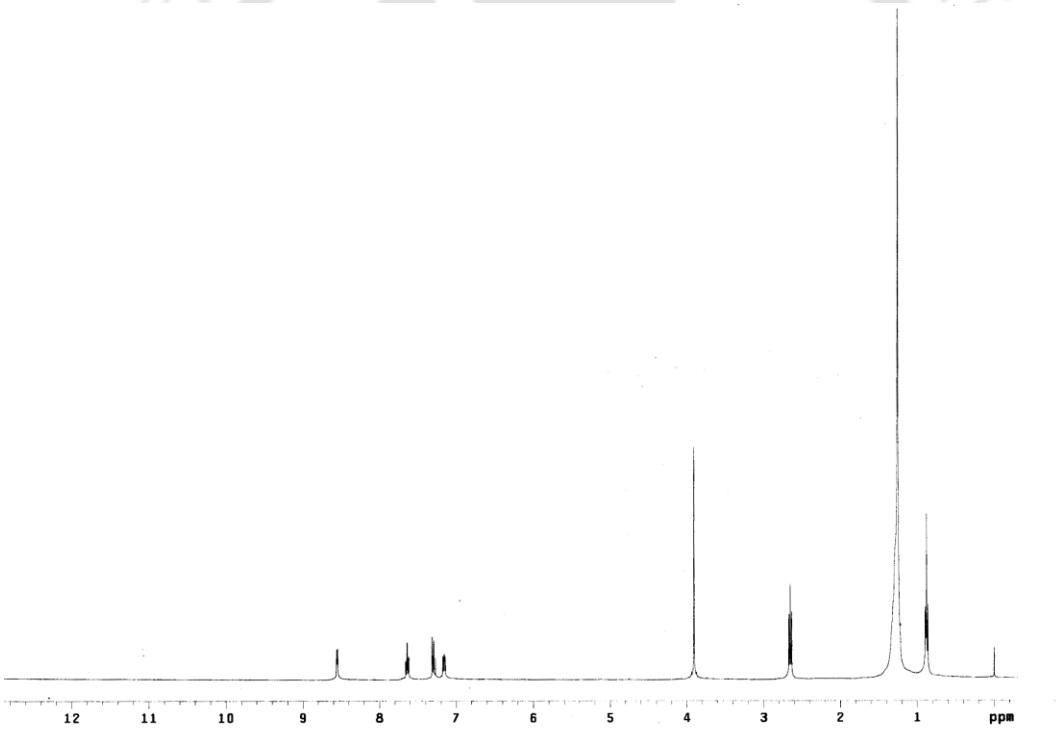

Figure A2.1. ^{1}H NMR spectra of **compound 3** in $CDCl_3$ solution.

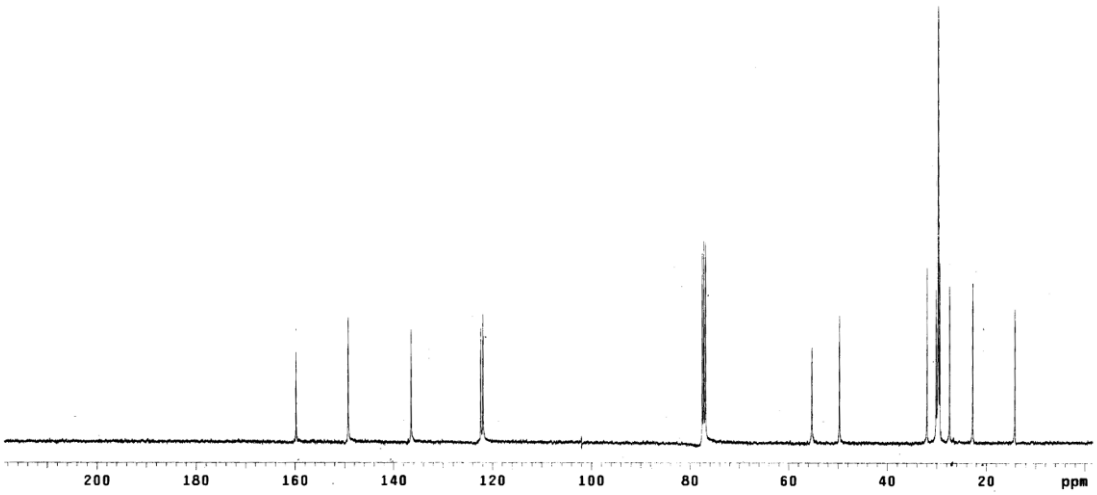

Figure A2.2. ^{13}C NMR spectra of **compound 3** in $CDCl_3$ solution.

A2.2.2. Characterization of Compound 4

^{1}H NMR [400 MHz, DMSO-d_6, δ (ppm)]: 9.077 (1H, d, J=0.014), 8.739 (1H, t, J=0.020), 8.551 (1H, d, J=0.020), 8.152 (1H, t, J=0.017), 6.813 (3H, s), 5.458 (2H, s), 4.869 (2H, t, J=0.011), 4.381-4.544 (20H, m), 2.781 (3H, t, J=0.014), ^{13}C NMR [100 MHz, $CDCl_3$, $SiMe_4$, δ (ppm)]: 149.385, 148.714, 148043,147.723, 146.579, 51.185, 40.744, 31.356, 29.068, 28.786, 26.148, 25.644, 23.707, 22.128, 13.601. ESI-MS (neutral mode, m/z). Calcd for $C_{19}H_{36}IN_2$: 418.18. Found: 418.18.

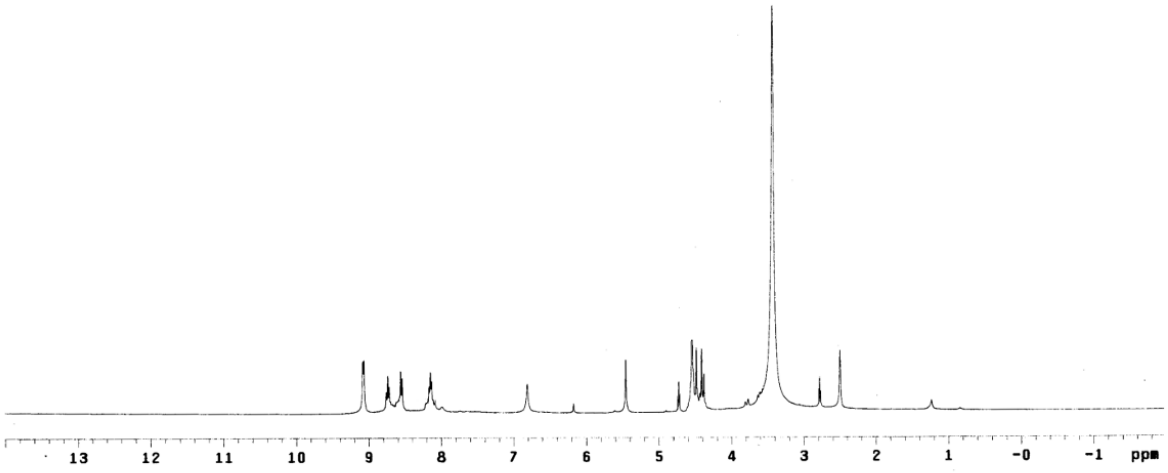

Figure A2.3. ^{1}H NMR spectra of **compound 4** in DMSO-d_6 solution.

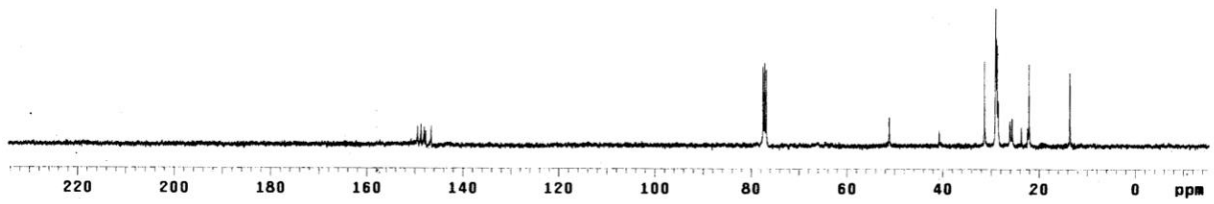

Figure A2.4. ^{13}C NMR spectra of **compound 4** in $CDCl_3$ solution.

A2.2.3. Characterization of Compound 5

^{1}H NMR [400 MHz, $CDCl_3$, δ (ppm)]: 8.512 (2H, d, J=0.013), 7.646 (2H, t, J=0.019), 7.305 (2H, d, J=0.020), 7.13 (2H, t, J=0.015), 3.807 (4H, s), 2.529 (2H, d, J=0.019), 1.235 (20H, broad multiplate), 0.0878 (3H, t, J=0.018), ^{13}C NMR [100 MHz, $CDCl_3$, $SiMe_4$, δ (ppm)]: 160.184, 148.905, 136.344, 122.860, 121.838, 60.528, 54.549, 31.943, 29.655, 29.503, 29.373, 27.345, 27.108, 22.715, 14.151. ESI-MS (positive mode, m/z). Calcd for $C_{24}H_{37}N_3$: 367.2987. Found: 368.3066 ($M + H^+$).

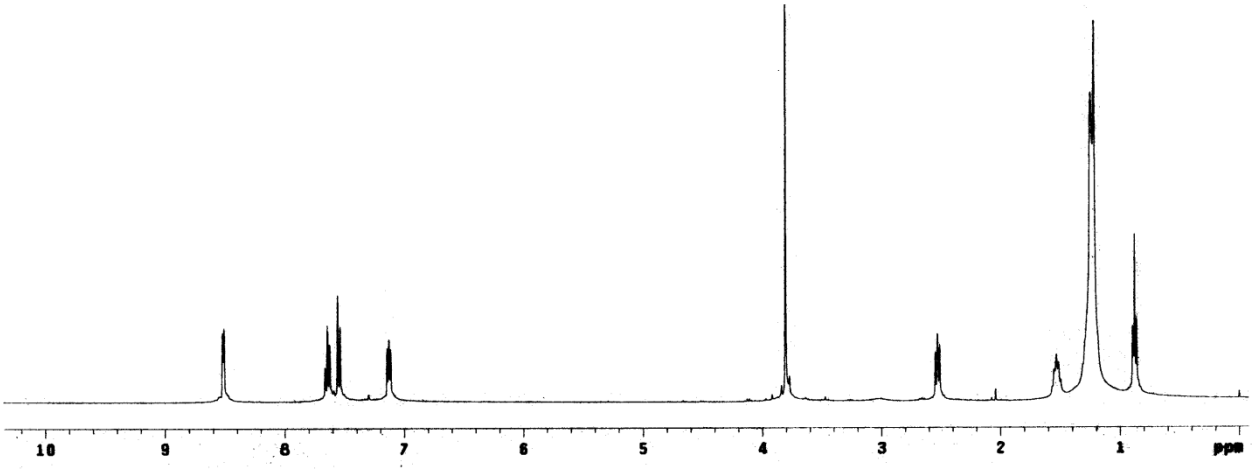

Figure A2.5. ^{1}H NMR spectra of **compound 5** in $CDCl_3$ solution.

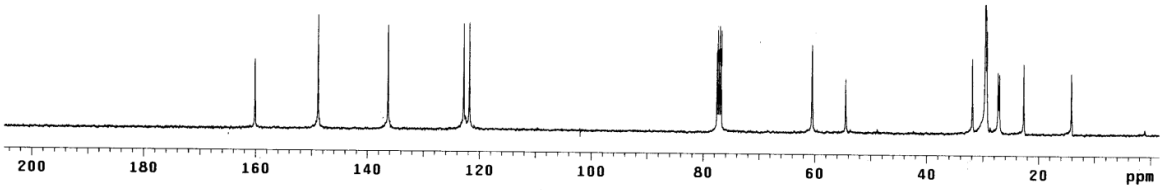

Figure A2.6. ^{13}C NMR spectra of **compound 5** in $CDCl_3$ solution.

*A2.2.4. Characterization of **Compound 6***

^{1}H NMR [400 MHz, DMSO-d_6, δ (ppm)]: 8.686 (2H, t, J=0.011), 8.604 (2H, t, J=0.020), 8.355 (2H, d, J=0.020), 8.232 (2H, d, J=0.009), 6.665 (6H, s), 5.690 (4H, s), 4.238-4.496 (22H, m), 2.788 (3H, t, J=0.015), ^{13}C NMR [100 MHz, $CDCl_3$, $SiMe_4$, δ (ppm)]: 157.719, 154.135, 146.744, 145.822, 144.838, 78.983, 65.888, 46.730, 46.471, 45.891, 37.288, 28.907. ESI-MS (positive mode, m/z). Calcd for $C_{26}H_{43}I_2N_3$: 651.15. Found: 325.58 (M/2)

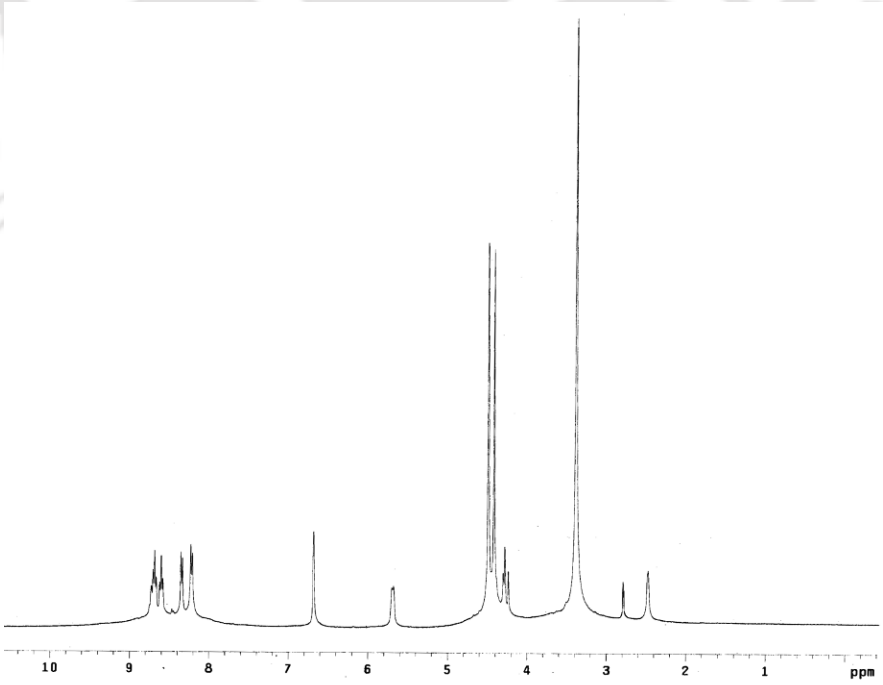

Figure A2.7. ^{1}H NMR spectra of **Compound 6** in DMSO-d_6 solution.

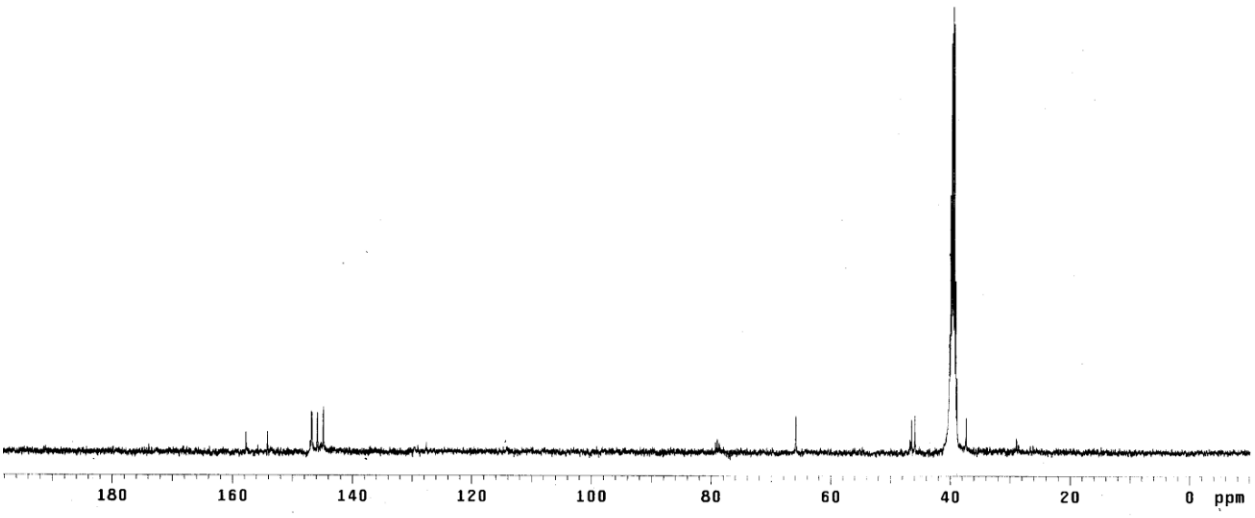

Figure A2.8. ^{13}C NMR spectra of **Compound 6** in $CDCl_3$ solution.

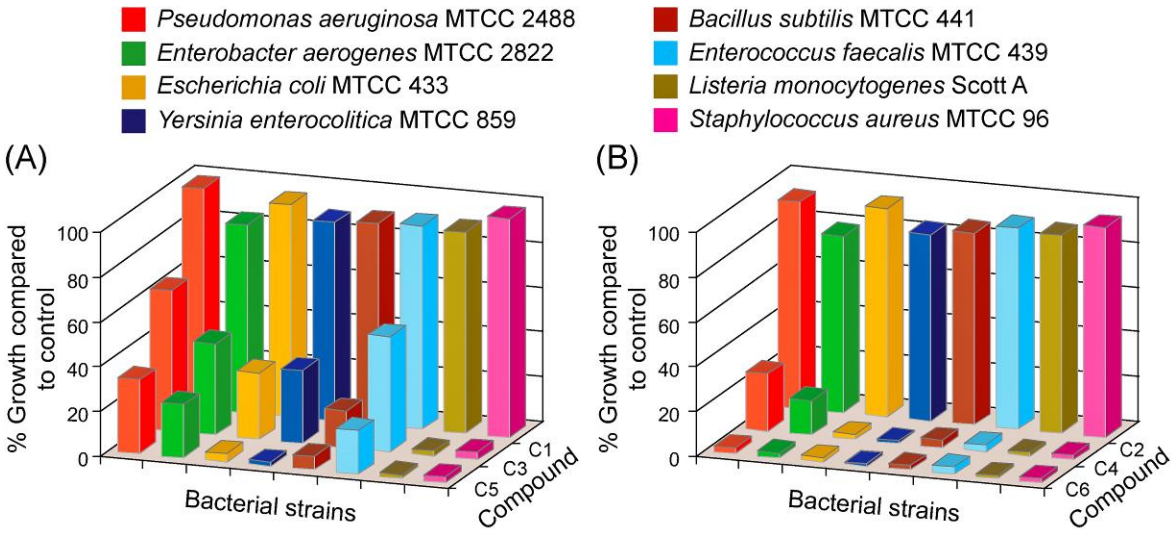

Figure A2.9. Antimicrobial activity of (a) neutral **(compound 1, 3 and 5)** and (b) charged amphiphiles **(compound 2, 4 and 6)** against pathogenic bacterial strains. Bacterial cells were treated with 50 mg mL^{-1} of amphiphile for 6 h.

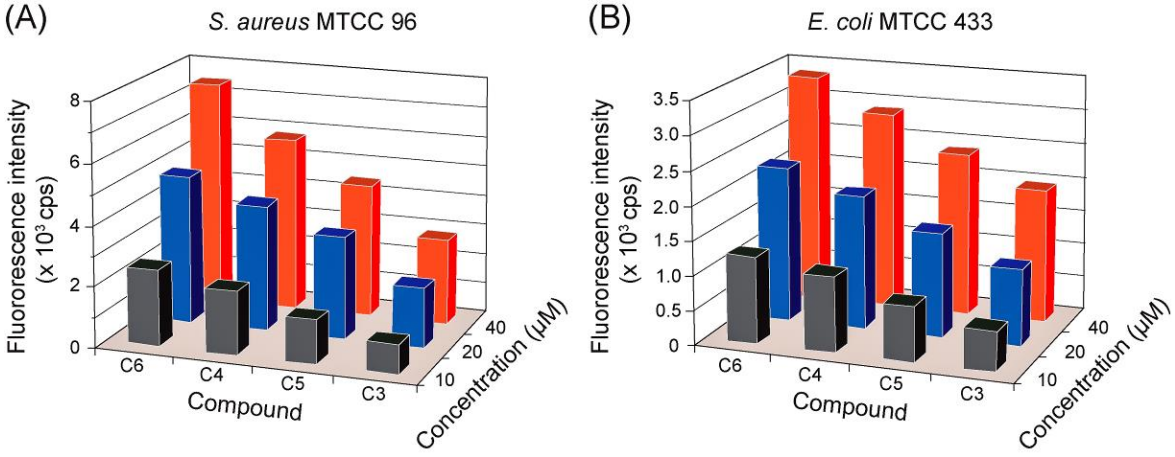

Figure A2.10. Assessment of membrane damage in amphiphile-treated bacteria by PI uptake assay.

Appendix

Table A2.1. Calculated hydrophobicity (LogP value) of neutral amphiphiles.

Synthetic Amphiphile	Hydrophobicity* (LogP value)
C5	5.16
C3	4.37
C1	2.94

* Hydrophobicity of the amphiphiles was calculated using the software jlopP Version 1.1(Brian White, 2004) (http://www.vls3d.com/JME_EditorOK.dir/run_jlogp.html)

Table A2.2. MIC and MKC of antibacterial amphiphiles.

Synthetic Amphiphile	*S. aureus* MTCC 96		*L. monocytogenes* Scott A		*E .coli* MTCC 433		*E. aerogenes* MTCC 2822	
	MIC (µM/ µg/mL)	MKC (µM/ µg/mL)	MIC (µM/ µg/mL)	MKC (µM/ µg/mL)	MIC (µM/ µg/mL)	MKC (µM/ µg/mL)	MIC (µM/ µg/mL)	MKC (µM/ µg/mL)
C3	40 / 26	100 / 65	40 /26	100 / 65	128 / 83.3	200 / 130	160 / 104	>200 / 130
C4	20 / 13	50 / 32.5	20 / 13	50 / 32.5	80 / 52	160 / 104	100 / 65	160 / 104
C5	25 / 16.2	64 / 41.7	25 / 16.2	64 / 41.7	100 / 65	160 / 104	128 / 83.3	160 / 104
C6	16 / 10.4	40 / 26	16 / 10.4	40 / 26	64 / 41.7	160 / 104	80 / 52	128 / 83.3

Table A2.3. Comparative cytotoxic effect exerted by the bactericidal amphiphiles on human cell lines HeLa, MCF-7 and HT-29.

Sl. No.	Comparison Group	Significant difference in % cell viability measured by MTT assay*	Concentration of amphiphiles in MTT assay
1.	**C6** versus **C5**	No	Equivalent to 2X MIC and 3X MIC of *S. aureus* MTCC 96
2.	**C6** versus **C4**	Yes	
3.	**C6** versus **C3**	Yes	
4.	**C5** versus **C4**	Yes	
5.	**C5** versus **C3**	Yes	
6.	**C4** versus **C3**	No	

* Significant difference implies *p* value < 0.001 based on analysis of variance (ANOVA) followed by all pair wise multiple comparisons (Holm-Sidak method) of % cell viability obtained in MTT assay.

Table A2.4. Comparative cytotoxic effect exerted by equimolar concentrations of bactericidal amphiphiles on human cell lines HeLa, MCF-7 and HT-29.

Sl. No.	Comparison Group	Significant difference in % cell viability measured by MTT assay*	Concentration of amphiphiles in MTT assay
1.	**C6** versus **C5**	Yes	40 µM and 60 µM
2.	**C6** versus **C4**	Yes	
3.	**C6** versus **C3**	Yes	
4.	**C5** versus **C4**	Yes	
5.	**C5** versus **C3**	Yes	
6.	**C4** versus **C3**	Yes	

* Significant difference implies *p* value < 0.001 based on analysis of variance (ANOVA) followed by all pair wise multiple comparisons (Holm-Sidak method) of % cell viability obtained in MTT assay.

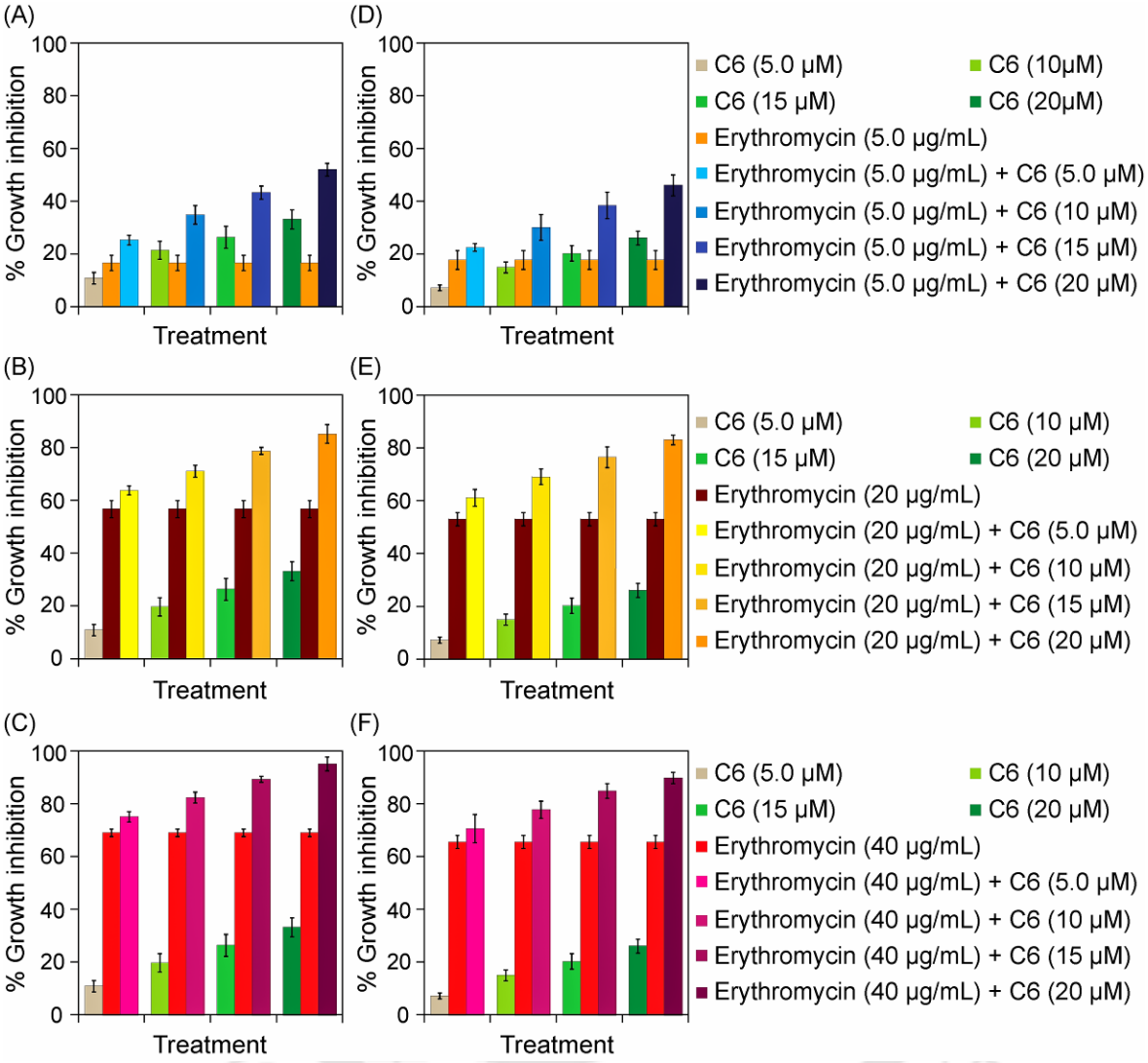

Figure A3.1. Effect of combined treatment of **C6** and erythromycin on the growth of (A, B and C) *E. coli* MTCC 433 and (D, E and F) *E. aerogenes* MTCC 2488.

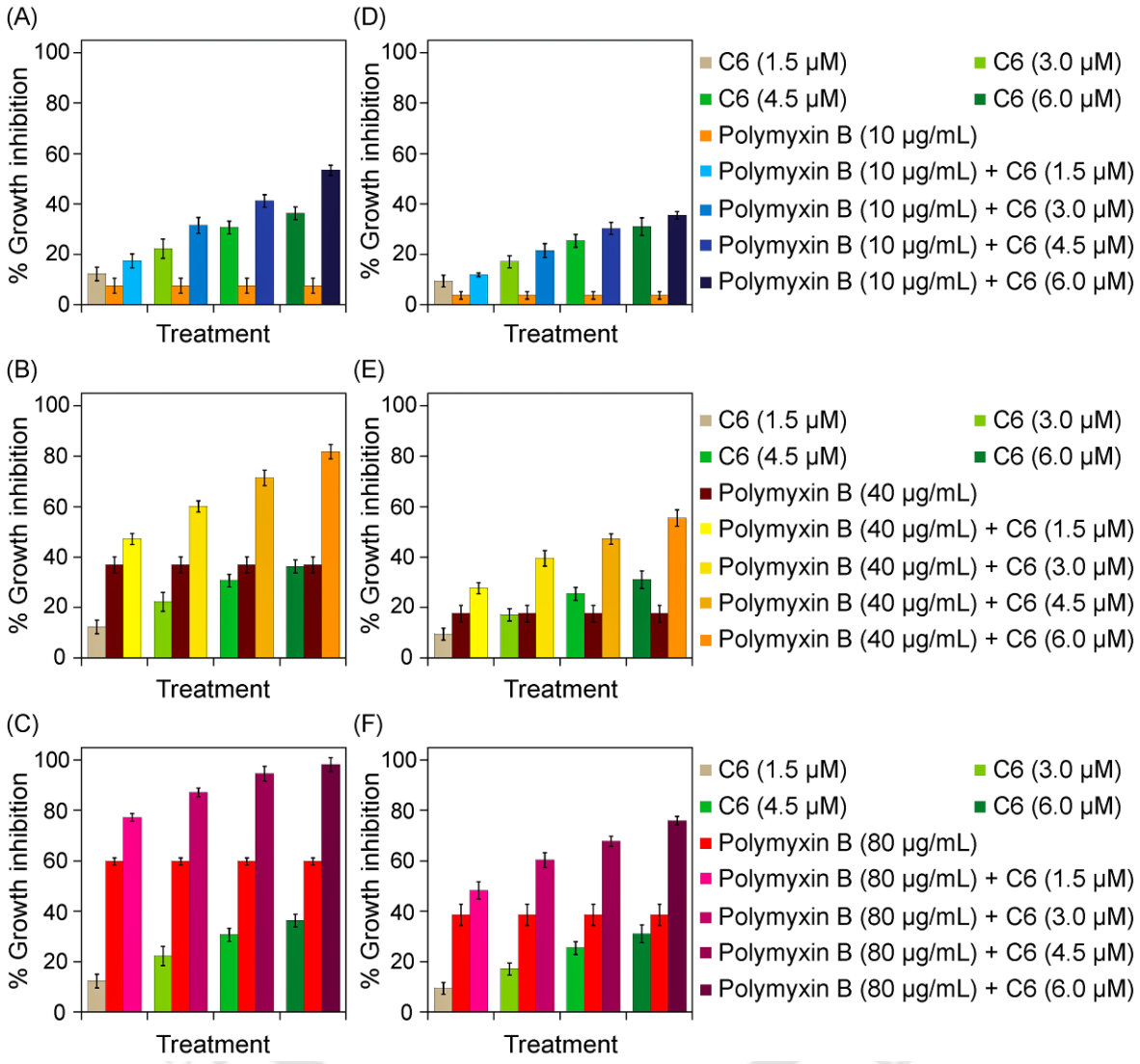

Figure A3.2. Effect of combined treatment of **C6** and polymyxin B on the growth of (A, B and C) *S. aureus* MTCC 96 and (D, E and F) *L. monocytogenes* Scott A.

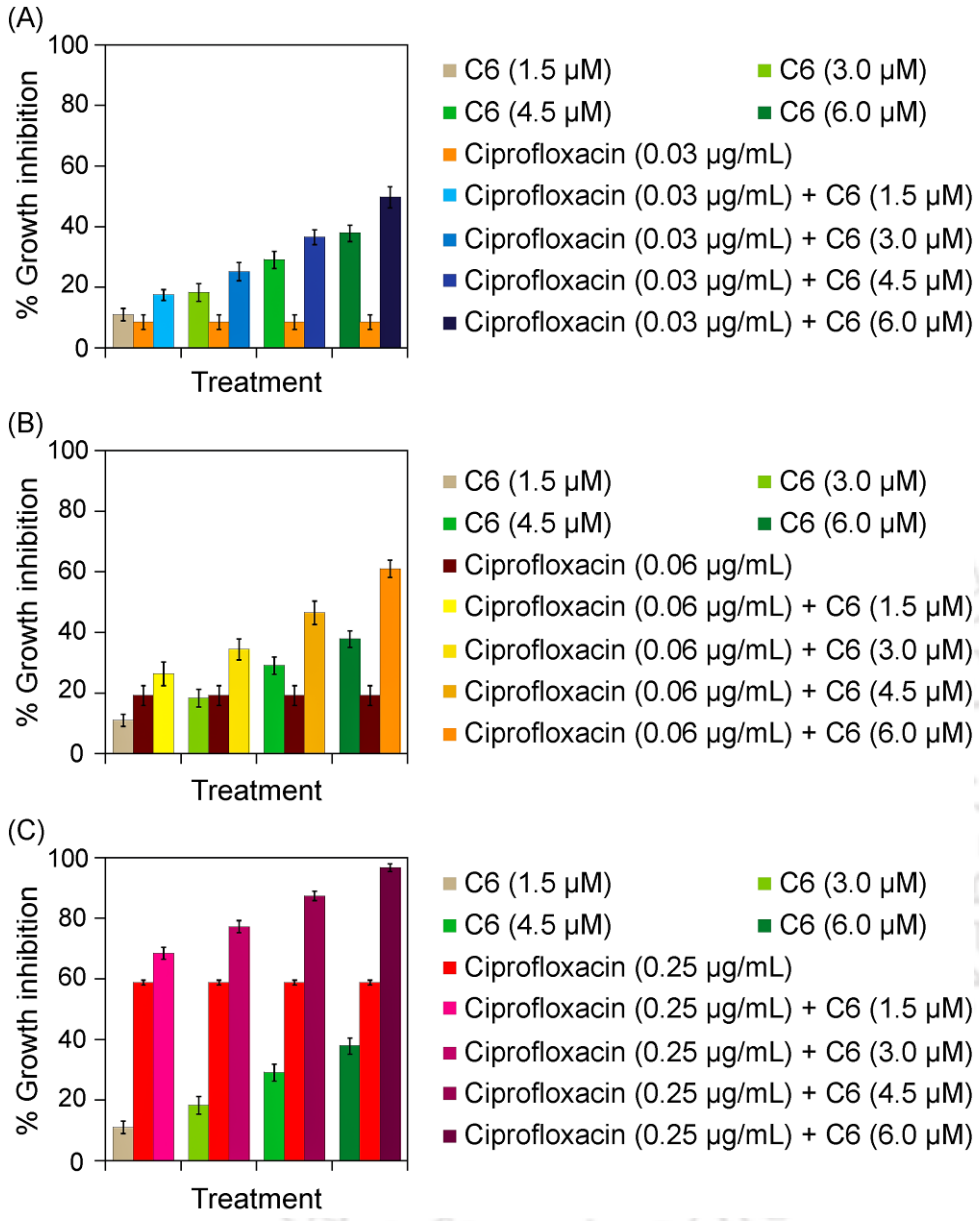

Figure A3.3. Effect of combined treatment of **C6** and ciprofloxacin on the growth of *S. aureus* MTCC 96.

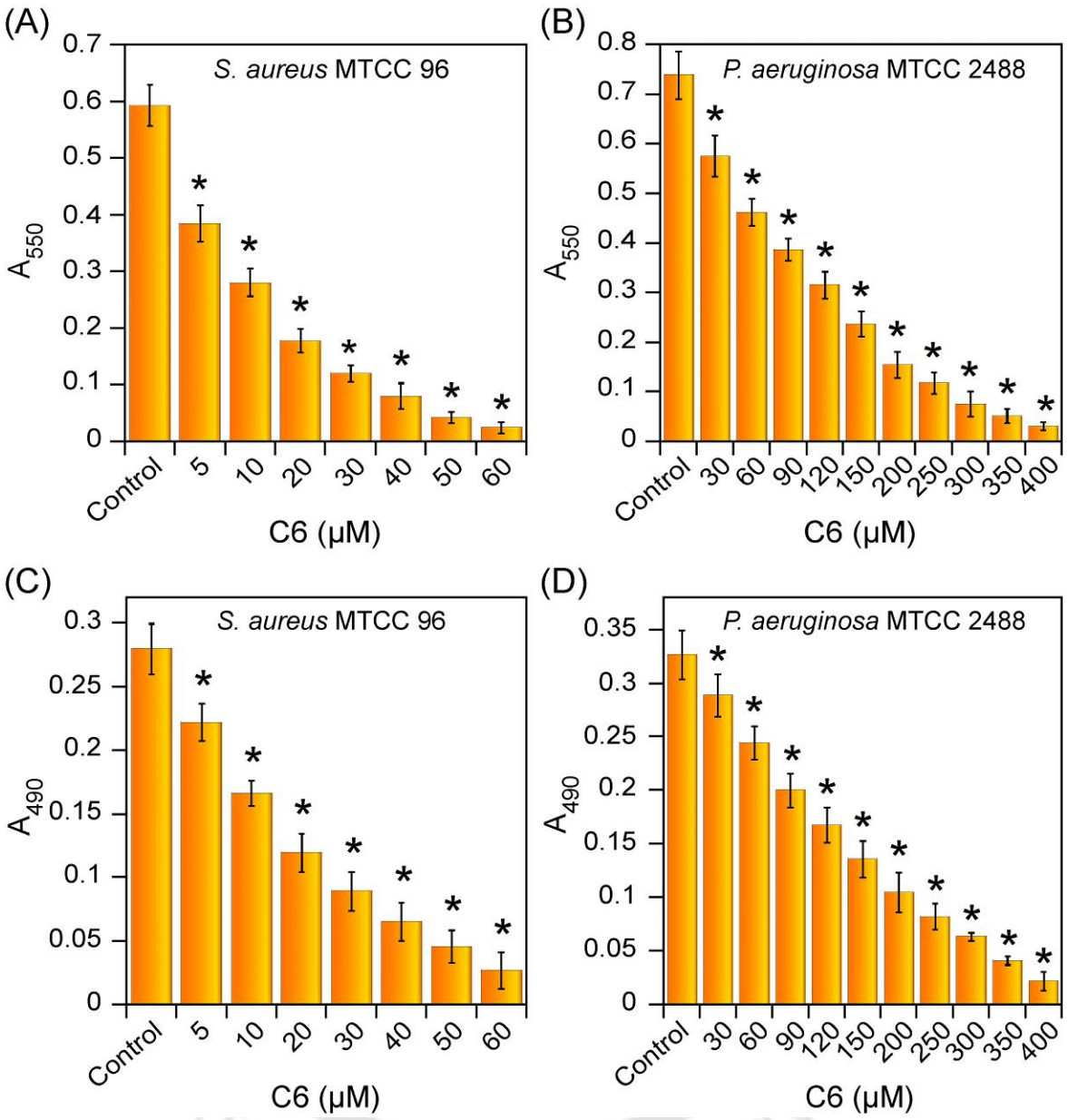

Figure A4.1. MTT assay to estimate the viability of (A) *S. aureus* MTCC 96 biofilm and (B) *P. aeruginosa* MTCC 2488 biofilm upon treatment with **C6**. Congo red binding assay for estimation of matrix formation in (C) *S. aureus* MTCC 96 biofilm and (D) *P. aeruginosa* MTCC 2488 biofilm upon treatment with **C6**. Statistically significant values derived by ANOVA are indicated by asterisk marks. * indicates p value < 0.001.

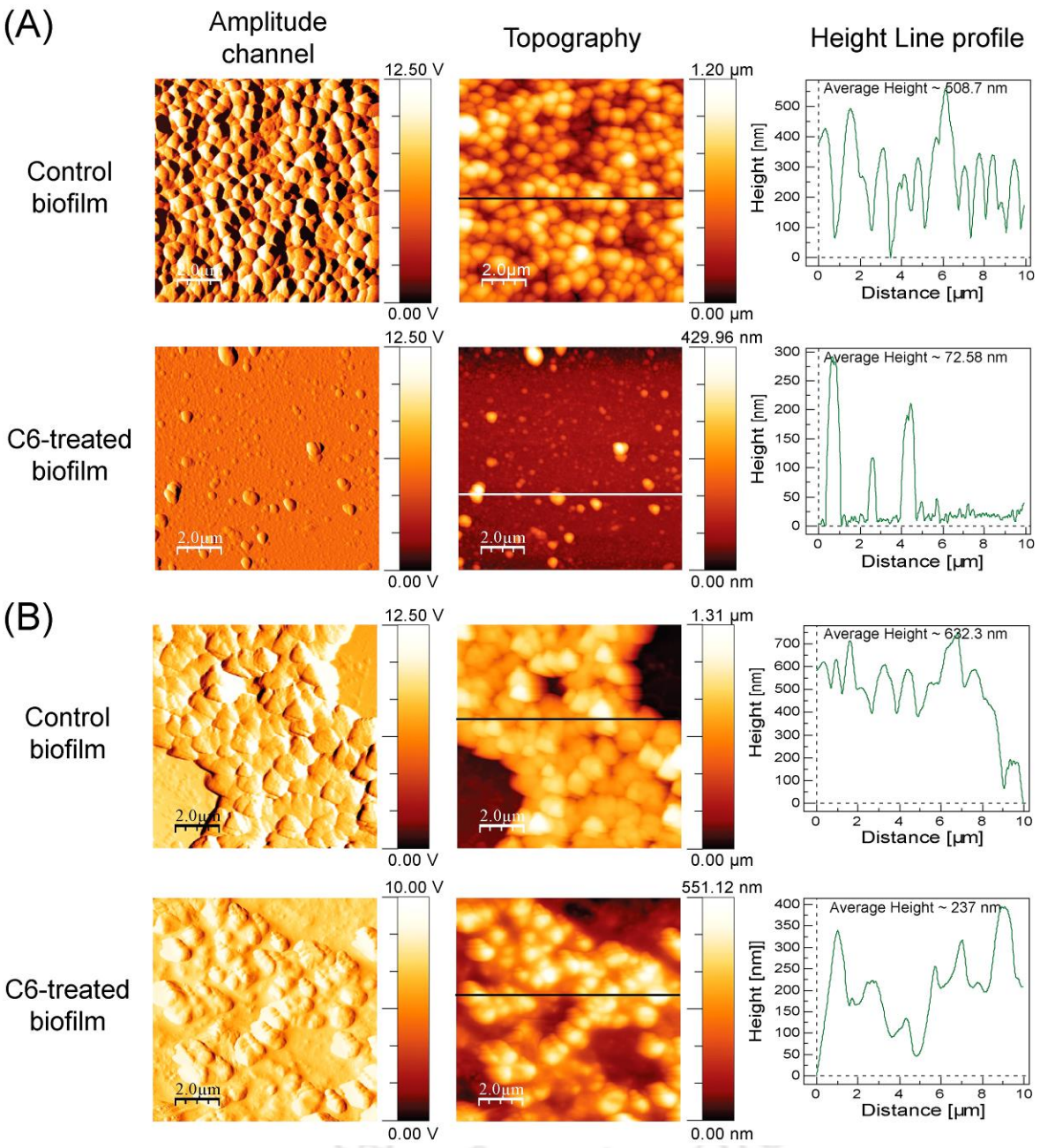

Figure A4.2. AFM analysis indicating amplitude channel, two-dimensional topographic images and height line profile obtained for (A) *S. aureus* MTCC 96 biofilm and (B) *P. aeruginosa* MTCC 2488 biofilm. In case of treated samples, *S. aureus* MTCC 96 biofilm was treated with 30 µM **C6** and *P. aeruginosa* MTCC 2488 biofilm was treated with 200 µM **C6**. All images are shown for an area of 10 µm x 10 µm.

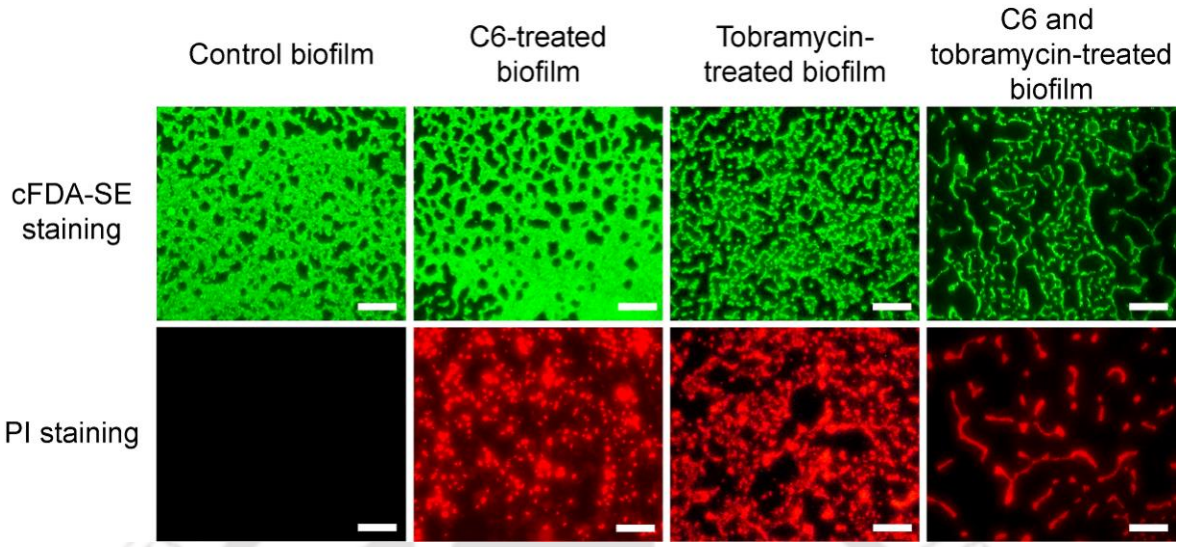

Figure A4.3. Representative fluorescence microscopic images of cFDA-SE and PI labeled *P. aeruginosa* MTCC 2488 biofilm treated with 30 μM **C6**, 0.08 μg/mL tobramycin, and 30 μM **C6** in combination with 0.08 μg/mL tobramycin. Scale bar for the images are 50 μm.

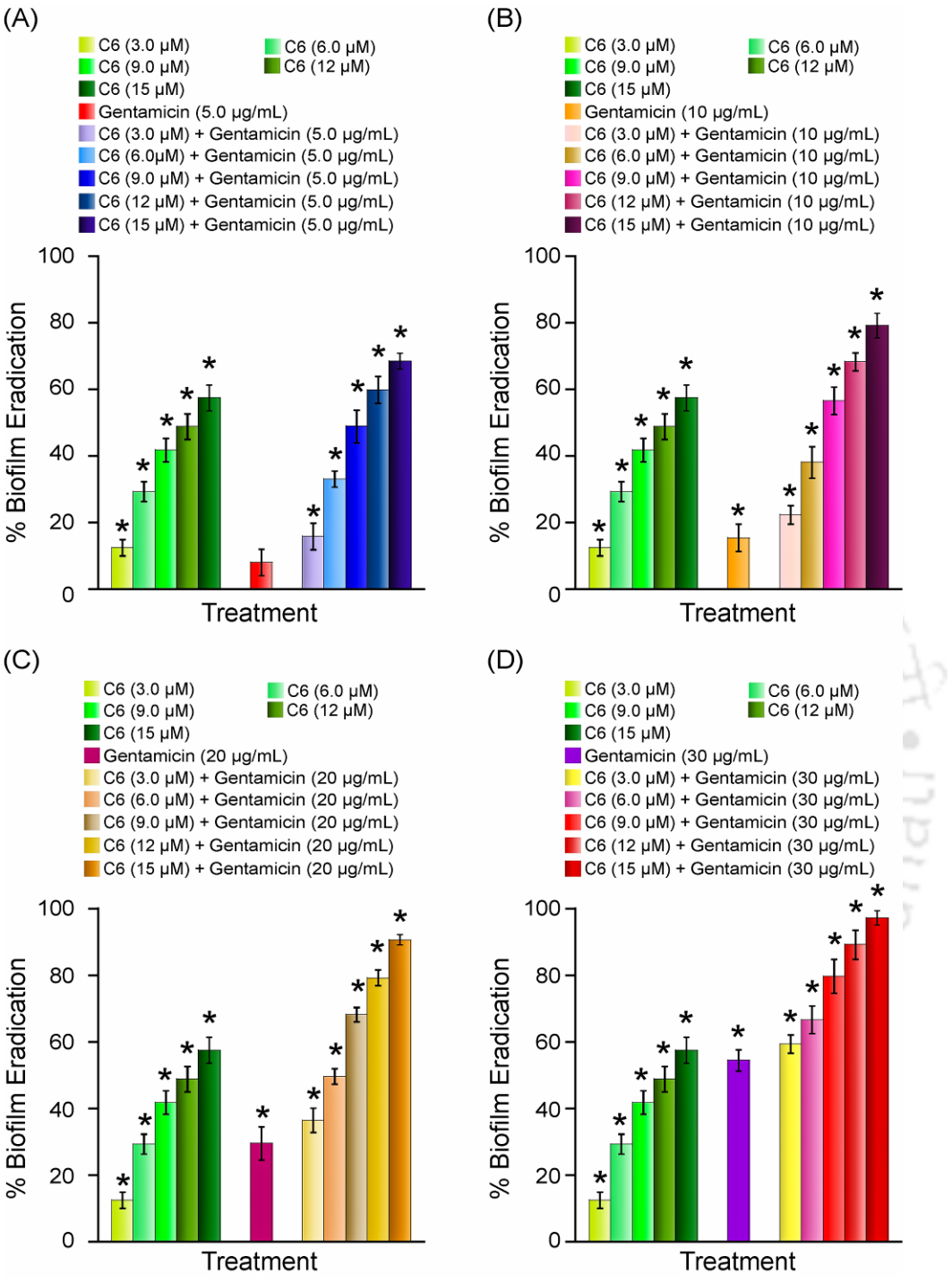

Figure A4.4. Effect of combined treatment of **C6** with (A) 5.0 µg/ml gentamicin, (B) 10 µg/ml gentamicin, (C) 20 µg/ml gentamicin and (D) 30 µg/ml gentamicin on *S. aureus* MTCC 96 biofilm measured by crystal violet assay. Statistically significant values derived by ANOVA are indicated by asterisk marks. * indicates *p* value < 0.001.

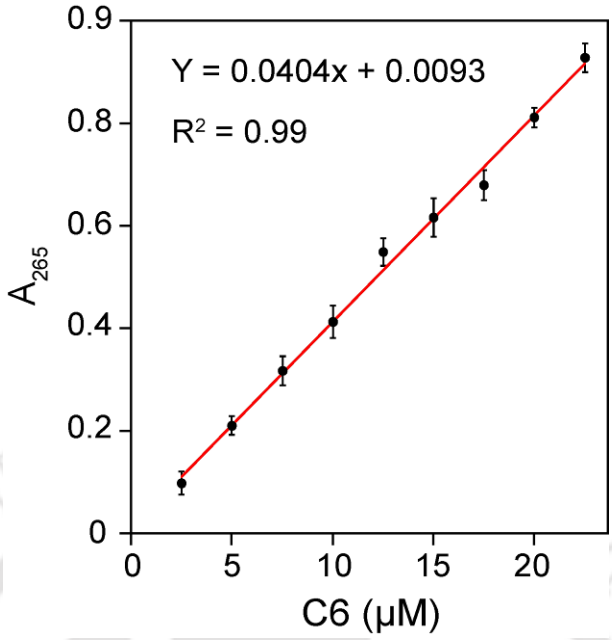

Figure A5.1. Calibration plot of absorbance versus concentration for **Compound 6**.

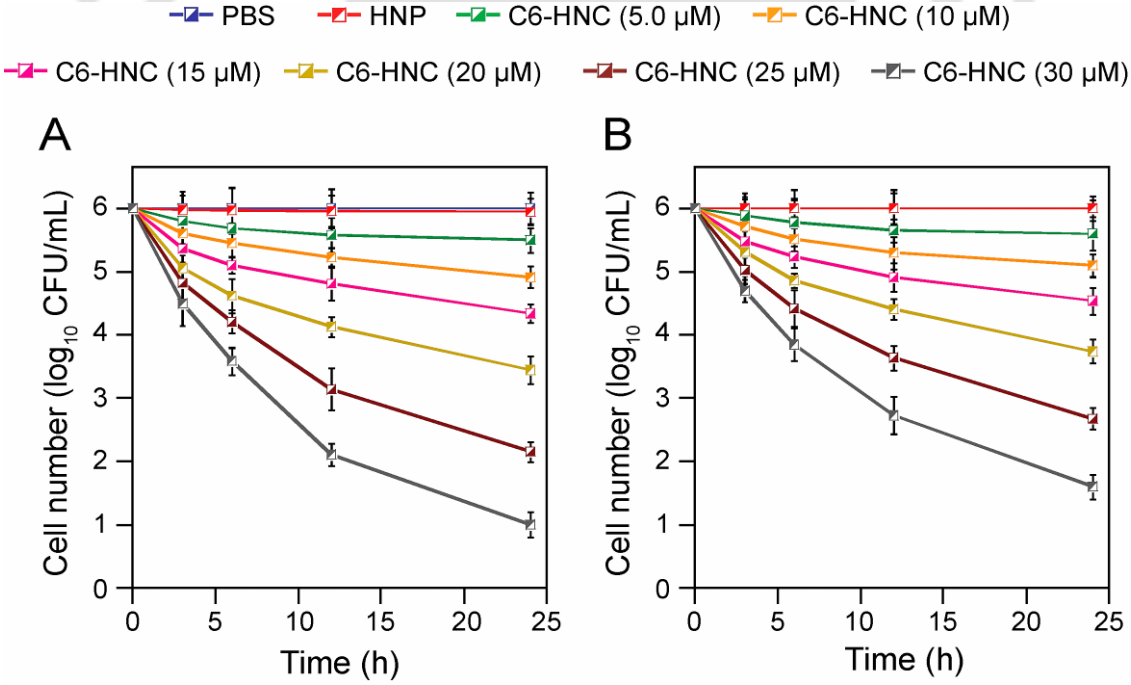

Figure A5.2. Time-kill curves for (A) *S. aureus* MTCC 96 and (B) *E.coli* MTCC 433 treated with **C6**-HNC bearing varying concentrations of **C6** (5.0 μM, 10 μM, 15 μM, 20 μM, 25 μM and 30 μM).

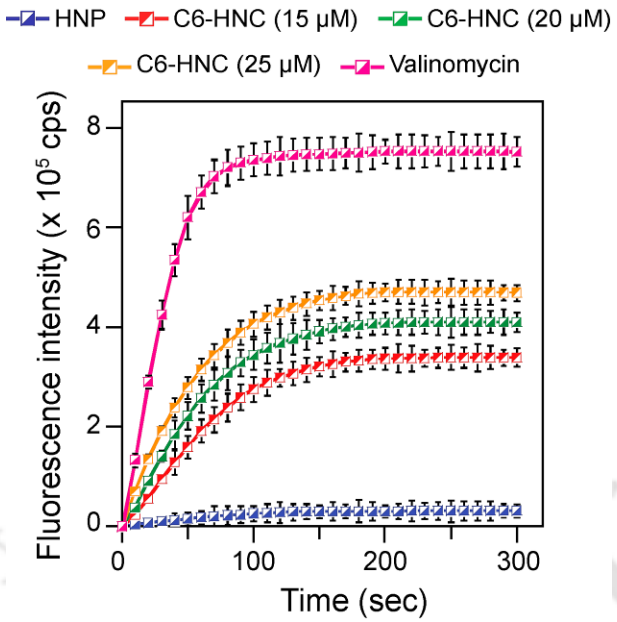

Figure A5.3. DiSC$_3$5-based membrane depolarization assay for *E. coli* MTCC 433 cells treated with **C6**-HNC representing varying concentrations of **C6** (15 μM, 20 μM and 25 μM). Cells treated with 30 μM valinomycin were used as positive control in the assay.

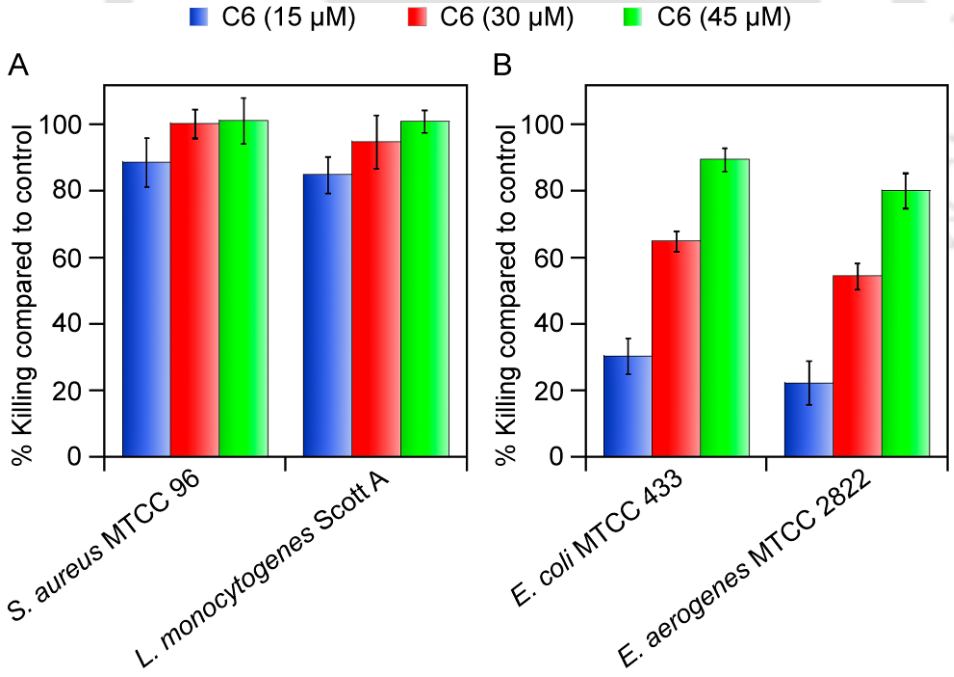

Figure A5.4. Antibacterial activity of **C6** against representative (A) Gram-positive bacteria and (B) Gram-negative bacteria following *in vitro* release from **C6**-HNC incubated in 10 mM HEPES buffer (pH 7.4). The concentration of released **C6** corresponds to 15 μM, 30 μM and 45 μM.

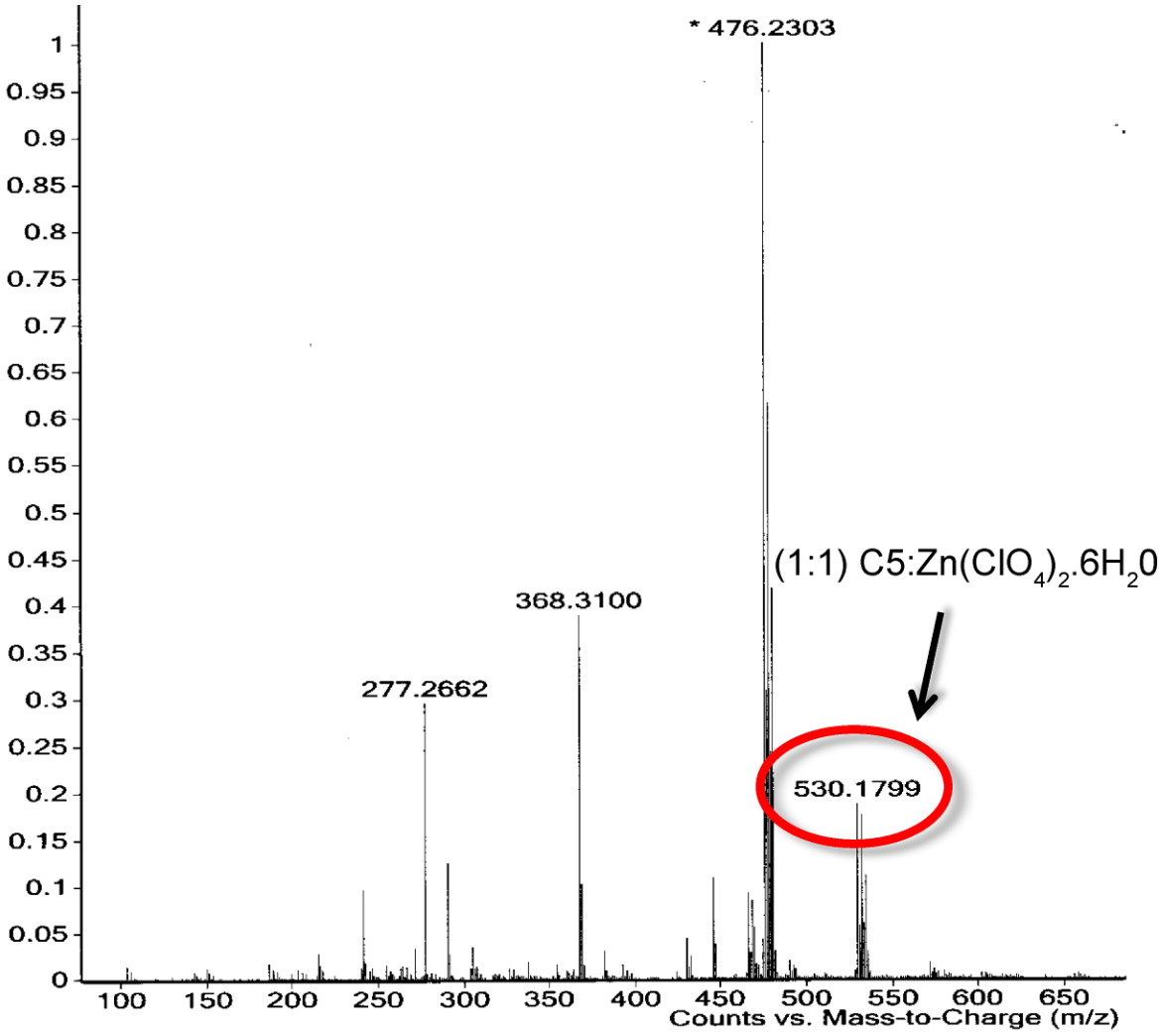

Figure A6.1. ESI-MS spectra of **C5**-zinc perchlorate complex.

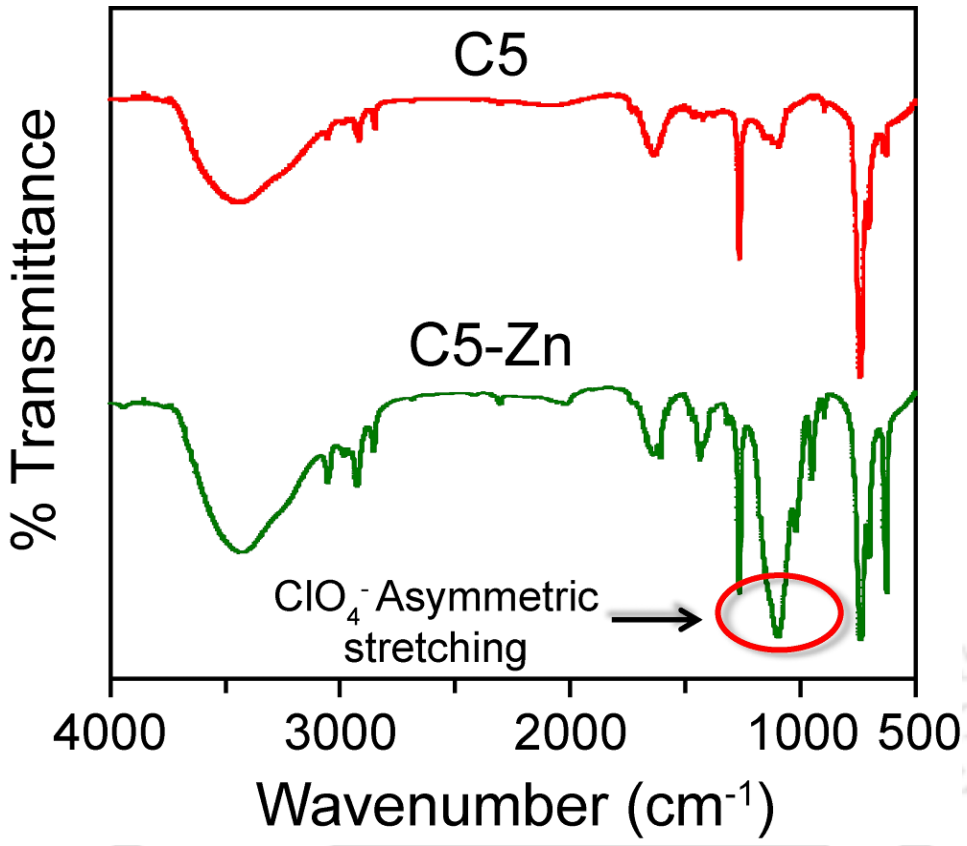

Figure A6.2. FTIR analysis of **C5**-Zn. The asymmetric stretching frequency of perchlorate at 1100 cm^{-1} indicates formation of **C5**-Zn complex.

Indian Institute of Technology Guwahati

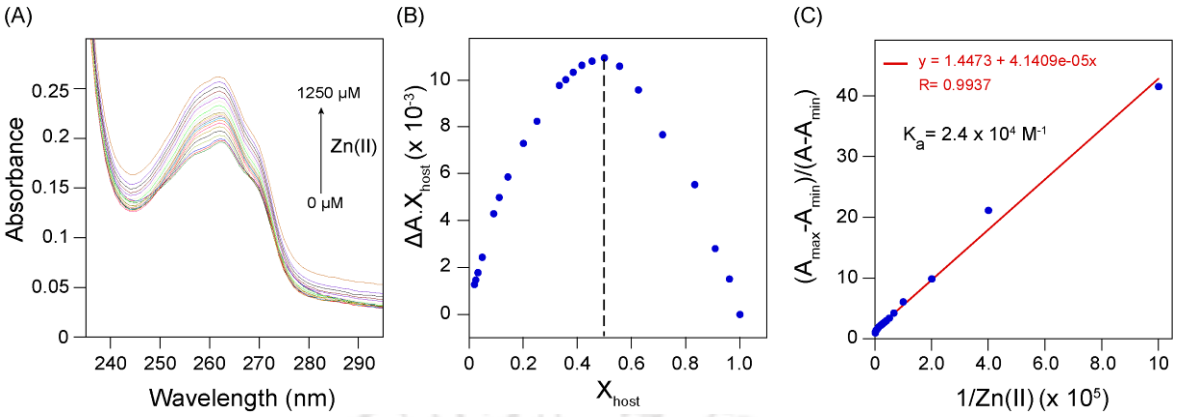

Figure A6.3. (A) Changes in absorption spectra of **C5** upon incremental addition of Zn(II). (B) Job's plot for **C5**-Zn complex formation derived from UV-visible titration experiment. (C) Bensei-Hildebrand plot obtained from UV-visible titration experiment.

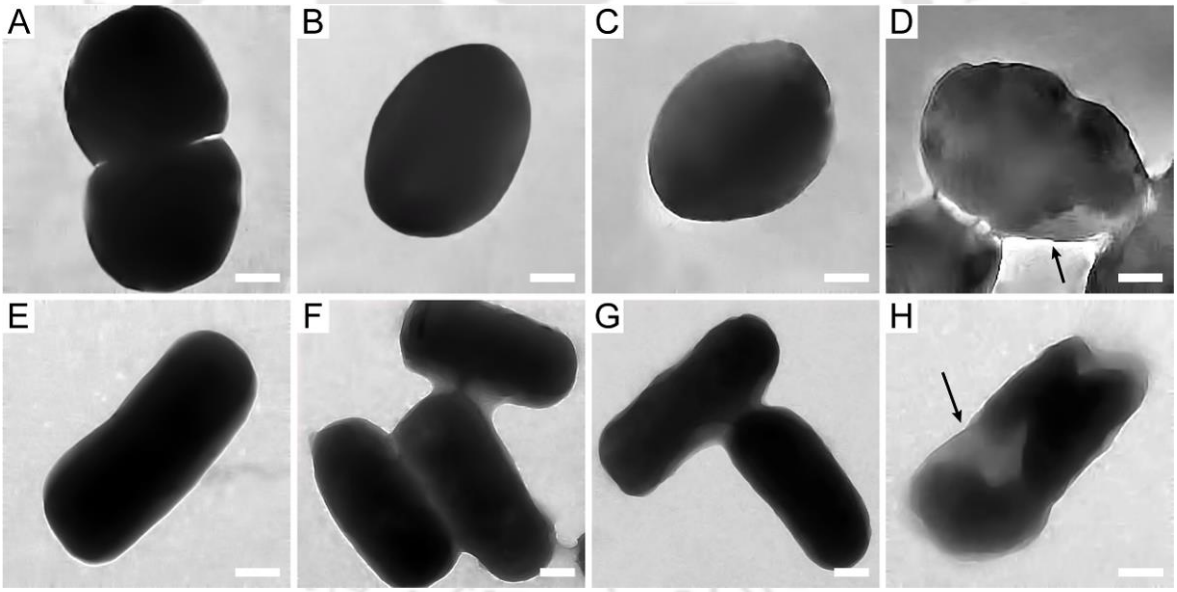

Figure A6.4. TEM images of (A-D) *S. aureus* MTCC 96 cells and (E-H) *E. coli* MTCC 433 cells. (A and E): untreated cells, (B and F): cells treated with Zn(II), (C and G): cells treated with **C5** and (D and H): cells treated with **C5**-Zn. Arrow in panels D and H indicate disintegration and loss of electron density in cells treated with **C5**-Zn. Scale bar for the images is 0.2 µm.

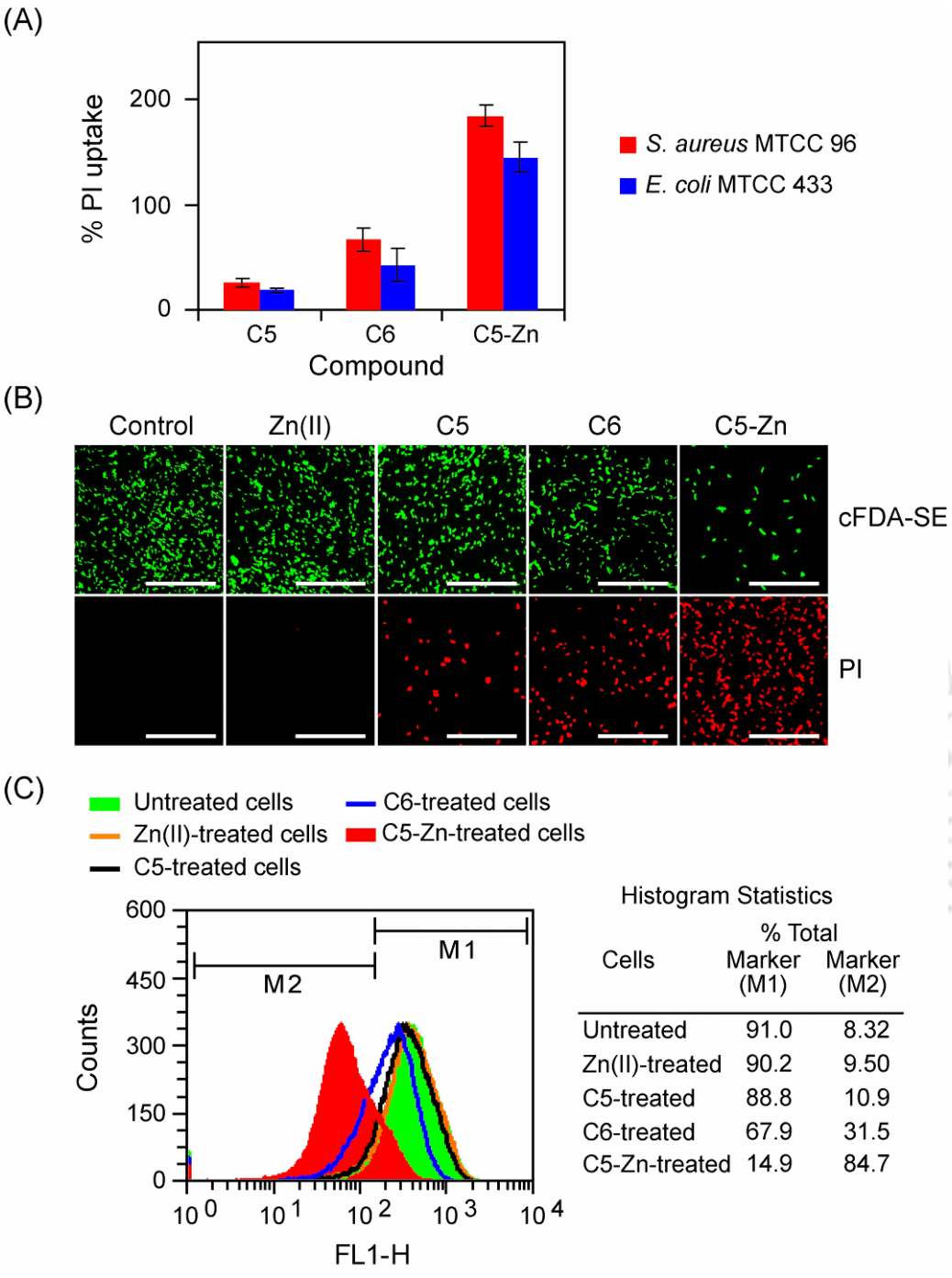

Figure A6.5. (A) PI uptake assay for target bacterial cells treated with amphiphiles (6.0 µM each for 6 h). (B) Fluorescence microscope analysis of *E. coli* MTCC 433 cells treated with Zn(II) and amphiphiles (6.0 µM each for 6 h). Scale bar for the images is 50 µm. (C) Flow cytometry analysis of cFDA-SE labelled cells of *E. coli* MTCC 433 treated with Zn(II) and the amphiphiles (6.0 µM each for 6 h).

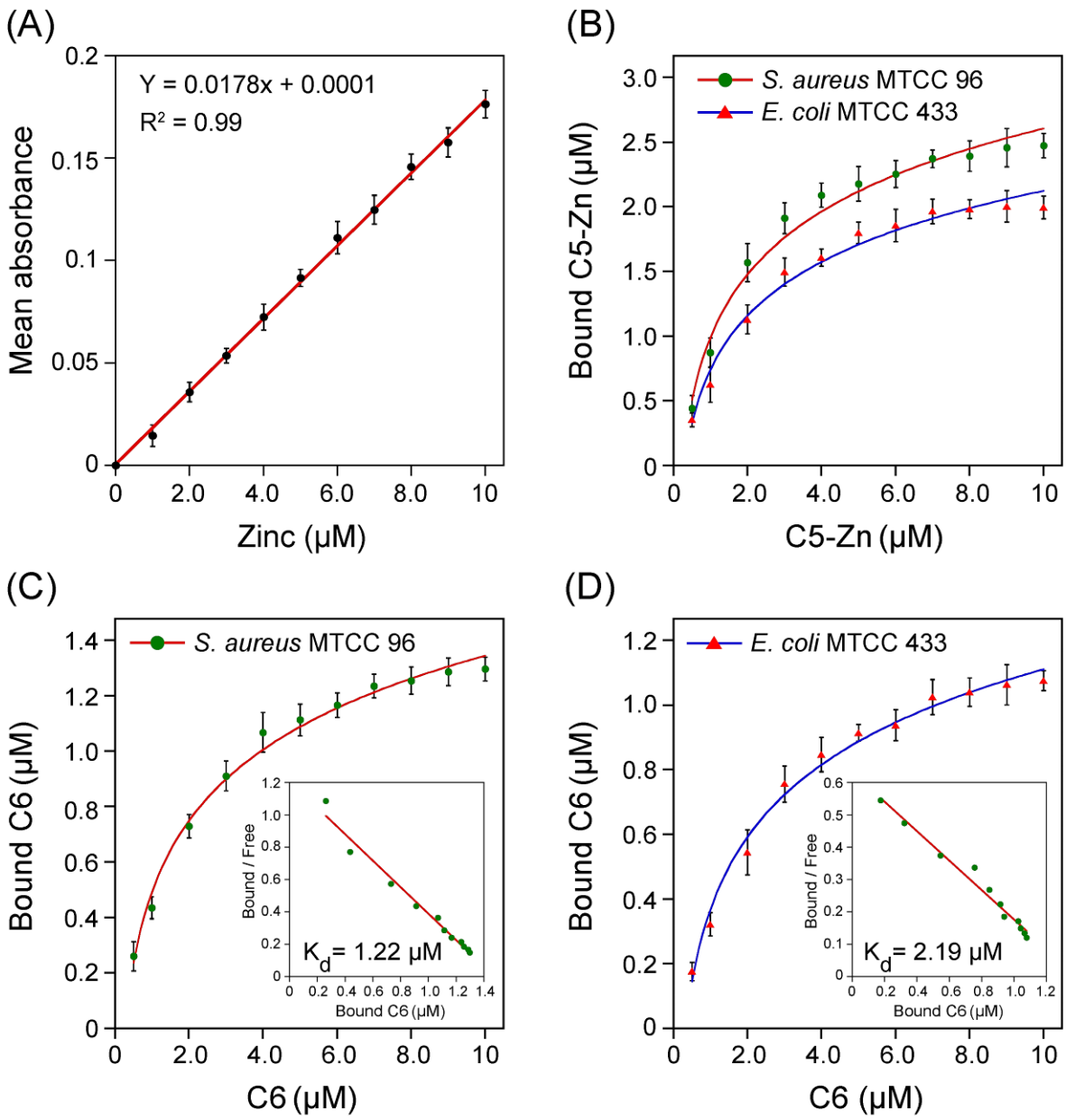

Figure A6.6. (A) Calibration plot of absorbance versus concentration for zinc measured by atomic absorption spectroscopy. (B) Concentration-dependent binding of **C5**-Zn on bacterial cells. (C-D) Concentration-dependent binding of **C6** on bacterial cells. Inset in (C) and (D) indicate Scatchard plot for determination of binding affinity of **C6**.

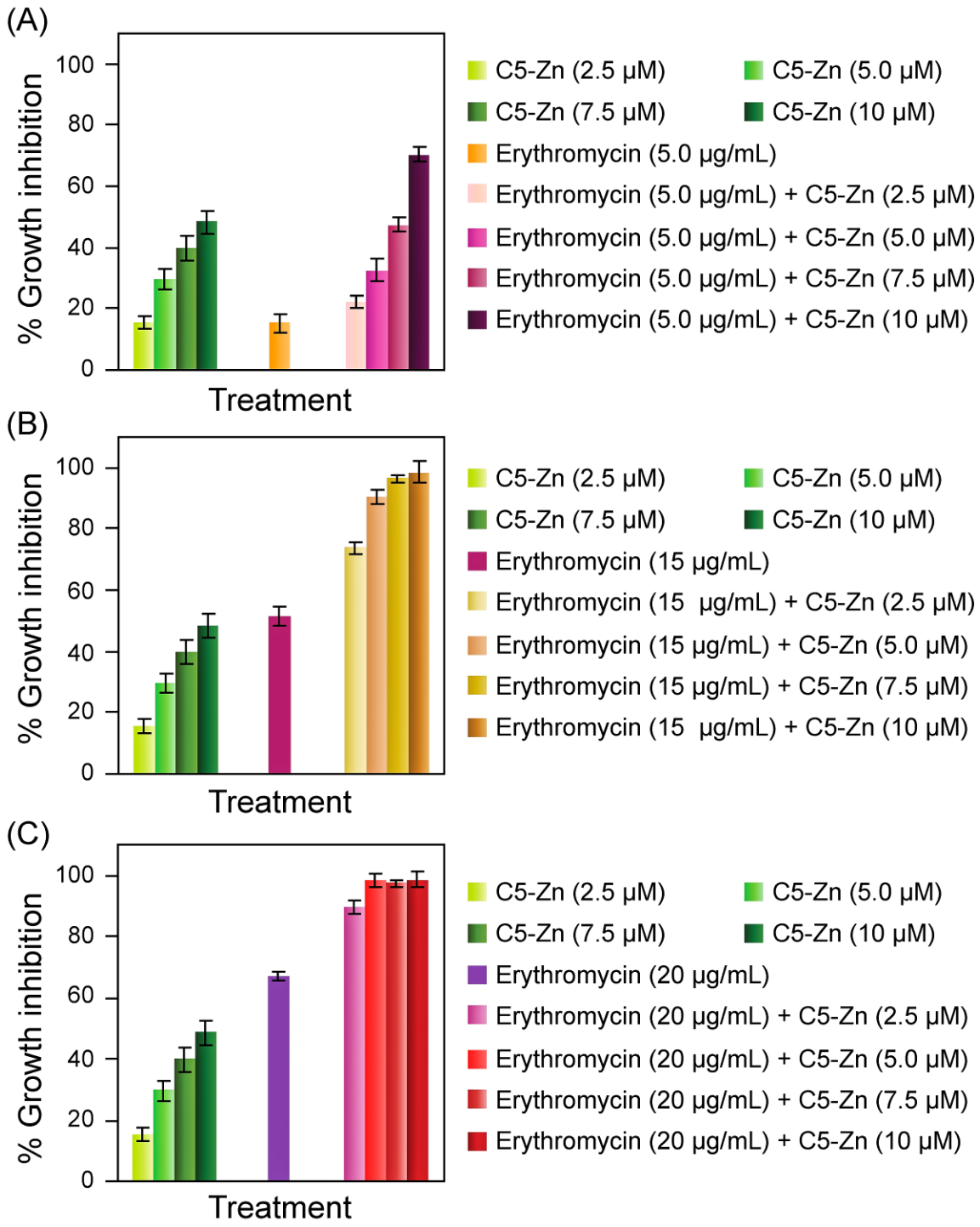

Figure A6.7. Effect of combined treatment of **C5**-Zn and erythromycin on the growth of *E. coli* MTCC 433.

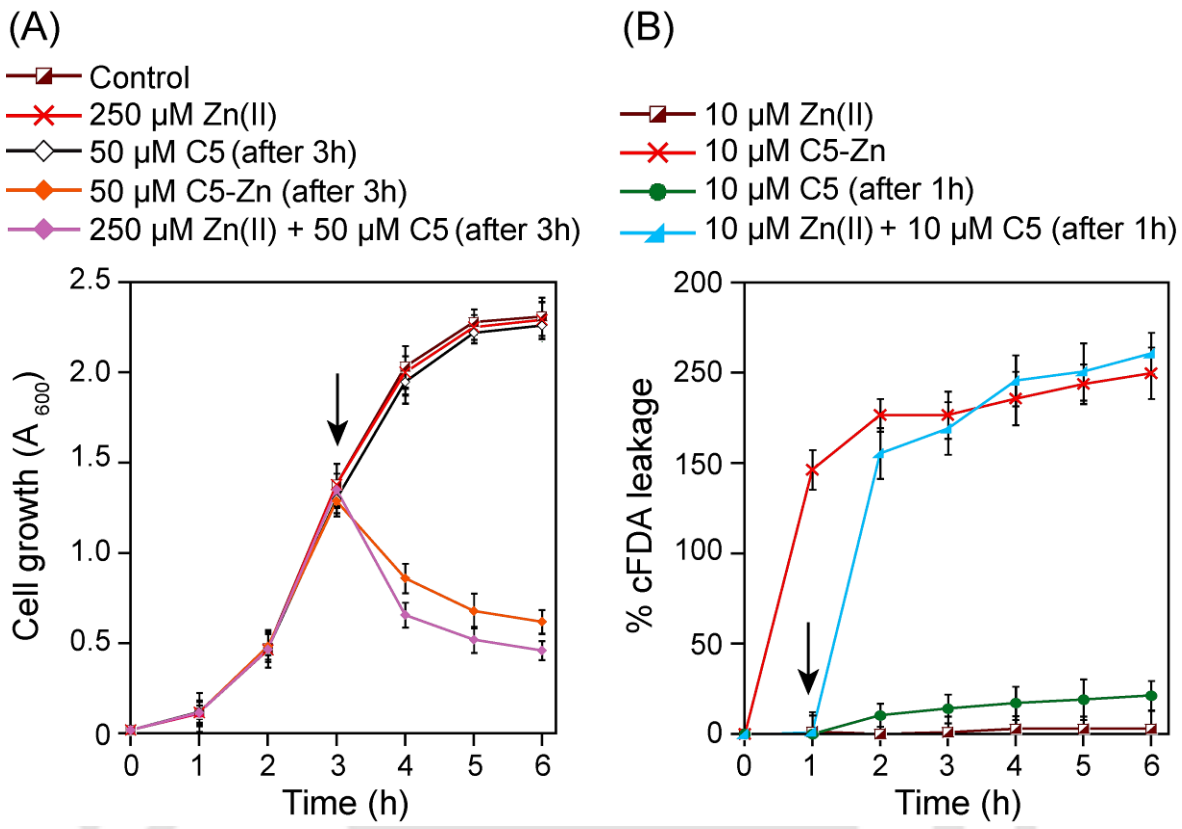

Figure A6.8. (A) Effect of addition of **C5** on *E. coli* MTCC 433 cells grown in presence of 250 μM Zn(II). (B) cFDA-Se leakage assay in *E. coli* MTCC 433 cells incubated in 5.0 mM HEPES buffer in presence of 10 μM Zn(II) followed by addition of **C5**. Arrow in (C) and (D) indicate the time of addition of **C5.**

Indian Institute of Technology Guwahati

TH-1410_10610607

LIST OF PUBLICATIONS

TH-1410_10610607

TH-1410_10610607

List of Publications

Publications from Ph.D. Research Work:

(A) Journal Publications:

1. **Goswami, S.**, Adhikari, M. D., Kar, C., Thiyagarajan, D., Das, G., and Ramesh, A. (2013) Synthetic amphiphiles as therapeutic antibacterials: lessons on bactericidal efficacy and cytotoxicity and potential application as an adjuvant in antimicrobial chemotherapy. *Journal of Materials Chemistry B* **1**, 2612-2623.

2. **Goswami, S.**, Thiyagarajan, D., Das, G., and Ramesh, A. (2014) Biocompatible nanocarrier fortified with a dipyridinium-based amphiphile for eradication of biofilm. *ACS Applied Materials & Interfaces* **6**, 16384-16394.

3. **Goswami, S.**, Thiyagarajan, D., Samanta, S., Das, G. and Ramesh, A. (2015). A zinc complex of a neutral pyridine-based amphiphile: a highly efficient and potentially therapeutic bactericidal material. *Journal of Materials Chemistry B* **3**, 7068-7078.

(B) Conference Presentations:

1. **Goswami, S.**, Adhikari, M. D., Kar, C., Das, G. and Ramesh, A. (2011). Structural modulation of synthetic amphiphiles for enhanced bactericidal efficacy. Abstract No. MVM 84. Presented in 52nd Annual Conference of Association of Microbiologists of India (AMI), Chandigarh, 03-06 November 2011.

Publications from Other Research Projects:

1. Vudumula, U., Adhikari, M. D., Ojha, B., **Goswami, S.**, Das, G. and Ramesh, A. (2012). Tuning the bactericidal repertoire and potency of quinoline-based amphiphiles for enhanced killing of pathogenic bacteria. *RSC Advances* **2**, 3864-3871.

2. Adhikari, M. D., **Goswami, S.**, Panda, B. R., Chattopadhyay, A. and Ramesh, A. (2013). Membrane-directed high bactericidal activity of gold nanoparticle-polythiophene composite for niche applications against pathogenic bacteria. *Advanced Healthcare Materials* **2**, 599-606.

3. Samanta, S., **Goswami, S.**, Ramesh, A., and Das, G. (2014) A new fluorogenic probe for solution and intra-cellular sensing of trivalent cations in model human cells. *Sensors & Actuators B* **194**, 120-126.

4. Thiyagarajan, D., **Goswami, S.**, Kar, C., Das, G., and Ramesh, A. (2014) A prospective antibacterial for drug-resistant pathogens: a dual warhead amphiphile designed to track interactions and kill pathogenic bacteria by membrane damage and cellular DNA cleavage. *Chemical Communications* **50**, 7434-7436.

5. Uday, S. P., Thiyagarajan, D., **Goswami, S.**, Adhikari, M. D., Das, G., and Ramesh, A. (2014) Amphiphile-mediated enhanced antibiotic efficacy and development of a payload nanocarrier for effective killing of pathogenic bacteria, *Journal of Materials Chemistry B* **2**, 5818-5827.

6. Samanta, S., **Goswami, S.**, Hoque, M. N., Ramesh, A., and Das, G. (2014) An aggregation-induced emission (AIE) active probe renders Al(III) sensing and tracking of subsequent interaction with DNA, *Chemical Communications* **50**, 11833-11836.

7. Kar, C, Samanta, S., **Goswami, S.**, Ramesh, A. and Das, G. (2015). A single probe to sense Al(III) colorimetrically and Cd(II) by turn-On fluorescence in physiological conditions and live cells, corroborated by X-ray crystallographic and theoretical studies. *Dalton Transactions* **44**, 4123-4132.

8. Samanta, S., **Goswami, S.**, Ramesh, A., Das, G. (2015). A new chemodosimetric probe for the selective detection of trivalent cations in aqueous medium and live cells. J*ournal of Photochemistry and Photobiology a-Chemistry* **310**, 45-51.

भारतीय प्रौद्योगिकी संस्थान गुवाहाटी • Indian Institute of Technology Guwahati •